Proceedings of the Indian Academy of Sciences

Volume 92, 1983

CONTENTS (Chemical Sciences)

Inorganic and Analytical

Oxotransition metal complexes of O,O-diethylphosphonyl-dithiocarbamate *B Khera, G S Sodhi and N K Kaushik* 73–76

Polarographic study of mixed ligand complexes of Pb(II) with ethylenediamine-malonate and propylene-diamine-malonate *J K Gard, P S Verma and D S Jain* 77–82

Preparation, characterization and thermal properties of di-N-isothiocyanato-dihydrazine metal(II) *K C Patil, J P Vittal and C C Patel* 83–89

Polarographic study of mixed ligand complexes: Pb(II)-succinate-imidazole system *Madhu Shivhare and Mukhtar Singh* 91–97

Kinetics and mechanism of anation of hydroxopenta-aquo chromium(III) ion by DL-alanine in aqueous solution *B K Nigy and G S De* 153–161

Preparation and structural studies of a new series of bimetallic complexes *T N Ojha and S B Sharma* 163–166

Effect of several auxiliary ligands on the extraction of cadmium(II) with 2-thenoyl-trifluoroacetone (TTA) *G N Rao and Roma Lahiri* 167–172

3*d*-metal complexes of salicylaldehyde ethoxythiocarbonyl hydrazone *N K Singh, S C Srivastava and R C Aggarwal* 173–179

Manganese(II) complexes of some nitrogen-oxygen and nitrogen sulphur donor ligands *Sulekh Chandra and Yogendra Kumar* 249–255

Reactions of silylated Schiff bases with organotitanium(IV) and organotin(IV) chlorides *K Dey, S Ray and D Koner* 257–264

Stereochemistry of copper(II), nickel(II) and cobalt(II) 2′-hydroxy-5′-X-chalconeoxime complexes *C Natarajan and M Palaniandavar* 265–270

Copolymers and their polychelates derived from hydroxy benzoic (*o*- and *p*-) acids as antifungal and antibacterial agents *M M Patel, R Manavalan and K Prabhakaran* 271–278

Synthesis and characterisation of hexa, hepta and octa-coordinated Nb(V) complexes of N,N′-(substituted) formamidino-N′-(substituted) carbamides and thiocarbamides *K L Madhok* 605–612

Organic

Addition products of dimethyl acetylenedicarboxylate to thioureas—studies on 2-(*p*-bromophenyl) imino-3-methyl-5-carbomethoxy-methylidene-thiazolidin-(4)-one *K Nagarajan, M D Nair, S J Shenoy and C*

Oxidation of phenylmethylcarbinols by bromamine-*T* *S Gunasekaran and N Venka*

Chiral synthesis of optically active S(+)-2,6,7,7a-tetra-hydro-1-hydroxy-4-formyl-7αβ-methylindene *D K Banerjee, T R Kasturi and A Sarkar* 181–187

Synthesis and characterization of some novel β-aminodiketones *Stephen P Roe and John O Hill* 189–196

The crystal structure of 5α-cyano-3-keto-10-methyl-octahydronaphthalene *Puttaraja and D S Sake Gowda* 279–282

Micellar catalysed oxidative cyclisation of 1,3,5-triaryl formazans *R Balakrishnan, P S Raghavan and Vangalur S Srinivasan* 283–290

Physical and Theoretical

Predictive character of solid state chemistry: Relation between structure, chemical bonding and physical properties of solids *P Hagenmuller* 1–26

The principles of chemical conversion of organic molecules using sheet silicate intercalates *William Jones, D Tilak, B Tennakoon, John M Thomas, Laurice J Williamson, James A Ballantine and J Howard Purnell* 27–41

X-ray photoelectron and Auger studies of $Ag_{2+\delta}S$ *A K Shukla, D D Sarma and G Sankar* 43–46

Effect of ring aza substitution on luminescence of aromatic ketones. Luminescence of isomeric acetylpyridines *S K Sarkar, S K Ghoshal and G S Kastha* 47–58

Infrared spectral evidence for mono-, bi- and tetra-dentate behaviour of hexamethylenetetramine *I S Ahuja, Raghuvir Singh and C L Yadava* 59–63

Photoacoustic spectra of As_2S_3—As_2Se_3 glasses *T Somasundaram, P Ganguly and K J Rao* 65–71

Stability of mixed ligand complexes of copper(II): ESR studies *B S Prabhananda* 113–126

On the vibrational structure involving C=O stretch in the vapour phase phosphorescence of *p*-benzoquinone-h_4 and -d_4 *V N Pandey and S N Thakur* 127–131

The near UV vapour absorption spectra of 1-hydroxynaphthalene and 2-hydroxynaphthalene *V N Pandey and S N Thakur* 133–138

Structural, electrical and reflectance studies of the system $ZnMn_{2-2x}Ni_xTi_xO_4$ *B A Mulla and V S Darshane* 139–145

Viscometry in the study of molecular complexes *Bharati Bhattacharjee and S N Bhat* 147–152

Electronic spectra of paramethoxy benzyl alcohol and parachloro benzyl cyanide *A K Sarkar, P K Mallick, S Chakravorti and S B Banerjee* 197–201

Conductance behaviour of HCl in water-ethylene glycol, water-diethylene glycol and ethylene glycol-diethylene glycol mixtures *P Sivaprasad and C Kalidas* 203–209

Isotopic invariants of pyramidal symmetrical XY_3 molecules and evaluation of molecular constants *A Natarajan and V A Chinnappan* 211–219

Uncatalysed oscillations in the bromate-pyrogallol system *R Ramaswamy and S Ramanathan* 221–225

Sulphonated macroporous resin catalysts: studies on the dehydration of 2-butanol *S P Sivanand, R S Singh and D K Chakrabarty* 227–232

Role of salt effect and adsorption on the Liesegang ring formation of lanthanum molybdate *K V Kurien, V K Vaidyan and M A Ittyachen* 233–237

Periodic crystallisation of magnesium hydroxide in agar agar gel: Influence of temperature *S Ambrose, F D Gnanam and P Ramasamy* 239–247

Very anharmonic molecular vibrations *Foil A Miller* 563–587

Thermodynamics of exchange in clays: Ion exchange equilibria of transition metals and sodium ions on illite *O P Bansal* 589–596

EPR studies of phosphine photofragments in cancrinite matrix at 77K *P Raghunathan and S K Sur* 597–604

Polymer Science and Engineering

Recent advances in the polymerisation of propylene *S Sivaram* 613–621

Polymer alloys: Science and practice *Vikas M Nadkarni* 623–637

Whither polymer engineering *R A Mashelkar* 639–671

Simulation and optimization of polyethylene terephthalate (PET) reactors *Santosh K Gupta* 673–680

Papers dedicated to S Ramaseshan on his 60th birthday

Crystallography

The phase problem of x-ray crystallography *Herbert Hauptman* 291–321

The efficient generation of phase sets by the random approach *K Henderson and M M Woolfson* 323–328

An assessment of criteria of fit in Patterson search *C E Nordman* 329–334

The probability of large structure amplitudes: The space group $P\bar{1}$ *A J C Wilson* 335–339

Maximum entropy—A new approach to the crystallographic phase problem *Ramesh Narayan, Rajaram Nityananda and G V Vani* 341–358

Extinction correction and synchrotron radiation *P Suortti* 359–377

Mathematical methods for the analysis of charge densities from x-ray diffraction *T N Guru Row* 379–384

Determination of one-dimensional crystal structures using the double Patterson function *Peter Main* 385–396

Precision of determination of *d*-spacings using a Guinier camera
Svend Erik Rasmussen 397–401

The phase problem in neutron diffraction
S K Sikka 403–414

Neutron diffraction using an electron linear accelerator *B T M Willis* 415–420

Electro- and magnetogyration *I S Zheludev and O G Vlokh* 421–427

A theoretical consideration of the intermediate phase in α-β transition of quartz
N Kato 429–435

Crystal and molecular structure of pyrrolidine dithio carbamate cobalt(III) chelate
Gopinath Kartha and Kotra V Krishnamurthy 437–441

Electron density distribution in potassium *bis*-(carbonato) cuprate(II)
E N Maslen, N Spadaccini and K J Watson 443–448

Crystallographic study of push-pull ethylenes
D Adhikesavalu, Nirupa U Kamath and K Venkatesan 449–456

Structural evidence for the radical scavenging mechanism of some aminothiol group of radioprotectants
Kalyani Vijayan, B M Vedavathi and A Mani 457–462

Structure and interactions of aspirin-like drugs *M Vijayan* 463–471

Structural changes in the monomeric despentap[illegible]e (B30-B26) insulin crystal
Ru Chang Bi, Zbigniew Dauter, Eleano[illegible]odson, Guy Dodson, Federico Gordiano, Rod Hubbard and Colin Reynolds 473–483

X-ray structural studies on metal complexes with nucleotides and pyridoxal-amino acid Schiff bases. Models for platinum binding to DNA and pyridoxal catalyzed reactions
M Damodara Poojary, S P Sudhakara Rao and H Manohar 485–495

Macromolecular crystallography research at Trombay
K K Kannan and R Chidambaram 497–508

On the polymorphism of the smectic A phases of highly polar compounds
N V Madhusudana 509–525

XANES and EXAFS of copper compounds: Studies of copper carboxylates with metal-metal bonds of the complex formed by *Pseudomonas aeruginosa*
P R Sarode, G Sankar and C N R Rao 527–542

Miscellaneous

Optical birefringence in a fluid near its critical point with stratification under gravity
S Chatterjee and E S R Gopal 543–550

Anomalous dielectric dispersion in glycolchitosan—carboxy methyl cellulose poly-electrolyte complex containing alkali ions
R Srinivasan and Pushpa Viswanathan 551–562

Proc. Indian Acad. Sci. (Chem. Sci.), Vol,. 92, No. 1, January 1983, pp. 1-26.
© Printed in India.

Predictive character of solid state chemistry: Relation between structure, chemical bonding and physical properties of solids

P HAGENMULLER

Laboratoire de Chimie du Solide du C.N.R.S., Universite de Bordeaux I, 351, Courts de la Liberation 33405, Talence, Cedex, France

MS received 10 June 1982

Abstract. Better models to interpret physical properties as well as use of new preparative techniques have allowed in recent years the development of the predictive character of solid state chemistry. Various examples of this evolution have been given in this paper.

It has been shown for instance that new materials (sometimes metastable ones) can be prepared, either by ion exchange or by chemical (or electrochemical) intercalation-deintercalation methods. The structural requirements of such reactions will be discussed. Another example is provided by the way one selects fast ionic conductors for energy storage. Various factors like amorphous nature, covalency, bond competition, presence of vacancies, influence of cationic lone pairs are discussed in the case of alkali ion or fluorine ion electrolytes.

Attention is also paid to the stabilization of unusual electronic configurations, particularly for high oxidation states of transition elements, on the base of relevant structural and bonding considerations.

In the field of magnetic properties, the possibility of obtaining new ferrimagnetic or ferromagnetic materials is discussed, as well as the ability to modify 1D- or 2D- behaviour of chain-or layer-type materials.

Examples are also given showing how the performance of non-linear materials can be modified by playing with the factors determining structural distortions.

Optical properties of materials are also strongly influenced by structural and bonding properties. It will be shown for instance how thanks to the relevant choice of a host, the lattice as well as the chemical composition of the material may lead to pure monochromatic $4f^7$ UV emission in a Eu^{2+}—doped material. Another example illustrates the possibility of obtaining a strong green emission in a $[Ce^{3+}, Tb^{3+}]$ doped phosphate by choosing a formulation leading to best possible over-lapping of the Ce^{3+} emission spectrum under appropriate UV illumination and the $^5D_4 \rightarrow {}^7F_5$ excitation spectrum of Tb^{3+}

Keywords. Electronic configuration; intercalation compounds; magnetism; non-linear materials; optical properties; soft chemistry; superionic conductivity; chemical bonding; structural bonding; fast ionic conductors; energy transfer.

1. Introduction

A few chosen examples will clearly demonstrate how solid state chemistry is increasingly acquiring more and more predictive character in recent years. This is due to the better models available to interpret physical properties and the development of new preparative methods. It has become possible now in many instances to choose the materials which are most appropriate to provide the desired properties.

1.1 *Soft chemistry*

It is possible now to modify the composition of 1-D or 2-D materials a diffusion of alkali ions by room temperature techniques, either by actior or reducing organic solutions or by electrochemical intercalation des methods.

A classic example is given by TiS_2 which has an O1 structure (ABAB p sulphur atoms, layers of titanium in octahedral coordination alternatin Waals gaps). Lithium can be intercalated in the empty gaps (rougl composition $LiTiS_2$), ideally in the available octahedral sites, either by re for instance *n*-butyl lithium dissolved in hexane or by the action of a galv organic solution of Li/Li giving a potential of about 2.4 V (Steele 1974). lithium atoms give rise to Li^+ cations which, after having crossed the elec into TiS_2 forming Li_xTiS_2 ($0 \leq x \leq 1$) and free electrons which in the e move to the TiS_2 cathode and are responsible for the discharge current: $e^-) + TiS_2 \rightarrow Li_xTiS_2$.

The above process is of great interest because of the high specific ene formation of the border material $LiTiS_2$ theoretically 480 wh/kg and c of Li_xTiS_2 which keeps the same structure in the entire homo ($0 \leq x \leq 1$). These features and the reversibility of the above reactio using such a chain for secondary batteries (figure 1). The practical d reactivity of the organic electrolyte with the electrodes; this is wl tendency is to employ superconducting molten lithium salts or solid

Substitution of sulphides by oxides could give higher voltages an capacities, but their utilization in lithium batteries is limited both b reactivity with the electrolyte and by instability of most binary oxides smaller homogeneity ranges of the obtained Li_xMO_2 phases especial charge-discharge cycles.

The case of sodium (or of potassium) differs from that of lithiu storage performances are indeed much lower due to smaller electrc higher mass of the alkali element; however, because of the strong rep the oxide sheets (the M–O bond is less covalent than the M–S bond) the large Na^+ (or K^+) ions may stabilize such layer structures. Lik introduce Coulomb interactions in the van der Waals gap, but they p oxygen layers strongly aside. As a rule, when the transition metal c oxidation power, Na_xMO_2 or K_xMO_2 layer compounds exist only ciently high (at least $x > 0.50$). Furthermore, as intercalation or de sodium (or to a certain extent potassium) leads to relatively high v tions, phase transitions occur leading often to new metastable mat

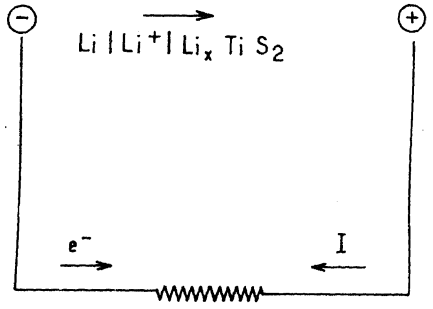

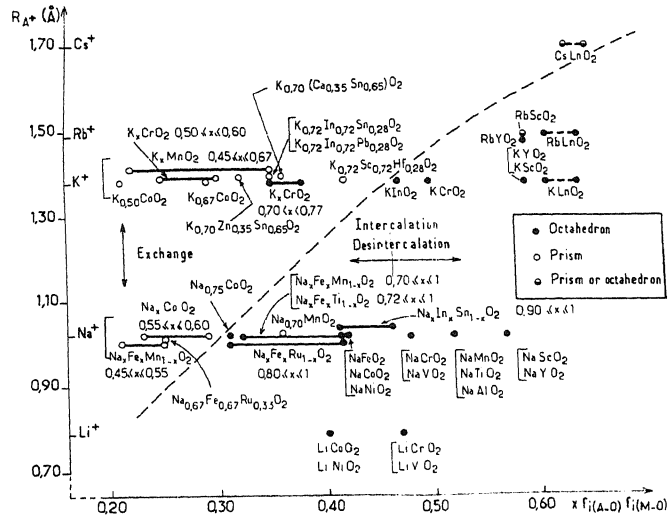

Figure 2. Classification of the A_xMO_2 sheet phases in a R_{A^+} Vs $xf_{i(A-O)}f_{i(M-O)}$ diagram.

The structure-ionicity diagram of figure 2 established by Delmas *et al* (1976) for intercalation oxides on the basis of the model proposed earlier by Rouxel (1976) for sulphides reveals a clear border-line between two different types of oxygen surroundings for Na^+ (or K^+) ions. Octahedral coordination is favoured by high values of x and low oxidation states of M^{n+} (*i.e.* when the repulsions between adjacent oxygen layers through the gap become very large due to strong attraction by the alkali ions as well as to lower covalency of the M–O bonds). For smaller x and higher M^{n+} oxidation states, the coordination is often of trigonal prismatic type. In sheet oxides, octahedral coordination is always found for Li^+ ions, trigonal prismatic coordination for Cs^+ ions. We have neglected here factors such as Jahn-Teller distortion of the M^{n+} ion or energy levels of the trapped electrons. A similar borderline had been observed by Rouxel *et al* (1971) for sulphides. Na_xTiS_2 possesses the O3 type structure for $0.79 \leq x \leq 1$ and the P3 type structure for $0.38 \leq x \leq 0.72$ due to stronger covalency of the TiS_2 sheets*. A comparison of $KTiS_2$ and $KZrS_2$ shows a change from a trigonal prismatic coordination of potassium in the former to an octahedral coordination in the latter one due to weaker Zr–S bonding (Rouxel *et al* 1971).

Electrochemical desintercalation or intercalation of Na_xCoO_2 leads to O3 ←→ O'3 ←→ P'3 reversible transitions, each phase being characterized by a voltage change in the V *vs* x diagram (figure 3). Figure 4 shows that the phases differ simply by sheet gliding without breaking of the Co–O bonds (O'3 has an intermediate structure close to O3) (Delmas *et al* 1981).

Four phases actually appear in the high temperature equilibrium CoO_2 (Fouassier *et al* 1973): P'3 ($0.55 \leq x \leq 0.60$), P2 ($0.64 \leq x \leq 0.7$ and O3 ($x = 1$). Surprisingly enough, P2 is not obtained from the th electrochemical reaction. If one uses P2 as the starting phas preserved over a large composition range: $0.46 \leq x \leq 0.83$ (Delm one can show that a structural transition to a P3 or O3 phase v

* O or P characterises the coordination type of the alkali ion 1,2 or 3 the nu unit cell.

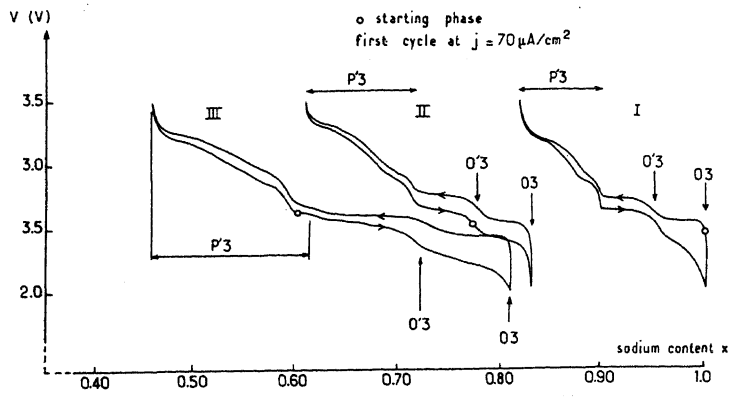

Figure 3. Electrochemical behaviour of $Na_x CoO_2$ phases with P'3, O'3 and O3 structures.

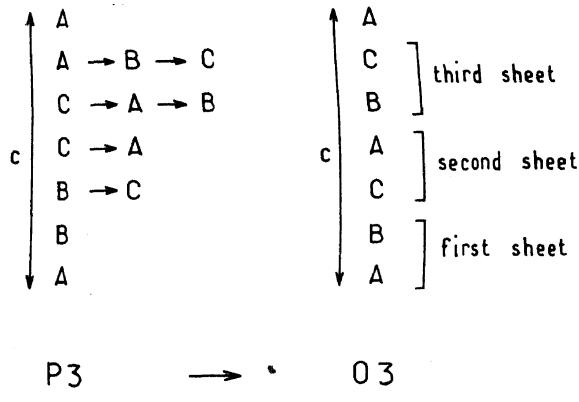

Figure 4. Relationships between P3 and O3 structural types.

sheet shifting, but also Co–O bond breaking due to $\pi/3$ rotation of the (CoO_6) octahedra; the energy available at room temperature is not sufficient to realize such a structural modification.

A similar electrochemical reaction allows the transformation of $NaTiO_2$ (O3) into $Na_{0.71}TiO_2$ (O'3) which differs only by crystallographic distortion. Partial oxidation of $NaTiO_2$ can also be carried out with an iodine solution, but the oxidizing power of the latter is not sufficient to desintercalate $NaMO_2$ phases with high potential like $NaNiO_2$ (Murphy *et al* 1977).

In potassium oxides which are less stable than the homologous sodium oxides, desintercalation can also be achieved by removing the potassium metal under vacuum. At 700° C, this method allows the decomposition of $KCrO_2$ (O3) into so far unpublished K_xCrO_2 (O'3) with $0.70 \leq x \leq 0.77$ and K_xCrO_2 (P3) with $0.50 \leq x \leq 0.60$ (Delmas *et al* 1982).

Another method consists of replacing an alkali ion by another one by using a molten nitrate or a solution of an alkali salt in an organic solvent (*e.g.* methanol), the solvent excess being readily evaporated at relatively low temperature. The first exchange method has been used for preparing $LiFeO_2$ from $NaFeO_2$ (O3) without any structural change by Goodenough *et al* (1979). The second method has allowed the transforma-

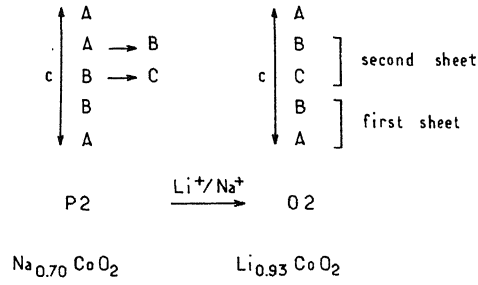

Figure 5. Relationships between P2 and O2 structural types.

tion of $Na_{0.70}CoO_2$ (P2) into a new $Li_{0.93}CoO_2$ (O2) variety (Delmas *et al* 1982). Figure 5 shows that the structures of both materials differ only by sheet shifting. A similar exchange reaction leads to the transformation of $Na_{0.60}CoO_2$ (P3) to $LiCoO_2$ (O3), which again differ only by simple sheet gliding (figure 4). Heating transforms the metastable O2 lithium-cobalt oxide into the stable O3 variety (Delmas *et al* 1982).

In the structure-ionicity diagram of figure 2, intercalation-desintercalation reactions are characterized by horizontal shifts, ion exchange reactions by vertical lines.

Many examples can be given for the preparation of new materials by soft chemistry. For instance, hydrolysis of $K_2Ti_4O_9$ in acidic medium followed by evaporation of H_2O at 500° C leads to a new B variety of TiO_2 formed by blocks of four (TiO_6) octahedra sharing edges. Chemical or electrochemical intercalation of lithium leads to Li_xTiO_2 up to $x=0.85$ (Marchand *et al* 1980). Desintercalation of lithium by electrochemical methods or with iodine from Li_2FeS_2 (obtained by interaction of Li_2S and FeS at 700° C) leads reversibly to $LiFeS_2$ which has the $LiTiS_2$ structure (Brec 1981).

2. Selection of fast ionic conductors

Solid state chemists are paying more and more attention to solid electrolytes with high ionic conductivity from the fundamental point of view and also because of their potential utilization in secondary batteries for energy storage. It has been shown that to obtain a current density of 10 mA/cm^2 in an "all solid" battery for a maximum internal power loss of 1 mW and a minimum electrolyte thickness of 50 μm, the specific conductivity of the electrolyte must exceed $10^{-3}\,\Omega^{-1}cm^{-1}$ at room temperature (Steele 1974). Comparative investigations using precise information given by neutron diffraction as well as by local characterization techniques such as NMR and EPR spectroscopy on doped materials have permitted the determination of the essential requirements of fast ionic conductors (Hagenmuller and Van Gool 1978). Two important features are the presence of available vacancies in the lattice and the low coordination of the mobile ions. The best ionic conductors so far prepared are Cu^+ or Ag^+ compounds where many available sites are empty and the coordination number of the mobile Cu^+ or Ag^+ ions is small (AgI or $RbAg_4I_5$ for instance). The role of coordination of the mobile cation may be explained by the area of the faces constituted by the surrounding anions. The moving cations have to cross these faces as if they were real windows. The smaller the coordination number, the larger is the window opening and the easier the diffusion from an occupied site to an empty one. These considerations can be extended to sheet structures where mobile alkali ions may occupy either octahedral or trigonal prismatic sites in the van der Waals gap.

Table 1. Comparison of the electrical properties of some $A_x In_x Sn_{1-x} O_2$ sheet structure materials.

	Structure type	σ/σ_{NaInO_2}(500K)	E(eV)
$NaInO_2$	O3	1	1.09
$Na_{0.90}In_{0.90}Sn_{0.10}O_2$	O3	8	0.93
$KInO_2$	O3	32	0.87
$K_{0.72}In_{0.72}Sn_{0.28}O_2$	P2	2.6×10^6	0.69
extrap. $K_{0.72}In_{0.72}Sn_{0.28}O_2$	O3	10^3	

Table 1 gives a comparison made by Delmas *et al* (1979b) of the conductivities and the activation energies of several sheet oxides of general formula $A_xIn_xSn_{1-x}O_2$. The conductivity increases while the activation energy decreases from $NaInO_2$ to $Na_{0.90}In_{0.90}Sn_{0.10}O_2$ because of the appearance of octahedral vacancies in the O3-type lattice. We may expect a similar effect due to substitution by Sn in $KInO_2$ (O3): however, a comparison with the value of the conductivity obtained for $K_{0.72}In_{0.72}Sn_{0.28}O_2$ which has a P2-type structure, shows that the latter has a conductivity which is roughly 10^3 times higher than that expected for a similar composition with O3 structure. Trigonal prismatic coordination of the mobile alkali ion enhances strongly the conductivity. Figure 6 shows the diffusion paths in both cases. The diffusion of the cation is slackened when it moves from an octahedral site to another after crossing an intermediate tetrahedron. Such a slowing does not occur when it crosses a prism while diffusing between two similar trigonal prismatic positions. The presence of two cations belonging to the adjacent oxide sheets of the P2 structure near the base-triangles of this intermediate prism is even able to accelerate the crossing process. Figure 7 summarizes a calculation of the variation of the steric part of the activation energy during cation diffusion for both environments which takes into account the alkali cation-oxygen distances inside the polyhedra. Trigonal prismatic surrounding is clearly favoured in the diffusion process (Delmas *et al* 1979b).

Another important property of solid electrolytes is the following. The weaker the bonding between the mobile ion and the lattice, the higher is the mobility. Thus from table 1 we see that the conductivity of K^+ ions is higher in $KInO_2$ than that of the stronger bond Na^+ in the isostructural $NaInO_2$. Lowering of the activation energy is also indicative of the enhancement of the mobility. Consequently, the more covalent the host structure, the looser are the bonds with the mobile ion; this in turn increases the conductivity and lowers the activation energy.

Table 2 allows the comparison of the electrical performances of $K_x(L_{x/2}Sn_{1-x/2})O_2$ sheet oxides of P2 structure. Decreasing the electronegativity difference between oxygen and the sheet cations (*i.e.* higher covalency of the sheets) brings about higher conductivity and smaller activation energy (Maazaz *et al* 1979). Nevertheless, a comparison set-up by Delmas *et al* (1979a,b) of the performances of the zinc-tin oxides ($x=0.80$ and $x=0.70$) whose sheets have the same electronegativity difference shows that higher conductivity and smaller activation energy for $x=0.70$ do not result from the covalency effect, but from the presence of more T.P. vacancies in the material (at least at first approximation since decrease in the number of K–O bonds strengthens bonding within the sheets). This result also explains why the conductivity in layered sulphides is significantly higher than in the homologous oxides and the activation

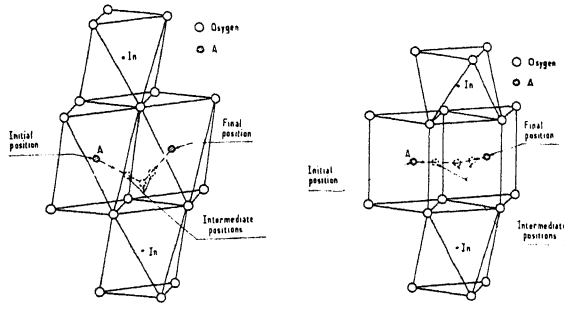

Figure 6. Diffusion paths of the alkali ion in octahedral and trigonal prismatic anionic surroundings between oxide sheets.

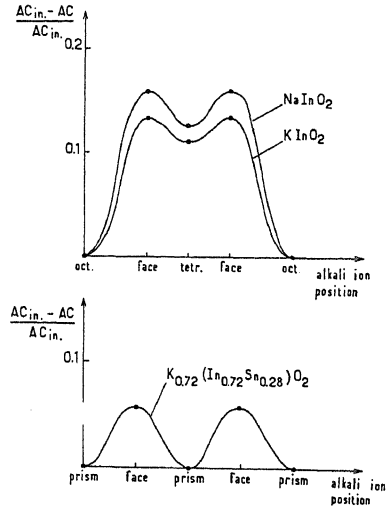

Figure 7. Variation of the steric part of the activation energy during diffusion processes in sheet structures.

Table 2. Influence of the electronegativity difference in the (L, Sn)–O sheets in some $K_x(L_{x/2})O_2$ oxides.

		Str. type	$(\Omega^{-1}cm^{-1})$ 300 K	$(\Omega^{-1}cm^{-1})$ 500 K	E(eV)	$f_{i(L,Sn)-O}$
	L = Zn	P2	7.5×10^{-6}	7.9×10^{-3}	0.45	0.54
$K_{0.70}(L_{0.35}Sn_{0.65})O_2$	L = Mg	P2	1.6×10^{-6}	5.0×10^{-3}	0.52	0.59
	L = Ca	P2	4.5×10^{-7}	6.3×10^{-4}	0.54	0.61
$K_{0.80}(Zn_{0.40}Sn_{0.60})O_2$		P2	1.0×10^{-6}	2.3×10^{-3}	0.50	0.54

energy smaller due to stronger covalency of the sulphide sheets (Trachet and Rouxel 1977).

The influence of the skeleton covalency on the electrical performances of fast ionic conductors is indeed not a property specific to sheet materials alone. Similar results

have been found in substituted β–aluminas or hollandites. Delmas *et al* (1982 a,b) have shown recently such a behaviour in cristobalite-type A_xMO_2 electrolytes which are characterized by large A^+ and small M^{n+} cations. Figure 8 shows that the conductivity of the $K_x(Zn_xGe^{1-x/2})O_2$ phases increases with decreasing x due to an increase in the number of K^+ vacancies as well as the enhanced covalent character resulting from zinc-germanium substitution in the common corner-sharing tetrahedra of the lattice. A comparison with the homologous $K_x(Ga_xGe_{1-x})O_2$ solid solution allows distinction between the influence of these two factors. For the same value of x the first series has a higher conductivity due to the larger Ge content (Zn^{2+} and Ga^{3+} have the same ionicity factors $f_i=0.59$ while Ge^{4+} with $f_1=0.51$ increases the covalency). The activation energy varies very little as the substitution does not modify the crystallographic parameters significantly, *i.e.* the width of the diffusion tunnels in the skeleton (Maazaz and Delmas 1982).

Figure 8 also gives the behaviour of a glassy $K_{0.70}(Zn_{0.35}Ge_{0.65})O_2$ sample. The conductivity is much lower and the activation energy higher than that expected for a crystallized material. Local disordering corresponding to glass formation narrows the tunnels partially in the vitreous state giving rise to bottlenecks. This is however not a general behaviour of glasses. When a vitreous material is formed by isolated glass blocks, the conductivity increases (and the activation energy decreases) with the covalent character of the matrix. Figure 9 established by Levasseur *et al* (1981) shows that the conductivity of the B_2X_3—0.50 Li_2X—0.10 LiI glass increases when the B–O bonds give place to B–S bonds in the vitreous framework; the corresponding activation energy decreases. Li^+ conductivity, despite stronger bonding to the matrix, surpasses that of Na^+ due to the smaller size of the mobile ion which makes the diffusion process through the glass easier (the conductivity at room temperature attains $10^{-3}\,\Omega^{-1}cm^{-1}$). Covalency and steric effects seem to be in competition in such vitreous materials.

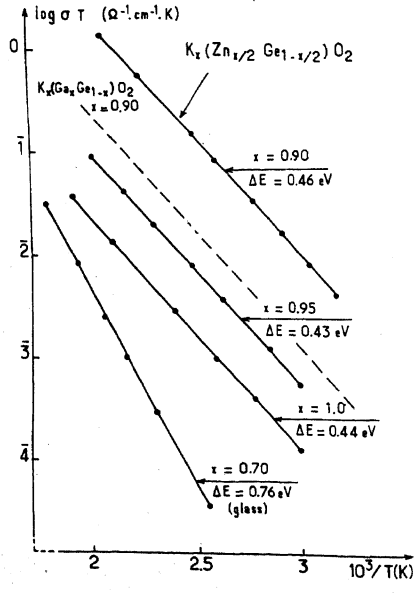

Figure 8. Variation of log σT vs reciprocal temperature for some crystallized $K_x(Zn_{x/2}Ge_{1-x/2})O_2$ compounds and for a vitreous $K_{0.70}(Zn_{0.35}Ge_{0.65})O_2$ sample. Comparison with crystallized $K_{0.90}(Ga_{0.90}Ge_{0.10})O_2$.

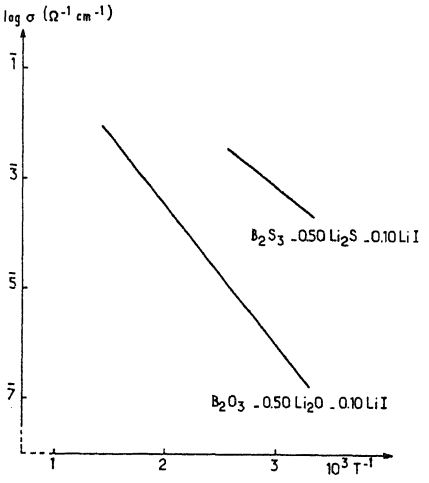

Figure 9. Comparison of the log σ vs T^{-1} curves for two homologous oxide and sulphide glasses.

Another illustration of the role played by diffusion paths is given in figure 10, which clearly shows that the conductivity of B_2O_3-Li_2O-yLiX glasses (X = halogen) increases with increasing size of X which enlarges the diffusion paths. The existence range of the glasses is all the more reduced (Levasseur *et al* 1979).

Much information concerning the behaviour of solid electrolytes has been provided in recent years through investigations of the F^- ion conductivity in fluorite-type materials. This structure may be considered ideally as formed by F^- cubes sharing faces. Half of the cubes is occupied by the M^{2+} cations while the other half is empty, allowing diffusion of the F^- ions from one corner to another through the available central positions, provided the final position is free(figure 11).

The factors that favour F^- anion conduction are weak M–F bonds and the presence of cations with lone pairs which appear to repel the anions during the diffusion process. In figure 12 the low-temperature conductivities of CaF_2, SrF_2 and β–PbF_2 (all of cubic fluorite-type structure) are compared; we see readily that β–PbF_2 is by far the best material.

According to an extensive study by Réau *et al* (1978a) presence of an excess of F^- ions in the material enhances the conductivity by creating a disordered situation in the anionic sublattice. This is clearly shown for instance by the variation of the conductivity of $Pb_{1-x}Bi_xF_{2+x}$ with x (figure 13) (Hagenmuller *et al* 1981). The extra F^- anions occupying the empty sites in the cube centres modify their surroundings by pushing some of the fluorine atoms away from ideal cube corner positions to other available central sites. The resulting disorder increases the conductivity up to $x = 0.25$. Figure 14 shows results of neutron diffraction determinations for $x < 0.25$; the proportion of vacancies in the normal F_I positions increases markedly giving rise to a number of interstitial F_{II} atoms.

When $x > 0.25$, the proportion of F_I vacancies increases more slowly, the number of F_{II} atoms attaining $2x$ as $x = 0.50$, which corresponds to the upper limit of the solid solution range. This composition range is characterized by decreasing conductivity. The conductivity decrease results from a new ordering first at short range and later at long range, leading to an ordered $PbBiF_5$ compound with tetragonal symmetry and $CaYF_5$ structure (Hagenmuller *et al* 1981). The composition $x = 0.25$ corresponds, as expected, to a minimum of activation energy.

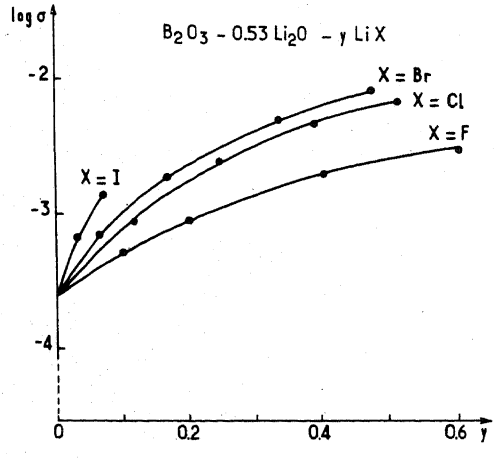

Figure 10. Variation of the conductivity at 300° C vs LiX content in B_2O_3 — 0.5(LiX (X = F, Cl, Br, I).

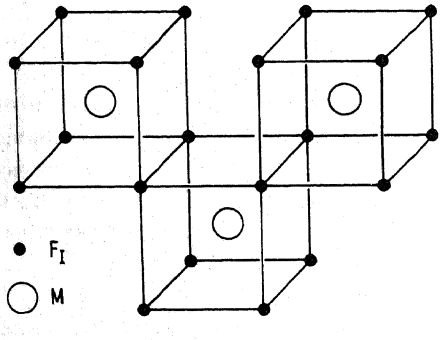

Figure 11. Fluorite-type structure.

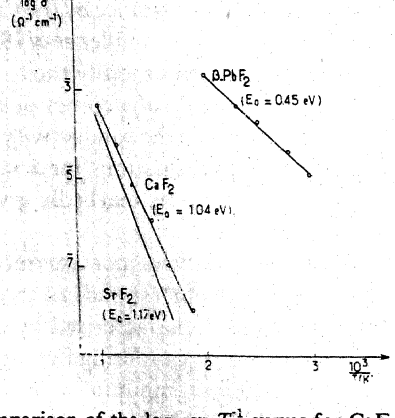

Figure 12. Comparison of the log σ vs T^{-1} curves for CaF_2, SrF_2 and β–PbF

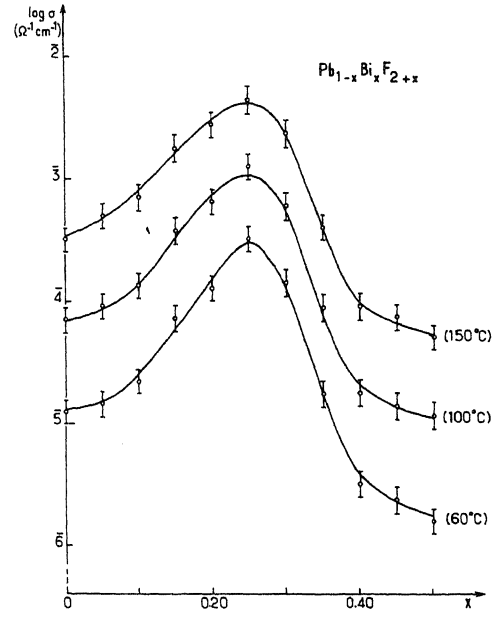

Figure 13. Variation of the logarithm of the conductivity with x for $Pb_{1-x}Bi_xF_{2+x}$ solid solutions vs x at various temperatures.

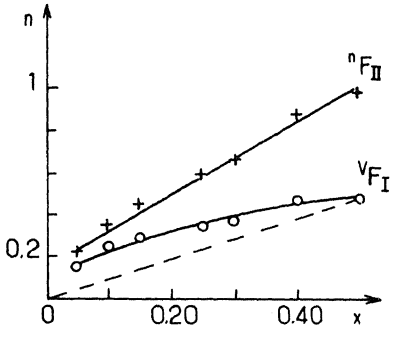

Figure 14. Normal F_I ions, V_{F_I} vacancies and interstitial F_{II} ions in $Pb_{1-x}Bi_xF_{2+x}$. The dashed line indicates the value of x for each material.

A behaviour similar to that $Pb_{1-x}Bi_xF_{2+x}$ has been observed for $Pb_{1-x}Sb_xF_{2+x}$ (Darbon *et al* 1981a), $Pb_{1-x}Zr_xF_{2+2}$ (Darbon *et al* 1981b), $Pb_{1-x}Rh_xF_{2+2x}$ (Réau *et al* 1978a) and $Pb_{1-x}V_xF_{2+2x}$ and more recently for $Pb_{1-x}In_xF_{2+x}$ (Réau *et al* 1982). As a rule maximum conductivity and minimum activation energy correspond approximately to the middle of the solid solution range.

Figure 15 gives an overview of the performances obtained with some fluorite-type related fluorides. Conductivity is enhanced by large cation-fluorine distances, ability of the cations to give rise to lone pairs and by anionic disorder. The best material is $PbSnF_4$, which at 100° C has a conductivity of about $10^{-1}\,\Omega^{-1}cm^{-1}$ with an activation energy of 0.14 eV (Réau *et al* 1978b).

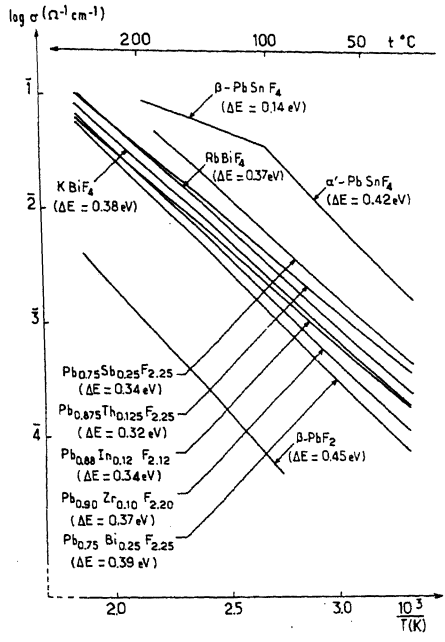

Figure 15. Plot of log σ vs T^{-1} for various fluorite-type fluorides.

Use of fluoride fast ionic conductors in galvanic cells has allowed the setting-up of sensors for measuring P_{O_2} or reducing gas pressures (HF, H_2, NH_3). The determined voltage varies linearly with the logarithm of the gas pressure following a Nernst equation (Portier *et al* 1980).

3. Materials with unusual electronic configurations

Thanks to the development of high pressure techniques, it is now possible to prepare materials containing transition elements with quite unusual electronic configurations. By an appropriate choice of structure and composition, stabilization of several unknown or unusual oxidation states or electronic contributions has been achieved. Extensive studies on metal oxides have been carried out be Demazeau *et al* (1982) who have given a new thrust to a research area initiated 25 years ago by Klemm and his co-workers in FRG.

A good example of such an investigation is given by compounds containing high spin $Fe^{4+}(t^3_{2g}e^1_g)$ in octahedral coordination. In pure Fe^{4+} oxides so far prepared, mostly perovskites, Fe^{4+} had a low spin configuration ($SrFeO_3$) (Takeda *et al* 1972) or showed a certain electronic delocalization of the e_g electron ($CaFeO_3$) (Takeda *et al* 1978). By choosing a material of the K_2NiF_4-type layer structure and allowing competition between Fe-O and Li-O bonds inside the perovskite-type sheets, Demazeau *et al* (1980) have prepared $Sr_{0.5}La_{1.5}Li_{0.5}Fe_{0.5}O_4$. Due to the elongation of the (FeO_6) octahedra which favours Jahn–Teller distortion ($c/a = 3.46$), Fe^{4+} in this compound has the expected high-spin configuration with all the *d* electrons localized. Figure 16 illustrates the influence of the layer structure and of the Li^+ ions in the perovskite planes on the elongated (FeO_6) octahedra. The electronic configuration in this system was ascertained by magnetic measurements and Mössbauer spectroscopy.

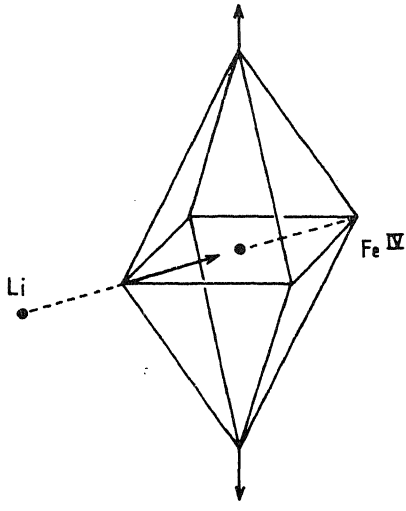

Figure 16. Elongation of the (FeO_6) octahedron in $Sr_{0.5}La_{1.5}Li_{0.5}Fe_{0.5}O_4$.

Another worthy system is the perovskite $La_{1-x}Ca_xFeO_{3-y}$ containing $\tau = x - 2y$ Fe^{4+} ions. At high temperature, these phases are stabilized due to strong hopping between high spin Fe^{3+} and Fe^{4+} ions (at 300 K, $\sigma = 10^{-1}\,\Omega^{-1}cm^{-1}$). This hopping is favoured as x increases because of the broadening of the σ^* levels to a narrow band. As it could be expected from the electronic structure, the hopping mechanism may be "frozen" at low temperature, giving rise to disproportionation: $2Fe^4 \rightarrow Fe^{3+} + Fe^{5+}$ (Komornicki *et al* 1981). This phenomenon is clearly illustrated by the Mössbauer spectra at 4.2 K given in figure 17; the mechanism has been previously described for $CaFeO_3$ and related perovskites (Takano *et al* 1977; Takeda *et al* 1979, Takano *et al* 1980). It suggested the possibility of an eventual stabilization of Fe^{5+} in an octahedral surrounding owing to its t^3_{2g} configuration.

Compounds with Fe^{5+} had been so far prepared only in absence of other iron ions in a tetrahedral environment, which due to strong covalency strengthened the Fe^{5+}–O bonding (Wahl *et al* 1956; Scholder *et al* 1955; Scholder 1965). We selected a perovskite structure with Li–Fe ordering in the B sites with the intention of obtaining Fe^{5+} in an undistorted octahedral site where the t_{2g} levels would be stabilized. The predicted formula of this compound was La_2LiFeO_6. After preparation under 60 kb oxygen pressure, evidence of the oxidation state +V was given from Curie constant determination as well as Mössbauer and EPR measurements (Demazeau *et al* 1981a). It must be emphasized that neither Fe^{4+} nor Fe^{5+} exist in fluorides because of the very small cyrstal field and very high t_{2g} energy levels. Nevertheless, iron (+IV) may be encountered in oxide fluorides (Ménil *et al* 1981).

Cobalt 3+ has provided an interesting development recently. In an octahedral environment, Co^{3+} ions are usually either of low spin $t^6_{2g}e^0_g$ or of high spin $t^4_{2g}e^2_g$ configuration (with the ground term $^1A_{1g}$ or ^5E_g). The first electronic structure is common in oxides and the second is most frequent in fluorides at least at high temperatures. It has been shown on the basis of a Tanabe-Sugano type diagram that an intermediate medium spin configuration with two single electrons corresponding to a $^3B_{2g}$ ground term ($d^2_{zx}d^2_{yz}d^1_{xy}d^1_{z^2}d^0_{x^2-y^2}$) may occur in an octahedron, provided the crystal field/Raccah parameter ratio is high enough and the site sufficiently elongated (figure 18) (Demazeau *et al* 1980). In $La_2Li_{0.5}Co_{0.5}O_4$ due to the strong crystal field

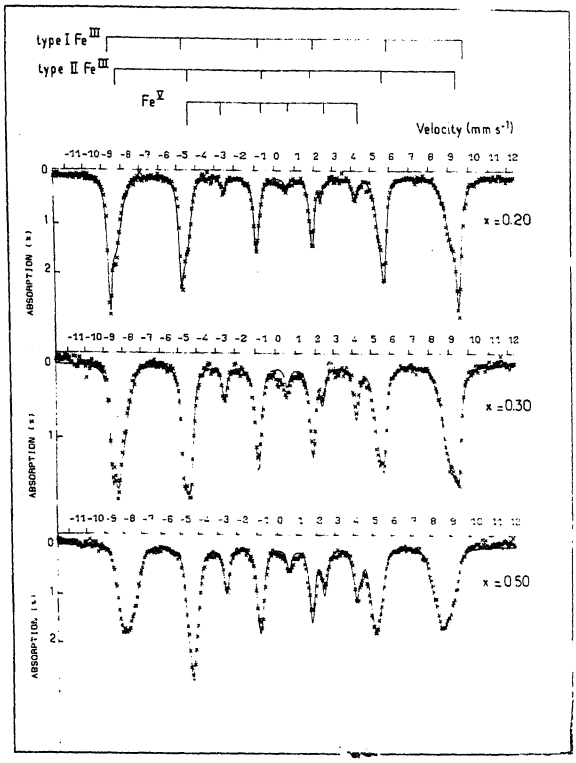

Figure 17. Mössbauer spectra of $La_{1-x}Ca_xFeO_{3-y}$ at 4.2 K for various values of X.

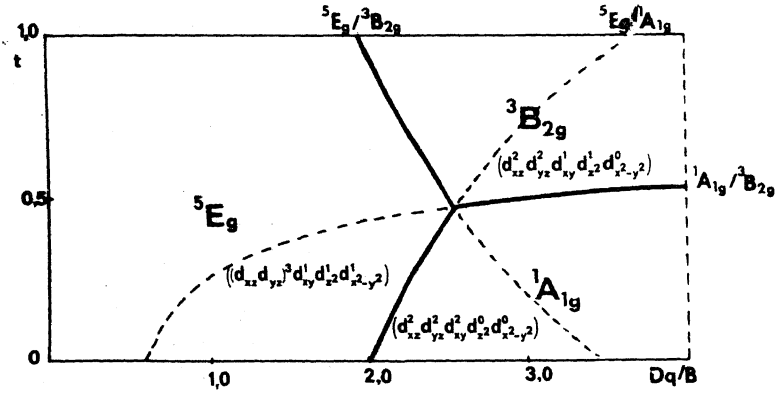

Figure 18. Stability domains for the ground terms $^1A_{1g}$, $^3B_{2_g}$, and ^5E_g vs distortion parameter t and D_g/B.

and a $c/a = 3.39$, a great proportion of cobalt 3+ has the medium spin configuration as shown by fitting the calculated magnetic susceptibility data with the experimental values. Figure 19 allows us to understand the influence of the crystallographic elongation on the energy level splittings.

A further development relates to the possibility of obtaining Ni^{3+} which is generally in the low-spin state $(t_{2g}^6e^1_g)$ to occur in the high-spin configuration $(t_{2g}^5e^2_g)$. Demazeau *et al* (1982) used as the starting point $SrLaNiO_4$ where Ni^{3+} has the low spin

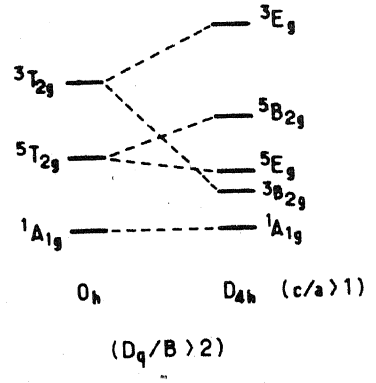

Figure 19. Splitting of the energy levels of an octahedrally surrounded Co^{3+} ion under the influence of a strong elongation.

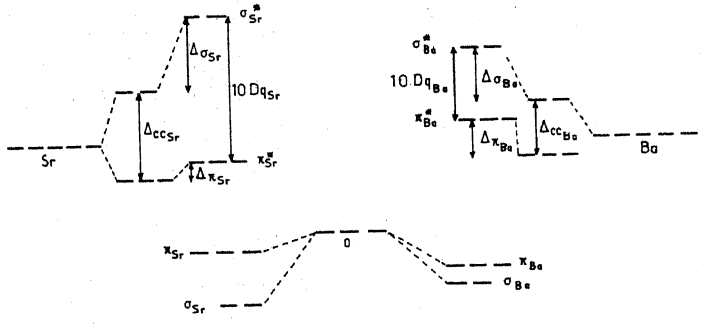

Figure 20. Energy diagrams giving the positions of the σ^* and π^* orbitals of Ni^{3+} ions in $SrLaNiO_4$ and $BaLaNiO_4$.

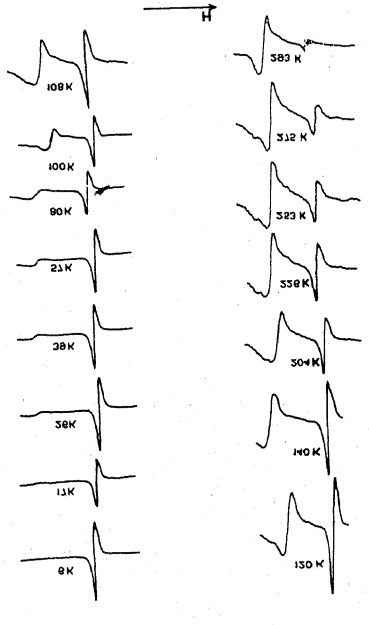

Figure 21. EPR spectra of $BaLaNiO_4$ as a function of temperature.

configuration due to the K_2NiF_4-type structure which favours Jahn-Teller distortion. Substitution of strontium by barium renders formation of the high-spin configuration easier due to larger Ni^{3+} ions and lower σ^* level resulting from the smaller crystal field. These effects are enhanced by a higher π^* (Ni–O) level resulting from the weaker σ(Ba–O) bond, which competes with the π(Ni–O) bond (figure 20) (Demazeau *et al* 1982). Magnetic susceptibility and EPR measurements give evidence of a low spin → high spin transition at rising temperature in $BaLaNiO_4$. The EPR spectra given in figure 21 show that this transformation is achieved at room temperature.

In $SrLaNiO_4$ because of the strong σ(Ni–O) bonds, the $e^1{}_g$ electron is delocalized in a narrow band. $La_2Li_{0.5}Ni_{0.5}O_4$ has been prepared to localize this e_g electron; the structure and composition favour the low-spin configuration of Ni^{3+}, but isolation of the (NiO_6) octahedra leads to localization of the $e^1{}_g$ electron. This interpretation is ascertained by Curie constant determination, EPR spectrum and electrical measurements. It is illustrated by the high value of c/a which attains 3.43 (Demazeau *et al* 1981).

In fluorides nickel 3+ has the high-spin configuration, provided the temperature is high enough. By magnetic susceptibility measurements and x-ray crystallographic studies, evidence was obtained for a low spin → high spin transition in the Na_3NiF_6, K_3NiF_6 and Cs_2KNiF_6 elpasolites (Grannec *et al* 1976). The crystal field of Ni^{3+} is very small here since only one Ni–F bond competes with three (even weak) alkali element-fluorine bonds. Similar results have been obtained by Hoppe and his co-workers who prepared many new fluorides of high oxidation state transition elements.

In the perovskite $LaCuO_3$, the strong Cu^{3+} –O bonding gives rise to metallic behaviour in contrast to the behaviour of the isomorphous $LaNiO_3$ (Goodenough *et al* 1973). Whereas in the former compound, antiferromagnetic e_g–$p\sigma$–e_g correlations lead to a half-filled narrow σ^* band, in the latter ferromagnetic correlations give rise to a quarter-filled band with higher Pauli-type susceptibility. On the contrary, $La_2Li_{0.5}Cu_{0.5}O_4$ which has the K_2NiF_4 structure and where each ($Cu^{3+}O_6$) octahedron is surrounded in the perovskite layers by 4(LiO_6) octahedra is an insulator. The layer structure and the competition with weak Li–O bonds induces an elongation of the (CuO_6) octahedron, which is enhanced by a Jahn-Teller effect. The very high value of c/a (3.54) and diamagnetic behaviour are consistent with the $t^6_{2g}d^0_{x^2-y^2}$ configuration of copper 3+ (Demazeau *et al* 1972).

Similar investigations have been carried out on 4*d* or 5*d* cations. The perovskites La_2LiRuO_6 and La_2LiOsO_6, where Ru^{5+} ($4t^3_{2g}e^0_g$) and Os^{5+} ($5t^3_{2g}e^0_g$) have the same surroundings as Fe^{5+} ($3t^3_{2g}e^0_g$) in La_2LiFeO_6 have already been prepared at ordinary pressures. The $t^3{}_{2g}$ configuration is easily stabilized here by higher crystal fields (Hayashi *et al* 1981). But oxidation state +V, which is quite unusual in solid state chemistry for molybdenum ($4d^1$) or tungsten ($5d^1$), has only been obtained for those elements either in on-stoichiometric molybdenum and tungsten bronzes (or related compounds) due to electronic delocalization in the conduction band, or in materials like $AlMoO_4$, $AlWO_4$ or $CrWO_4$ where two Mo^{5+} (or W^{5+}) ions are coupled sharing an electron pair through a common edge of their coordination octahedra in the VO_2 M_2-type structure (Doumerc *et al* 1975, 1976).

PdF_3, which has an ordered $LiSbF_6$ structure actually corresponds to the composition $Pd^{2+}Pd^{4+}F_6$, and is hence a ferromagnetic (T_c = 16 K) insulator at ordinary pressure (ΔE = 1.34eV). Under high pressures one observes a Pd^{2+} + Pd^{4+} → $2Pd^{3+}$ transition leading to a half-filled Pd^{3+} band with metallic behaviour (Demazeau *et al* 1980a). This material is not stable when the pressure is released. On the contrary, $NaPdF_4$ whose structure is derived from the $KBrF_4$-type and which has been obtained at 700° C from NaF and Pd_2F_6 mixture under high pressure is a stable

insulator. The formation of $NaPd^{III}F_4$ is actually in competition with appearance of a $Pd^{II}F_2 + NaPd^{IV}F_6$ mixture which is the reaction product at low temperature and low pressure.

Such a competition explains the difficulty of preparing $KPdF_4$, $AgPdF_4$ or $TlPdF_4$ (Langlais *et al* 1979; Tressaud *et al* 1982). But K_2NaPdF_6 was recently synthesized by the same authors with the elpasolite structure, which is flexible enough to allow the Jahn-Teller distortion required by the $4d^7$ configuration of Pd^{3+}. Obtaining new electronic configurations is often not only a question of correct thinking but also a matter of patience.

4. Magnetic materials

In this field, we have a relatively sound knowledge of the sign and strength of magnetic interactions as given by the Goodenough-Kanamori rules, which allow us to make good predictions of the properties provided the crystallographic structures are not too complex. In the past ten years, many new series of ferrimagnetic materials have been discovered. This is specially true for fluorides. Because of the relatively weak couplings through fluorine, which has a much lower polarizability than oxygen, molecular field theory may be applied and the interactions depend essentially on the nearest neighbouring cations.

A good example of such fluorides is $Na_2M^{II}M^{III}F_7$ or $Ag_2M^{II}M^{III}F_7$ weberites where chains of $(M^{II}F_6)$ corner-sharing octahedra are linked by isolated $(M^{III}F_6)$ octahedra (figure 22) When both M^{2+} and M^{3+} cations are magnetic, the material is generally ferrimagnetic due to $M^{2+} - F - M^{3+}$ superexchange (Na_2NiFeF_7 for instance has a $T_c = 90$ K).

When M^{2+} is diamagnetic isolated $(M^{III}F_6)$ octahedra give rise to paramagnetic behaviour (unless indeed M^{3+} is also diamagnetic as in Na_2MgAlF_7). If M^{3+} alone is diamagnetic, the $(M^{II}F_5)_n$ chains show 1-D magnetic behaviour down to a very low temperature (Na_2NiAlF_7 for instance only becomes antiferromagnetic below 14 K). $Na_2Mn^{II}Fe^{III}F_7$ is antiferromagnetic by magnetic compensation effect ($T_N = 9.7$ K) (Tressaud *et al* 1974).

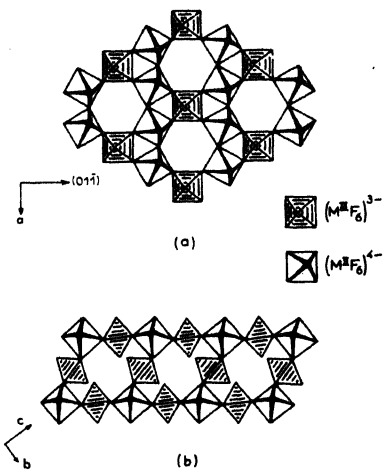

(a) Projection idealisee des couches d'octaèdres sur le plan (011)
(b) Connexion des couches par les octaèdres $(M^{III}F_6)^{3-}$

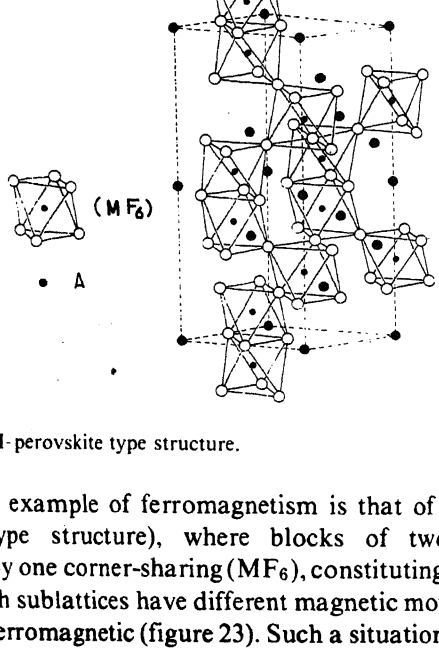

Figure 23. 6H-perovskite type structure.

Another significant example of ferromagnetism is that of 6H-type fluorides (of hexagonal $BaTiO_3$-type structure), where blocks of two-face-sharing (MF_6) octahedra are linked by one corner-sharing (MF_6), constituting unequivalent cationic sublattices. When both sublattices have different magnetic movements with opposite signs, the material is ferromagnetic (figure 23). Such a situation is realized in $CsFeF_3$, as the $Fe^{2+}-Fe^{2+}$ couplings between the face-sharing octahedra are positive, while they are negative between the corner-sharing ones ($T_c = 60$ K) (Portier *et al* 1968). In the prevailing sublattice, the strongest ferromagnetic interactions are of 90° $e_g - p\sigma' - e_g$ type. This explains why in the analogous 6H-$RbFeCl_3$ phase T_c is higher ($T_c = 110$ K) due to stronger Fe–Cl bonds. In $CsMnF_3$, which has the same structure all the neighbouring Mn^{2+} cations are coupled antiparallely: $CsMnF_3$ must therefore be antiferromagnetic ($T_N = 54$ K) (Lee *et al* 1963).

It is possible to make equally good predictions regarding ferromagnetic fluorides. Ferromagnetic behaviour requires direct or indirect magnetic interactions between unequally occupied orbitals which as a rule are positive. A typical example is the $MMnF_6$ series which is of $LiSbF_6$-type structure (ordered VF_3 structure) and where Mn^{4+} is a $t_{2g}^3 e_g^0$ ion. Ferromagnetic couplings may occur if M^{2+} has full t_{2g} orbitals and half-filled or completely filled e_g orbitals. This is the case when $M^{2+} = Ni^{2+}$, Zn^{2+} or Cd^{2+} (Lorin *et al* 1981). With $T_c = 39$ K $NiMnF_6$ has the highest Curie temperature so far obtained for ferromagnetic fluorides.

Much emphasis has been placed in recent year on 1D- or 2D- magnetism (*i.e.* magnetic interactions in chains or layers) prevailing largely over the interchain or interlayer couplings). 2D-type behaviour explains for instance why $CaLaFeO_4$ and $SrLaFeO_4$ with K_2NiF_4-type structure have the same J/K (–37 K) and similar T_c values (373 K and 380 K) despite the different distances between successive magnetic ion-oxygen layers (Le Flem *et al* 1981). In the solid solution $CaLa_{1-x}Y_xCrO_4$, the 2D character of the magnetic interactions disappears as X increases. The (Y–O) bonds are stronger than the σ(La–O) bonds for reasons of cationic size. Their appearance weakens the competing $\pi(Cr\,t_{2g}\text{–}O)$ bonds which are responsible for the 2D behaviour in $CaLaCrO_4$. This magnetic evolution is clearly illustrated by figure 2 which shows the decreasing value of $|J|/K$ and the appearance of a three-dimensional Neel point (Le Flem *et al* 1981; Berjoan *et al* 1982).

V^{2+} ions ($t_{2g}^3 e_g^0$) have provided convenient cases to illustrate the existence of 1D or 2D-magnetism (Niel *et al* 1977). Thus, $CsVX_3$ compounds (X=Cl, Br or I

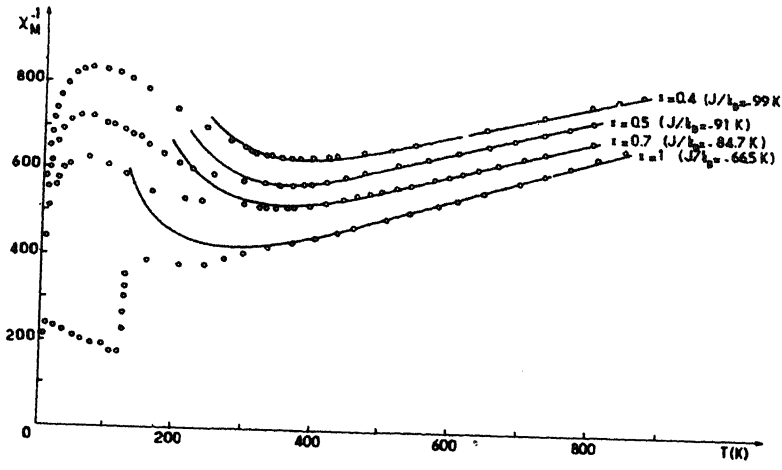

Figure 24. Variation of χ^{-1}_M vs T for $CaLa_{1-x}Y_xCrO_4$.

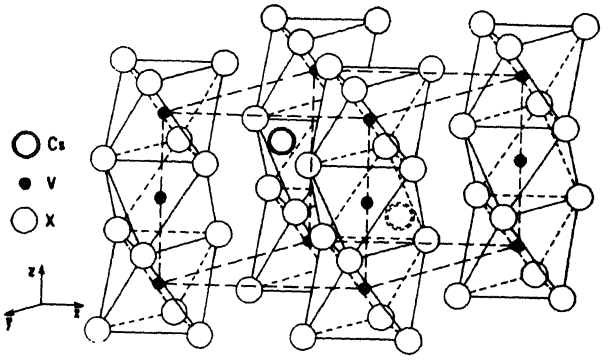

Figure 25. 2H-type structure of the $CsVX_3$ compounds.

constitute a good example of chain magnetism (figure 25) as they are formed by slabs of face-sharing (VX_6) octahedra linked by the Cs^+ ions. The thermal susceptibility curves are characterized by a smooth maximum. The intrachain exchange integrals may be determined by fitting the experimental values to those calculated from an appropriate high temperature series model (figure 26). For X = Cl, Br and I, the exchange integrals, J/K, are about -115 K, -85 K, -60 K. Ferromagnetic e_g–$p\sigma$–$p\sigma'$–e_g interactions are in competition with direct antiferromagnetic t_{2g}–t_{2g} interactions. As the size of the halogens increases, the ferromagnetic couplings become stronger due to higher covalency, whereas the antiferromagnetic ones decrease because of the bigger V^{2+}—V^{2+} distance. Both effects explain why J/K increases (Niel *et al* 1977a).

A similar behaviour is observed in the VX_2 (X = Cl, Br, I) series which has on OI layer structure (figure 27). The HTS calculation method leads to J/K values equal to -23 K, -16 K and -6 K (figure 28). The evolution of J/K with increasing size of the halogen can be explained in the same way as that of the corresponding $CsVX_3$ phases (Niel *et al* 1977b).

It is worthwhile to compare these results with those obtained for the homologous CrX_3 phases. Cr^{3+} has the same electronic structure as V^{2+} ($t_{2g}^3 e_g^0$), and both haloge-

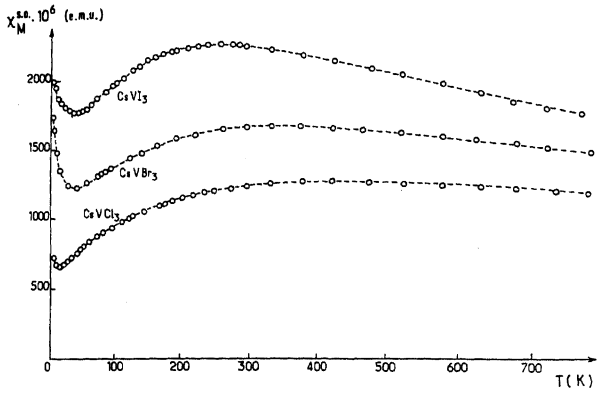

Figure 26. Thermal variation of the magnetic susceptibility for $CsVCl_3$, $CsVBr_3$ and $CsVCl_3$.

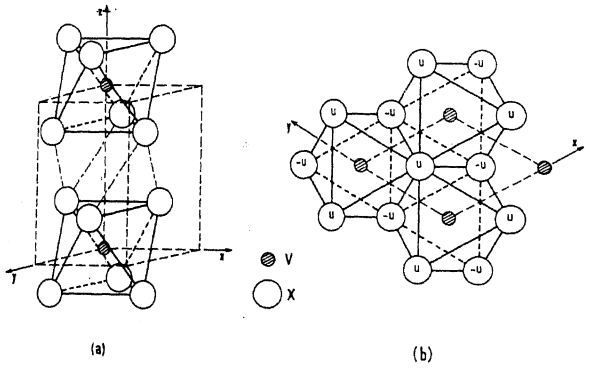

Figure 27. OI-type structure of the VX_2 compounds.

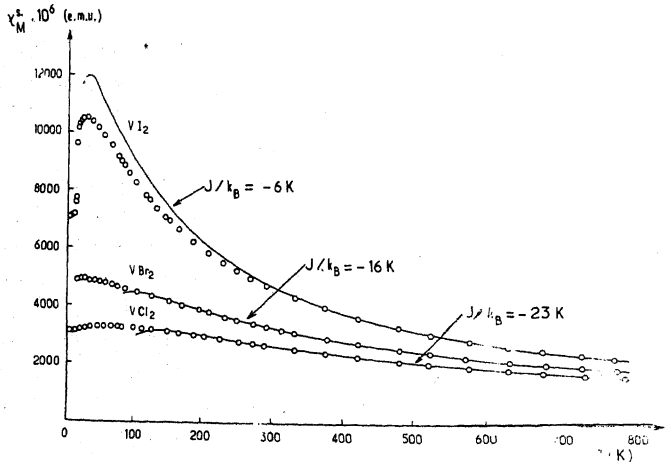

Figure 28. Experimental values of χ^S_M for the VX_2 phases and calculated thermal variations.

nides have a similar layer structure but only 2/3 of the cationic sites are occupied by Cr^{3+} in the CrX_3 sheets. The higher covalency of the Cr^{3+} — X bonds enhances the ferromagnetic couplings and leads to higher J/K values. These become equal to 5.2 K, 8.2 K and 13.5 K for $CrCl_3$, $CrBr_3$ and CrI_3 (Samuelson *et al* 1971).

5. Modifications of non-linear properties of materials by change in chemical composition

Piezoelectric materials are of particular interest because of their applications (for instance in second harmonic generation of laser beams). It becomes necessary to enhance or to weaken the structural distortion responsible for their noncentrosymmetrical character depending on the requirement. This distortion becomes greater as the Curie temperature (transition from a non-linear behaviour to a paraelectric one) increases (Abrahams *et al* 1978).

A good example of the possibility to modulate nonlinear properties by changing the chemical composition is given by the tetragonal tungsten bronze (TTB)-like structures (Ravez *et al* 1976b). Most of these are ferroelectric (*i.e.* the spontaneous polarization which characterizes their piezoelectric behaviour is reversible generally along a unique axis) and their Curie points can be modified by appropriate substitutions. The structure is given in figure 29, the general formulation corresponding to $A_2BC_2M_5O_{15}$ where A, B, C cations occupy tunnels of pentagonal, square or triangular cross-sections. Their coordination numbers are 15, 12 and 9. The M_5O_{15} skeleton is formed by (MO_6) octahedra linked by common corners. The cation distribution in the tunnels depends essentially on their size. Oxygen may be partially or completely replaced by fluorine, *e.g.* in the K_xFeF_3 fluoride bronzes of de Pape (1965). The ferroelectric distortion is due to the positions of the M cation in the (MO_6) octahedra. One generally finds alternating short and long M-O distances along the *c*-axis which is the polar axis; this gives rise to lengthening of the *c* parameter.

Several composition rules have been found. The first one is that the distortion of the octahedra is greater (and T_c becomes higher) as the M^{n+} cation becomes smaller. From $SrK_2(Nb_4Mo)O_{15}$ to $SrK_2(Nb_4W)O_{15}$, for instance, T_c increases from 310 K to 338 K

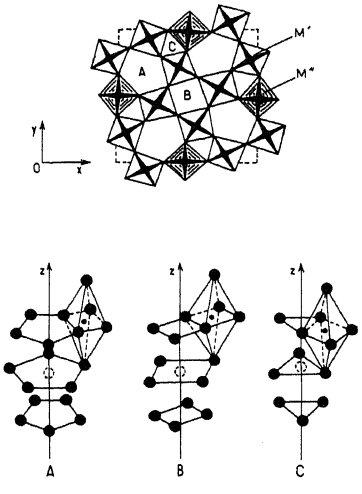

Figure 29. Projection of the TTB structure on a xOy plane. Skeleton of the ABC tunnels.

because of the smaller ionic radius of W^{6+} (Elouadi *et al* 1975). This is the reason why Nb^{5+} which accommodates an ideal octahedral position in oxides with some difficulty, generally gives rise to high Curie points. Substitution of Ta^{5+} for Nb^{5+} markedly decreases T_c despite similar sizes. It has been shown that the π(Ta-O) bonds are weaker than the π(Nb-O) bonds and that the thermal energy required to remove the crystallographic distortion of the octahedron is reduced (Pouchard *et al* 1975). The Curie temperature increases as the size of the *A* cations increase and as that of B cations decrease. The influence of the cation occupying the A site results probably from the weakening of the A-O bond which strengthens the competing (M-O) bonds, increasing their covalent nature. This is clearly brought out in the variation of the Curie point of homologous $[Sr_2]NaNb_5O_{15}$ (T_c=539 K), $[BaSr]NaNb_5O_{15}$ (T_c=547 K) and $[Ba_2]NaNb_5O_{15}$ (T_c=853 K) TTB compounds (Ravez and Budin 1972). The role of the B cation is illustrated by the comparison of $[Ba_2]KNb_5O_{15}$ (T_c=668 K) and $[Ba_2]NaNb_5O_{15}$ (T_c=853 K) (Ravez and Budin 1972) or of the $K_2LnNb_5O_{15}$ compounds where the rare earths occupy the B sites (figure 30) (Scott *et al* 1961). It is likely that small B cations contribute to the crystallographic distortion. Very large A cations and small B cations lead indeed to particularly high Curie temperatures (*e.g.* $Ba_2NaNb_5O_{15}$: T_c=853 K).

Introduction of cations with a lone pair (Tl^+, Pb^{2+}, Bi^{3+}) in an A or B site increases generally T_c due to higher polarizability. Let us compare for instance $Sr_2RbNb_5O_{15}$ (T_c=412 K) and $Sr_2TlNb_5O_{15}$ (T_c=468 K), $Sr_2KNb_5O_{15}$ (T_c = 437 K) and $Pb_2KNb_5O_{15}$ (T_c=630 K), and $K_2NdNb_5O_{15}$ (T_c=442 K) and $K_2BiNb_5O_{15}$ (T_c=633 K). Replacement of an alkaline earth cation by Pb^{2+} also changes the orientation of the spontaneous polarization which rotates from the *c* to the *b*-axis. The material gets a ferroelectric-ferroelastic coupling, which means that two similar structures are in equilibrium but due to the coupling they may substitute for each other on applying an electrical field, a property that is useful in signal transmissions through "optical windows" (Ravez *et al* 1976). C sites can only be occupied by small cations (Li^{2+}, Mg^{2+}, Ni^{2+}, Cu^{2+}). As they generally participate in lattice distortions, their presence in the C tunnels increases the Curie temperature, as shown by a comparison of $Sr_2KNb_5O_{15}$ (T_c=437 K) and $Sr_2KLi_2Nb_4TiO_{15}$ (T_c=663 K) (Pouchard *et al* 1975).

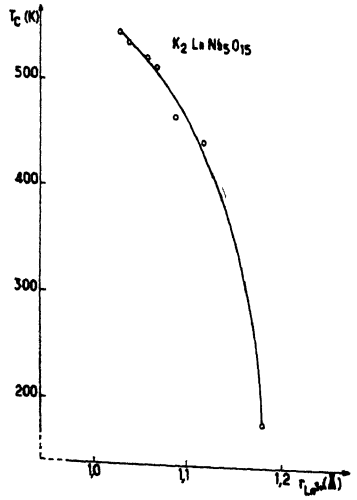

Figure 30. Variation of T_c with the ionic radius of Ln^{3+} for the $K_2LnNb_5O_{15}$ compounds.

Another important feature is the role of oxygen-fluorine substitution. In all ferroelectric materials, replacement of oxygen by fluorine (which decreases the covalency of the non-centrosymmetrical polyhedra) markedly decreases the Curie point. Whereas going from $Sr_2KNb_5O_{15}$ to $SrK_2Nb_4WO_{15}$ decreases T_c only by 100 K, passing from $Sr_2KNb_5O_{15}$ to $SrK_2Nb_5O_{14}F$ results in a 340 K decrease (Ravez and Dabadie 1973). Because of the numerous applications of such materials, the possibility to modify the Curie temperature and hence the structural distortion related to T_c is of prime importance.

6. Materials with selected optical properties

Study of the optical properties has been for a long time an area of research dominated by physicists. Their increasing importance in modern-day life now offers a challenge for solid state chemists to propose new materials possessing specific optical properties. A good example is given by the optical emission properties of Eu^{2+}. In most lattices, it consists of a band corresponding to transitions originating from the lowest states of the $4f^65d^1$ configuration. Hence the produced colour depends mainly on the position of the $4f^65d^1$ configuration (Blasse *et al* 1968). If Eu^{2+} is only weakly bound to the surrounding anions, the smaller covalency lifts the $4f^65d^1$ band, which may then lie above the first excited $4f$ level ($^6P_{7/2}$). As optical pumping in $4f^65d^1$ is easy and the $4f^65d^1 \rightarrow {}^6P_{7/2}$ transition non radiative, such an electronic configuration leads to a monochromatic $^6P_{7/2} \rightarrow {}^8S_{7/2}$ transition around 27000 cm^{-1} (with eventual Stark lines) with a strong intensity due to long life time on $^6P_{7/2}$. Figure 31 gives a schematic representation of both emission mechanisms. A pure monochromatic emission is only possible at room temperature with fluorides because of the weakness of the Eu^{2+} F bond. A detailed investigation shows that other requirements are necessary to raise sufficiently the bottom of the $4f^65d^1$ band: Eu^{2+} has to substitute for Ba^{2+} rather than for Sr^{2+} or Ca^{2+}, C.N. of Eu^{2+} must be 12, the Eu^{2+} F bond has to compete either with another bond of high covalency or with several other bonds. All these conditions lead to further weakening of the Eu^{2+} F bonds. It has been shown, in particular by Fouassier *et al* (1976), that Eu^{2+}-doped $BaAlF_5$, $BaSiF_6$ and BaY_2F_8 give a pure monochromatic emission.

With the exception of Ce^{3+} and Eu^{3+}, trivalent rare earths generally cannot be excited in an efficient way by UV radiation, but most of them have absorption levels in the vicinity of the $^6P_{7/2}$ level of Eu^{2+}, so that resonant or phonon-excited energy transfer from Eu^{2+} may be expected. As BaY_2F_8 may be simultaneously doped with

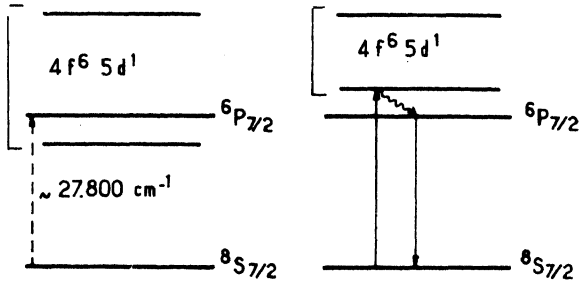

Figure 31. Representation of the Eu^{2+} emission possibilities depending on bond strength with anionic surrounding.

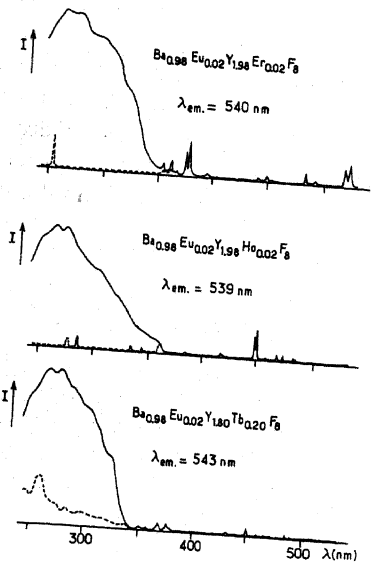

Figure 32. Excitation spectra of Tb^{3+}, Ho^{3+} and Er^{3+} in doped BaY_2F_8 (dashed lines) and $Ba_{0.98}Eu_{0.02}Y_2F_8$ (solid lines).

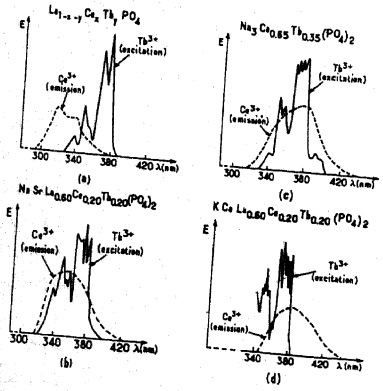

Figure 33. Overlapping between Ce^{3+} emission (for = 254 mm) and $^5D_4 \rightarrow {}^7F_5$ Tb^{3+} excitation spectra at 300 K in: **a**: $La_{1-x-y}Ce_xTb_yPO_4$. **b**: $NaSrLa_{0.60}Ce_{0.20}Tb_{0.20}(PO_4)_2$. **c**: $Na_3Ce_{0.65}Tb_{0.35}(PO_4)_2$. **d**: $KLa_{0.60}Ce_{0.20}Tb_{0.20}(PO_4)_2$.

Eu^{2+} and a small rare earth replacing Y^{3+} (Tb^{3+}, Ho^{3+} or Er^{3+}), the result is a strong emission in the green which would not occur in absence of Eu^{2+}. Figure 32 allows us to compare the corresponding excitation spectra with or without Eu^{2+} (Latourrette *et al* 1979).

Another example of the role solid state chemistry is able to play in the optical properties of materials is related to the green $^5D_4 \rightarrow {}^7F_5$ emission of Tb^{3+} which may be enhanced by the presence of Ce^{3+}, a property being exploited in phosphors employed in low pressure mercury lamps. Phosphates are particularly relevant for such applications, as the strong P O bonds lead to small crystal fields at the rare earth sites. The emission in the green is all the stronger as overlapping between Ce^{3+} emission and Tb^{3+} excitation spectra is better. Whereas the latter is relatively insensitive to the host

structure, the emission of Ce^{3+} is strongly influenced by the crystal field. The higher the alkali ion content and the electropositivity of the alkali element, the greater is the shift of the emission spectrum of Ce^{3+} towards longer wavelengths. This displacement corresponds to a stronger covalency of the Ce–O bonds and to a lowering of the $Ce^{3+}5d$ band (Bochu *et al* 1981; Parent *et al* 1980; Bourcet and Fong 1974). In other words, Ce^{3+} emission may be adjusted to Tb^{3+} excitation by choosing a relevant chemical composition. Figure 33 shows clearly that among the various investigated phosphates, $Na_3Ce_{0.65}\ Tb_{0.35}\ (PO_4)_2$ is the most efficient since the spectra exhibit the best overlapping.

One could multiply examples of physical problems which can be solved by an appropriate selection of the material. Quite frequently one comes across cases where two different physical properties are required for the material the choice of two-phase composite materials would be an attractive solution in such instances. The adopted strategy not only requires a good interface with solid state physics, but also involves mastering of advanced chemical preparation techniques.

References

Abrahams S C, Kurtz S K and Jannieson P R 1978 *Phys. Rev.* **172** 551

Berjoan R, Coutures J P, Le Flem G and Saux M 1982 *J. Solid State Chem.* **42** 75

Blasse G, Wanmaker W, Ter Vrugt J W and Bril A 1968 *Philips Res. Rep.* **23** 189

Bochu P, Parent C, Daoudi A, Le Flem G and Hagenmuller P 1981 *Mater. Res. Bull.* **16** 883

Bourcet J C and Fong K F 1980 *J. Chem. Phys.* 7 913

Brec. R 1981 Private Communication

Darbon P, Reau J M and Hagenmuller P 1981a *Mater. Res. Bull.* **16** 273

Darbon P, Réau J M, Hagenmuller P, Laval J P and Frit B 1981b *Mater. Res. Bull.* **16** 389

Delmas C, Fouassier C and Hagenmuller P 1976 *Mater. Res. Bull.* **11** 1483

Delmas C, Maazaz A, Fouassier C, Réau J M and Hagenmuller P 1979a *Fast ion transport in solids* (eds) Vashishta, J N Mundy and G K Shenoy, (Amsterdam: North Holland) p. 451

Delmas C, Maazaz A, Fouassier C, Reau J M and Hagenmuller P 1979b *Mater. Res. Bull.* **14** 329

Delmas C, Braconnier J J, Fouassier C and Hagenmuller P 1981 *Solid State Ionics* **3/4** 165

Delmas C, Braconnier J J and Hagenmuller P 1982a *Mater. Res. Bull.* **17** 117

Delmas C, Braconnier J J, Maazaz A and Hagenmuller P 1982b *Rev. Ch. Minér.* (in press)

Demazeau G, Parent C, Pouchard M and Hagenmuller P 1972 *Mater. Res. Bull.* 7 913

Demazeau G, Langlais F, Portier J, Tressaud A and Hagenmuller P 1980a *High pressure science and technology* **1** 579

Demazeau G, Pouchard M, Churean N, Colombet J F, Thomas M, Menil F and Hagenmuller P 1980b *J. Less Common Metals* **26** 279

Demazeau G, Pouchard M, Thomas M, Colombet J G, Granier J C, Fournés L, Soubeyroux J L and Hagenmuller P 1980c *Mater. Res. Bull.* **15** 451

Demazeau G, Buffat B, Ménil F, Fournés L, Pouchard M, Dance J M, Fabritchnyi P and Hagenmuller P 1981a *Mater. Res. Bull.* **16** 1465

Demazeau G, Marty J L, Pouchard M, Rojo T, Dance J M and Hagenmuller P 1981b *Mater. Res. Bull.* **16** 47

Demazeau G, Marty J L, Buffat B, Dance J M, Pouchard M, Dordor P and Chevalier B 1982 *Mater. Res. Bull.* **17** 37

de Pape R 1965 *C. R. Acad. Sci.* **260** 4527

Doumerc J P, Vlasse M, Pouchard M and Hagenmuller P 1975 *J. Solid State Chem.* **14** 144

Doumerc J P, Angelov S, Menil F and Pouchard M 1976 *Mater. Res. Bull.* 7 913

Elouadi B, Réau J M and Ravez J 1975 *Bull. Soc. Chem Fr.* **3** 467

England W A, Mizushima K, Wiseman P J and Goodenough J B 1979 *Proc. Eur. Comm. Meeting on Adv. Batteries* p. 199

Fouassier C, Matejka G, Réau J M and Hagenmuller P 1973 *J. Solid. State Chem.* **6** 532

Fouassier C, Latourette B, Portier J and Hagenmuller P 1976 *Mater. Res. Bull.* **11** 933

Goodenough J B, Mott N F, Pouchard M, Demazeau G and Hagenmuller P 1973 *Mater. Res. Bull.* **8** 647
Grannec J, Soube P, Chevalier B, Etourneau J and Portier J 1976 *C. R. Acad. Sci.* **282** 915
Hagenmuller P and Van Gool W 1978 *Solid electrolytes* (New York: Academic Press)
Hagenmuller P, Réau J M, Lucat C, Matar S and Villeneuve G 1981 *Solid State Ionics* 3/4 341
Hayashi K, Dazazeau G and Pouchard M 1981 *C. R. Acad. Sci.* **292** 1433
Komornicki S, Fournés L, Grenier J C, Ménil F, Pouchard M and Hagenmuller P 1981 *Mater. Res. Bull.* **16** 967
Langlais F, Demazeau G, Tressaud A, Portier J and Hagenmuller P 1979 *Solid State Commun.* **29** 473
Latourrette B, Guillon F and Fouassier C 1979 *Mater. Res. Bull.* **14** 865
Lee K, Portis A M and Witt G L 1963 *Phys. Rev.* **132** 144
Le Flem G 1982 *C. R. Acad. Sci.* **294** 29
Le Flem G, Courbin P, Delmas C and Soubeyroux J L 1981 *Z. Anorg. Allg. Ch.* **476** 69
Levasseur A, Brethous J C, Reau J M and Hagenmuller P 1979 *Mater. Res. Bull.* **14** 1979
Levasseur A, Olazcuaga R, Kbala M, Zahir M and Hagenmuller P 1981 *C. R. Acad. Sci.* **293** 563
Lorin D, Dance J M, Soubeyroux J L, Tressaud A and Hagenmuller P 1981 *J. Magn. and Magn. Mater.* **20** 1
Maazaz A, Delmas C, Fouassier C, Reau J M and Hagenmuller P 1979 *Mater. Res. Bull.* **14** 193
Maazaz A and Delmas C 1982 *Solid State Commun.* (in press)
Marchand R, Brohan L and Tournoux M 1980 *Mater. Res. Bull.* **15** 1129
Ménil F, Kinomura N, Fournés L, Portier J and Hagenmuller P 1981 *Phys. Status Solidi* **64** 261
Murphy D W, Cros C, Di Salvo F J and Waszczak J V 1977 *Inorg. Chem.* **16** 3027
Niel M, Cros C, Pouchard M and Chaminade J P 1977a *J. Solid State Chem.* **20** 1
Niel M, Cros C, Le Flem G, Pouchard M and Hagenmuller P 1977b *Nouv. J. chimie 1 n° 2* 127
Parent C, Fava J, Salmon R, Le Flem G and Hagenmuller P 1980 *Solid State Commun.* **35** 451
Portier J, Tressaud A, Pauthenet R and Hagenmuller P 1968 *C. R. Acad. Sci.* **267** 1329
Portier J, Couturier G, Danto A, Hakam A, Lucat C, Kleitz M, Cot L, Salardenne J and Hagenmuller P 1980 *ANVAR patent*
Pouchard M, Chaminade J P, Perron-Simon A, Ravez J and Hagenmuller P 1975 *J. Solid State Chem.* **14** 274
Ravez J and Budin J P 1972 *C. R. Acad. Sci.* **274** 635
Ravez J and Dabadie M 1973 *Rev. Ch. Miner.* **10** 765
Ravez J, Perron-Simon A, Elouadi B, Rivoalloan and Hagenmuller P 1976a *J. Phys. Chem. Sol.* **37** 349
Ravez J, Perron-Simon A and Hagenmuller P 1976b *Ann. Ch.* 1–251
Réau J M, Moali J and Hagenmuller P 1977 *J. Phys. Chem. Sol.* **38** 1395
Réau J M, Rhandour A, Lucat C, Portier J and Hagenmuller P 1978a *Mater. Res. Bull.* **13** 827
Réau J M, Lucat C, Portier J, Hagenmuller P, Cot L and Vilminot S 1978b *Mater. Res. Bull.* **138** 877
Reau J M, Matar S, Kacim S, Champarnaud-Mesjard J C and Frit B 1982 *Solid State Ionics* (in press)
Rouxel J 1976 *J. Solid State Chem.* **17** 223
Rouxel J, Danot M and Bichon J 1971 *Bull. Soc. Chim. Fr.* **11** 3930
Samuelson E J, Silberglitt R and Sheriane G 1971 *Phys. Rev.* **B3** 157
Scholder R 1965 *Bull. Soc. Chem.* **4** 1112
Scholder R, Bunsen H V, Kindervater and Zeiss N 1955 *Z. Anorg. Allg. Ch.* **282** 268
Scott B A, Giess E A, Burns G and O'Kane D F 1961 *Mater. Res. Bull.* **3** 861
Steele B C H 1974 *Philos. Trans. R. Soc. (London)* **A302** 361
Takano M, Nakanishi N, Takeda Y, Naka S and Takada 1977 *Mater. Res. Bull.* **12** 923
Takano M, Kawachi, Nakanishi N and Takeda Y 1980 *Proc. 3rd Int. Conf. Ferrites,* Kyoto, Japan
Takeda T, Yamaguchi Y and Watanabe W 1972 *J. Phys. Soc. Jpn.* **33** 967
Takeda Y, Naka S, Takano M, Shinjo T, Takeda T and Shimada M 1978 *Mater. Res. Bull.* **13** 61
Takeda Y, Naka S and Takano M 1979 *J. Phys.* **40 C2** 331
Tressaud A, Dance J M, Portier J and Hagenmuller P 1974 *Mater. Res. Bull.* **9** 1219
Tressaud A, Khairoun S, Dance J M, Grannec J, Demazeau G and Hagenmuller P 1982 *C. R. Acad. Sci.* (in press)
Trichet L and Rouxel J 1977 *Mater. Res. Bull.* **12** 345
Wahl K, Klemm W and Wehrmeyer G 1956 *Z. Anorg. Allg. Ch.* **285** 322

Proc. Indian Acad. Sci. (Chem. Sci.), Vol. 92, No. 1, January 1983, pp. 27–41.
© Printed in India.

The principles of chemical conversion of organic molecules using sheet silicate intercalates

WILLIAM JONES, D TILAK, B TENNAKOON,
JOHN M THOMAS*, LAURICE J WILLIAMSON,
JAMES A BALLANTINE† and J HOWARD PURNELL†
Department of Chemistry, University of Cambridge, Lensfield Road, Cambridge, CB2 1EP, UK
† Department of Chemistry, University College of Swansea, Singleton Park, Swansea, SA2 8PP, UK

MS received 19 October 1982

Abstract. Several recently identified commercially significant processes involving a range of organic reactants are catalyzed by certain cation-exchanged sheet silicates, which can be derived from a number of commonly available clay minerals. Methods of characterizing these catalysts, as well as techniques that throw light on the chemical nature and orientation of the intercalated reactants are discussed with the aid of specific examples utilizing various spectroscopic and diffraction methods. A unified mechanistic interpretation, based on the Brönsted acidity of the catalysts, accounting for the facile production of esters, ethers, certain dimers and polymeric hydrocarbons, is given.

Keywords. Catalysis; sheet silicates; smectites.

1. Introduction

Several distinct categories of organic reaction that proceed efficiently in the presence of cation-exchanged montmorillonites and hectorites have come to light since we first reported (Adams *et al* 1978, 1979) the facile production of di-(alk-2-yl) ethers from alk-1-enes three years ago. These include the production of esters from intercalated carboxylic acids (Ballantine *et al* 1981b); of di-(alk-1-yl) ethers by elimination of water from primary alcohols (Ballantine *et al* 1981a); of alkenes from secondary and tertiary alcohols (Ballantine *et al* 1981a); of dialkyl sulphides by elimination of H_2S from thiols (Ballantine *et al* 1981a); and of secondary amines by elimination of NH_3 from primary amines (Ballantine *et al* 1981b). In addition, many other types of organic reactions have been identified including dimerizations (Thomas *et al* 1977 and Adams *et al* 1977), low-temperature thermal decompositions of amines (Tricker *et al* 1975) and esters [Adams *et al* (in press)], intermolecular hydrogen transfer (Adams *et al* 1979a), lactonization Davies (1980) and polymerization (Ballantine *et al* 1981b) quite apart from the already substantial (Thomas 1982) list of reaction types which earlier workers such as Weiss (1969), Fripiat and Cruz-Cumplido (1974) Pinnavaia and Welty (1975) and others (Brindley 1970; Theng 1974; Barrer 1978) have uncovered. New classes

* Honarary fellow of the Academy
To whom correspondence should be made

of organic reaction involving sheet silicate intercalates continue to emerge, and it is now obvious (Thomas 1982) that considerable scope for controlled synthesis exists by judicious manipulation of the interlamellar regions of the expandable sheet silicates obtained from readily available clays of the montmorillonite type (also designated smectites).

During the course of our work we have paid increasing attention to two aspects of the behaviour of these so-called clay catalysts: the detailed characterization of the montmorillonite prior to use and under conditions that simulate those of the catalytic reactions, and the elucidation of reaction mechanisms.

In this paper we draw together the various threads of the arguments pertaining to the mode of preferred reaction exhibited by the intercalates, and in so doing focus attention on the characterization of the parent or ion-exchanged silicate with a view to emphasizing the key features of the catalysis. By highlighting the principal parameters that influence the catalytic properties of the sheet silicate, it permits a broader appreciation of the factors that may be manipulated to achieve a given catalytic end.

2. Structural considerations

Clay minerals are composed of two distinct types of layers containing SiO_4 tetrahedra and M $(O, OH)_6$ octahedra, with M being, in general, Al, Mg or Fe. The silicates of principal interest here result when one octahedral layer is sandwiched by two tetrahedral layers (see figure 1). If the ion M is divalent (*e.g.* Mg^{2+}), then all the possible octahedral sites within the structure are occupied and the silicate is of the trioctahedral

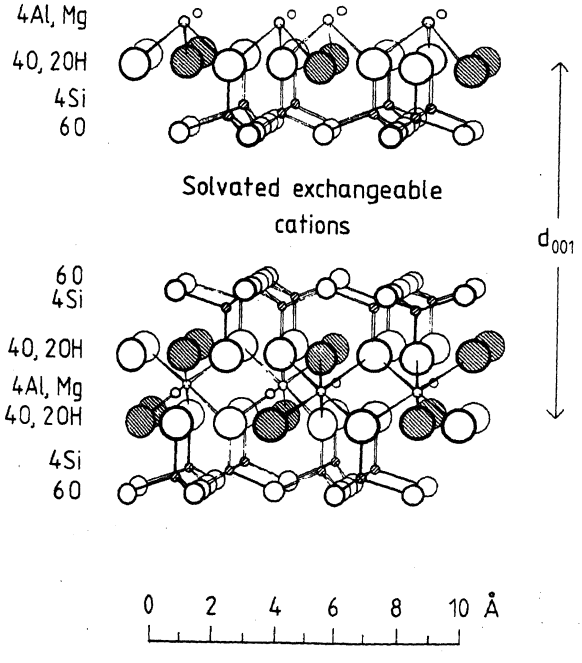

Figure 1. Schematic illustration of the structure of montmorillonite (after Brindley and MacEwan 1953).

type. For trivalent ions (*e.g.* Al^{3+}) only two-thirds of the available sites are occupied leading to a dioctahedral silicate. In addition the tetrahedral and octahedral layers may be partially substituted by ions of lower valency. This produces a negative charge on the layers which is balanced by interlamellar exchangeable cations, which are often Na^+ or Ca^{2+} in naturally occurring clays. The ideal formulae of some smectites are shown in table 1.

With regard to the intercalated organic molecules, figure 2 shows three of the possible ways in which an organic molecule with a hydrocarbon chain may be accommodated in the interlamellar space. Information on the actual orientation adopted may be obtained from x-ray diffraction studies of oriented films of the intercalate (Thomas *et al* 1977; Adams *et al* 1977; Kanamaru and Vand 1970; Adams *et al* 1977a; Williamson *et al* (unpublished)). For smaller molecules information pertaining to orientation is a little less reliable, but we do know some of the broad details of the disposition adopted by butyrolactone and related molecules (Adams *et al* 1977a; Williamson *et al* (unpublished)).

Table 1. Idealised formulae for some selected clay minerals.

Montmorillonite	$(\frac{1}{2}Ca, Na)_x\ (Si_8)\ (Al_{4-x}Mg_x)$	$O_{20}(OH)_4.nH_2O$
Beidellite	$(\frac{1}{2}Ca, Na)_x\ (Si_{8-x}Al_x)\ (Al_4)$	$O_{20}(OH)_4.nH_2O$
Hectorite	$(\frac{1}{2}Ca, Na)_x\ (Si_8)\ (Mg_{6-x}Li_x)$	$O_{20}(OH)_4.nH_2O$
Saponite	$(\frac{1}{2}Ca, Na)_x\ (Si_{8-x}Al_x)\ (Mg_6)$	$O_{20}(OH)_4.nH_2O$

$x = 0.66 - 1.0$

$(Mg_6)\quad O_{20}(OH)_4.nH_2O$

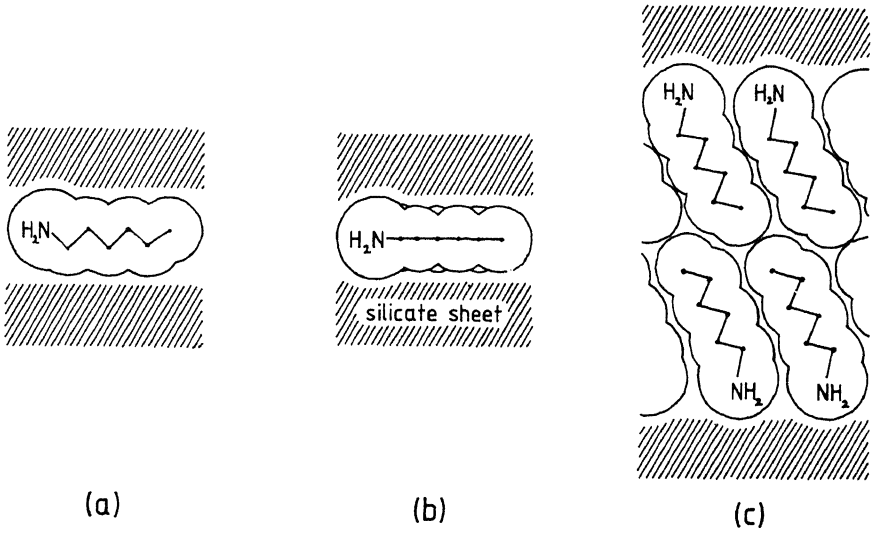

Figure 2. Schematic diagram showing three possible orientations of the intercalated *n*-hexylamine molecule: **(a)** the α_I-configuration, with chain parallel to sheets. **(b)** the α_{II}-configuration, also with chain parallel to sheets, (but rotated by $\pi/2$ with respect to **(a)** and **(c)** the β-configuration, with chain inclined to sheets Nomenclature after Brindley and Hoffman (1962)

3. Chemical composition of montmorillonites

In practice the distinction between the different silicates described above is rarely clear-cut and in particular many clays have substitutions both in the octahedral and in the tetrahedral sites. In addition to the types substitution listed above and in table 1, other elements, particularly iron, are frequently found. Some idea of the variety in composition that exists can be gained from table 2, which lists some structural formulae of several clays taken from the literature.

The unambiguous determination of such structural formulae presents a number of difficulties. Firstly, the clays are often found in deposits containing such impurities as quartz, micas and iron oxides. If these are not removed by sedimentation or other methods, the results of a bulk chemical analysis may be misleading.

Secondly, conversion of the analytical results into a structural formula involves several assumption concerning the allocation of the different elements to the sites available. For example, it is usually assumed that all silicon is present in tetrahedral sites, and that any remaining tetrahedral sites are filled by Al^{3+} and Fe^{3+} ions. Until

Table 2. Typical compositions of some clays.

	Tetrahedral layer	Octahedral layer	CEC*
Montmorillonite[a] "Gelwhite L"	$Si_{7.65}Al_{0.35}$	$Al_{3.20}Fe^{III}_{0.09}Mg_{0.74}$	100
Montmorillonite[b] Chambers, Arizona (Cheto)	$Si_{7.7}Al_{0.3}$	$Al_{2.67}Fe_{0.44}Mg_{0.90}$	150
Montmorillonite[b] Belle Fourche, South Dakota	$Si_{7.86}Al_{0.14}$	$Al_{3.03}Fe_{0.43}Mg_{0.45}$	110
Montmorillonite[c] Camp Berteau Morocco	$Si_{7.75}Ti_{0.03}(Al,Fe^{III})_{0.22}$	$(Al,Fe^{III})_{3.22}Mg_{0.69}$	115
Montmorillonite[d] Wyoming ("Volclay")	$Si_{7.84}Al_{0.16}$	$Al_{3.10}Fe^{III}_{0.38}Mg_{0.52}$	87
Beidellite[c] Black Jack mine	$Si_{6.92}Al_{1.08}$	$Al_{3.92}Fe^{III}_{0.08}$	142
Beidellite[c] Rupsroth	$Si_{7.35}Ti_{0.03}(Al,Fe^{III})_{0.64}$	$(Al,Fe^{III})_{3.54}Mg_{0.45}$	148
Hectorite[c]	$Si_{8.0}$	$Mg_{5.45}Li_{0.55}$	92
Kozakov[c] saponite	$Si_{6.6}Al_{1.36}Fe_{0.04}$	$Mg_{5.0}Fe^{III}_{0.48}Fe^{II}_{0.52}$	120

* The cation exchange capacities are expressed in units of milliequivalents per 100 g. (1 electron/unit cell is *ca.* 140 meq/100 g).

[a] Georgia Kaolin Co., New Jersey.

[b] Cicel and Machajdik (1981).

[c] Chourabi and Fripiat (1981).

[d] Tsunashima *et al* (1981).

other methods are developed for confirming the resulting formula, this approach, which is widely used, should be viewed with some scepticism. Possible confirmatory techniques might include infra-red spectroscopy to determine the location of the negative charge within the sheets (Chourabi and Fripiat 1981), and Mössbauer spectroscopy to determine the oxidation state and location of any iron present (Goodman 1980).

Due to very small particle size of montmorillonites ($< 2\mu m$ diameter) the information that can be obtained concerning their structure and that of their intercalates is generally limited to that available from x-ray powder diffraction or selected area electron diffraction. Several workers have, however, successfully grown organic intercalates of a closely-related solid, vermiculite (a clay mineral not generally so active catalytically), which does form single crystals, and information obtained concerning the arrangements and contacts within these intercalates may also be relevant to those of the montmorillonites.

4. Techniques and results of characterization

Alongside the determination by chemical analysis the *cation exchange capacity* (CEC) is determined. Several methods are available. The one used by us involves measuring the decrease in concentration of ammonium ions (using an ammonium ion selective electrode) in a solution of ammonium chloride when a known weight of clay is added. Typical values for a range of montmorillonites are given in table 2.

The *water content* of the clay is an important quantity. The differences in the operational sense, between 'one, two- and three-layer clays' are schematized in figure 3. 'Layers', in this context refer to the interlamellar water, though the precise chemical nature of this entrained water is not easily established and in any case is a function of the parent silicate. In some sheet silicates, the water is believed to take up an ice-like mono-layer (Hendricks *et al* 1940). What is clear from TGA and IR, however, is that primary and secondary hydration of the interlamellar cation, itself a rather mobile entity, takes place. Such water is rather readily, but not completely, displaced by various organic species, especially amines and carboxylic acids. As a consequence,

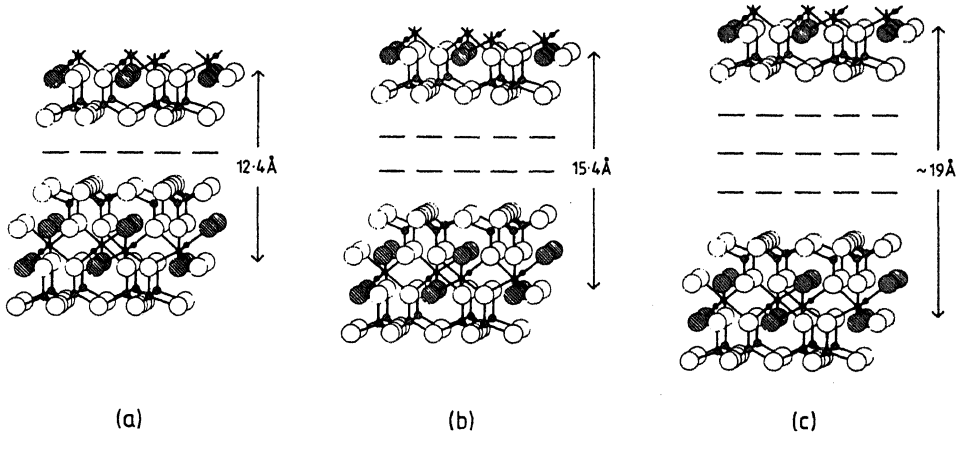

Figure 3. Diagram showing the arrangement of layers of water molecules (dashed lines) in hydrated montmorillonites, and the corresponding interlayer spacings of: (**a**) a one-layer clay, (**b**) a two-layer clay, (**c**) a three-layer clay.
The spacing adopted by a clay depends upon the nature of the silicate layer and the exchangeable cations, as well as the humidity and temperature.

Scheme

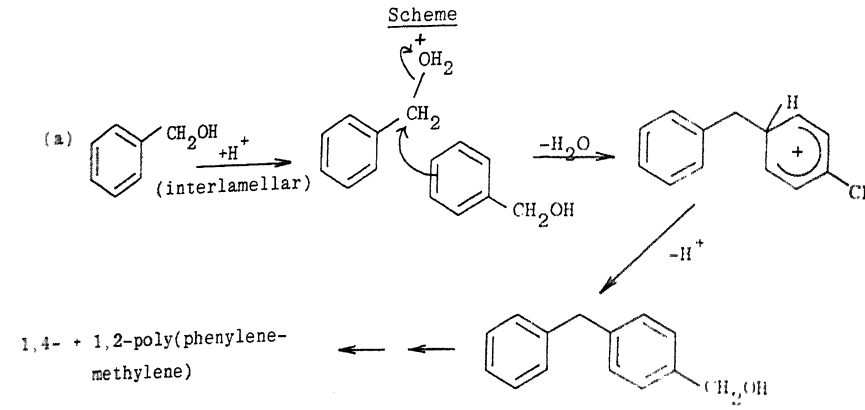
(a)
CH_2OH
$+H^+$
(interlamellar)
$+OH_2$
CH_2
CH_2OH
$-H_2O$
H
$-H^+$
1,4- + 1,2-poly(phenylene-methylene)
CH_2OH

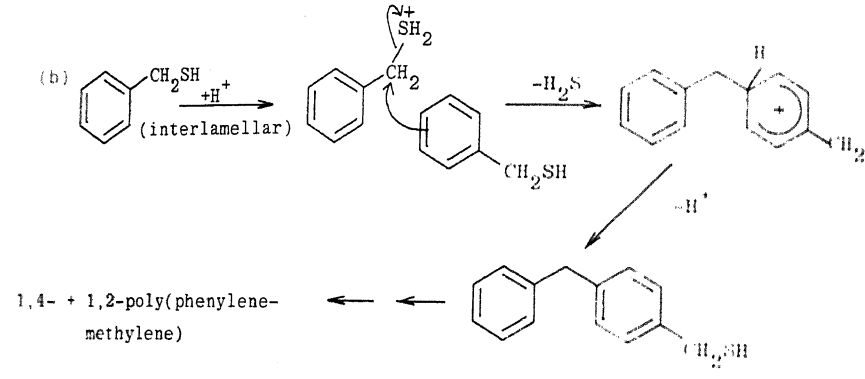
(b)
CH_2SH
$+H^+$
(interlamellar)
$+SH_2$
CH_2
CH_2SH
$-H_2S$
H
$-H^+$
1,4- + 1,2-poly(phenylene-methylene)
CH_2SH

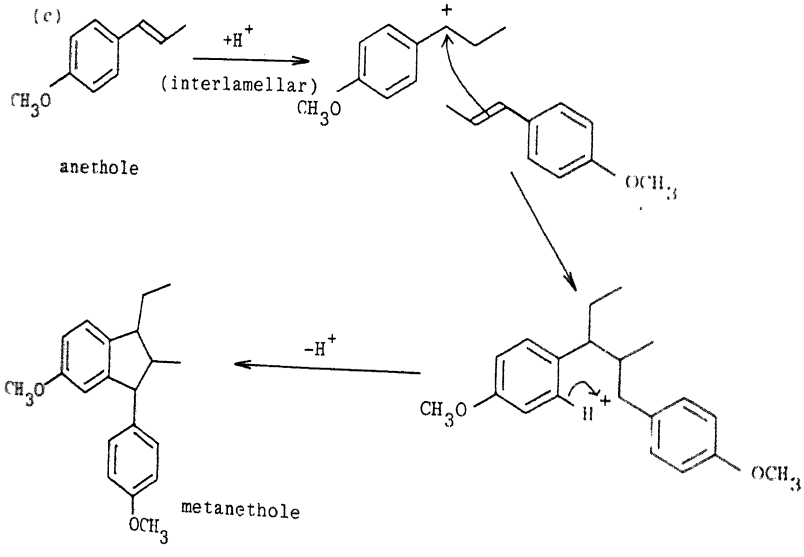
(c)
$+H^+$
(interlamellar)
CH_3O
anethole
OCH_3
$-H^+$
CH_3O
H
OCH_3
CH_3O
OCH_3
metanethole

Scheme (cont.)

(d)

the interlamellar microenvironment is converted from a predominantly hydrophilic to an oleophilic state, making it more conducive to the further insertion of organic species which may otherwise be difficult to intercalate into the original, water-rich montmorillonite.

The ^{57}*Fe Mössbauer spectrum* (taken with a transmission geometry) readily detects structural changes which may result in iron-containing smectites as a result of purification or ion-exchanged as well as during or after catalysis (Rozenson and Heller-Kallai 1978). There is little doubt that the silicate layers are modified during ion-exchange. Figure 4 demonstrates the complete absence of the initial structural ferrous species (a) following cation exchange by chromium (b). Although rigorous quantitative assessment of of site population is, in general, extremely difficult, such major changes in oxidation state are readily studied using this technique. At one time it was suspected

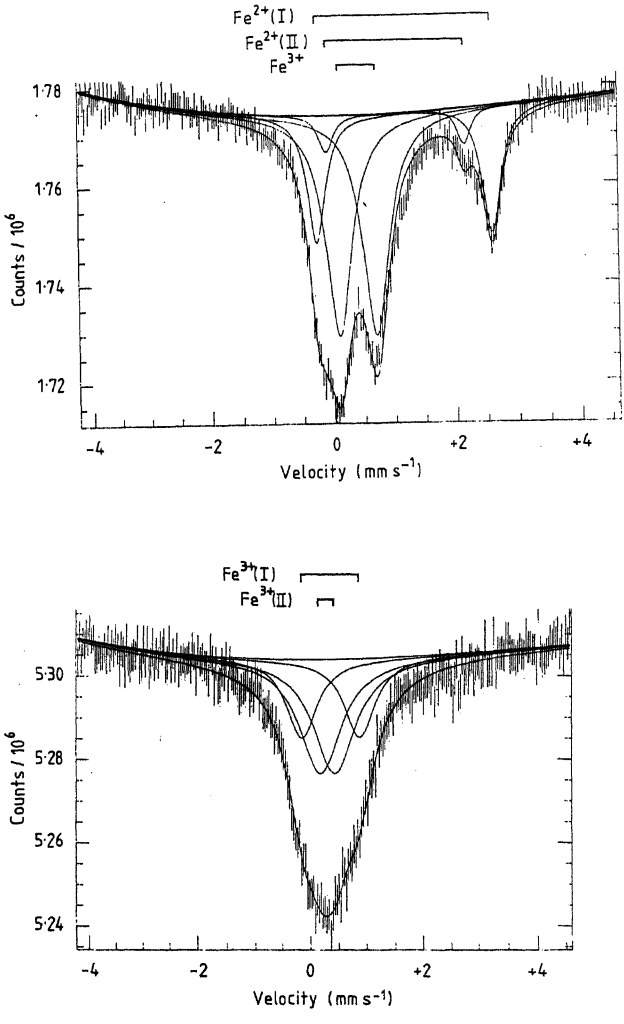

Figure 4. Mössbauer spectra of the naturally occurring montmorillonite before and after exchange by Cr^{3+}. The absence of a ferrous absorption after exchange is evident.
[Fe^{2+} (I) $\delta = 1.17$, $\Delta = 2.86$; Fe^{2+} (II) $\delta = 1.03$, $\Delta = 2.26$; Fe^{3+} (I) $\delta = 0.40$, $\Delta = 0.60$ mm sec^{-1} for natural montmorillonite].
[Fe^{3+} (I) $\delta = 0.34$, $\Delta = 1.08$; Fe^{3+} (II) $\delta = 0.31$, $\Delta = 0.33$ mm sec^{-1} for chromium exchanged montmorillonite].

(by us) that the constitutional iron was involved, either directly or indirectly, in certain of the reactions of the organic intercalates. This now seems unlikely, at least when Bronsted rather than Lewis acidity holds sway, as results we have obtained recently using a commercially available montmorillonite known as Gelwhite (which is essentially free from iron) are not significantly different from those obtained with iron-rich montmorillonites.

IR *spectroscopy* carried out using thin self-supporting films (Farmer 1974) ($\leq 50\,\mu$m thickness) of the appropriate purified montmorillonite, has proved most illuminating, as may be seen from figures 5 and 6. Figure 5 shows the spectrum of a purified sample of Wyoming montmorillonite and figure 6 shows the effect on the spectrum as the

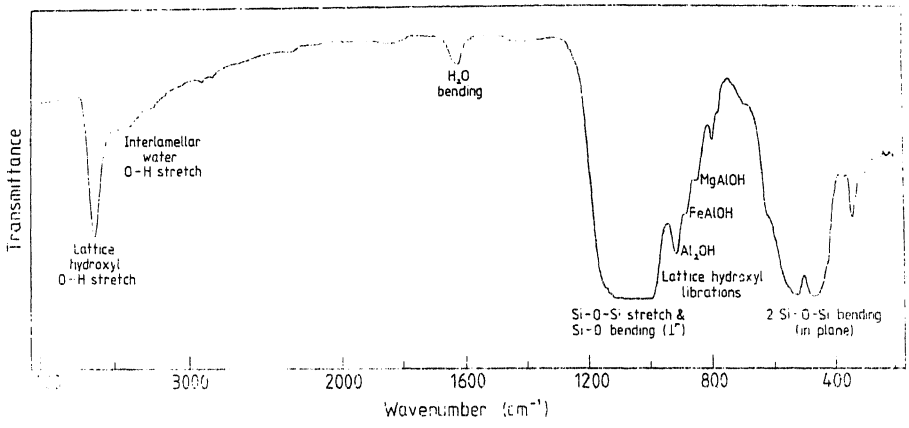

Figure 5. Infrared spectrum of a typical natural bentonite. Small amounts of residual silica (absorbing at ~ 797, 760 and 695 cm^{-1}) are present.

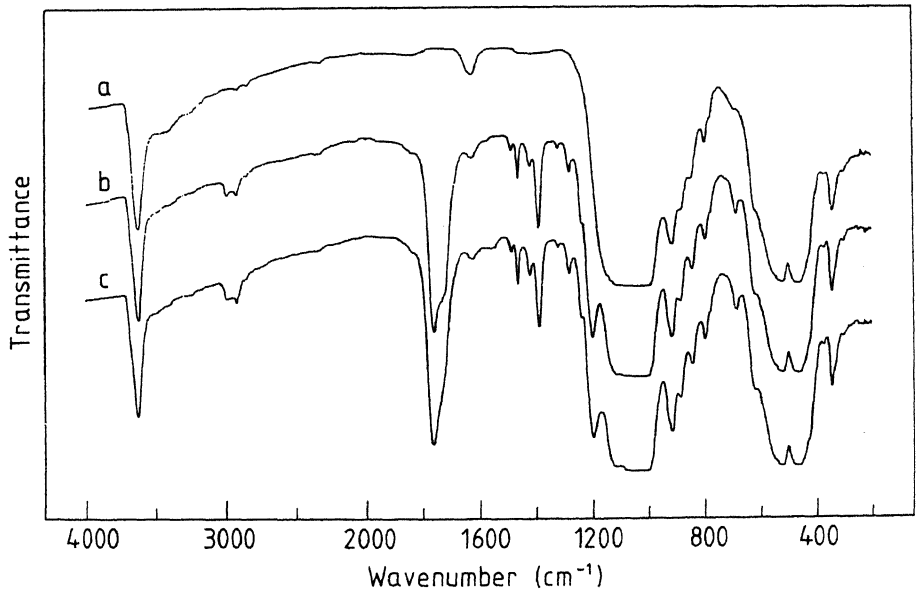

Figure 6. Intercalation of sedimented bentonite by γ-butyrolactone: (**a**) before exposure, (**b**) after 90 min exposure to vapour at 25° C, (**c**) after 14 days exposure to vapour.

sample is exposed to γ-butyrolactone (γ-BUL) vapour. It can be seen that the intensities of the interlamellar water vibrations are decreased, and that new absorptions, due to the organic molecule, have arisen. X-ray diffraction indicates that intercalation has indeed occurred: the interlamellar spacing changes from 12.4 Å for the hydrated material to 18.22 Å after 10 days in the vapour of γ-BUL. This spacing corresponds to a double layer of γ-BUL molecules between the sheets. After 1½ hr in the vapour, the x-ray diffraction pattern has an irrational series of peaks, indicating that a mixture of at least two different spacings is present. The shoulder on the low wave number side of the carbonyl absorption at *ca* 1760 cm^{-1} in the IR spectrum indicates that γ-BUL molecules exist in two types of environment in this sample, and is consistent with the existence of a proportion of one-layer intercalated material.

IR is particularly useful in determining (a) the relative amounts of protonated and unprotonated organic species (see figure 7) or of dissociated and undissociated or dimerized acids, and (b) the rate of uptake of organic species (in a given molecular form) as a function of the interlamellar cation. Figure 8 reveals the important role played by the interlamellar ion in governing uptake kinetics.

Another essential characterizing tool is *x-ray diffractometry* since it provides generally reliable clues as to the occurrence of intercalation by the change in *d*-spacing*. Also one-dimensional Fourier projection maps, which may be extracted from the intensity of (00*l*) reflexions when highly oriented films (and hence large values of *l*) of the intercalate are formed yield instructive information pertaining to the 'time-averaged' orientation of the relatively rigidly held guest species in the interlamellar space (see figure 9). Thus, figure 9 (a) shows the electron density projection along the *z*-direction of a sample of vermiculite, obtained by Fourier synthesis using the observed intensities of the 00*l* reflections (up to $l = 17$) and calculated phases based upon the accepted framework structure. Figure 9 (b) is an electron density projection obtained by Fourier synthesis of calculated structure factors (to 00, 17) for a model structure of the vermiculite (see also legend to figure).

X-ray diffractometry is of additional value, however, since it may be utilized to characterize the clay catalysts under conditions close to, or the same as, those that prevail under actual reaction conditions. Thus figure 10 shows the variable temperature X-ray diffractometric traces, in the region of 2θ corresponding to reflections from the basal (00*l*) planes of an Al^{3+}-exchanged montmorillonite intercalate containing (a) water and (b) 1-pentanol. Clearly this tool gives some insight as to whether a three-layer, two-layer or single-layer or a collapsed (9.5 Å repeat distance) clay exists under certain circumstances. 1-Pentanol which yields principally either 1,1 dialkyl ether or 1-pentene, depending upon the precise reaction conditions, is still retained as a 'one-layer' intercalate, with a d-spacing of 12.6 Å giving a van der Waals gap (or interlamellar space) of about 3.1 Å, at 175° C, at which temperature the heterogeneous reaction (pentanol vapour/solid Al^{3+}-exchanged montmorillonite) proceeds briskly to yield considerably more 1-alkene than when the reaction is carried out in presence of surplus liquid pentanol, in a bomb at 180°.

NMR, using conventional spectrometers (*i.e.* without 'magic-angle spinning' and/or cross-polarization techniques (Fyfe *et al* 1981; Andrew 1981) which are, in general, the preferred aids for extracting chemical shift data from solids), may be profitably used to reveal instructive information about guest entities in sheet silicates. For relatively mobile organic molecules within the interlayer region dipolar broadening is

*This is not an infallible guide: sometimes, when intercalation is known to have occurred, there is essentially no change in d-spacing (Adams 1974).

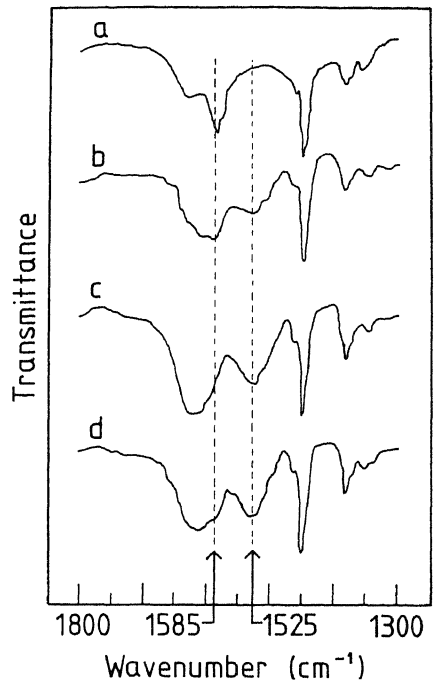

Figure 7. NH and CH bending absorptions in the infrared spectra of cyclohexylamine intercalated into bentonite: (**a**) naturally occurring clay (exchangeable cation principally Na^+) (**b**) after Cu^{2+} exchange, (**c**) Ni^{2+} exchange, (**d**) after Al^{3+} exchange.
The absorptions at 1585 and 1525 cm^{-1} are characteristic of the neutral and protonated cyclohexylamine molecules, respectively.

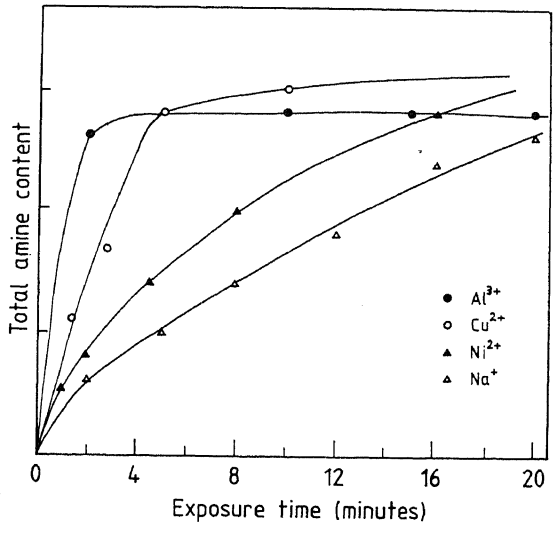

Figure 8. Comparison of rates of cyclohexylamine uptake by differently exchanged bentonite samples. Ordinate proportional to intensity of a CH breathing absorption and hence to the total amount of amine absorbed (protonated and non-protonated).

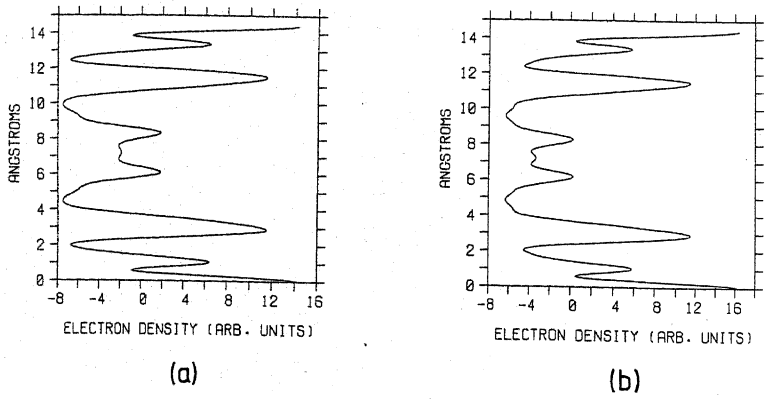

Figure 9. (**a**) Experimentally based and (**b**) theoretically deduced electron density projections for a vermiculite: water intercalate. The framework composition and structure follows closely that used by Mathieson and Walker (1954). The amount of water present in (**b**) was obtained by thermogravimetric analysis and the positions of the water molecules were obtained by refinement using our recorded intensity data.

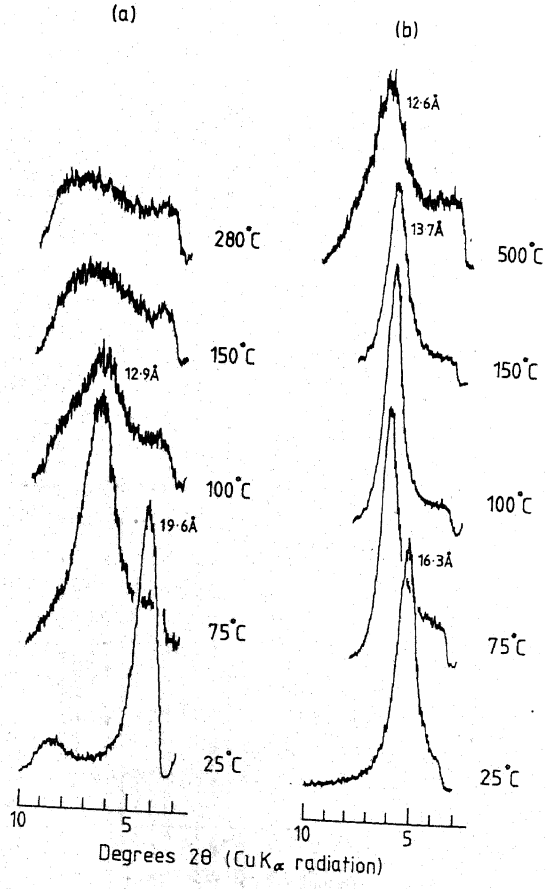

Figure 10. Positions and relative intensities of the (00*l*) reflections obtained with: (**a**) an Al-montmorillonite:water intercalate, and (**b**) an Al-montmorillonite: pentanol intercalate as a function of temperature. The presence of 1-pentanol clearly results in a more temperature-stable expanded structure. The shoulder present within these traces at *ca* 3.5° (2θ) is an instrumental artefact.

minimal so that quite good resolution may be achieved, adequately, in fact, to yield chemical shifts and relaxation times which, in turn, afford information pertaining to the precise degree of molecular freedom, keto-enol equilibria of certain organic species loosely constrained in the micro environment of the interlamellar space and the composition of the guest (especially if there are mixtures of organic species). ^{13}C-spectra recorded at 20 MHz, as well as straight forward ^{13}C spin-lattice relaxation time measurements of a *p*-xylene intercalate of a synthetic hectorite point (Fyfe *et al* 1981; Andrew 1981) to the integration of the xylene guest into the sheet-silicate host–all three structurally distinct carbon atoms have relaxation times (*ca* 450 msecs) that are essentially indistinguishable from one another. The ^{13}C NMR spectrum of cyclohexylamine intercalated within the sheets of a synthetic hectorite is shown in figure 11. Mass analysis and x-ray diffraction (the interlayer spacing increasing from *ca* 12 Å to *ca* 16 Å) clearly support the view that the signal originates from intercalated material. Loss of motional freedom, compared with that of the liquid state, is suggested by the increased line widths.

Other techniques, such as acidity measurements using probe molecules (van Roosmalen 1980) are potentially of use in distinguishing one particular clay catalyst from another. As well as Hammett indicators and pyridine, which have been used to determine acidity, an IR absorption at *ca* 1290 cm^{-1} which appears when *t*-butylamine is introduced into a clay catalyst, could in principle also be used to compare the Brönsted acidity of related clays, since the intensity of this absorption increases with the polarising power of the exchangeable cations (*e.g.* $I_{Na^+} < I_{Ni^{2+}} < I_{Al^{3+}}$). This band may be attributable to the *t*-butyl carbenium ion: the fact that NMR measurements did not confirm its presence might be ascribed to either the low probability of such a cation having sufficient mobility in the interlamellar space to give an observable resonance or to a very short lifetime associated with the carbenium ion. Another method as yet inadequately exploited, is the protonic conductivity of the clay (Sheffield and Howe 1979): this too reflects directly the Brönsted acidity of the catalyst. Lastly high-resolution electron microscopy, as a post-mortem implement, reflects directly (Williamson 1980) the extent of intercalation and its uniformity, or otherwise, within individual crystallites.

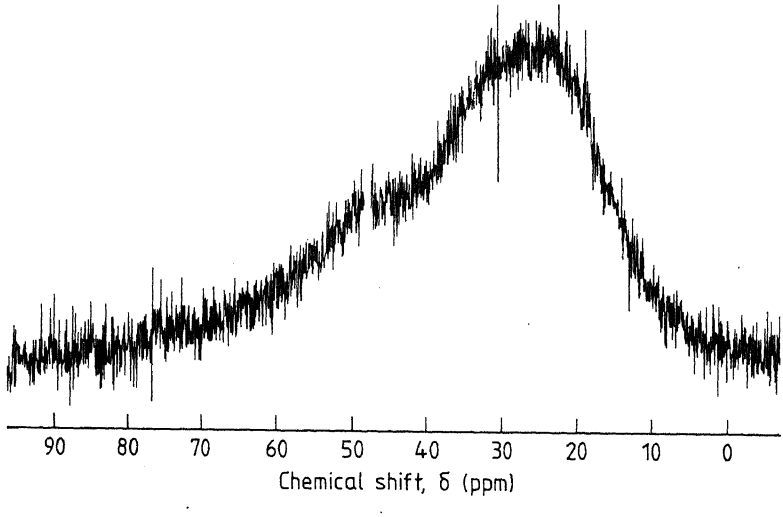

Figure 11. ^{13}C NMR spectrum of 0.16 g cyclohexylamine intercalated into 0.75 g of a synthetic hectorite. The ppm scale is relative to TMS.

5. Summary of catalytic features

We now proceed to enumerate the kinds of conclusion that may be drawn pertaining to reaction conditions and mechanisms from the application of one or more of the techniques discussed in the preceding section. Thus:

(a) *Proof* of the occurrence and nature *of intercalation* comes from x-ray diffractometry and infrared spectroscopy (both of which may be utilized under conditions that closely simulate those that prevail under actual reaction conditions) as well as from NMR studies. TGA provides further circumstantial evidence.

(b) *Proof* that protonation of at least one of the species is an essential requirement for certain reactions comes from infra-red measurements. Moreover, infrared has shown directly the coexistence of protonated and unprotonated amines, a feature which is responsible in part for the unique character of chemical conversions of organic molecules using sheet silicate intercalates.

(c) *Proof* of motional freedom of the intercalated entity comes partly from x-ray diffraction but more directly from NMR line shape and relaxation time data (^{13}C and ^{1}H, see Fyfe *et al* 1981 and Andrew 1981).

(d) *Proof* of the direct or indirect *participation* of certain framework ions (*e.g.* Fe^{2+} or Fe^{3+} in the octahedral or tetrahedral sub-lattices of the sheet silicate) is sometimes provided by spectroscopic measurements, especially Mössbauer absorption technique (Tennakoon *et al* 1974). (By taking two distinct kinds of montmorillonite, one rich in iron the other relatively free of it we have shown that the facile production of ethyl acetate from acetic acid and ethylene is not significantly influenced by so-called lattice iron).

6. Significance of results

The overwhelming majority of novel reactions that may be effected with the agency of sheet silicate intercalates are proton-catalyzed. Some typical examples are shown in the scheme. The production of 1,4- and 1,2-poly (phenylenemethylene) from benzyl alcohol and thio benzylalcohol (Ballantine *et al* 1981a) ((a)and (b)) as well as metanethole from anethole (Adams *et al* in preparation) (c) and sec-ethers from 1-alkenes (Adams 1978, 1979) (d) are shown to have common mechanistic features. In this sense clay catalysts may be pictured in broadly the same mechanistic terms as zeolite catalysts. The solid silicate serves principally as a rich source of protons. But whereas a zeolite possesses a well-defined pore structure (and connectivity between the pores) with access only to relatively small organic molecules, the sheet silicate is in principle capable of 'opening' to accommodate reactant and product molecules of much greater dimensions. A delicate balance of opposing forces dictates whether or not intercalation of a guest by a layered host may take place: energy has to be expended whenever the distance between a central, interlamellar cation and the sheet-anion is increased, but energy is released if the guest is strongly bound to the cation or the interior surface of the silicate. Quantitative discussions of the various factors involved, including identification of separate energetic terms, have recently been given (Barrer 1978; Jenkins and Hartman in press). But it is not yet possible accurately to predict which reactant species will be preferentially intercalated for a given type of cation-exchanged sheet silicate. Greater understanding of the principles of clay catalysis are likely to emerge from the development of techniques for the *in situ* study of chemical reaction by XRD, IR and Mössbauer spectroscopy.

Acknowledgements

The authors thank the University of Cambridge, the University College of Swansea, B P Research (Sunbury) and SERC for support. Discussions with Dr T Rayment and the assistance of Dr P Bowen and Mr S Martin are appreciated.

References

Adams J M 1974 *J. Chem. Soc. Dalton* 2286
Adams J M, Ballantine J A, Graham S H, Laub R J, Purnell J H, Reid P I, Shannon W Y M and Thomas J M 1978 *Angew. Chem. Int. Ed. Engl.* **90** 280
Adams J M, Ballantine J A, Graham S H, Laub R J, Purnell J H, Reid P I, Shannon W Y M and Thomas J M 1979 *J. Catal.* **58** 238
Adams J M, Davies S E, Graham S H and Thomas J M 1979a *J. Chem. Soc. Chem. Commun.* 527
Adams J M, Davies S E, Graham S H and Thomas J M 1982 *J. Catal.* **78** 197
Adams J M, Graham S H, Reid P I and Thomas J M 1977 *J. Chem. Soc. Chem. Commun.* 67
Adams J M, Lukawski K S, Reid P I, Thomas J M and Walters M J 1977a *J. Chem. Res. (M)* 0301
Andrew E R 1981 *Int. Rev. Phys. Chem.* **1** 195
Ballantine J A, Davies M, Purnell J H, Rayankorn M, Thomas J M and Williams K H 1981a *J. Chem. Soc. Chem. Commun.* 427
Ballantine J A, Galvin R P, O'Neil R M, Purnell J H, Rayanakorn M and Thomas J M 1981b *J. Chem. Soc. Chem. Commun.* 9
Barrer R M 1978 *Zeolites and clay minerals as sorbents and molecular sieves* (London and New York: Academic Press)
Brindley G W 1970 *Reunion Hispano-Belga de Minerales de la Arcilla, Madrid* p. 55
Brindley G W and Hoffman R W 1962 *Clays Clay Miner.* **9** 546
Brindley G W and MacEwan D M C 1953 in *Ceramics-a symposium* (eds) A T Green and G H Stewart (Stoke-on-Trent: Br. Ceram. Soc.) p. 15
Cicel B and Machajdik D 1981 *Clays Clay Miner.* **29** 40
Chourabi B and Fripiat J J 1981 *Clays Clay Miner.* **29** 260
Davies S E 1980 *Catalytic Properties of smectites* Ph.D. Thesis, University of Wales, U.K.
Farmer V C 1974 in *The infrared spectra of minerals* (ed) V C Farmer (London: The Mineralogical Society)
Fripiat J J and Cruz-Cumplido M I 1974 in *Annual review of earth and planetary sciences* (eds) F A Donath, F G Stehli and G W Wetherill, (California: Annual Reviews Inc.) Vol. 2, p. 239
Fyfe C A, Thomas J M and Lyerla 1981 *Angew. Chem. Int. Ed. Engl.* **20** 96
Goodman B A 1980 in *Advanced chemical methods for soil and clay minerals research* (eds) J W Stucki and W L Banwart (Dordrecht: D. Reidel Publ. Co.) p.1
Hendricks S B, Nelson R A and Alexander 1940 *J. Am. Chem. Soc.* **62** 1457
Jenkins H D B and Hartman P 1982 *Philos. Trans. R. Soc. (London)* **A304** 397
Kanamaru F and Vand V 1970 *Am. Miner.* **55** 1550
Mathieson A McL and Walker G F 1954 *Am. Miner.* **39** 231
Pinnavaia T J and Welty P K 1975 *J. Am. Chem. Soc.* **97** 3819
Rozenson I and Heller-Kallai L 1978 *Clays Clay Miner.* **26** 88
Sheffield S H and Howe A T 1979 *Mater. Res. Bull.* **14** 929
Tennakoon D T B, Thomas J M and Ticker J M 1974 *J. Chem. Soc. Dalton* 2211
Theng B K G 1974 *The chemistry of clay-organic reactions* (London: Adam Hilger)
Thomas J M 1982 in *Intercalation chemistry* (eds) M S Whittingham and A J Jacobson (New York: Academic Press) p. 55
Thomas J M, Adams J M, Graham S H and Tennakoon D T B 1977 *Adv. Chem. Ser.* **163** 298
Tricker M J, Tennakoon D T B, Thomas J M and Graham S H 1975 *Nature (London)* **253** 110
Tsunashima A, Brindley G W and Bastovanov M 1981 *Clays Clay Miner.* **29** 10
van Roosmalen A J and Mol J C 1980 *J. Chem. Soc. Chem. Commun.* 704
Weiss A 1969 in *Organic geochemistry* (eds) G Eglington and M T J Murphy (Berlin: Springer-Verlag) p. 737
Williamson L J 1980 *CPGS Dissertation*, (UK: University of Cambridge)
Williamson L J, Jones W and Rayment (unpublished work)

Proc. Indian Acad. Sci. (Chem. Sci.), Vol. 92, No. 1, January 1983, pp. 43–46.
© Printed in India.

X-ray photoelectron and Auger studies of $Ag_{2+\delta}S$ †

A K SHUKLA*, D D SARMA and G SANKAR
Solid State and Structural Chemistry Unit, Indian Institute of Science, Bangalore 560 012, India

MS received 21 October 1982

Abstract. The metal-insulator transition induced by changing the stoichiometry (δ) in $Ag_{2+\delta}S$ has been investigated employing x-ray photoelectron and Auger electron spectroscopies. Changes in the valence band structure in x-ray photoelectron are found to reflect the conductivity behaviour in these samples. The valence bands have been examined in a novel fashion by interatomic transitions in x-ray induced Auger spectra.

Keywords. X-ray photoelectron spectra; Auger electron spectra; silver sulfide; metal-insulator transition.

1. Introduction

Photoelectron spectroscopy has been found to be effective in studying metal-insulator transitions in transition metal oxides (Vasudevan *et al* 1978; Rao and Sarma 1982). It has been shown that the binding energies of the valence band peaks as well as the core levels shift as the temperature is changed through the transition temperature (Rao and Sarma 1982). Since UV photoelectron spectroscopy probes the valence band region with a high resolution, it has been possible to examine subtle changes in the shape of the band near the Fermi energy (E_F) across the transitions; HeI spectra of transition metal oxides such as V_2O_3 and VO_2 show a sharp cut-off in the photoemission intensity at the Fermi energy in the metallic phase (Rao and Sarma 1982; Beatham *et al* 1980).

Silver chalcogenides exhibit interesting metal-insulator transitions as a function of the stoichiometry (Shukla *et al* 1981; Shukla and Schmalzried 1979). Although detailed investigations of the transitions have been carried out using electrical and other measurements (Shukla *et al* 1981; Shukla and Schmalzried 1979; Vasan and Shukla 1981; Shukla *et al* 1982), no electron spectroscopic investigation of these systems has been reported todate. We therefore considered it useful to investigate the metal-insulator transition in the $Ag_{2+\delta}S$ system as a function of the stoichiometry, δ, employing x-ray photoelectron spectroscopy (XPS) as well as Auger electron spectroscopy.

2. Experimental

$Ag_{2+\delta}S$ was prepared by direct solid state reaction of pure silver powder (Johnson Matthey) and sulphur (Alpha Inorganic) *in vacuum* at 400° C. The specimens with

† Contribution No. 186 from the Solid State and Structural Chemistry Unit.
*To whom all correspondence should be made.

various stoichiometry (different δ values) were prepared by solid state coulometric technique (Shukla *et al* 1981). The cell used for this purpose can be denoted as Ag/AgI/$Ag_{2+\delta}S$/Pt. Two samples were prepared, one with $\delta = 0.007 \times 10^{-3}$ (nearly stoichiometric composition, referred to in the text as the sample with $\delta = \delta^\circ$) and the other with $\delta = 2 \times 10^{-3}$ (silver excess composition referred to in the text as the sample with $\delta = \delta^*$).

X-ray photoelectron and x-ray induced Auger spectra were recorded using an ESCA 3 Mark II spectrometer of V.G. Scientific Ltd., U.K. The spectrometer has been described elsewhere (Rao *et al* 1979). As this spectrometer is provided with twin anode, both AlKα(1486.6 eV) and MgKα (1253.6 eV) radiations were used for unambiguous assignments of XPS and AES. However, the spectra reported here are taken with MgKα, as it offers lower natural width of the excitation source, compared to AlKα.

The samples of $Ag_{2+\delta}S$ were freshly cleaned just before the sample introduction into the vacuum to minimize surface contamination. Ar^+ etching was entirely avoided as it reduces the sample surface.

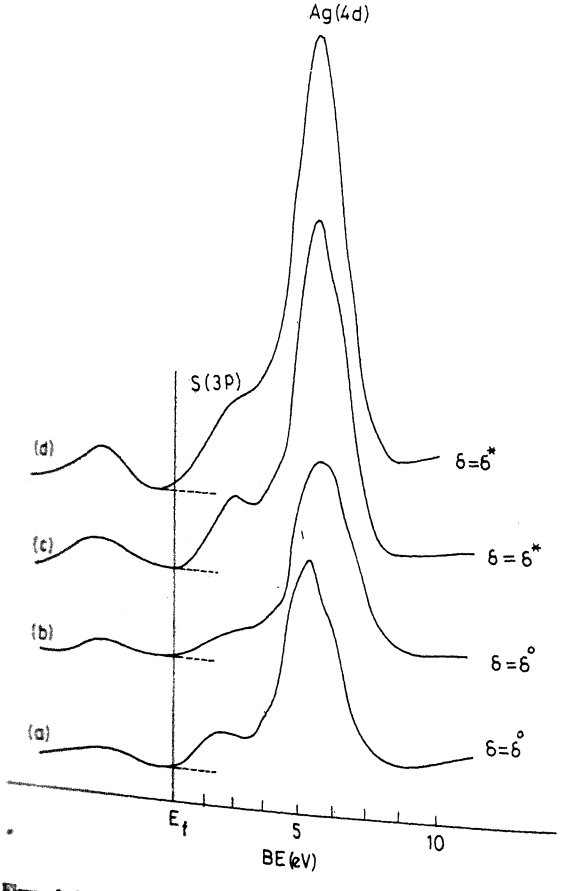

Figure 1. X-ray photoelectron spectra of the valence band in: (a) $Ag_{2+\delta}S$ ($\delta = \delta^\circ$) at 295 K; (b) $Ag_{2+\delta}S$ ($\delta = \delta^*$) at 473 K (c) $Ag_{2+\delta}S$ ($\delta = \delta^*$) at 295 K; and (d) $Ag_{2+\delta}S$ ($\delta = \delta^*$) at 473 K.

3. Results and discussion

XPS valence bands of the two samples of $Ag_{2+\delta}S$ (with $\delta = \delta^{\circ}$ and $\delta = \delta^{*}$) are shown in figure 1 at temperatures above and below the transition temperature (449 K). We see that the S(3*p*) derived band in the low-temperature α -phase of both the samples show a well-defined peak around 2 eV characteristic of a localized band. These peaks have no intensity at E_F indicating that the bands are localized well below the Fermi level in these insulating phases. This band becomes considerably broader in the high-temperature β -phase. The high-temperature phase with $\delta = \delta^{\circ}$, while showing considerable broadening of the S(3*p*) derived band, does not have any intensity at the Fermi energy, corroborating the semiconducting behaviour of this sample at high temperatures. However, the sample with $\delta = \delta^{*}$, not only shows a distinct broadening of the topmost occupied valence band, but also has finite intensity at E_F as should be expected due to its metallic behaviour.

No significant change is found in binding energies of core levels (in XPS) with composition and temperature. The silver core level spectra of these compounds show negative chemical shifts with respect to those of silver metal, as reported earlier by Romand *et al* (1978). This negative chemical shift varies between –0.2 and –0.4 eV depending on the stoichiometry and temperature.

X-ray induced Auger signals due to the Ag($M_{45}N_{45}N_{45}$)transition are seen in the 345–360 eV kinetic energy range (figure 2). Weak intensity features are seen at higher kinetic energies due to interatomic M_{45}(Ag)VV process where V represents a $S(3p)$ derived band. We see from figure 2 that the onset of this interatomic structure differs depending on the stoichiometry and temperature. The Auger energy of a MVV transition is given by,

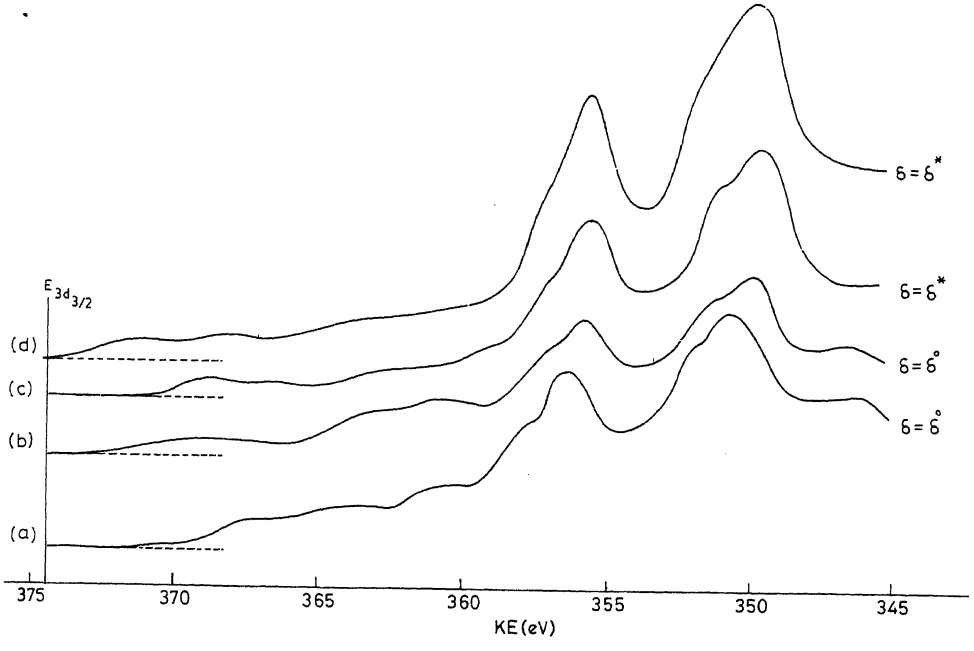

Figure 2. X-ray induced Auger electron spectra of the Ag($M_{45}N_{45}N_{45}$) region in: (a) $Ag_{2+\delta}S$ ($\delta = \delta^{\circ}$) at 295 K; (b) $Ag_{2+\delta}S$ ($\delta = \delta^{\circ}$) at 473 K; (c) $Ag_{2+\delta}S$ ($\delta = \delta^{*}$) at 295 K; and (d) $Ag_{2+\delta}S$ ($\delta = \delta^{*}$) at 473 K.

$$E_{MVV} = E_M - 2E_V - U_{\text{eff}} \tag{1}$$

where E_M and E_V are the binding energies of the corresponding levels and U_{eff} is a term arising out of hole-hole interaction (in the final state of the valence band) and various polarization effects. Thus, the highest energy $E^{\max}_{MVV}$ of MVV transition is achieved when the valence electron is at E_F ($E_V = 0$) and U_{eff} is equal to zero; in such a situation, $E^{\max}_{MVV}$ is equal to E_M. In this sense, E_M may be taken to be the counterpart of E_F in Auger transitions. We have therefore indicated the energy $E_{3d3/2}$ in figure 2.

Since the core level binding energies do not change in this system, E_M in equation (1) would remain unchanged. Figure 1 reveals that the mid-points of the $S(3p)$ derived bands in all the cases remain essentially constant. Broadening of this band at high temperatures is not likely to cause a drastic modification in the MVV transition, as the band gap in the insulating phase is small (<1 eV) (Shukla and Schmalzried 1979). Changes in E_{MVV} have therefore to be attributed to changes in U_{eff}. In such a situation, the occurrence of the onset of the interatomic structure at lower kinetic energies ($\sim$ 3.5 eV from the $3d_{3/2}$ energy) in the low temperature phases of both the samples (see figure 2) can be attributed to a considerably high U_{eff}. This indicates that in these cases, the $S(3p)$ derived band is a localized band forcing the two holes to be in close proximity. High temperature spectra of the sample with $\delta = \delta^{\circ}$ show the onset of the interatomic transition around 2 eV from $E_{3d3/2}$ indicating a considerably broader band; a finite U_{eff} would however still indicate a localized band in accordance with the semiconducting nature of the sample even at high temperatures. The high temperature spectrum of the sample with $\delta = \delta^*$, on the other hand, shows a rise in intensity at $E_{3d3/2}$ indicating that U_{eff} is nearly equal to zero in this case. This observation confirms the delocalized (metallic) behaviour of the $Ag_{2+\delta}S$ sample with $\delta = \delta^*$ at high temperature.

Acknowledgement

The authors express their gratitude to Professor C N R Rao for suggesting the problem and helpful discussion. Financial support from the Department of Science and Technology, Government of India is gratefully acknowledged.

References

Beatham N, Fragala I L, Orchard A F and Thornton G 1980 *J. Chem. Soc. Faraday Trans.* II **76** 929
Rao C N R, Sarma D D, Vasudevan S and Hegde M S 1979 *Proc. R. Soc. (London)* **A367** 239
Rao C N R and Sarma D D 1982 *J. Solid State Chem.* **45** 14
Romand M, Roubin M and Deloume J P 1978 *J. Electron Spectrosc. Rel. Phenom.* **13** 229
Shukla A K and Schmalzried H 1979 *Z. Phys. Chem. Neue Folge* **118** 59
Shukla A K, Sen P and Sarma D D 1982 *Ber. Bunsenges. Phys. Chem.* **86** 198
Shukla A K, Vasan H N and Rao C N R 1981 *Proc. R. Soc. (London)* **A376** 619
Vasan H N and Shukla A K 1981 *Bull. Mater. Sci.* **3** 399
Vasudevan S, Hegde M S and Rao C N R 1978 *Solid State Commun.* **27** 131

Proc. Indian Acad. Sci. (Chem. Sci.), Vol. 92, No. 1, January 1983, pp. 47–58.
© Printed in India.

Effect of ring aza substitution on the luminescence of aromatic ketones. Luminescence of isomeric acetylpyridines

S K SARKAR, S K GHOSHAL and G S KASTHA*
Optics Department, Indian Association for the Cultivation of Science, Jadavpur, Calcutta 700 032, India

MS received 3 September 1982

Abstract. The absorption and luminescence characteristics of 2-, 3- and 4-acetyl-pyridines (ACP) and acetophenone have been examined in polar and nonpolar media at room temperature and low temperature (77 K). All the ACP exhibit intense and structured phosphorescence emission of $n\pi^*$ character. Though the triplet yields of these ketones are very high, the phosphorescence quantum yield and lifetime of ACP decrease significantly in the order 4-ACP > 3-ACP > 2-ACP > acetophenone. The distinctive differences in the spectral properties and the luminescence characteristics of ACP from their phenyl analogue have been interpreted in terms of the perturbing influences of the inductive effect of the pyridinic nitrogen, the vibronic interaction between the $n\pi^*$ and $\pi\pi^*$ states and the photochemical reaction occurring from the lowest triplet state.

Keywords. Isomeric acetylpyridines; absorption; emission; inductive effect; vibronic interaction; photochemical reaction; luminescence.

1. Introduction

The luminescence properties of many aromatic carbonyl compounds *viz* benzaldehyde, acetophenone, benzophenone and their derivatives have been extensively studied (Shimada and Goodman 1965; Takemura and Baba 1969; Olmsted and El-Sayed 1971; Cheng and Hirota 1974; Ghoshal *et al* 1981). Unlike their hydrocarbon counterparts the photophysical behaviours of this system are primarily determined by the relative energy positions of $n\pi^*$ and $\pi\pi^*$ states and the interaction between them in the singlet and triplet manifolds. It is also known that the radiative and nonradiative properties of aromatic molecules are markedly altered when a N-hetero atom is introduced in the phenyl ring of these molecules (Hotchandani and Testa 1973; Babiak and Testa 1976; Hotchandani and Testa 1977; Sarkar *et al* 1982a) because of the presence of additional $n\pi^*$ states arising from the non-bonding electrons of nitrogen atom in the singlet and triplet manifolds of the parent molecules. It is therefore surprising that except for a preliminary study on the location of the lowest triplet states (Arnold 1968), no attention has been given to a systematic study of the luminescence of the simple N-heterocyclic carbonyls. Moreover, though it is known that in suitable media many of the carbonyl compounds undergo photochemical reaction in their lowest $n\pi^*$ triplet states (Yang *et al* 1967; Arnold 1968; Turro 1978) no such investigation appears to have been made with their N-heterocyclic counterparts. The object of the present work is to study how the photophysical properties of the parent carbonyl molecules are modified with the introduction of a nitrogen atom in

*To whom all correspondence should be made.

the phenyl nucleus of these molecules. With this in view, the absorption and luminescence characteristics of three isomeric pyridylketones (or acetylpyridines) in the vapour phase and in polar as well as nonpolar solvents at room temperature and low temperature (77 K) have been studied and compared with those of acetophenone reported earlier (Ghoshal *et al* 1981).

2. Experimental

2.1 *Materials*

All the isomeric acetylpyridines procured from Schuchardt, Munchen (Germany) were subjected to repeated fractional distillation under reduced pressure till no impurity could be detected with a flame ionization detector column (Hewlett-Packard, Model 5730A). Spectrograde solvents were further purified by fractional distillation. Freshly prepared and deoxygenated solutions of concentrations 10^{-4} 10^{-5} M were used for recording all the spectra except for $T \leftarrow S_0$ absorption where solutions of higher concentration (*ca* 10^{-3} M) were employed.

2.2 *Spectroscopic measurements*

The solution and vapour phase absorption spectra at room temperature (300 K) were recorded with a Shimadzu 210A UV-VIS absorption spectrophotometer. Low temperature (77 K) emission, excitation and polarization spectra were obtained with a Perkin-Elmer model MPF 44A fluorescence spectrophotometer. The phosphorescence lifetimes were determined by using a Molectron UV-1000 N_2-Laser as the excitation source (337 nm) in conjunction with an EC storage oscilloscope. The energy in the laser beam was 3 mJ with a pulse duration of 5 nsec and a repetition frequency of 5/sec.

The triplet yields (Φ_T) of these acetylpyridines in methylcyclohexane were estimated following the method described by Favaro (1973). Assuming unitary triplet yield for benzophenone, the Φ_T values of the isomeric acetylpyridines were determined by their efficiency in sensitizing biacetyl phosphorescence.

3. Results

3.1 *Absorption spectra and phosphorescence excitation spectra*

Like acetophenone each of the three isomeric acetylpyridines (ACP) shows two systems of singlet $\pi\pi^*$ absorption bands corresponding to $^1L_a \leftarrow S_0$ and $^1L_b \leftarrow S_0$ transitions in the spectral region 200–300 nm in the vapour phase and in ethanol and *n*-hexane solutions at room temperature (figures 1 and 2). The phosphorescence excitation spectra of these compounds in *n*-hexane at 77 K reproduced in figure 3 also clearly display these two bands with their associated vibronic structures. A comparison of the absorption and excitation spectra of the acetylpyridine molecules with those of acetophenone reveals that: (i) While the ^1L_b bands of acetophenone are sharp and structured, the corresponding bands in the ACP are broad and structureless. (ii) The band origins of this system in 2- and 3-ACP are located at frequencies higher than that of acetophenone and their intensities are significantly larger while in the 4-isomer the 0,0 band is shifted towards lower frequencies by a small amount. (iii) The ^1L_a bands of all the ACP molecules, on the other hand, appear with markedly reduced intensity and are considerably blue shifted with respect to acetophenone. This shift is largest in the 4-isomer.

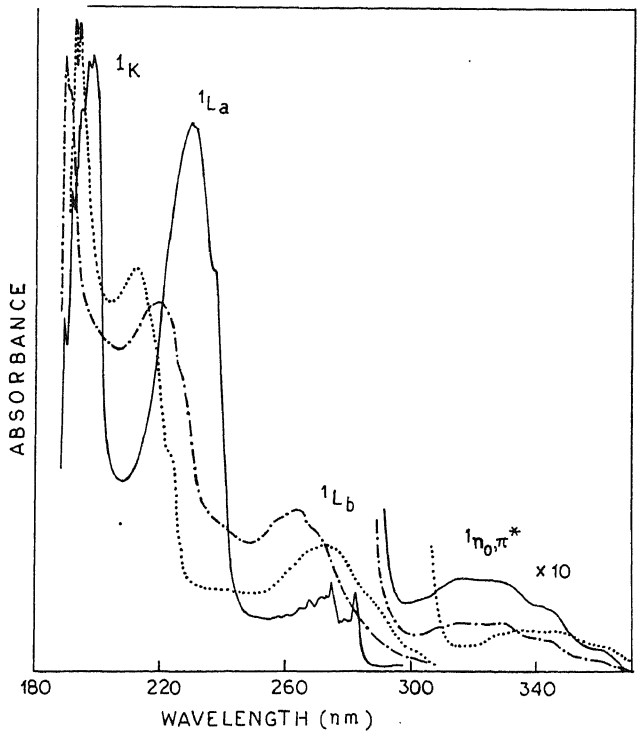

Figure 1. Vapour phase absorption spectra of acetophenone (_____), 2-ACP (—.—) and 4-ACP (.....) at 330 K and 0.1 torr. $^1n_O,\pi^*$ corresponds to singlet-singlet π^*–n transition due to n electrons on carbonyl oxygen atom.

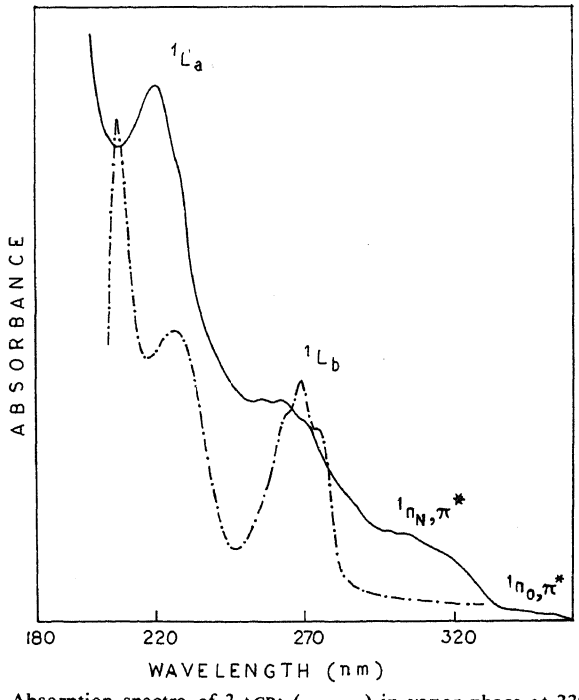

Figure 2. Absorption spectra of 3-ACP: (_____) in vapor phase at 330 K and 0.1 torr; (—.—) in 1% HCl at 300K. ^1n_N, π^* and $^1n_O,\pi^*$ correspond to singlet-singlet π^*—n transitions due to n electrons on the pyridinic nitrogen and carbonyl oxygen atom, respectively.

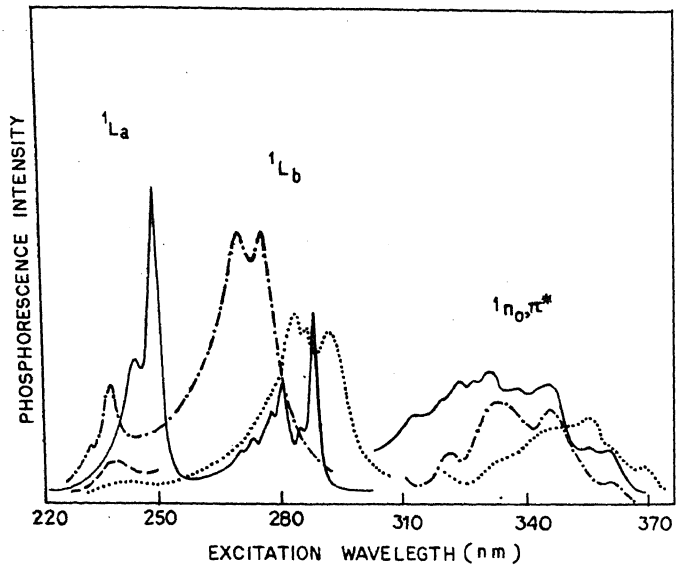

Figure 3. Phosphorescence excitation spectra of acetophenone (_____), 2-ACP (—.—) and 4-ACP (....) in *n*-hexane at 77 K. Only a part of the spectrum corresponding to 3-ACP (---) is shown in the figure for the sake of clarity of the diagram. $^1n_0,\pi^*$ corresponds to singlet-singlet π^*—n transition due to n electrons on carbonyl oxygen atom.

Besides these distinctive features of the $\pi\pi^*$ bands, the absorption spectrum of each of the ACP exhibits weak band system in the spectral region 300–370 nm as in acetophenone (figure 1). They are also evident from the excitation spectra (figure 3). By analogy these bands are attributed to transitions involving the *n*-electrons on the oxygen atom of the carbonyl group and have been designated as $^1n_0\pi^*$ bands. Comparison of the vapour phase absorption spectra of the ACP molecules with that of acetophenone (figure 1) reveals that there exists another region of absorption between the ^1L_b and $^1n_0\pi^*$ band systems. Though these bands are not clearly separated because of the overlapping by the tail of the much stronger ^1L_b bands, their occurrence can reasonably be inferred from the fact that in the same spectral region such absorption bands appear distinctly in the case of pyridylaldehydes which have also been studied in this laboratory. The relevant spectral data are shown in table 1.

In strongly hydrogen bonding and acidic media (*e.g.* 1% HCl in ethanol) both the weak absorption bands at the tail part of ^1L_b bands and the more distinct $^1n_0\pi^*$ bands disappear completely as is seen from the spectra of 3-ACP (figure 2). It is also observed that in the absorption spectrum of acidic solution the ^1L_b bands appear with more resolved vibronic structure presumably because of the disappearance of the overlapping $n\pi^*$ bands. This observation is similar to that reported in the case of pyridine and some of its derivatives (Sarkar *et al* 1982a). By comparison the weak absorption region has been associated with the singlet–singlet π^*–n transition due to the excitation of *n*-electrons on the pyridinic nitrogen atom and is henceforth referred to as $^1n_N\pi^*$ band to distinguish them from the $^1n_0\pi^*$ band. Unfortunately the $^1n_N\pi^*$ bands could not be detected in the phosphorescence excitation spectra of the acetylpyridine molecules.

In addition to the bands arising from the singlet–singlet transitions described above, the solution phase absorption spectra of all the isomeric acetylpyridines display weak

Table 1. Observed singlet $\pi\pi^*$ and $n_0\pi^*$ energy levels of acetophenone and acetylpyridines (ACP) and $^1n_N\pi^*$ energy levels of pyridinealdehydes (PAD) from room temperature absorption and 77 K phosphorescence excitation spectra.

Molecules	^1L_a ($\pi\pi^*$) ν_{00} in cm^{-1}			^1L_b ($\pi\pi^*$) ν_{00} in cm^{-1}			$^1n_0\pi^*$ ν_{00} in cm^{-1}			$^1n_N\pi^*$ ν_{00} in cm^{-1}		
	Vapour	EtOH	*n*-hexane	Vapour	EtOH	*n*-hexane	Vapour	EtOH	*n*-hexane	Molecules	Vapour	*n*-hexane
Aceto-phenone[c]	42997	41395 (39749)	42092 (39892)	35387	34712 (34532)	34954 (34675)	27886	31736 (28240)	27692 (27776)			
2-ACP	45647	43654 (42003)	44234 (42058)	36885	36286 (36051)	36485 (36194)	27769	31075 (27548)	27886 (27464)	2-PAD	33547	33888 (33774)
3-ACP	45337	43846 (41481)	44039 (41500)	36889	36415 (36345)	36485 (36352)	27784	31873 (27700)	27900 (27624)	3-PAD	33103	33323 (32885)
4-ACP	47154	45143	45234	34591	34109 (34160)	34203 (34178)	27720	— (27322)	27880 (27166)	4-PAD	—	32885 (32777)

[a] Figures in paranthesis indicate the positions of the band origins of the respective transitions as determined from phosphorescence excitation spectra at 77 K

[b] Studied in the present investigation.

[c] From Ghoshal *et al* 1981.

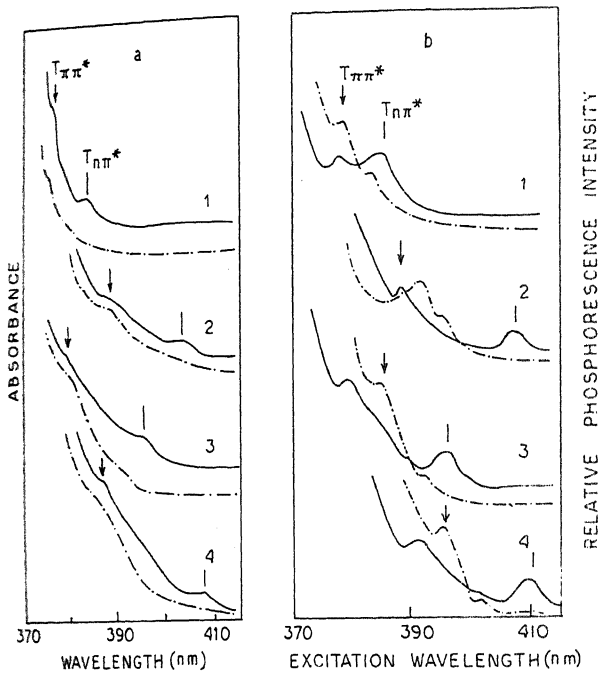

Figure 4. Singlet-triplet absorption and phosphorescence excitation spectra of acetophenone (1), 2-ACP (2), 3-ACP (3) and 4-ACP (4) in *n*-hexane (_____) and ethanol (- . -). **a.** Absorption at 300 K. **b.** Excitation at 77 K.

Table 2. Observed triplet $\pi\pi^*$ and $n_0\pi^*$ energy levels of acetophenone and acetylpyridines (ACP) from room temperature absorption and 77 K phosphorescence excitation and emission spectra[a]

	Absorption				Phosphorescence			
	$^3\pi\pi^*$	ν_{00} in cm^{-1}	$^3n_0\pi^*$	ν_{00} in cm^{-1}	$^3n_0\pi^*$	ν_{00} in cm^{-1} 77 K	$\Delta E(^3\pi\pi^* - ^3n_0\pi^*)$[c] in cm (77 K)	
Molecules	EtOH	*n*-hexane	EtOH	*n*-hexane	EtOH	*n*-hexane	EtOH	*n*-hexane
Aceto-phenone[b]	26510 (26377)	26517 (26383)	— (26034)	26000 (25933)	26007	25819	360	507
2-ACP	25600 (25470)	25666 (25568)	— (25213)	24745 (24502)	24899	24538	414	1048
3-ACP	26308 (25966)	26329 (26200)	— (25438)	25245 (25181)	25633	24899	430	1160
4-ACP	25765 (25245)	25799 (25568)	— (24868)	24502 (24383)	24654	24235	484	1259

[a] Figures in paranthesis indicate the positions of band origins of the respective transitions as determined from phosphorescence excitation spectra at 77 K.
[b] From Ghoshal *et al* 1981.
[c] Indicates average of the values of $^3n_0\pi^*$ energy positions obtained from the position of band origins in the phosphorescence excitation and emission spectra.

bands in the spectral region 370–410 nm. Inspection of the spectra (figure 4a) reveals, that as in acetophenone, each of the ACP exhibits a weak but distinct band and a barely resolved band to the higher energy side of the former. These bands are more distinctly observed in the excitation spectra shown in figure 4b. In analogy with acetophenone (Ghoshal *et al* 1981) and on the basis of the spectral positions and solvatochromic effects the lower and higher energy bands are assigned to triplet singlet π^*–n_0 and π^*–π transitions respectively. In neither of the room temperature absorption nor 77 K phosphorescence excitation spectra could the bands due to $^3n_N\pi^* \leftarrow S_0$ transition be detected. However, their approximate energy positions have been inferred in the following way.

We have already shown that the energy positions of $^1n_N\pi^*$ states should be similar to that in 2-, 3- and 4- pyridinealdehydes, at least in hydrocarbon solvents at 77 K. Further, the singlet-triplet separations in some substituted pyridines is *ca* 2000 cm^{-1}. In cyanopyridines the position of $^3n_N\pi^*$ state is at about 28,000 cm^{-1} (Sarkar *et al* 1982a) and in 4-aminopyridine it is located at *ca* 29000 cm^{-1} (Sarkar *et al* 1982b). So the $^3n_N\pi^*$ state in the ACP is expected to lie between 31000-30000 cm^{-1} which is at least 3000 cm^{-1} above the respective $^3\pi\pi^*$ level in these substituted pyridine molecules. In ethanol solvents the $^3n_N\pi^*$ states will be shifted to higher energy region. Table 2 shows all the relevant experimental data.

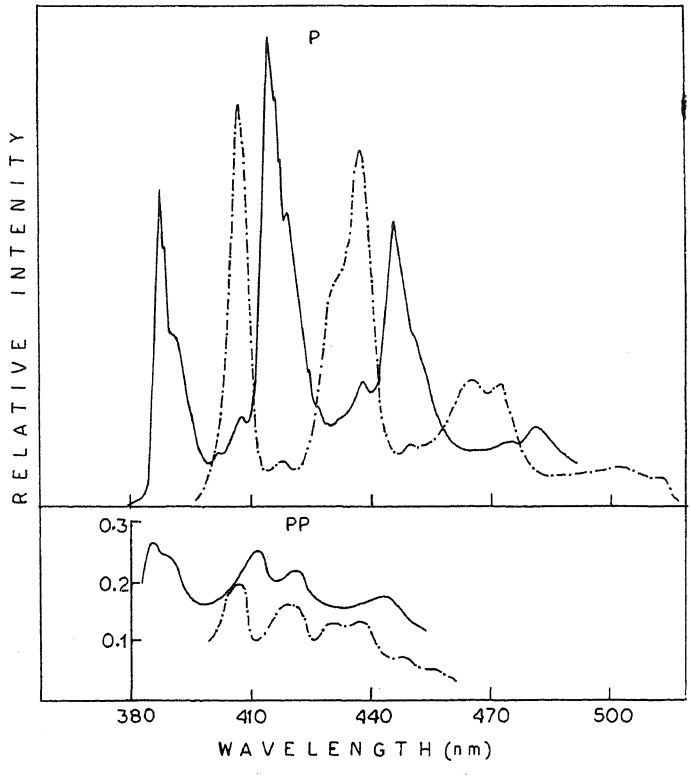

Figure 5. Phosphorescence (P) and phosphorescence polarization (PP) spectra of acetophenone (_____) and 2-ACP (—.—) in 3-methylpentane glass at 77 K.

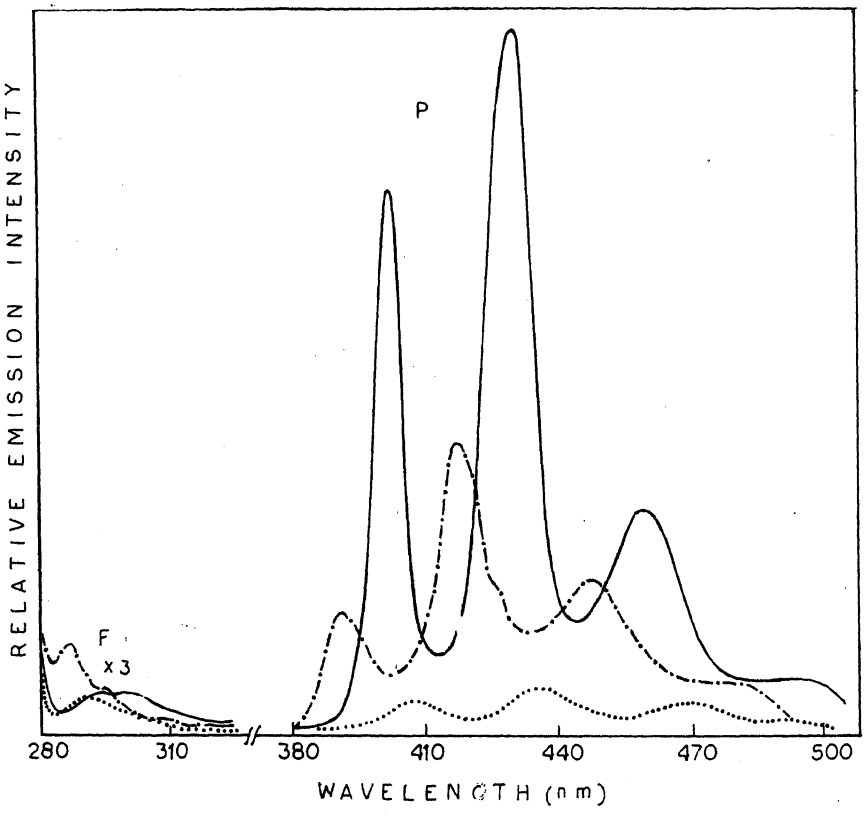

Figure 6. Fluorescence (F) and Phosphorescence (P) spectra of 2-ACP (_____), 3-ACP (—.—) and 4-ACP (.....) in ethanol glass at 77 K.

3.2 *Luminescence spectra*

All the isomeric acetylpyridines exhibit fairly strong ketone like phosphorescence in rigid nonpolar and moderately polar glassy solvents at 77 K. Moreover, all of them are nonfluorescent in hydrocarbon solvent but emit a very weak fluorescence in protic media at low temperature. Despite close resemblance in the appearance of the phosphorescence spectra of the pyridylketones and acetophenone, several distinguishing features are revealed from careful examination of the spectra presented in figures 5 and 6.

(i) In contrast to the moderately sharp and structured phosphorescence spectrum of acetophenone, the spectra of ACP are markedly broader and less structured. Also, these spectra are considerably red-shifted relative to acetophenone.

(ii) The phosphorescence spectra of all the ACP exhibit a vibrational progression of carbonyl stretching frequency which is found to be reduced significantly in comparison with that of acetophenone.

(iii) The phosphorescence intensity is observed to decrease in the order acetophenone >2-ACP>3-ACP>4-ACP (figure 6).

As in acetophenone, the degree of phosphorescence polarization (P) for all the isomeric ACP in 3-methylpentane glass at 77 K is positive with respect to $^1L_a \leftarrow S_0$ excitation and this indicates a predominantly in-plane polarization of the phosphores-

Table 3. Measured phosphorescence yield (Φ_p) and lifetime (τ_p), triplet yield (Φ_T) and carbonyl stretching frequency ($\nu_{C=O}$) in the phosphorescence emission spectra of acetophenone and acetylpyridines (ACP) at 77 K

Molecules	τ_p(ms)		Φ_p		Φ_T	$\nu_{(C=O)}$in cm^{-1}	
	EtOH	Methylcyclo-hexane	EtOH	Methylcyclo-hexane	Methylcyclo-hexane	EtOH	Methylcyclo-hexane
Acetophenone[a]	5.0	2.5	0.6	0.65	0.90	1666	1710
2-ACP	0.9	0.8	0.3	0.42	0.90	1657	1698
3-ACP	0.7	0.6	0.16	0.24	0.85	1631	1666
4-ACP	0.4	0.3	0.04	0.06	0.80	1605	1617

From Ghoshal *et al* (1981)

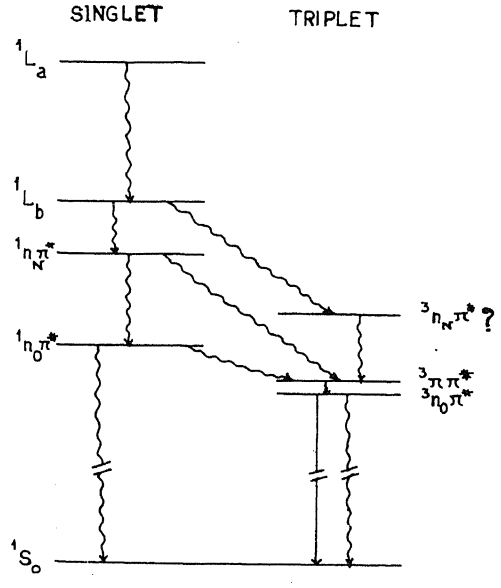

Figure 7. Schematic energy level diagram and probable radiative and nonradiative processes of acetylpyridines. Radiative and nonradiative transitions are shown by the vertical solid line and wavy curves respectively.

cence emission from these compounds. Further, the (P) value outside the band origin shows significant alteration (figure 5), which is attributable to the occurrence of a nontotally symmetric out-of-plane vibronic activity arising from vibronic interaction between the closely spaced triplet states in these molecules.

It is also observed that the decay nature of the phosphorescence emissions from all the pyridyl ketones are almost nonexponential even in protic media in contrast to the markedly exponential nature observed in the case of acetophenone in such media (Ghoshal *et al* 1981). Further, the phosphorescence lifetimes (τ_p) of all the ACP are significantly shorter than that of acetophenone, the τ_p values are found to decrease in the order acetophenone > 2-ACP > 3-ACP > 4-ACP, which is parallel to the change in Φ_p-values. Incidentally, the triplet yields (Φ_T) of acetophenone and acetylpyridines in methylcyclohexane glass at 77 K (determined by the usual method) do not show large

variations. The luminescence data for all the ketones are presented in table 3.

The short phosphorescence lifetime, significant blue shifts of the phosphorescence bands in protic media, the vibrational structure and the predominantly in-plane polarization of the phosphorescence emission strongly suggest that the lowest triplet state in each of the pyridylketones is $n_0\pi^*$ in nature. The approximate energy level scheme and the various probable radiative and nonradiative processes may be sketched as in figure 7.

4. Discussion

The distinctive differences in the spectral properties of acetylpyridines and acetophenone and the observed trends in the luminescence characteristics among the isomers clearly point to the influence of the pyridinic nitrogen atom. Moreover, these perturbations are found to vary from one isomer to the other depending on the relative positions of the acetyl group and the pyridinic nitrogen atom.

4.1 *Inductive effect*

It is known that an electron withdrawing substituent stabilizes the $n\pi^*$ states of the carbonyls. If the pyridinic nitrogen atom is considered to be an electron withdrawing substituent, the energy positions of the singlet and triplet $n_0\pi^*$ states of the acetylpyridines will be lowered with respect to those of acetophenone. The observed bathochromic shifts (tables 1 and 2) are found to be consistent with that expected from the inductive effect of the pyridinic nitrogen atom. Moreover, the red shifts suffered by either the band origin of $^1n_0\pi^* \leftarrow S_0$ or $^3n_0\pi^* \leftarrow S_0$ transitions of the isomeric acetylpyridines are different for the different isomers.

4.2 *Vibronic interaction*

Pyridinic nitrogen atom manifests its influence somewhat indirectly. It is seen from table 1 that $^1L_b(\pi\pi^*)$ state in the ACP are fairly close to the inferred position of the $^1n_N\pi^*$ state in each of the molecules. It is known that such proximity of energy states of the same multiplicity gives rise to vibronic interactions between the two states and its magnitude depends on their energy separation. The noticeable broadening of the ^1L_b bands observed in the absorption spectra (figure 1) and in the excitation spectra (figure 3) of the ACP relative to that of acetophenone is a clear indication of the occurrence of such vibronic interactions. This observation thereby points to the perturbation caused by the pyridinic N atom.

4.3 *Conjugative effect*

The conjugation effect of the strongly electron accepting acyl group leads to a large stabilization of the ^1L_a and $^3L_a(\pi\pi^*)$ states of benzene. As a result the energy positions of these bands in acetophenone are lowered by *ca* 7130 and 2790 cm^{-1} respectively relative to the corresponding bands of benzene. In the ACP one of the CH groups has been replaced by the strongly electronegative nitrogen atom and this renders the migration of electrons towards the carbonyl group difficult. The aza substitution tends to counteract the effect of conjugation due to the acyl group, which leads to some destabilization of the $\pi\pi^*$ states of ACP relative to acetophenone. The large hypsochromic shifts of the ^1L_a bands of the ACP with respect to that in acetophenone support this view (table 1).

The most interesting aspects of the effect of the pyridinic nitrogen atom are observed through the variations in phosphorescence quantum yields (Φ_p) and phosphorescence lifetime (τ_p) among the ACP isomers in comparison with those of acetophenone in ethanol glass and hydrocarbon matrices at 77 K. It is seen from table 3 that the efficiency of triplet formation (Φ_T) measured in methylcyclohexane (MCH) glass at 77 K is almost unity but this also shows a slowly decreasing tendency in the order acetophenone > 2-ACP > 3-ACP > 4-ACP. This implies that a very small part ($1-\Phi_T$) of the primary excitation is lost through $S_1 \rightsquigarrow S_0$ nonradiative process in these pyridyl ketones. Indeed, we have observed that there is some vibronic interaction between the $^1\pi\pi^*$ (^1L_b) and $^1n_N\pi^*$ states of these ketones which favours nonradiative process. Our data also indicate that such interaction is greatest in the 4-isomer.

The large Φ_T-values in these aromatic ketones suggest that most of the primary excitation is transferred to the lowest triplet $n_0\pi^*$ state through the various internal conversion and inter-system crossing mechanisms. On the other hand, the gradually decreasing values of Φ_p in these molecules show that a large part of this triplet excitation is lost through various deactivation processes. This is reflected in the large reduction of the observed phosphorescence lifetimes of the pyridyl ketones as compared to acetophenone. Of the various deactivation mechanisms the two probable nonradiative processes, (i) vibronic interactions and (ii) possibility of photochemical reaction in the triplet $n_0\pi^*$ state, are considered to be important.

From the 'proximity effect' on radiationless transition (Wassam and Lim 1978) it is known that distortion of the potential surface of the lowest emitting triplet state due to vibronic interaction with a close lying upper triplet level favours nonradiative transitions. The magnitude of the interaction depends on the proximity of the two interacting states and as a result of vibronic mixing the lower state acquires some of the characteristics of the upper state. A perusal of the data given in table 2 shows that in each of the pyridyl ketones the energy separation between the $^3\pi\pi^*$ and $^3n_0\pi^*$ states in hydrocarbon matrices is more than twice as large as in ethanol glass while the observed phosphorescence lifetime (τ_T) in the former is slightly smaller than in the latter. This is in contrast to what is obtained with acetophenone where the value of τ_p in methylcyclohexane is only half the value in ethanol glass though the energy separation in the former is *ca* 1.5 times more than in the latter. The large energy separation between the two interacting $^3\pi\pi^*$ and $^3n_0\pi^*$ states of the acetylpyridines in *n*-hexane would lead to very little vibronic interaction and therefore to little mixing of the two states. As a result the $^3n_0\pi^*$ state would be expected to retain its pure $n_0\pi^*$ character and the lifetime would be appropriate for this state. Hence the vibronic interaction may not be mainly responsible for the decrease in the τ_p values of the acetyl pyridines, particularly for the 3- and 4- isomers.

It is seen from table 3 that both the Φ_T and τ_p values of acetophenone are considerably reduced with the introduction of a N-atom in the phenyl ring of the aromatic ketone and this reduction becomes more and more pronounced as one moves from 2-ACP to 4-ACP. It is quite reasonable that the observed decrease in the Φ_p and τ_p values is due to the effect of the pyridinic N-atom. The possibilities by which the N-atom may produce the observed modifications mainly arise from the vibronic interactions between the $^3n_N\pi^*$ state and the lowest energy $^3n_0\pi^*$ state and/or from photochemical reactions occurring in the $^3n_0\pi^*$ state. We have already seen that the $^3n_N\pi^*$ states are at least 3000 cm^{-1} above the $^3\pi\pi^*$ states in the pyridylketones and therefore, are less likely to produce the large decrease in τ_p-values by enhancing the nonradiative rate through vibronic interaction.

The possibility of photochemical reactions in the triplet $n_0\pi^*$ state is now considered to account for the large reductions in the Φ_p-and τ_p-values of the 3- and 4-acetylpyridines. During the measurement of phosphorescence lifetimes of the ketones in ethanol and methylcyclohexane rigid matrices at 77 K by the method described under experimental section, it was observed that in the case of acetophenone and 2-acetylpyridine neither the maximum of the phosphorescence signal nor its decay nature is altered to any appreciable extent during successive excitation flashes. In the case of 3-acetylpyridine, on the other hand, there was a measurable reduction in the maximum of phosphorescence signal after five successive flashes. With the 4-acetyl pyridine this reduction was so large that during the second pulse the phosphorescence signal maximum was reduced to about one-half of the value observed with the first pulse and in the third pulse, the phosphorescence signal was barely detectable. In view of the known fact that in suitable solvents (*viz.* isopropyl alcohol) acetophenone photoreacts in the $^3n_0\pi^*$ state with the formation of pinacol (Arnold 1968; Turro 1978) the above observations may be rationalized by postulating that a part of the molecules excited to the $^3n_0\pi^*$ state of 3- and 4-ACP's is removed by photochemical reactions between the excited pyridyl ketone molecules and the solvent in which they are dispersed. The photoreaction rate in 3-ACP is larger than that in acetophenone and 2-acetylpyridine while in the 4-isomer the rate is the largest. The observed phosphorescence lifetime which is the reciprocal of the combined radiative, nonradiative and photochemical reaction rates would therefore decrease in the order 2-ACP>3-ACP> 4-ACP among the pyridylketones as has been experimentally determined. This incidentally, would also account for the observed decrease of the experimental Φ_p-values of the pyridylketones and the order of their decrement. Though, it has not been possible to obtain quantitative values of the reaction rates from these observations, it seems probable that in the 3- and 4-ACP, the photoreaction rate constant would be comparable with the phosphorescence rate constant.

References

Arnold D R 1968 *Adv. Photochem.* **6** 301
Babiak S and Testa A C 1976 *J. Phys. Chem.* **80** 1882
Cheng T H and Hirota N 1974 *Mol. Phys.* **27** 281
Favaro G 1973 *Chem. Phys. Lett.* **21** 401
Ghoshal S K, Sarkar S K and Kastha G S 1981 *Bull. Chem. Soc. Jpn.* **54** 3536
Hotchandani S and Testa A C 1973 *J. Chem. Phys.* **59** 596
Hotchandani S and Testa A C 1977 *J. Chem. Phys.* **67** 5201
Olmsted J and El-Sayed M A 1971 *J. Mol. Spectrosc.* **40** 71
Sarkar S K, Ghoshal S K and Kastha G S 1982a *J. Chem. Phys.* **76** 825
Sarkar S K, Ghoshal S K and Kastha G S 1982b *Can. J. Chem.* (communicated)
Shimada R and Goodman L 1965 *J. Chem. Phys.* **43** 2027
Takemura T and Baba H 1969 *Bull. Chem. Soc. Jpn.* **42** 2756
Turro N J 1978 *Modern molecular photochemistry* (New York: Benjamin)
Wassam W A and Lim E C 1978 *J. Mol. Struct.* **47** 129
Yang N C, McClure D S, Murov S L, Houser J J and Dusenbery 1967 *J. Am. Chem. Soc.* **89** 5466

Proc. Indian Acad. Sci. (Chem. Sci.), Vol. 92, No. 1, January 1983, pp. 59–64.
© Printed in India.

Infrared spectral evidence for mono-, bi- and tetra-dentate behaviour of hexamethylenetetramine

I S AHUJA*, RAGHUVIR SINGH and C L YADAVA
Chemistry Department, Banaras Hindu University, Varanasi 221 005, India

MS received 24 June 1982; revised 2 December 1982

Abstract. Infrared spectral features to distinguish the different modes of hexamethylenetetramine in metal complexes have been presented. The tentative mode of metal-hexamethylenetetramine bonding has been arrived at from the pattern of the two ν_{CN} bands at 1225 and 1000 cm^{-1}. It is shown that in complexes with terminal monodentate, bidentate and tetradentate the bands show differing behaviour. Except for the splitting of ν_{CN} bands the IR spectra are superimposable on that of the uncoordinated molecule supporting the theory that chair configuration of the uncoordinated hexamethylenetetramine is retained in all the complexes.

Keywords. Infrared spectra; hexamethylenetetramine; monodentate; bidentate; tetradentate.

1. Introduction

Hexamethylenetetramine (HMTA), a potentially tetradentate ligand, has until recently been known to act only as bidentate ligand bridging between two metal ions (Negita *et al* 1965). A number of complexes of metal salts have been prepared with this ligand (Ahuja *et al* 1979, 1980, 1981a,b; 1982) and in this paper the IR spectral features to distinguish the different modes of metal HMTA bondings are reported.

2. Experimental, results and discussion

The complexes studied are listed in table 1.

HMTA is a heterocyclic system with three fused rings in the chair configuration and four bridge-head nitrogen atoms. The chemical and steric equivalence of the four nitrogen atoms (donor sites) has been demonstrated by various physicochemical methods (Andersen 1957). It is considered to act as a mono-, bi-, tri- or tetra-dentate ligand. Framework molecular models suggest that the lone pair of electrons on each of the four nitrogen atoms point outwards and the simultaneous coordination of more than one site to the same metal ion is ruled out. It can, however, act as a bidentate-bridging ligand resulting in polymeric structures or that all the bonding sites may coordinate simultaneously to four metal ions resulting in tetranuclear structures.

The 1300–200 cm^{-1} region IR spectrum of uncoordinated HMTA (nujol mull) shows absorption bands at 1225s, 1180w, 1040m, 1000s, 813w, 803s, 714w, 664s, 610m and 508s cm^{-1}. Of these the two strong bands at 1225 and 1000 cm^{-1} are assigned to the fundamentals of the CN stretching modes (Mecke and Spiescke 1955). Negita *et al* (1965) pointed out that both these ν_{CN} bands are split into two well-defined and well-separated bands in complexes in which the HMTA was considered as bidentate-

*To whom all correspondence should be made

Table 1. Hexamethylenetetramine complexes with metal salts.

Complex	Tentative stereochemistry	Mode of Metal–HMTA bonding
$UO_2(HMTA)_2SO_4$	Polymeric 8-coordinate	BB
$UO_2(HMTA)(NO_3)_2$	Polymeric 8-coordinate	BB
$UO_2(HMTA)(NCS)_2$	Polymeric 8-coordinate	BB
$Hg(HMTA)CL_2$	Polymeric tetrahedral	BB
$Hg(HMTA)Br_2$	Polymeric tetrahedral	BB
$Hg(HMTA)(CN)_2$	Polymeric tetrahedral	BB
$Hg_4(HMTA)(NCS)_8$	Monomeric tetranuclear three-coordinate	T
$Co(HMTA)(NO_3)_2$	Polymeric octahedral	BB
$Ni(HMTA)(NO_3)_2$	Polymeric octahedral	BB
$Cu(HMTA)_2(NO_3)_2$	Polymeric octahedral	BB
$Zn(HMTA)(NO_3)_2$	Polymeric tetrahedral	BB
$Ag(HMTA)(NO_3)$	Polymeric two-coordinate	BB
$Cd(HMTA)_2(NO_3)_2$	Polymeric octahedral	BB
$Mn(HMTA)_2(NCS)_2(EtOH)_2$	Monomeric octahedral	TM
$Mn(HMTA)_2(NCS)_2$	Polymeric octahedral	BB
$Co(HMTA)_2(NCS)_2(EtOH)_2$	Monomeric octahedral	TM
$Co(HMTA)_2(NCS)_2$	Monomeric tetrahedral	TM
$Ni(HMTA)_2(NCS)_2(EtOH)_2$	Monomeric octahedral	TM
$Ni(HMTA)_2(NCS)_2$	Polymeric octahedral	BB
$Cu(HMTA)_2(NCS)_2$	Polymeric octahedral	BB
$Zn(HMTA)_2(NCS)_2$	Polymeric octahedral	BB
$Cd(HMTA)(NCS)_2$	Polymeric tetrahedral	BB
$Ni(HMTA)_2(OAc)_2$	Monomeric octahedral	TM
$Zn(HMTA)_2(OAc)_2$	Monomeric tetrahedral	TM
$Mn(HMTA)\ SO_4$	Polymeric octahedral	BB
$Co(HMTA)SO_4$	Polymeric octahedral	BB
$Ni(HMTA)SO_4$	Polymeric octahedral	BB
$Zn(HMTA)SO_4$	Polymeric octahedral	BB
$Cd(HMTA)SO_4$	Polymeric octahedral	BB

BB = Bidentate bridging; T = Tetradentate; TM = Terminal monodentate

bridging ligand. We find, however, that most of the complexes exhibit bidentate bridging nature of HMTA (figure 1). (Evidence of stereochemical environments deduced from their room temperature magnetic moment values, electronic spectral bands and ligand field parameters being considered is consistent with the bidentate-bridging behaviour of HMTA). Apart from some intensity changes and splitting of ν_{CN} bands the IR spectra due to coordinated HMTA in all these complexes are almost superimposable on that of the uncoordinated ligand. This may be because the chair configuration of the uncoordinated HMTA is retained in the complexes irrespective of the mode of metal- HMTA bonding. The 1225 cm^{-1} band splits into ~1215 and 1235 cm^{-1} and the 1000 cm^{-1} into ~1010 and 970 cm^{-1} providing a means to distinguish the bidentate-bridging behaviour of HMTA (Negita *et al* 1965; Ahuja *et al* 1979, 1980, 1981, 1982). It may be pointed out that the geometry of HMTA rules out the possibility of it acting as a bidentate-chelating ligand.

The room temperature magnetic moment values, electronic spectral bands and ligand field parameters of the complexes $Mn(HMTA)_2(NCS)_2(EtOH)_2$, $Co(HMTA)_2(NCS)_2(EtOH)_2$, $Co(HMTA)_2(NCS)_2$, $Ni(HMTA)_2(NCS)_2(EtOH)_2$ and $Ni(HMTA)_2(OAc)_2$ are consistent with octahedral environments (tetrahedral)

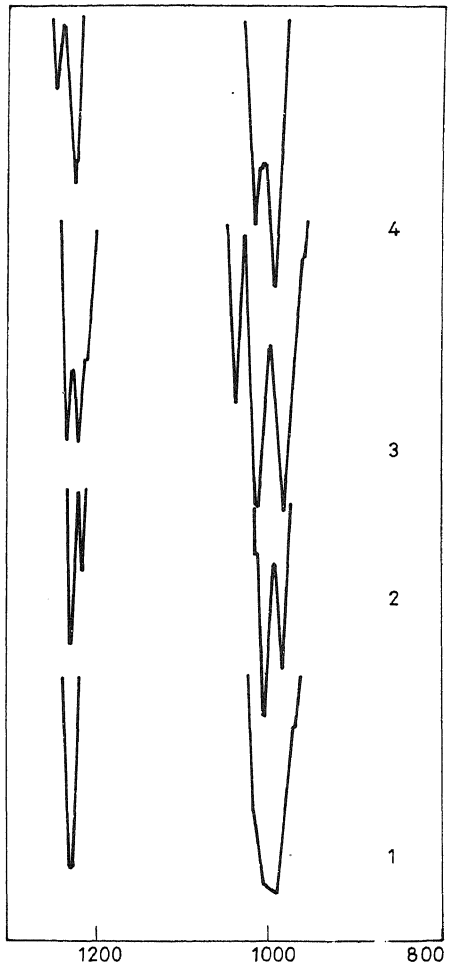

Figure 1. 1. Uncoordinated HMTA; 2. Hg(HMTA) $(CN)_2$; 3. Hg(HMTA)Br_2; 4. Co(HMTA)Cl_2.

(Ahuja *et al* (1982) in the case of Co(HMTA)$_2$(NCS)$_2$) around the respective metal ion (Ahuja *et al* 1981). Moreover, the fundamental frequencies due to the thiocyanate groups are consistent with the presence of terminally N-bonded NCS groups (Ahuja *et al* 1981). IR frequencies due to the acetate groups are consistent with bidentate chelating (acetato) ligands in the Ni(HMTA)$_2$(OAc)$_2$ complex (Ahuja *et al* 1981). These considerations lead one to conclude that HMTA molecules must be terminally-bonded monodentate ligands in all these complexes. The two ν_{CN} bands at 1225 and 1000 cm^{-1} in these complexes suffer only very minor splitting resulting in closely-spaced doublets or triplets (Ahuja *et al* 1982). Moreover, except for intensity changes of some absorption bands the IR spectra due to coordinated HMTA in these complexes are almost superimposable on that of the uncoordinated HMTA supporting the theory that the chair configuration of the uncoordinated HMTA is retained. It is thus evident that complexes in which HMTA is terminally-bonded monodentate ligand, only very minor splitting of the two ν_{CN} bands at 1225 and 1000 cm^{-1} occurs resulting in closely-spaced doublets or triplets (figure 2).

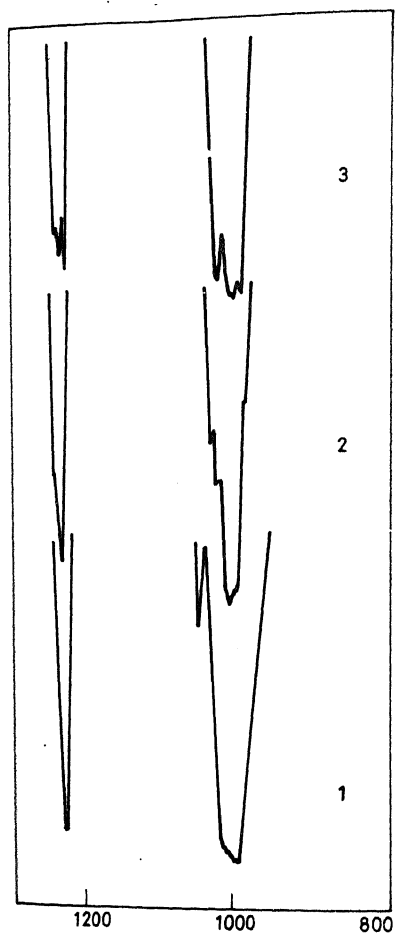

Figure 2. 1. Uncoordinated HMTA; 2. $Co(HMTA)_2(NCS)_2(EtOH)_2$; 3. $Ni(HMTA)_2(NCS)_2(EtOH)_2$.

Although HMTA is a potentially tetradentate ligand not more than one donor site can coordinate to the same metal ion. These donor sites can, however, coordinate to four metal ions resulting in tetranuclear structures. Tetradentate HMTA would have the same symmetry as the uncoordinated molecule. With all the four donor atoms equivalent, *i.e.* coordinated (tetradentate HMTA), the IR spectrum due to tetradentate HMTA would not be expected to suffer any splitting of ν_{CN} bands and would indeed be superimposable on that of the uncoordinated HMTA.

Except for some intensity changes and the slightly lower frequencies of some absorption bands (which provides good evidence for the absence of free ligand), cf. coordinated 1,4-dioxane (Mikawa *et al* 1966) the IR spectrum due to coordinated HMTA in 4:1 mercury (II) thiocyanate–HMTA complex is superimposable on that of the uncoordinated HMTA. The two ν_{CN} bands at 1225 and 1000 cm^{-1} do not suffer any splitting at all (figure 3) (Ahuja *et al* 1982). This close similarity in the IR spectra of uncoordinated HMTA and the coordinated HMTA and the non-splitting of the ν_{CN} bands in this complex may be attributed to the fact that the overall symmetry and the chair configuration of uncoordinated HMTA is retained, or in other words, all the four donor sites are equivalent, that is coordinated in this compound.

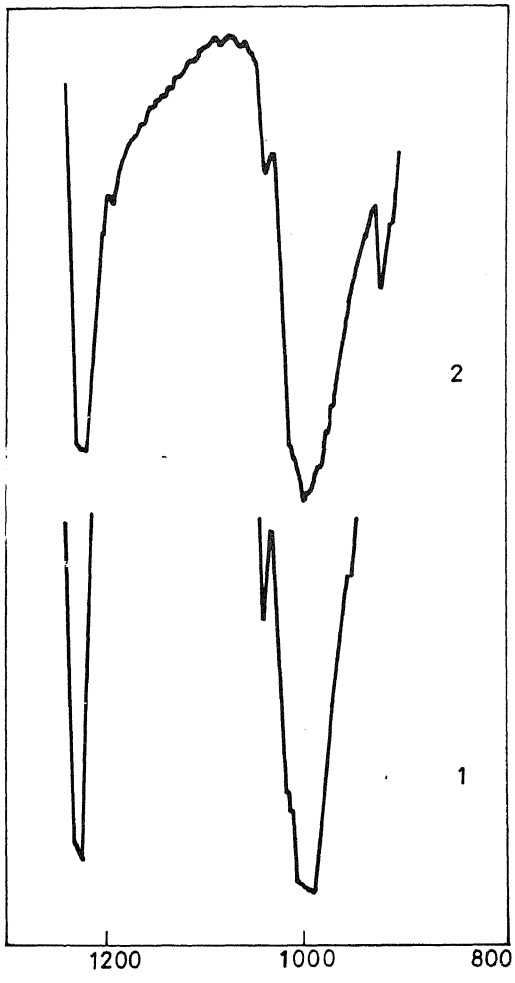

Figure 3. 1. Uncoordinated HMTA; 2. $Hg_4(HMTA)(NCS)_8$.

It is thus concluded that the comparison of IR spectra of the coordinated HMTA with that of its uncoordinated spectrum in the ν_{CN} region lends considerable support for distinguishing the mode of metal–HMTA bonding in metal complexes with this potentially tetradentate ligand. However, x-ray and Raman studies would lead to more conclusive support for the mode of metal–HMTA bonding.

References

Negita H, Nishi Y and Koga K 1965 *Spectrochim. Acta* **21** 2144
Ahuja I S, Singh R and Rai C P 1979 *Spectrochim. Acta* **A35** 193
Ahuja I S, Singh R and Yadava C L 1980 *J. Mol. Struc.* **68** 333
Ahuja I S, Singh R and Yadava C L 1981a *Curr. Sci.***50** 317, 1017
Ahuja I S, Singh R and Yadava C L 1981b *Spectrochim. Acta* **A37** 407
Ahuja I S, Singh R and Yadava C L 1982 *J. Mol. Struc.* **81** 229, 289
Andersen A F 1957 *Acta Crystallogr.* **10** 107
Mecke R and Spiescke H 1955 *Ber.* **88** 1997
Mikawa Y, Jackobsen R J and Brasch J N 1966 *J. Chem. Phys.* **45** 4528

Photoacoustic spectra of As_2S_3 — As_2Se_3 glasses[+]

T SOMASUNDARAM, P GANGULY and K J RAO*
Solid State and Structural Chemistry Unit, Indian Institute of Science, Bangalore 560 012, India

MS received 7 December 1982

Abstract. Photoacoustic spectra of As–S, As–Se glasses as well as the $As_2(S,Se)_3$ glasses have been investigated. Photoacoustic spectra of powdered samples give results comparable to those obtained from transmission spectra, the latter studies requiring preparation of thin films. Temperature-dependent studies of the As_2S_3 glass have been carried out. Optical behaviour of these glasses has been interpreted in terms of homoatomic bonding defects.

Keywords. Arsenic chalcogenide glasses; homoatomic bonding defects; optical absorption edge; photoacoustic spectroscopy.

1. Introduction

It has been recognized (Ganguly and Rao 1981) that photoacoustic spectroscopy (PAS) is a sensitive method for studying solids which are difficult to study by normal transmission or reflectance spectroscopic techniques. Arsenic chalcogenide glasses which exhibit absorption edges in the visible region (Tanaka 1976) possess high extinction coefficients and are highly reflecting and thin films of the material have to be taken for studying their optical behaviour. Arsenic sulphide, As_2S_3 and arsenic selenide, As_2Se_3 glasses also exhibit interesting photo-structural effects (Treacy *et al* 1980; De Neufville 1976). We therefore consider it instructive to investigate the PAS of As_2S_3 and As_2Se_3 glasses and extend the previous preliminary study of Ganguly and Rao (1981) to other systems. In view of the many investigations reported about these glasses by Mohan (1981), it should be possible to assess the viability of PAS as a useful investigative tool to study glasses. We show in this investigation that the absorption edges are indeed easily located and that many useful inferences about the behaviour of chalcogenide glasses may be drawn from PAS studies.

2. Experimental

As_2S_3, As_2Se_3 and three different $As_2(S,Se)_3$ glasses were prepared from 5N purity elements (Koch-light). Proper mixtures of the elements were melted in quartz ampoules sealed under low pressure of argon. The melts were agitated in a rotary furnace for over 8 hours at 1000° C and quenched in water. Powders of these glasses suitable for PAS studies were prepared by grinding the glass thus obtained.

[+] Communication No. 193 from the Solid State and Structural Chemistry Unit.

* To whom correspondence should be made

PA spectra were recorded with a spectrometer consisting of a 250 W tungsten halogen lamp; schoeffel 1/4m G250 monochromator, 163 PAR chopper and 124 A PAR lock in amplifier. The details of the PAS cell have been described elsewhere by Ganguly and Rao (1981). Low temperature measurements were made in a cell described earlier by Ganguly and Rao (1981). The normalised PA spectra were obtained by dividing by carbon black power spectrum. The resolution chosen was 5 nm and the spectra were recorded at a drive of 50 nm/min with a time constant of 1 sec.

3. Results and discussion

PA spectra of As_2S_3, As_2Se_3 glasses and of crystalline samples are shown in figure 1. PA spectra of the three $As_2(S,Se)_3$ glasses are shown in figure 2. These results are essentially independent of chopping frequencies.

PA spectrum of As_2S_3 glass indicates a steep rise in photoabsorption between 500 and 600 nm. In conventional absorption spectroscopy this absorption region is observed only with thin samples (Young 1971). Reported values of absorption edge wavelengths in As_2S_3 and As_2Se_3 glasses corresponding to extinction coefficients, α, of $\simeq 10^3$ cm^{-1} are 510 and 670 nm respectively (Treacy *et al* 1980). These wavelengths correspond to 90% of realizable PAS intensity for these glasses. Since the absorption edge in our PAS study is at shorter wavelength compared to normal transmission studies using thin films, we feel that the position of the absorption edge in our PA spectra is not much affected by saturation effects. These results therefore clearly indicate the suitability of PAS for the study of such glasses. The absolute value of PAS intensities are difficult to interpret in view of their dependence on many other factors (Ganguly and Rao 1981 and references therein). Absorption band edges are fixed, in

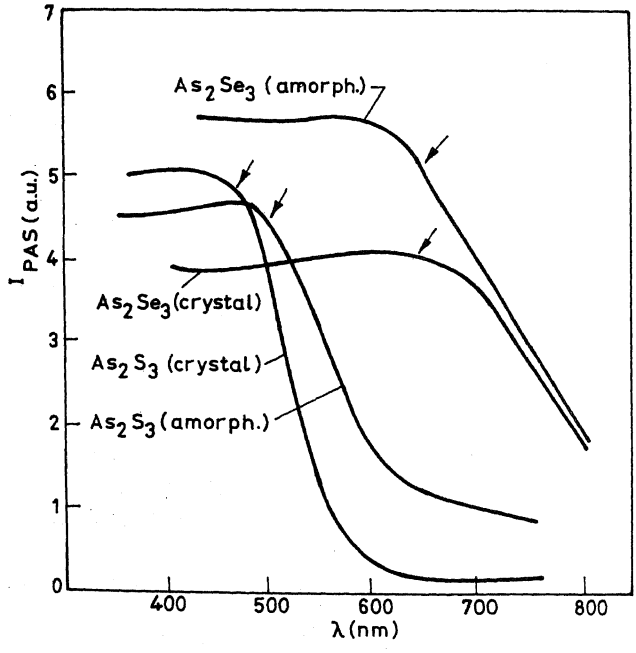

Figure 1. Normalised PA spectra of amorphous and crystalline As_2S_3 and As_2Se_3.

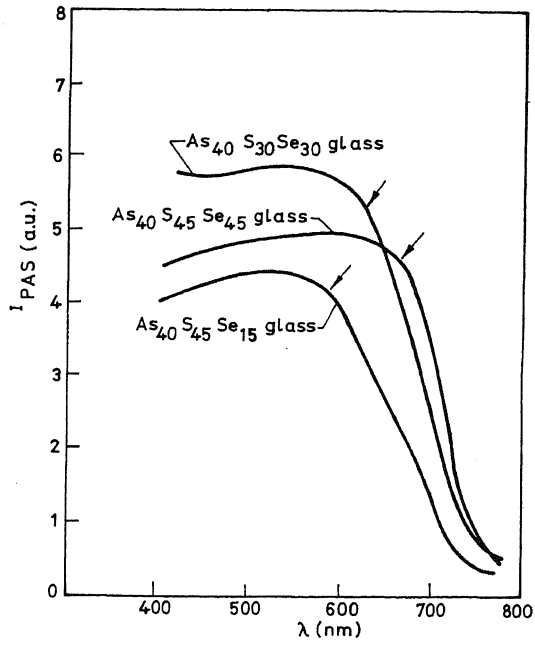

Figure 2. Normalised PA spectra of various $As_2(S,Se)_3$ glasses.

Table 1. Absorption band edges from PAS.

Compound	Absorption band edges from PAS[a] ± 5 nm
As_2S_3 (crystalline)	470
As_2Se_3 (crystalline)	670
As_2S_3 glass	520
$As_{40}S_{45}Se_{15}$ glass	620
$As_{40}S_{30}Se_{30}$ glass	655
$As_{40}S_{15}Se_{45}$ glass	675
As_2Se_3 glass	680

(a) 90% of the normalised saturation intensity.

certain cases, by taking the intersection of the extrapolated absorption edge and the saturation curve (Bhatnagar and Subrahmanyam 1982). To make a reference point with respect to the reported band edge wavelengths we have chosen 90% maximum normalised PAS intensity for the band edge. The absorption edges thus determined by PAS are given in table 1. In both As_2S_3 and As_2Se_3 we notice that the band edges are higher for crystalline than for glassy states. Young (1971) suggested that this difference arose from the generally higher atomic spacing (lower density) in the vitreous state. However this implies that the rather large difference in the energies between vitreous and crystalline states of As_2S_3 with identical first shell of neighbours is almost entirely from density-dependent bond energy differences. An alternative explanation which

we believe more appropriate is that the loose packing inherent to disordered chalcogenides gives rise to a greater spread of the non-bonding levels originating from chalcogens and these levels are known to constitute the top of the valence band (Kastner 1972). Hence a decrease in the optical gap in vitreous state ensures from such spread of valence band levels. In the case of vitreous As_2S_3 the large difference in the densities of crystalline and glassy states (3.49 and 3.16 gm/cc respectively) may arise at least in considerable part from realgar-like structures (Nemanich *et al* 1978) involving >As–As< and, –S–S– linkages. Indeed the antibonding levels corresponding to >As–As< bonds should constitute the bottom of the conduction band. Populating these levels by optical excitation weakens the >As–As< linkages and bond rearrangements of the type, shown in scheme 1,

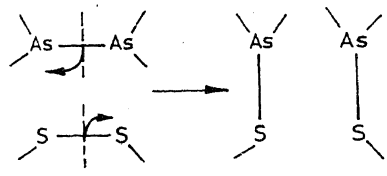

Scheme 1

are facilitated. We feel that such rearrangements constitute the likely steps in the large ('giant') photo structural changes (Singh *et al* 1980) in amorphous As_2S_3. Presence of such homoatomic bonds in As_2S_3 glass and glasses rich in As_2S_3 has been inferred from structural studies by Parthasarathy *et al* (1982) using EXAFS. It is a surprising coincidence that the energy released in such rearrangements is 0.2 eV (energies of As–As, S–S, As–S bonds are respectively 2.07, 2.69 and 2.48 eV (Rao and Mohan 1981) and the difference in the energies of the absorption band edges between crystalline and glassy states of As_2S_3 is about 0.26 eV. The agreement is quite close and suggests that band edge energies of perfectly annealed, defect-free As_2S_3 glass and As_2S_3 crystals should not be different by more than 0.06 eV ($\sim$500 cm^{-1}).

As_2Se_3 glass has been shown to possess a chemically ordered structure through a number of investigations. Density differences between As_2Se_3 glass (4.58 g/cc) and As_2Se_3 crystals (4.75 g/cc) is 0.33 g/cc which is just about 3.6% as compared to 10% difference in the case of As_2S_3. This again indicates in comparison with As_2Se_3 that As_2S_3 glasses involve considerable homoatomic bonding defects. In As_2Se_3 glass, therefore, we expect little difference in the absorption band edge though the edge itself is expected to be more 'smeared' out in the glass.

The temperature dependance of the PA spectra of the As_2S_3 glass presented in figure 3 indicates a red shift consistent with the observation of Young (1971). Edge energies are plotted in the inset of figure 3 and the choice of the PAS edges is indicated by arrows. The thermal coefficient of band edge energy is 7.1×10^{-4} eV dg^{-1} in rather good agreement with the reported literature value (7.0×10^{-4} eV dg^{-1}).

Band edge energies of intermediate compositions $As_2(S_{1-f}Se_f)_3$ decrease as the selenium content in the glass increases as shown in figure 4. Assuming a simple Kastner (1972)-type band picture wherein the band widths are proportional to the concentration of the bond species, substitution of sulphur by selenium should result in a fairly linear decrease in band gap (the decrease being proportional to f, the mole fraction of As_2Se_3 referred to in figure 4). However, the variation is rather steep in the

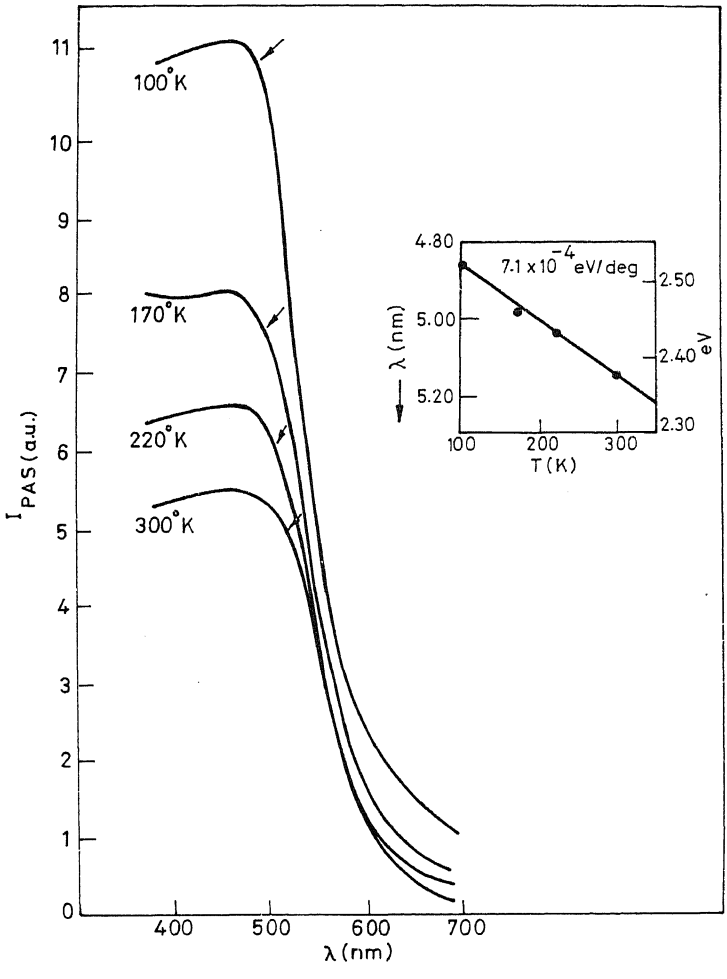

Figure 3. Temperature dependance of PA spectra of As_2S_3 glass. Inset shows the variation of band edge energies. The band edges are marked by arrows.

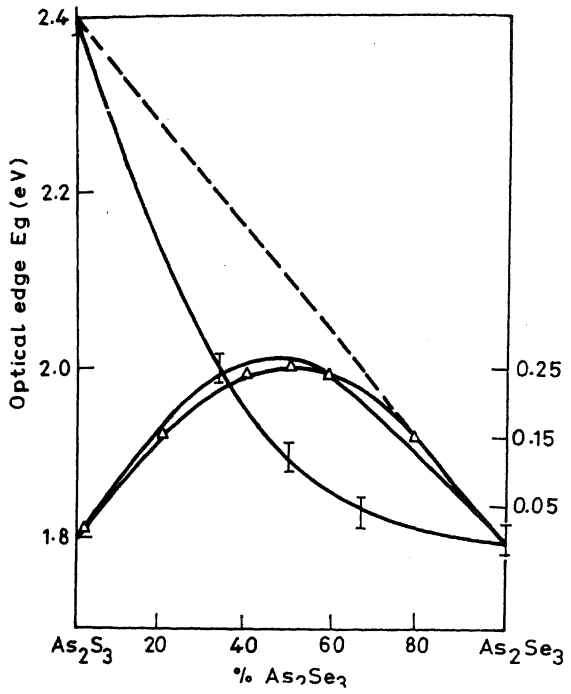

Figure 4. Variation of band edge energies as a function of composition. The dotted straight line is the hypothetical linear variation. The full line dome represents the difference between straight line and actual edge energies. The triangles and thin lines correspond to $f(1-f)$ function, the scale of which is given on the right ordinate.

initial stages of substitution. The difference between the linear (shown as broken line) and actual variation is also plotted in figure 4 (dotted line). The dome shape of the dotted line suggests that the additional decrease of band gap responsible for the nonlinearity has the form of $(f(1-f))$ function (shown as Δ marks on an adjusted scale). This, we believe, is due to the elimination of homoatom bonds upon As_2Se_3 substitution which therefore involves participation of As–Se bonds as intermediate steps. Such steps are essential for reorienting >As–As< and –S–S– linkages in the vitreous phases. One may visualize such a step through scheme 2:

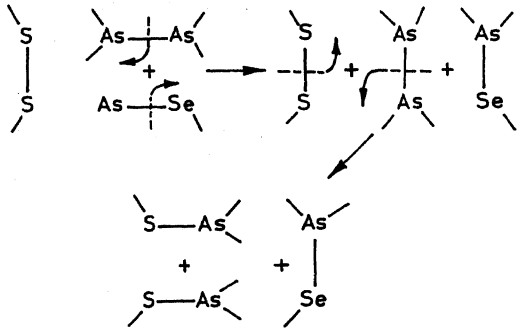

Scheme 2

The reaction mechanism thus requires participation of >As–Se–linkages and hence the process itself is dependent on the concentrations of both As_2S_3 (f) (which determines >As–As< and –S–S–linkages) and As_2Se_3 ($1-f$), (which determines concentration of As–Se links).

4. Conclusions

The present investigation shows that, (a) photoacoustic spectroscopy can be effectively used to investigate spectroscopic behaviour of glasses and (b) As_2S_3 and As_2Se_3 rich glasses contain homoatomic bonding defects which determine their optical behaviour.

Acknowledgement

The authors thank the Indian National Science Academy and the Department of Science and Technology, Government of India, for support of this research.

References

Bhatnagar A K and Subrahmanyam S V 1982 *Solid State Commun.* **42** 281
De Neufville J P 1976 in *Optical properties of solids-New developments* (ed) B O Seraphin (Amsterdam: North Holland) p. 437
Ganguly P and Rao C N R 1981 *Proc. Indian Acad. Sci. (Chem. Sci.)* **90** 153 (and references therein)
Kastner M 1972 *Phys. Rev. Lett.* **28** 355
Mohan R 1981 *Study of As–Se glasses* Ph.D. Thesis, Indian Institute of Science, Bangalore
Nemanich R J, Connel G A N, Hayes T M and Street R A 1978 *Phys. Rev.* **B18** 6900
Parthasarathy R, Rao K J and Rao C N R 1982 *J. Phys.* **C15** 3649
Rao K J and Mohan R 1981 *Solid State Commun.* **39** 1065
Singh B, Rajagopalan S, Bhat P K, Pandya D K and Chopra K L 1980 *J. Non-cryst. Solid* **35–36** 1053
Tanaka K 1976 in *Structure and excitations of amorphous solids* (eds) G Lncovsky and F L Galeener, (p.148 Am. Inst. Phys.)
Treacy D J, Strom U, Klein P B, Taylor P C and Martin T P 1980 *J. Non-cryst. Solid* **35–36** 1035
Young P A 1971 *J. Phys.* **C4** 93

Oxotransition metal complexes of O,O-diethylphosphonyldithiocarbamate

B KHERA, G S SODHI and N K KAUSHIK*
Department of Chemistry, University of Delhi, Delhi 110 007, India

MS received 24 July 1982; revised 11 October 1982

Abstract. O,O-Diethylphosphonyldithiocarbamato complexes of oxovanadium(IV), oxoniobium(V), oxomolybdenum(V), oxotungsten(V, VI) and oxouranium(VI), formulated as $VO(DPD)_2$, $NbO(DPD)_3$, $Mo_2O_3(DPD)_4$, $W_2O_3(DPD)_4$, $WO_2(DPD)_2$ and $UO_2(DPD)_2$ [DPD = $(EtO)_2P(:O)NHCS_2^-$] have been prepared. These have been characterised on the basis of elemental analyses, electrical conductance, magnetic susceptibility and spectral studies. IR spectral data indicate bidentate nature of the ligand. These complexes are fairly stable in inert atmosphere but decompose on standing in air.

Keywords. O,O-Diethylphosphonyldithiocarbamate; oxovanadium(IV); oxoniobium(V); oxomolybdenum(V); oxotungsten(V, VI); oxouranium(VI).

1. Introduction

The dithiocarbamate derivatives find their use as fungicides and pesticides (Thorn and Ludwig 1962). Besides their biological significance, the dithiocarbamate ligands possess structural importance too. Dithiocarbamate derivatives often exhibit unusual coordination phenomena because in some complexes, the dithiocarbamate ligand behaves as a monodentate group (Johnson *et al* 1969; Domenicano *et al* 1966), while in others it acts as a bidentate group (Kaushik *et al* 1978, 1979).

In an earlier communication, we reported (Sodhi and Kaushik 1981) a number of O,O-diethylphosphonyldithiocarbamate complexes of the type $[(EtO)_2P(:O)NHCS_2]_nM$ {M = Cu(I), (n=1); Cu(II), Zn(II), Cd(II), Hg(II), Pb(II), Ni(II), (n=2); Co(III), Fe(III), Mn(III), As(III), Sb(III) and Bi(III), (n=3)}. Our interest in the investigation of bonding mode of O,O-diethylphosphonyldithiocarbamato moiety prompted us to synthesise and characterise some oxotransition metal dithiocarbamates.

2. Experimental

2.1 *Materials and methods*

Potassium O,O-diethylphosphonyldithiocarbamate was prepared by the method described by Addor (1970). Nitrobenzene for conductance measurements was purified as given in the literature (Fay *et al* 1967). The metal contents in these compounds were determined by standard methods (Vogel 1978). Nitrogen was estimated by Kjeldahl's method and sulphur as barium sulphate.

*To whom all correspondence should be made.

Conductance measurements were made in nitrobenzene at 30 ± 0.1 using an Elico Conductivity Bridge (Model CM–82). Infrared spectra were recorded (KBr pellets) in the 4000–200 cm^{-1} region with a Perkin-Elmer 621 spectrophotometer. Magnetic moment studies were made by the Gouy's method using mercury tetrathiocyanato cobaltate(II) as calibrant.

2.2 *Preparation of the complexes*

2.2a *Oxobis(diethylphosphonyldithiocarbamato)vanadium(IV)*, $VO(DPD)_2$: To an aqueous solution of $VOSO_4.2H_2O$ was added an aqueous solution of the ligand in 1:2 molar ratio at 0–5° C and the contents stirred for about 15 min at this temperature when yellowish precipitate appeared. It was washed with ice cold water followed by an aqueous ethanol. It was then reprecipitated from an acetone solution by adding petroleum ether (60–80°), dried and stored *in vacuo* over P_4O_{10}.

2.2b *Oxotris(diethylphosphonyldithiocarbamato)niobium(V)*, $NbO(DPD)_3$: It was prepared by mixing an aqueous solution of the ligand to an aqueous solution of niobium pentachloride in 1:3 metal to ligand molar ratio, followed by stirring for 10 min. The white precipitate obtained was washed with ice-cold water and aqueous ethanol. These were recrystallised from an acetone solution by adding petroleum ether (60–80°) and dried *in vacuo* over P_4O_{10}.

2.2c *μ-Oxodioxobis (diethylphosphonyldithiocarbamato) dimolybdenum (V)*, $[MoO(DPD)_2]_2O$: Addition of a fresh aqueous solution of sodium dithionite to a stirred solution of the ligand (0.02 mol) and sodium molybdate (0.01 mol) in water resulted in the formation of a brownish-green precipitate. It was washed with cold water and ethanol. It was finally recrystallised from an acetone solution by adding petroleum ether (60–80°) dried and kept in vacuum over P_4O_{10}.

2.2d *μ-Oxodioxobis(diethylphosphonyldithiocarbamato)ditungsten(V)*, $[WO(DPD)_2]_2O$: It was prepared by adding an aqueous solution of ligand in excess of an aqueous solution of sodium tungstate at 0–5° C and the contents stirred for about 15 min at this temperature. The metal complex thus precipitated was washed with ice cold water followed by aqueous ethanol. It was then recrystallised from an acetone solution by adding petroleum ether (60–80°), dried and kept *in vacuo* over P_4O_{10}.

2.2e *Dioxobis (diethylphosphonyldithiocarbamato) tungsten* (VI), $WO_2(DPD)_2$: It was prepared by adding dilute hydrochloric acid to a cold aqueous solution of the ligand (0.02 mol) and sodium tungstate (0.01 mol). The light green precipitate thus obtained was washed with cold water followed by aqueous ethanol. It was reprecipitated from an acetone solution by adding petroleum ether (60–80°) and dried under vacuum.

2.2f *Dioxobis (diethylphosphonyldithiocarbamato) uranium (VI)*, UO_2 $(DPD)_2$: It was prepared by mixing an aqueous solution of ligand to an aqueous solution of uranyl acetate in 1:2 molar ratio and the contents stirred for about 15 min at 0–5° C. The orange-coloured complex thus precipitated was washed with ice cold water followed by aqueous ethanol. It was reprecipitated from an acetone solution by the addition of petroleum ether (60–80°), dried and stored *in vacuo* over P_4O_{10}.

3. Results and discussion

The analytical data and some physical characteristics of the complexes are listed in table 1. All the complexes are soluble in common organic solvents. Conductance measurements show that all the complexes are nonelectrolytes in nitrobenzene. All the complexes are fairly stable in inert atmosphere and decompose on standing in air.

3.1 *Magnetic moments*

All the complexes except those of oxovanadium (IV) are diamagnetic. The magnetic moments of oxovanadium (IV) complexes lie in the range 1.70-1.72 BM at room temperature. These values lie within the range reported for oxovanadium (IV) complexes having one unpaired electron.

3.2 *Infrared spectra*

Table 2 lists the important infrared frequencies of the complexes. All the complexes exhibit only one strong band at ~ 1000 cm^{-1} supporting the bidentate nature of the dithiocarbamates and also suggesting the chelating nature of the ligand (Johnson *et al*

Table 1. Analytical data and physical characteristics of the complexes

Complex	Melting point (° C)	Colour	% of elements Calc. (Found)		
			M	S	N
$VO(DPD)_2$	107 (d)	Yellow	9.75(9.92)	12.23(12.01)	2.67(2.88)
$NbO(DPD)_3$	200 (d)	White	11.72(11.81)	8.07(8.19)	1.76(1.93)
$Mo_2O_3(DPD)_4$	208 (d)	Brownish green	16.66(16.80)	5.55(5.62)	1.21(1.09)
$W_2O_3(DPD)_4$	>250 (d)	White	27.71(27.83)	4.81(4.89)	1.05(1.16)
$WO_2(DPD)_2$	125 (d)	Light green	27.38(27.12)	9.52(9.77)	2.08(2.32)
$UO_2(DPD)_2$	120 (d)	Orange	32.78(32.93)	8.81(9.02)	1.92(2.14)

DPD = O,O-diethylphosphonyldithiocarbamate
(d) with decomposition

Table 2. Characteristic infrared bands (cm^{-1}) of the complexes.

Complex	ν(C....N)	ν(C....S)	ν(C-O)	ν(P=O)	ν(M-S)	ν(M=O)	
$VO(DPD)_2$	1355s	1005s	1120s	1260m	345m	945m	
$NbO(DPD)_3$	1340s	1000s	1105s	1275m	360m	925w	
$Mo_2O_3(DPD)_4$	1350s	1005s	1105s	1272m	350m	955w	ν(Mo-O-Mo) 430w 750m
$W_2O_3(DPD)_4$	1360s	1010s	1110s	1265m	355m	900w	
$WO_2(DPD)_2$	1355s	1000s	1100s	1270m	348m	910w	
$UO_2(DPD)_2$	1365s	1000s	1115s	1275m	355m		ν(U-O) 915s, 800w

1969; Brown and Smith 1972; Bonati and Ugo 1967). A doublet is expected in the region 1000 ± 50 cm^{-1} if the ligand is to behave as monodentate. The ligand band at ~ 1350 cm^{-1} is assigned to the ν(C....N). The occurrence of this band at lower energy in the complexes compared with those of corresponding dialkyl dithiocarbamate complexes, indicates considerably less double bond character of the (C....N) bond in these complexes. A strong band at ~ 1100 cm^{-1} is assigned to ν (C–O) in the C_2H_5OP group, while that at ~ 1260 cm^{-1} is due to ν (P=O). The ν (N–H) occurs at ~ 3075 cm^{-1}. The bands in the range 360–345 cm^{-1} are assigned to ν(M–S)vibrations(Bradley and Gitlitz 1969).

The new bands in the infrared spectra at *ca* 945 and 925 cm^{-1} in the oxovanadium (IV) and oxoniobium (V) complexes, respectively may be assigned to ν (M=O) vibrations (Selbin 1966; Sabatini and Bertini 1966). Complexes of the type Mo_2O_3 $(DPD)_4$ have a single Mo=O stretching mode at 955 cm^{-1}. In addition, two bands are observed at *ca* 430 and 750 cm^{-1} which may be assigned to a symmetrical and antisymmetrical Mo-O-Mo stretching modes (Cotton and Wing 1965) respectively. In the oxotungsten (V, VI) complexes, the absorption due to ν (W=O) was observed at ~ 900 cm^{-1}. In the oxouranium (VI) complex, two bands at *ca* 915 and 800 cm^{-1} may be assigned (Cattalini *et al* 1971) to ν $(U\text{-}O)_{asymm}$ and ν $(U\text{-}O)_{symm}$ modes. These observations indicate that the UO_2 moiety is virtually linear (Cattalini *et al* 1971).

A comparison of ν (M-O) stretching vibrations in the present complexes with other compounds of similar composition (Kumar and Kaushik 1981), reveals that these frequencies are not sensitive to any unusual geometry.

Acknowledgement

The authors (BK and GSS) are thankful to the CSIR, New Delhi for the award of fellowship.

References

Addor R W 1970 *J. Heterocycl. Chem.* **7** 381
Bonati F and Ugo R 1967 *J. Organomet. Chem.***10** 257
Bradley D C and Gitlitz M H 1969 *J. Chem. Soc.* (A) 1152
Brown T M and Smith J N 1972 *J. Chem. Soc.* (Dalton) 1614
Cattalini L, Croatto U, Degetto S and Tondello E 1971 *Inorg. Chim. Acta Rev.* **5** 19
Cotton F A and Wing R M 1965 *Inorg. Chem.* **5** 204
Domenicano A, Vaciago A, Zambonelli L, Loader P L and Venanzi L M 1966 *Chem. Commun.* 476
Fay R C and Lowry R N 1967 *Inorg. Chem.* **6** 1512
Johnson B F G, Al-Obaidi K H and McCleverty J A 1969 *J. Chem. Soc.* (A) 1668
Kaushik N K, Bhushan B and Chhatwal G R 1978 *Transition Met. Chem.* **3** 215
Kaushik N K, Bhushan B and Chhatwal G R 1979 *Z. Naturforsch.* **34b** 949
Kumar S and Kaushik N K 1981 *Gazz. Chim. Ital.* **111** 57
Sabatini A and Bertini I 1966 *Inorg. Chem.* **5** 204
Selbin J 1966 *Coord. Chem. Rev.* **1** 293
Sodhi G S and Kaushik N K 1981 *Indian J. Chem.* **20** 922
Thorn G D and Ludwig R A 1962 The dithiocarbamates and related compounds (London:Elsevier)
Vogel A I 1978 *A textbook of quantitative inorganic analysis* (London:Longmans)

Proc. Indian Acad. Sci. (Chem. Sci.), Vol. 92, No. 1, January 1983, pp. 77–82.
© Printed in India.

Polarographic study of mixed ligand complexes of Pb(II) with ethylenediamine-malonate and propylene-diamine-malonate

J K GARG*, P S VERMA† and D S JAIN†

Postgraduate Department of Chemistry, Government College, Ajmer 305 001, India
† Department of Chemistry, University of Rajasthan, Jaipur 302 004, India

MS received 5 March 1982; revised 27 September 1982

Abstract. Overall stability constants of mixed ligand complexes formed by Pb(II) with ethylenediamine-malonate and propylenediamine-malonate have been determined. The reductions were reversible and diffusion-controlled involving two electrons in both systems. The equilibrium concentration of the ligand is calculated from pH and the total amount present using pK values. The formation constants have been used to discuss the results.

Keywords. Mixed-ligand complexes; lead (II), ethylenediamine; propylenediamine malonate ion.

1. Introduction

Single ligand complexes have been studied by polarographic methods by several workers. However, it has been rarely applied to mixed ligand complexes. It was used to study mixed ligand complexes by Schaap and McMasters (1961) by extending the method of DeFord and Hume (1951) to cases where a metal ion forms complexes with two ligands simultaneously in solution.

Mixed complexes of Pb(II) with various organic ligands have been extensively studied (Gupta and Kaur 1979; Verma and Yadav 1980; Agarwal 1979; Garg *et al* 1982). The present investigation deals with mixed ligand complexes formed by Pb(II) with (i) ethylenediamine-malonate and (ii) propylenediamine-malonate. It was observed that Pb(II) forms 1:3 highest complexes with ethylenediamine (EN), propylenediamine (PN) and malonate ion (MALO).

2. Experimental

The chemicals used were of reagent grade. A manual polarograph was used for this work. Capillary characteristics for the open circuits were: $m = 1.89$ mg/sec and $t = 3.5$ sec. All the measurements were carried out at $298 \pm 0.5°$ K. pH measurement (Toshniwal pH meter) was adjusted with nitric acid solution or CO_2-free potassium hydroxide. Potassium nitrate was added to make the ionic strength equal to 1.5 M. The solution was placed in H-type cell coupled with saturated calomel electrode through an agar-agar saturated with KCl salt bridge. Prior to reduction at DME, oxygen was removed by bubbling pure nitrogen gas through the solution for 20 min. The pk values

* To whom all correspondence should be made

of the ligands were measured by generally accepted procedures and were found to be as follows:

Ligands	pk_1	pk_2
Ethylenediamine	6.5	9.48
Propylenediamine	7.0	9.78
Malonic acid	2.85	5.69

3. Results and discussion

3.1 *Simple systems*

The reduction of Pb(II) was reversible involving two electrons and diffusion-controlled in each case as revealed from the linear plots of i_d vs $h^{1/2}_{\text{eff}}$ of mercury column passing through the origin. The plots of log i/i_d-i vs E_{de} were linear with a slope of 31 ± 2 mV. No maximum suppressor was needed in these systems. The concentrations of "free" EN, PN and malonate were calculated from the pH and the total amount present using the pk values. The overall formation constants of simple complexes have been evaluated by DeFord and Hume's method and the results are summarized below:

System	Overall formation constants		
	log β_1	log β_2	log β_3
Pb (II) - EN	4.079	7.243	10.099
Pb (II) - PN	5.061	8.204	10.959
Pb (II) - MALO	2.857	3.663	4.268

3.2 *Mixed systems*

Three different mixed complexes of Pb(II) are possible with two bidentate ligands. These are [Pb(EN)(MALO)] $[Pb(EN)(MALO)_2]^{-2}$ and $[Pb(EN)_2(MALO)]$ for ethylenediamine-malonate system and [Pb(PN)(MALO)] $[Pb(PN)(MALO)_2]^{-2}$ and $[Pb(PN)_2(MALO)]$ for propylenediamine system.

A shift in $E_{1/2}$ to more cathodic potential with increase in EN or PN concentrations was observed in all the cases. The shift is greater in the presence of weaker ligand (MALO) than in its absence signifying mixed ligand formation. The Schaap and McMasters treatment was applied to the half-wave potential data and F_{io} functions evaluated. Leeden's (1941) graphical extrapolation method was then applied to calculate *A, B, C, D* and the calculations are given in tables 1 to 4.

Due to experimental advantage, malonate concentrations were held at two different fixed values (0.20 and 0.25 M) allowing the F_{00} functions to be evaluated as function of EN or PN concentration which varied with pH. Under this condition, for the lead systems, the F_{00} functions may be written:

$$F_{00}=A+B[X]+C[X]^2+D[X]^3,$$

where, $[X]$=EN or PN,

$$A=1+\beta_{01}[\text{MALO}]+\beta_{02}[\text{MALO}]^2+\beta_{03}[\text{MALO}]^3,$$

$$B=\beta_{10}+\beta_{11}[\text{MALO}]+\beta_{12}[\text{MALO}]^2,$$

$$C=\beta_{20}+\beta_{21}[\text{MALO}], \text{ and } D=\beta_{30}.$$

The values of A and D are known from the studies of the simple systems. However, B values must be evaluated at least at two appropriate malonate ion concentrations, so that the mixed constants β_{11} and β_{12} can be calculated.

Theoretically, log C must be equal to log β_{30}. Our results agree with this postulation The average log D values from both the series in the EN–MALO system were 10.040 and 10.056 which agree reasonably well with the value of log $\beta_{30}=10.099$. However, in PN-MALO system, the log D values were 10.932 and 10.945 which also agree with the corresponding value of log $\beta_{30}=10.959$.

Table 1. Lead-ethylenediamine-malonate system

$[\text{EN}]\times10^4$	log I_M/I_C	$\Delta E_{1/2}$	$F_{00}(X)$	$F_{10}(X)\times10^{-4}$	$F_{20}(X)\times10^{-8}$	$F_{30}(X)\times10^{-12}$
6.1485	0.1205	0.0830	849.6107	—	—	—
9.2228	0.1272	0.0863	1115.8145	69.2105	—	—
12.297	0.1339	0.0890	1398.4921	74.8957	0.8860	0.01106
15.371	0.1385	0.0912	1677.6756	78.0805	0.9160	0.01080
18.445	0.1408	0.0933	1986.4241	81.8067	0.9654	0.01168
21.519	0.1455	0.0951	2310.3830	85.1751	0.9840	0.01087
24.594	0.1478	0.0969	2672.3664	89.2440	1.0264	0.01124
27.668	0.1501	0.0985	3043.2666	92.7341	1.0385	0.01043
30.742	0.1525	0.1001	3466.4424	97.2267	1.0808	0.01076

$[\text{Pb}]^{+2}=0.5$mM; $\mu=1.5$ M; pH = 7.7; $I_M=65.0$ divs; $E_{1/2}=-0.4150$ volts vs SCE; [malonate] = 0.20 M

$A_{\text{cal}}=477.5$ $B=64\times10^4$ $C=0.75\times10^8$ log $D_{\text{av}}=10.040$

Table 2. Lead-ethylenediamine-malonate system

$[\text{EN}]\times10^4$	log I_M/I_C	$\Delta E_{1/2}$	$F_{00}(X)$	$F_{10}(X)\times10^{-4}$	$F_{20}(X)\times10^{-8}$	$F_{30}(X)\times10^{-12}$
6.1485	0.1272	0.0876	1234.7641	—	—	—
9.2228	0.1362	0.0908	1617.6032	93.1391	—	—
12.297	0.1408	0.0932	1971.0062	98.5937	1.0241	0.01091
15.371	0.1501	0.0951	2334.9844	102.5557	1.0771	0.01217
18.445	0.1549	0.0969	2716.4142	106.1433	1.0921	0.01096
21.519	0.1597	0.0986	3135.6240	110.4616	1.1367	0.01147
24.594	0.1670	0.1001	3584.1319	114.8870	1.1746	0.01157
27.668	0.1670	0.1017	4060.0182	119.3226	1.2044	0.01136
30.742	0.1695	0.1031	4554.1150	123.4635	1.2186	0.01069

$[\text{Pb}]^{+2}=0.5$mM; $\mu=1.5$ M; pH = 7.7; $I_M=65.0$ divs; $E_{1/2}=-0.4150$ volts vs SCE; [malonate] = 0.25 M

$A'_{\text{cal}}=758.6$ $B'=86\times10^4$ $C'=0.89\times10^8$ log $D_{\text{av}}=10.056$

Table 3. Lead-propylenediamine-malonate system

$[PN] \times 10^4$	$\log I_M/I_C$	$\Delta E_{1/2}$	$F_{00}(X)$	$F_{10}(X) \times 10^{-4}$	$F_{20}(X) \times 10^{-8}$	$F_{30}(X) \times 10^{-12}$
2.7536	0.1362	0.0833	901.7615	154.0752	—	—
4.1305	0.1400	0.08695	1208.9365	177.0818	4.1355	0.08123
5.5073	0.1431	0.08953	1488.7676	183.6231	4.2894	0.08887
6.8841	0.1455	0.0918	1786.3736	190.1299	4.3767	0.08378
8.2610	0.1525	0.0937	2105.3786	197.0559	4.4856	0.08300
9.6378	0.1573	0.0955	2449.1461	204.5743	4.6249	0.08556
11.014	0.1645	0.0971	2821.0923	212.7830	4.7924	0.09010
12.391	0.1695	0.0986	3206.8938	220.2723	4.8642	0.08588
13.768	0.1719	0.1001	3625.0934	228.6166	4.9838	0.08598

$[Pb]^{+2} = 0.5$mM; $\mu = 1.5$ M; pH = 7.7; $I_M = 65.0$ divs; $E_{1/2} = -0.4150$ volts vs SCE; [malonate] = 0.20 M

$A_{cal} = 477.5$; $B = 160 \times 10^4$; $C = 3.8 \times 10^8$; $\log D_{av} = 10.932$.

Table 4. Lead-propylenediamine malonate system

$[PN] \times 10^4$	$\log I_M/I_C$	$\Delta E_{1/2}$	$F_{00}(X)$	$F_{10}(X) \times 10^{-4}$	$F_{20}(X) \times 10^{-8}$	$F_{30}(X) \times 10^{-12}$
2.7536	0.1455	0.0870	1228.9672	170.819	—	—
4.1305	0.1501	0.0910	1696.4458	227.0538	4.6129	—
5.5073	0.1549	0.0933	2051.9746	234.8473	4.8749	—
6.8841	0.1621	0.0952	2419.1789	241.2195	4.8255	—
8.2610	0.1645	0.0971	2820.7461	249.6243	5.0386	0.08336
9.6378	0.1719	0.0987	3250.1844	258.5221	5.2421	0.09256
11.014	0.1769	0.1002	3695.6870	266.6685	5.3267	0.08868
12.391	0.1820	0.1016	4169.8574	275.3012	5.4315	0.08728
13.768	0.1845	0.1030	4677.8295	284.6622	5.5681	0.08848

$[Pb]^{+2} = 0.5$mM; $\mu = 1.5$ M; pH = 7.7; $I_M = 65.0$ divs; $E_{1/2} = -0.4150$ volts vs SCE; [malonate] = 0.20 M

$A'_{cal} = 758.6$ $B' = 208.0 \times 10^4$; $C' = 4.35 \times 10^8$; $\log D'_{av} = 10.945$.

The results are summarized in schemes 1 and 2 where $\log K$ of the steps is indicated. These trends may be understood if it is assumed in accord with evidence (not cited here) that the N → metal bond is appreciably more covalent than the O → metal bond with these ligands. The ethylenediamine or propylenediamine complexes would then be more strongly influenced by the stereochemistry of the hybridged sp^3 orbitals of lead than the more ionic malonate complexes and have a correspondingly greater tendency to be tetrahedral. Addition of either ethylenediamine/ propylenediamine molecule or malonate ion to $[Pb(EN)_2]^{+2}$ / $[Pb(PN)_2]^{+2}$ would be hindered, despite the opposite charges of the latter two species, while addition of either ligand to $[Pb(MALO)_2]^{-2}$ would proceed more readily, offsetting the repulsion of the like charges in the case of malonate addition.

For reactions

$$[Pb(X)_2]^{+2} + [Pb(Y)_2]^{-2} \rightleftharpoons 2[Pb(X)(Y)], \quad (1)$$

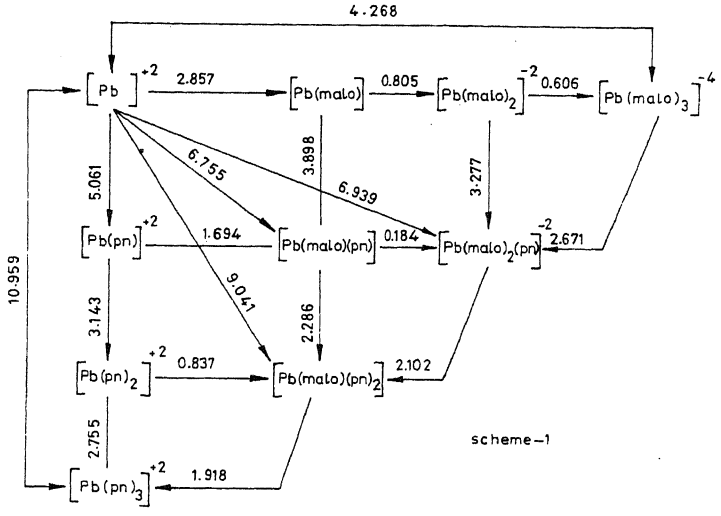

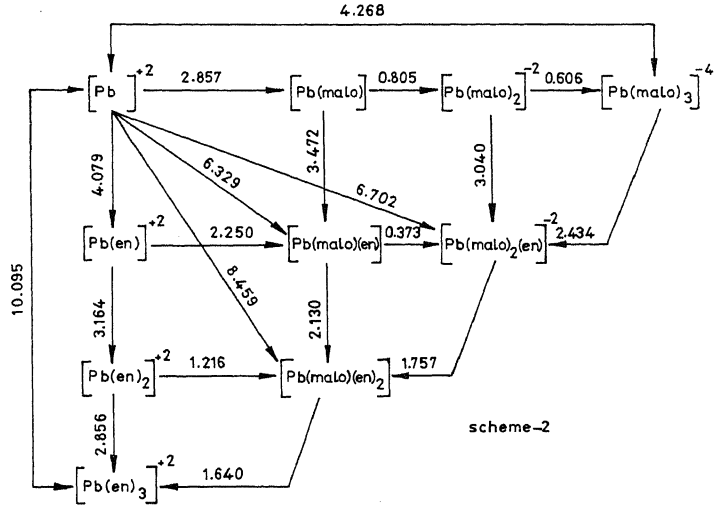

$$[Pb(X)_3]^{+2} + 2[Pb(Y)_3]^{-4} \rightleftharpoons 3[Pb(X)(Y)_2]^{-2}, \tag{2}$$

$$\text{and} \quad 2[Pb(X)_3]^{+2} + [Pb(Y)_3]^{-4} \rightleftharpoons 2[Pb(X)_2(Y)], \tag{3}$$

where $X =$ EN or PN and $Y =$ MALO.

The log values of X_{11}, X_{12} and X_{21} for both the systems were calculated and found as follows:

System	log X_{11}	log X_{12}	log X_{21}
Pb(II)-EN-MALO	1.753	1.471	0.911
Pb(II)-PN-MALO	1.644	1.322	0.937

The log X_{11} value on statistical grounds is 0.6, and the observed value of log X_{11} greater than 0.6 indicates favoured formation of mixed complexes. The observed log X_{12} and log X_{21} are also greater than the expected values on statistical basis.

Acknowledgement

Thanks are due to Sri G S Kachhawha for helpful discussion.

References

Agarwal L K 1979 Ph.D. Thesis Univ. of Rajasthan
DeFord D D and Hume D N 1951 *J. Am. Chem. Soc.*73 5321
Garg J K, Jain D S and Verma P S 1982 *Electrochim. Acta* (Communicated)
Gupta K C and Kaur T 1979 *Electrochim. Acta* **24** 1133
Leeden I 1941 *Z. Phys. Chem.* **A188** 160
Schaap W B and McMasters D L 1961 *J. Am. Chem. Soc.* **83** 4699
Verma P S and Yadav R D 1980 *J. Electrochem. Soc. India* **293** 145.7(A)

© Printed in India.

Preparation, characterization and thermal properties of di-N-isothiocynatodihydrazine metal (II)

K C PATIL*, J P VITTAL and C C PATEL
Department of Inorganic and Physical Chemistry, Indian Institute of Science, Bangalore 560 012, India.

MS received 6 May 1982; revised 12 November 1982

Abstract. Complexes of the type $[M(N_2H_4)_2(NCS)_2]$, where M = Mn(II), Fe(II), Co(II), Ni(II), Zn(II), Cd(II) and Mg(II) have been prepared and characterized by chemical analysis, infrared and Mössbauer spectroscopy and magnetic moments. Hydrazine acts as a bridge between the two metal ions through the N-atom forming a distorted octahedral environment around the metal ion. Thermal decomposition of the complexes was studied in air and nitrogen atmosphere using TG and DTA techniques. The thermal stability of the complexes in nitrogen and the M-N stretching frequencies of M-NCS and M-N_2H_4 obey Irwing-Williams order for the bivalent metal complexes *i.e.* $Mn^{2+} < Fe^{2+} < Co^{2+} < Ni^{2+} > Zn^{2+} > Cd^{2+}$

Keywords. Hydrazine complexes; infrared spectra; thermal decomposition.

1. Introduction

This work stems from our interest in metal complexes of hydrazine (Patil *et al* 1982, 1982a). Specifically, we deal here with the reactions of N_2H_5SCN with several transition metal ions as well as with Mg and Cd. Complexes of the type $[M(N_2H_4)_2(SCN)_2]$ have been isolated and thoroughly characterized using several physical methods. The thermal decomposition of the complexes is also examined. Several fragmentary studies on such complexes or related species are reported in literature (Srivastava *et al* 1980; Ray and Sarkar 1920; Anangnaostopoulus and Nicholls 1976; Aggarwal and Vallabhaneni 1978; Furlani *et al* 1970; Braibanti *et al* 1968; Ferrari *et al* 1961; Duval 1967). Our work constitutes the first systematic exploration of these complexes.

2. Experimental

Materials employed: Hydrazine hydrate, $N_2H_4.H_2O$ was a BDH product (99-100%). Ammonium thiocyanate was GR grade from Sarabhai M. Chemicals, India. The metal salts used were guaranteed pure reagents.

2.1 *Preparation of Di N-isothiocyanatodihydrazine metal(II)*

The complexes were prepared by the following two methods: *Method 1*: Stoichiometric quantities of metal(II) salts like chlorides or sulphates of Mn, Fe, Co, Ni, Zn or Cd in alcohol water mixture (1:1 by volume) were added to hydrazinium thiocyanate in 1:2 mole ratio. Alternatively, the metal salt was mixed with ammonium thiocyanate

*To whom all correspondence should be made

and hydrazine hydrate in the mole ratio 1:2:2 in each case, when the complex precipitated. The reaction can be represented as follows:

$$M^{2+} + 2N_2H_5SCN \rightarrow [M(N_2H_4)_2(NCS)_2] + 2H^+ \quad (1)$$

$$M^{2+} + 2NH_4SCN + 2N_2H_4H_2O \rightarrow [M(N_2H_4)_2(NCS)_2] + 2NH_4^+ + 2H_2O \quad (2)$$

The precipitated complex was filtered, washed with water followed by alcohol and dried over anhydrous calcium chloride in a desiccator. Yield ~95%. *Method 2*: Metal powders free from the oxide film, were dissolved separately in a solution of N_2H_5SCN as such or metathetically formed by the reaction of $N_2H_4H_2O$ with NH_4SCN. The reaction takes place as follows with the evolution of hydrogen.

$$M^{2+} + 2N_2H_5SCN \rightarrow [M(N_2H_4)_2(NCS)_2] + 2H^+ \quad (3)$$

All the reactions are exothermic but with different magnitude. Magnesium reacts violently, while the reactions with other metals such as Fe, Ni, Co and Zn are hastened by stirring the solution magnetically and raising the temperature to 40–45° C. The complexes precipitated were separated from the remaining metal powders magnetically and/or by centrifuging and filtered. The complexes were washed with water and alcohol as before and dried over anhydrous calcium chloride. Yield for magnesium complex ~95%; iron complex ~80%; cobalt, nickel and zinc ~30%.

The reaction of N_2H_5SCN with copper salts results in the reduction of Cu(II) to Cu(I) or metallic copper depending on the experimental conditions. The copper complex $[Cu(N_2H_4)_2(NCS)_2]$ could not be prepared as described by Srivastava *et al* (1980). The complex could not be prepared even starting with copper powder.

2.2 *Analyses*

The metal ions present in all the complexes were estimated using EDTA complexometric titration. The thiocyanate content was estimated gravimetrically as $Cu_2(NCS)_2$ while the hydrazine was estimated volumetrically using KIO_3 solution as a titrant under Andrews conditions after accounting for the thiocyanate interference (Vogel 1951).

2.3 *Physico-chemical studies*

Magnetic susceptibility was measured by the standard Gouy method at room temperature (23° C) using powdered samples of the complexes. The infrared spectra of the complexes in Nujol mull were recorded on a Perkin-Elmer spectrometer (model no. 597) in the region 200–4000 cm^{-1}. The Mössbauer spectrum of the complex $[Fe(N_2H_4)_2(NCS)_2]$ was recorded at room temperature (25° C) on an ECIL spectrometer (model MBS-35) with multichannel analyzer. The radioactive source (γ-ray emitter) was ^{57}Co in palladium matrix and the drive velocity was 0.06 mm sec^{-1}. The isomer shift was reported with reference to steel.

The DTA experiments were carried out by a DTA unit constructed for controlled atmosphere as described by Savant and Patel (1968), fitted with a two-pen strip chart recorder. About 100 mg of the powdered samples were used with close packing. The TG experiments were carried out using a Stanton Redcroft 750/770 thermobalance. The sample weight taken was about 7 mg. Both TG and DTA experiments were done in

air and nitrogen atmospheres with a flow rate of 25 ml min^{-1} with a heating rate of 10° C min^{-1}.

3. Results and discussion

Results of chemical analysis and the magnetic moment data are in table 1. All the complexes are insoluble in water except the magnesium complex. The complexes

Table 1. Chemical analyses and magnetic moments of $[M(N_2H_4)_2(NCS)_2]$.

$[M(N_2H_4)_2(NCS)_2]$ M(II)=	Colour	μ_{eff}(BM) 23° C		%Metal		$\%N_2H_4$		%NCS	
		Found	Calc. for spin only formula	Found	Calc.	Found	Calc.	Found	Calc.
Mn	White	5.87	5.91	23.24	23.38	26.98	27.25	49.84	49.37
Fe	White	4.91	4.89	23.33	23.68	27.73	27.14	48.25	49.18
Co	Pink	4.70	3.87	24.62	24.66	27.25	26.79	47.96	48.55
Ni	Blue	2.82	2.82	25.14	24.59	26.73	26.81	48.11	48.60
Zn	White	–	–	26.70	26.64	25.65	26.09	48.33	47.27
Cd	White	–	–	38.21	38.44	22.20	21.89	40.40	39.67
Mg	White	–	–	11.86	11.90	31.33	31.32	57.08	56.78

Table 2. Infrared spectra and the probable assignments for $[M(N_2H_4)_2(NCS)_2]$.

Mn	Fe	Co	Ni	Zn	Cd	Mg	Assignments
3222 s	3315	3308	3320	3328	3323	3332	
3300 s	3295	3290	3308	3304	3300	3312	
3215 s	3200	3200	3220	3212	3238	3224	N-H stretchings
3150 w	3135	3140	3142	3138	3155	3165	
2088 s	2070	2068	2092	2075	2070	2084	C-N stretchings
2024 sh	2010	2020	2024	2025	2020	2030	
1605 sh	1603	1600	1607	–	1588	1607	
1593 s	1590	1586	1593	1597	1587	1593	NH_2 bending
1580 s	1572	1568	1573	1578	1578	1573	
1558 sh	1558	–	1560	–	–	1560	
1409 sh	–	1418	1410	–	–	1410	
1364 sh	1368	–	1368	1368	1368	1350	
1339 m	1340	1338	1342	1342	1342	1313	NH_2 wagging
1296 m	1300	1302	1310	1306	1294	1310	
1174 m	1183	1191	1206	1189	1164	1195	
1140 s	1150	1152	1164	1153	1140	1156	NH_2 twisting
960 sh	–	–	–	–	–	974	
951 s	960	965	975	958	960	963	N-N stretching
941 sh	–	945	–	–	936	–	
793 m	796	794	795	792	788	802	C-S stretching
569 s	582	595	619	600	580	586	NH_2 asym rocking
494 s	515	539	575	536	502	523	NH_2 sym rocking
479 s	480	480	478	482	477	489	NCS bending
471 s	473	472	468	468	468	482	
460 sh	–	435	–	–	–	–	
330 m	354	367	395	354	335	383	M-N (of N_2H_4) stretching
312 sh	331	342	362	315	300	343	M-N (of NCS) stretching

Note: s-strong, w-weak, sh-shoulder and m-medium

prepared by both the methods are identical. The transition metal complexes are of high spin type, showing that hydrazine and thiocyanate are weak ligands. These values are in good agreement with those reported earlier. (Anagnaostopoulus and Nicholls 1976; Aggarwal and Vallabhaneni 1978).

3.1 *Bonding and structure of the complexes*

The infrared spectra of all the metal complexes are closely similar (table 2). The probable assignments of the frequencies are made on the basis of the comparison with earlier studies on hydrazine (Braibanti *et al* 1968; Sacconi and Sabatini 1963) as well as thiocyanate (Norbury 1975; Burmeister 1972) complexes. The thiocyanate is bonded to the metal through N-atom, as evidenced from the characteristic ν_{CN}, $\nu_{C\text{-}S}$ and δ_{NCS} around 2075, 790 and 480 cm^{-1} respectively. The N-N stretching frequency is observed around 960 cm^{-1} indicating the presence of hydrazine bridging between the two metal ions (Braibanti *et al* 1968). The metal-nitrogen stretching frequencies, $\nu_{M\text{-}N}$ of hydrazine and $\nu_{M\text{-}N}$ of thiocyanate are observed around 400 and 350 cm^{-1} respectively. The $\nu_{M\text{-}N}$ of hydrazine is almost of double intensity as that of $\nu_{M\text{-}N}$ of NCS, supporting the assignments since the NH_2:NCS ratio is 2:1 in these complexes. Further, since the two $\nu_{M\text{-}N}$ frequencies are observed, it shows that the bond strength of M-N of NCS is slightly lower than that of M-N of N_2H_4, suggesting that the molecular symmetry around the metal ion is not perfect octahedral, but a distorted one and the molecule is axially compressed. The molecular symmetry around the metal ion is therefore, D_{4h}. The IR assignments are in good agreement with the proposed polymeric structure (Ferrari *et al* 1961) as given below:

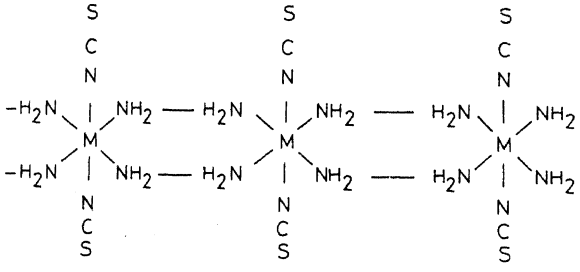

The Mössbauer spectrum of $[Fe(N_2H_4)_2(NCS)_2]$ shows a two-finger pattern with the isomer shift (IS) value of 1.03 mm sec^{-1} and the quadrupole splitting (QS) value of 1.54 mm sec^{-1}. The observed values indicate the presence of high spin Fe^{2+} in distorted octahedral environment (Bancroft and Platt 1972) and are comparable with those of $[Fe(IQ)_4(NCS)_2]$, where IQ = isoquinoline (C.S. = 1.37 mm sec^{-1} and QS = 1.50 mm sec^{-1}) and $[Fe(Py)_4(NCS)_2]$ (C.S., = 1.35 mm sec^{-1} and QS = 1.54 mm sec^{-1}).

3.2 *Thermal decomposition of* $[M(N_2H_4)_2(NCS)_2]$

The results of TG and DTA studies both in air and nitrogen atmospheres are summarized in tables 3 and 4 respectively. Both Mn(II) and Zn(II) complexes decompose to the corresponding metal isothiocyanates in the temperature range of 190–250° C with the loss of two molecules of hydrazine, producing nitrogen and ammonia which were identified by mass spectra. The solid intermediates were found to be metal isothiocyanates from the observed weight loss, qualitative tests and the IR spectra (ν_{CN} of NCS,

Table 3. Thermal decomposition of $[M(N_2H_4)_2(NCS)_2]$ in nitrogen.

$[M(N_2H_4)_2(NCS)_2]$	DTA peak temp. °C	TG Temp. region °C	% wt loss		Proposed reaction products
			Obsd.	Calcd.	
$[Mn(N_2H_4)_2(NCS)_2]$	197(+)	190–250	27.20	27.25	$Mn(NCS)_2$
	–	530–620	62.50	63.00	MnS
$[Fe(N_2H_4)_2(NCS)_2]$	218(+)	200–230	39.00	40.72	$Fe(NCS)_2^+$ $Fe(CN)_2$ or Fe(NCS) (CN)
	–	440–550	62.50	62.76	FeS
$[Co(N_2H_4)_2(NCS)_2]$	222(+)	215–260	39.21	40.19	$Co(NCS)_2$+ $Co(CN)_2$ or Co(NCS)(CN)
	334(+)	370–500	62.90	62.00	CoS
$[Ni(N_2H_4)_2(NCS)_2]$	240(+)	230–280	41.80	40.24	$Ni(NCS)_2$+ $Ni(CN)_2$ or Ni(NCS)(CN)
	–	–	–	62.02	NiS*
$[Zn(N_2H_4)_2(NCS)_2]$	198(−)				
	204(+)	195–240	25.00	26.08	$Zn(NCS)_2$
	–	450–600	58.70	60.33	ZnS
$[Cd(N_2H_4)_2(NCS)_2]$	207(+)	190–270	29.30	32.85	$Cd(NCS)_2$+ $Cd(CN)_2$ or Cd(NCS)(CN)
	–	450–650	50.00	50.63	CdS
$[Mg(N_2H_4)_2(NCS)_2]$	264(+)	230–360	47.00	47.00	$Mg(NCS)_2$+ $Mg(CN)_2$ or Mg(NCS)(CN)
	–	360–480	72.50	72.44	MgS

*The final product was identified to be NiS by qualitative analysis.
(+) exotherm and (−) endotherm

2060 and 2070 cm^{-1} respectively for Mn(II) and Zn(II) complexes). The thermal decomposition can, therefore, be represented as follows:

$$3[M(N_2H_4)_2(NCS)_2] \xrightarrow{190\text{–}250^\circ C} 3M(NCS)_2 + 8NH_3 + 2N_2 \quad (4)$$

The decomposition is more or less, similar to that of $[M(Py)_4(NCS)_2]$ (Liptay *et al* 1969a,b).

The metal(II) isothiocyanate formed as an intermediate further decomposes to the corresponding metal sulphide in the temperature range of 450-620° C according to the equation (Bell and Morcom 1979).

$$M(NCS)_2 \rightarrow MS + (CN)_2 + S \quad (5)$$

The observed weight loss corresponds to the formation of the corresponding metal sulphide (table 3). In air, the metal sulphides were oxidized forming the sulfate or oxide or their mixture depending on the metal ions (table 4). For example, $Zn(NCS)_2$ is oxidised directly to zinc oxide whereas $Mn(NCS)_2$ decomposes to Mn(NCS) (CN) at

Table 4. Thermal decomposition of $[M(N_2H_4)_2(NCS)_2]$ in Air

$[M(N_2H_4)_2(NCS)_2]$	DTA peak	TG temp.	% wt loss Obsd.	Calcd.	Proposed
$[Mn(N_2H_4)_2(NCS)_2]$	197(+)	180–250	27.26	27.25	$Mn(NCS)_2$
	503(+)	400–550	40.20	40.88	Mn(SCN)(CN)
	–	560–640	48.85	48.89	$2MnSO_4.Mn_2O_3$
$[Me(N_2H_4)_2(NCS)_2]$	173(+)	150–180	39.30	40.72	Fe(NCS)(CN)
	450(+)	350–500	–	66.18	Fe_2O_3*
$[Co(N_2H_4)_2(NCS)_2]$	190(+)	180–220	40.60	40.20	Co(NCS)(CN)
	443(+)	380–530	50.0	55.29	$CoSO_4.Co_2O_3$
$[Ni(N_2H_4)_2(NCS)_2]$	226(+)	220–280	39.20	40.29	Ni(NCS)(CN)
	485(+)	410–550	54.82	55.00	$NiO+NiSO_4$
$[Zn(N_2H_4)_2(NCS)_2]$	189(−)				
	198(+)	190–260	25.00	26.08	$Zn(NCS)_2$
	503(+)	550–900	67.30	66.87	ZnO
$[Cd(N_2H_4)_2(NNS)_\pi]$	203(+)	190–270	29.30	32.85	Cd(NCS)(CN)
	485(+)	450–650	49.00	50.60	CdS
$[Mg(N_2H_4)_2(NCS)_2]$	261(+)	230–360	47.00	47.00	Mg(NCS)(CN)
	–	360–500	72.50	72.44	MgS
	–	500–650	79.50	80.39	MgO

*The final residue was found to be Fe_2O_3 by qualitative analysis.
(+) exotherm and (−) endotherm

400–550° C and finally to a mixture of $MnSO_4$ and Mn_2O_3 in the temperature range of 560–640° C.

The iron(II), cobalt(II), nickel(II), cadmium(II) and magnesium(II) complexes decompose in a different way from those of Zn(II) and Mn(II) complexes. The weight loss does not correspond to the formation of metal isothiocyanate alone (table 3). But the intermediate residues contain thiocyanate as evidenced by qualitative tests and IR spectra. The intermediate solid product does not show the presence of sulphide, but the gaseous products of thermal decomposition contained H_2S. The intermediate formed at 230–360° C by the thermal decomposition of magnesium complex showed bands at 2200 and 2080 cm^{-1} corresponding to M-CN and M-NC of NCS respectively. Similarly, cadmium complex intermediate also shows bands at 2320 and 2035 cm^{-1}. On the basis of these observations, the intermediate of thermal decomposition of iron, cobalt, nickel, cadmium and magnesium complexes could be given as M(NCS)(CN) which subsequently decomposes slowly at higher temperature (~350 to 650° C) to the respective metal sulphides.

In air, the intermediate Fe(NCS)(CN) is oxidized to Fe_2O_3 while Mg(NCS)(CN) and Cd(CNS) decompose to the corresponding metal sulphides. Magnesium sulphide is further oxidized to magnesium oxide in air. The nickel and cobalt intermediates are oxidized to a mixture of the corresponding sulfate and oxide (table 4).

3.3 *Stability of the complexes*

The stability of the co-ordination compounds is usually determined from the strength of the metal ligand bonds. The NH_2 twisting, symmetric and asymmetric rocking, N-N stretching of N_2H_4, and M-N stretching of both M-NCS and M-N_2H_4 of the complexes (table 2) follow the Irving-Williams order of stability of the bivalent metal complexes

i.e. $Mn^{2+} < Fe^{2+} < Co^{2+} < Ni^{2+} > Zn^{2+} > Cd^{2+}$. A similar order was reported by Sacconi and Sabatini (1960; 1963) for $[M(N_2H_4)_2Cl_2]$.

The DTA peak temperature or the TG inception temperature of decomposition, in general, can be taken as a measure of the thermal stability of the metal complexes. The data in table 3 indicate the thermal stability order of $[M(N_2H_4)_2(SCN)_2]$ as $Mn^{2+} < Fe^{2+} < Co^{2+} < Ni^{2+} > Zn^{2+} > Cd^{2+}$. Thus, there appears to be a correlation between thermal stability and M-N of N_2H_4 or NCS bond strength.

References

Anagnaostopoulus A and Nicholls D 1976 *J. Inorg. Nucl. Chem.* **38** 615
Aggarwal R C and Vallabhaneni C S 1978 *Trans. Met. Chem.* **3** 309
Bancroft G M and Platt R H 1972 *Adv. Inorg. Radiochem.* **15** 59
Bell C F and Morcom R E 1979 *J. Therm. Anal.* **17** 7
Braibanti A I, Dallavalle F, Phellinghelli H A and Leporati E 1968 *Inorg. Chem.* **7** 1430
Burmeister J 1972 *Coordn. Chem. Rev.* **6** 407
Duval C 1967 *Inorganic thermogravimetric analysis* (New York: Elsevier) 2nd ed p. 336
Ferrari A, Braibanti A and Lanfredi A M 1961 *Gazz. Chim. Ita.* **4** 189
Liptay G, Papp-Molnar E and Burger K 1969a *J. Inorg. Nucl. Chem.* **31** 247
Liptay G, Burger K, Papp-Molnar E, Szobeni S and Ruff F 1969b *J. Inorg. Nucl. Chem.* **32** 2359
Norbury A H 1975 *Adv. Inorg. Radiochem.* **17** 232
Patil K C, Gajapathy D and Kishore K 1982a *Thermochim. Acta* **52** 113
Patil K C, Nesamani C and Pai Verneker V R 1982 *Synth. React. Inorg. Met. Org. Chem.* **12** 383
Ray P and Sarkar P V 1920 *J. Chem. Soc.* **117** 321
Sacconi L and Sabatini A 1960 *Nature (London)* **186** 549
Sacconi L and Sabatini A 1963 *J. Inorg. Nucl. Chem.* **25** 1389
Savant V V and Patel C C 1968 *Indian J. Technol.* **6** 231
Srivastava A K, Varshney A L and Jain P C 1980 *J. Inorg. Nucl. Chem.* **42** 47
Vogel A I 1951 *A text-book of quantitative inorganic analysis* (London: Longmans Green) p. 365

Proc. Indian Acad. Sci. (Chem. Sci.), Vol. 92, No. 1, January 1983, pp. 91–97.
© Printed in India.

Polarographic study of mixed ligand complexes: Pb(II)-succinate-imidazole system

MADHU SHIVHARE and MUKHTAR SINGH*
Department of Chemistry, Agra College, Agra 282 002, India.

MS received 12 January 1981; revised 23 April 1981

Abstract. The mixed ligand complexes of succinate ($Succ^{2-}$) and Imidazole (Im) with Pb(II) have been studied polarographically at constant ionic strength, $\mu = 2.0$ ($NaNO_3$) and at pH 6. The system has been studied at constant temperature, $25 \pm 0.1°$ C. The reduction of the complexes at dropping mercury electrode is reversible and diffusion-controlled. Three mixed complexes, *viz.*, $[Pb(Succ)(Im)]$: $[Pb(Succ)(Im)_2]$ and $[Pb(Succ)_2(Im)]^{2-}$ are formed.

Keywords. Polarographic study; mixed ligand complexes; succinate imidazole system.

1. Introduction

In the previous publication (Madhu and Mukhtar Singh 1981a,b,c) polarographic studies on simple and mixed complexes of Cd(II) with imidazole and tartrate, melonate and succinate have been reported. A survey of literature reveals that polarographic studies of the complexes of Pb(II) except Pb(II) succinate system (Gaur and Palrecha 1968) with imidazole have not been undertaken so far. But so far no polarographic study of mixed complexes of Pb(II) with imidazole and succinate ions has been made. With this aim in view a polarographic study of Pb(II)-imidazole-succinate system has been undertaken at a constant ionic strength, $\mu = 2.0$ ($NaNO_3$) and pH 6.

2. Materials and methods

All the chemicals used were of analytical reagent grade and their solutions were prepared in conductivity water. The ionic strength was maintained constant at $\mu = 2.0$ ($NaNO_3$). Imidazole and potassium succinate were used as ligands. The concentration of Pb(II) was kept at 1×10^{-3} M. Polarograms were obtained by means of a manual polarograph (Toshniwal CL 02) in conjunction with Toshniwal polyflex galvanometer (PL 50). Purified nitrogen was used for removing the dissolved oxygen. All the measurements were made at $25 \pm 0.1°$ C. Saturated calomel electrode (SCE) was used as reference electrode. The dme had the following characteristics (0.1 M $NaNO_3$, open circuit): $m = 1.5$ mg/sec, $t = 2.7$ sec, $m^{2/3}\, t^{1/6} = 1.55$ $mg^{2/3}$ $sec^{-1/2}$, $h_{corr} = 52$ cm.

3. Results and discussion

The reduction of Pb(II) in succinate and imidazole media, separately, was found to be reversible and diffusion-controlled. The same was true in the case of the mixed

* To whom all correspondence should be made.

system. The slopes on the linear plots of log i/i_d-i *vs* $E_{d.e.}$ were of the order of 30 mV and the plots of i_d *vs.* h_{corr} were linear and passed through the origin.

As imidazole (Im) (structure: 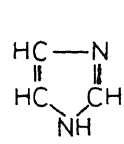)

is a base, it gets protonated in aqueous medium according to the following equilibrium:

$$Im + H_2O \rightleftharpoons ImH^+ + OH \quad (1)$$

Since hydrogen bound(protonated) base does not enter into complexation, the amount of the "free base" (*i.e.* unprotonated) only has to be taken for the concentration of the ligand. This can be calculated from the pH and pK_a value of the base as per the following equilibrium:

$$ImH^+ \rightleftharpoons Im + H^+ \quad (2)$$

$$K_a = \frac{[Im]\ [H^+]}{[ImH^+]}$$

or

$$\log\ [Im] = \log\ [ImH^+] + pH - pK_a$$

The pK_a value of imidazole at $25 \pm 0.1°$ C and at $\mu = 2.0$ ($NaNO_3$) has been determined by the titration method using glass electrode (Chaberek and Martell 1953). This worked out to be 7.09.

3. Pb(II)-succinate and Pb(II)-imidazole systems

The stability constants of simple complexes of Pb(II) with succinate and imidazole were determined separately prior to the study of mixed ligand system. Identical conditions were maintained in both the simple and mixed systems.

A plot of $E_{1/2}$ *vs* log [$Succ^{2-}$] and *vs* log [Im] (figure 1) gave smooth curves thereby showing the formation of successive complexes. DeFord and Hume's

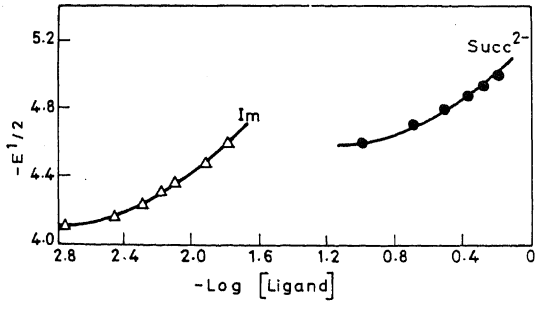

Figure 1. Plots of $E_{1/2}$ *vs.* log[$Succ^{2-}$] and log[Im] for Pb(II)-succinate and imidazole systems.

Table 1. Pb(II)-succinate system.
$[Pb^{2+}] = 1 \times 10^{-3}$ M; $\mu = 2.0$ ($NaNO_3$); pH 6; Temp. $25 \pm 0.1°$ C

$[Succ^{2-}]$ M	$-E_{1/2}$ V (SCE)	i_d div	$F_0[X]$	$F_1[X]$ x10^{-2}	$F_2[X]$ x10^{-4}	$F_3[X]$ x10^{-6}
0.00	0.400	100	–	–	–	–
0.10	0.460	90	119.30	11.83	–	–
0.20	0.470	89	263.10	13.10	40.52	7.76
0.30	0.480	88	580.10	19.30	47.66	7.55
0.40	0.488	87	1095.00	27.35	55.85	7.71
0.50	0.494	85	1788.00	35.74	61.48	7.29
0.60	0.500	85	2855.00	47.56	70.93	7.60

Table 2. Pb(II)-imidazole system.
$[Pb^{2+}] = 1 \times 10^{-3}$ M; $\mu = 2.0$ ($NaNO_3$); pH 6; Temp. $= 0.1°$ C

[Im] (Free ligand) M	$-E_{1/2}$ V (SCE)	i_d div	$F_0[X]$	$F_1[X]$ x10^{-2}	$F_2[X]$ x10^{-4}	$F_3[X]$ x10^{-6}
0	0.400	100	–	–	–	–
0.0016	0.411	90	2.61	–	–	–
0.0032	0.416	86	4.04	9.50	4.68	–
0.0047	0.423	85	7.06	12.89	10.40	–
0.0064	0.430	85	12.20	17.50	14.84	2.00
0.0079	0.436	83	19.93	23.96	20.20	2.33
0.0120	0.448	82	51.41	42.00	28.33	2.19
0.0162	0.458	81	113.40	69.38	37.08	2.21

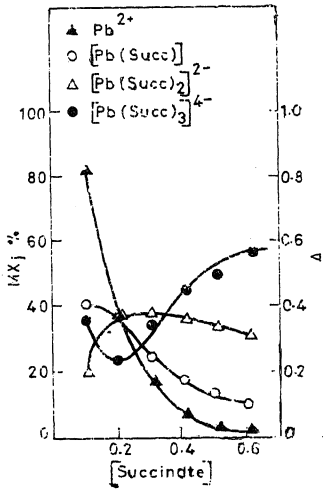

Figure 2. Percentage distribution of Pb(II) in its various forms as a function of [Succinate^{2-}]

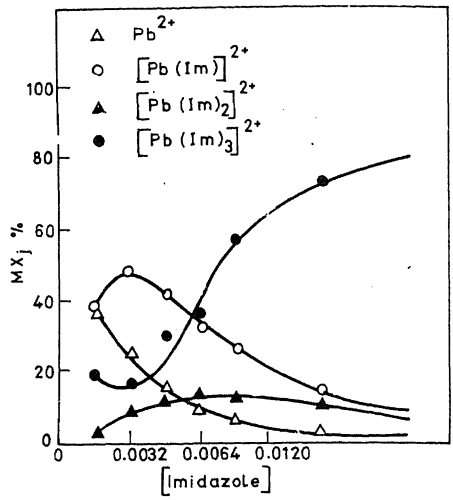

Figure 3. Percentage distribution of Pb(II) in its various forms as a function of [Im].

(1951) method has been applied to determine the stability constants of the successive complexes. The polarographic characteristics and $F_i[X]$ and $F_j[X]$ functions of Pb(II)- succinate and Pb(II)-imidazole systems have been presented in tables 1 and 2. Pb(II) forms three complexes with both the ligands. These are: [Pb(Succ)], $[Pb(Succ)_2]^{2-}$ and $[Pb(Succ)_3]^{4-}$ with stability constants $\log \beta_{10} = 2.7$, $\log \beta_{20} = 3.4$ and $\log \beta_{30} = 3.9$; and $[Pb(Im)]^{2+}$, $[Pb(Im)_2]^{2+}$ and $[Pb(Im)_3]^{2+}$ with stability constants $\beta_{01} = 2.90$, $\log \beta_{02} = 4.30$ and $\log \beta_{03} = 6.30$. The percentage distribution of Pb(II) in its various forms as a function of $[Succ^{2-}]$ and [Im] has been presented in figures 2 and 3.

3.2 *Pb(II)-succinate-imidazole system*

$[Succ^{2-}]$ was varied from 0–0.6 M [Im] was kept constant at 0.0032 M. It was found that the $E_{1/2}$ values were more negative than those obtained in the absence of imidazole thereby showing the formation of mixed complexes. The system was repeated at another concentration of imidazole (0.0064 M). The method of Schaap and McMasters (1961) was applied to determine the values of the stability constants of mixed complexes. The polarographic characteristics and $F_{ij}[X, Y]$ functions of the system have been presented in table 3. From the plots of F_{ij} data *vs* $[Succ^{2-}]$ (representative figure 4 for series 1) the following intercept values of constants (Crow 1963) A, B, C and D have been obtained which involve an error of ±0.5%. For series 1: $\log A = 0.7$, $\log B = 2.9$, $\log C = 3.8$ and $\log D = 3.9$. For series 2: $\log A = 1.3$, $\log B = 3.1$, $\log C = 3.9$ and $\log D = 4.1$.

The stability constants of the mixed complexes have been determined from the values of A, B, C and D. Three mixed complexes, *viz* [Pb(Succ)(Im)], [Pb(Succ)(Im)$_2$] and $[Pb(Succ)_2(Im)]^{2-}$ with stability constants $\log \beta_{11} = 4.9$ $\log \beta_{12} = 6.7$ and $\log \beta_{21} = 6.0$ respectively are formed. The mixing constant K_M (equilibrium constant) for the reaction:

$$1/2[Pb(Im)_2]^{2+} + 1/2[Pb(Succ)_2]^{2-} \rightleftharpoons [Pb(Succ)(Im)] \qquad (5)$$

indicates the relative stability of mixed complexes in solution as compared to paren

Table 3. Values of $F_{ij}[X,Y]$ functions for Pb(II)-succinate-imidazole system.

$[Succ^{2-}]$ M	$-E^{1/2}$ V (SCE)	i_d div.	$F_{00}[X,Y]$	$F_{10}[X,Y]$ x10^{-2}	$F_{20}[X,Y]$ x10^{-3}	$F_{30}[X,Y]$ x10^{-3}
Series 1 - Concentration of Imidazole, [Im] = 0.0032 M						
0.00	0.400	100	–	–	–	–
0.05	0.455	88	82.64	15.52	–	–
0.10	0.463	86	157.80	15.28	72.50	–
0.20	0.477	84	480.90	23.54	77.70	8.85
0.30	0.487	84	1053.00	34.94	89.76	8.92
0.40	0.494	83	1831.00	45.65	94.12	8.53
0.50	0.500	82	2959.00	59.08	102.16	8.43
0.60	0.505	81	4423.00	73.65	109.38	8.23
Series 2 - Concentration of Imidazole, [Im] = 0.0064 M						
0.00	0.400	100	–	–	–	–
0.50	0.460	85	126.20	21.64	–	–
0.10	0.467	81	228.80	20.88	88.80	–
0.20	0.480	82	625.50	30.27	91.35	–
0.30	0.490	81	1374.00	45.13	110.43	11.80
0.40	0.496	80	2095.00	64.37	130.92	13.98
0.50	0.504	80	4143.00	78.86	133.72	11.74
0.60	0.509	78	6273.00	101.20	148.66	12.27

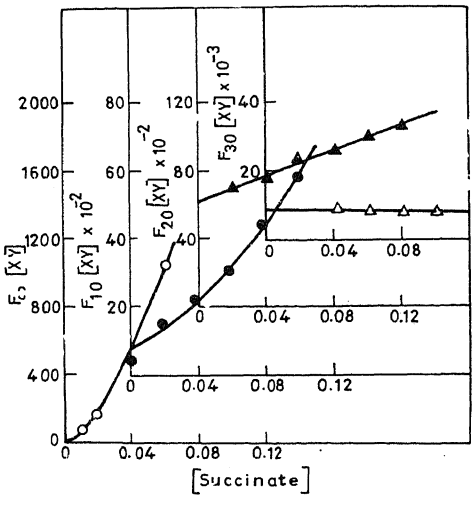

Figure 4. Plots of $F_{ij}[X,Y]$ *vs* [Succinate^{2-}] for Pb(II)-succinate-imidazole system.

binary complexes, this is given by

$$\log K_M = \log \beta_{11} - 1/2 \, (\log \beta_{02} + \log \beta_{20})$$

The value of log K_M works out to be +1.1 for the reaction (5). The positive value of log K_M shows that the mixed complex [Pb(Succ)(Im)] is more stable than the simple binary complexes, $[Pb(Succ)_2]^{2-}$ and $[Pb(Im)_2]^{2+}$.

Table 4. Equilibria involved in three mixed complexes and equilibrium constant (K) values.

Equilibria		log K at 25° C
1.	$Pb^{2+} + Succ^{2-} + Im \rightleftharpoons [Pb(Succ)(Im)]$	4.9
2.	$Pb^{2+} + Succ^{2-} + 2Im \rightleftharpoons [Pb(Succ)(Im)_2]$	6.7
3.	$Pb^{2+} + Succ^{2-} + Im \rightleftharpoons [Pb(Succ)_2(Im)]^{2-}$	6.0
4.	$[Pb(Succ)(Im)] + Im \rightleftharpoons [Pb(Succ)(Im)_2]$	1.8
5.	$[Pb(Succ)(Im)] + Succ^{2-} \rightleftharpoons [Pb(Succ)_2(Im)_2]^{2-}$	1.1
6.	$[Pb(Succ)_2(Im)]^{2-} + Im \rightleftharpoons [Pb(Succ)(Im)_2] + Succ^{2-}$	0.7
7.	$[Pb(Succ)] + Im \rightleftharpoons [Pb(Succ)(Im)]$	2.2
8.	$[Pb(Succ)_2]^{2-} + Im \rightleftharpoons [Pb(Succ)_2(Im)_2]^{2-}$	2.6
9.	$[Pb(Succ)] + 2Im \rightleftharpoons [Pb(Succ)(Im)_2]$	2.6
10.	$[Pb(Im)]^{2+} + Succ^{2-} \rightleftharpoons [Pb(Succ)(Im)]$	2.0
11.	$[Pb(IM)]^{2+} + 2Succ^{2-} \rightleftharpoons [Pb(Succ)_2(Im)]$	3.1
12.	$[Pb(Succ)_2]^{2-} + Im \rightleftharpoons [Pb(Succ)_2(Im)] + Succ^{2-}$	1.5
13.	$[Pb(Succ)_3]^{4-} + Im \rightleftharpoons [Pb(Succ)_2(Im)]^{2-} + Succ$	2.1
14.	$[Pb(Im)_2]^{2+} + 2Succ^{2-} \rightleftharpoons [Pb(Succ)_2(Im)]^{2-} + Im$	1.7

Disproportionation constant ($\Delta \log K$) for the equilibria:

$$2\ [Pb(Succ)(Im)] \rightleftharpoons [Pb(Succ)_2]^{2-} + [Pb(Im)_2]^{2+} \quad (6)$$

$$2\ [Pb(Succ)(Im)_2] \rightleftharpoons [Pb(Succ)_2]^{2-} + [Pb(Im)_2]^{2+} + 2Im \quad (7)$$

$$2\ [Pb(Succ)_2(Im)] \rightleftharpoons [Pb(Succ)_2]^{2-} + [Pb(Im)_2]^{2+} + Succ^{2-} \quad (8)$$

works out to be -2.1, -5.7 and -4.3 respectively. The positive value of $\Delta \log K$ for (6) shows that the mixed complex species, [Pb(Succ)(Im)] is less stable than the simple binary complexes, $[Pb(Succ)_2]^{2-}$ and $[Pb(Im)_2]^{2+}$. On the other hand negative values of $\Delta \log K$ for equilibrium (6)(7) (Bidkar *et al* 1977) show that the mixed species [Pb(Succ) (Im)], [Pb(Succ)(Im)$_2$] and $[Pb(Succ)_2(Im)]^{2-}$ are more stable than the simple binary complexes, $[Pb(Succ)_2]^{2-}$ and $[Pb(Im)_2]^{2+}$.

Pb(II) is hexa coordinated. Three mixed complexes existing in solution have the following equilibria (table 4). The equilibrium constants (log K values) have been calculated and written in front of each equilibrium.

From the equilibrium constant values, the relative tendency of $Succ^{2-}$ and Im to add to the mixed complex species, [Pb(Succ)(Im)] can be compared. It is seen that Im adds readily to [Pb(Succ)(Im)] as compared to $Succ^{2-}$ (equilibria 4 and 5). It is also seen that Im can replace $Succ^{2-}$ from the mixed complex, $[Pb(Succ)_2(Im)]^{-}$ Equilibria 10, 11, 12 and 13 indicate that complexing tendency of Im is much more than $Succ^{2-}$.

The stability of three mixed complexes as seen from their overall stability constants follows the order:

$$[Pb(Succ)(Im)_2] > [Pb(Succ)_2(Im)]^{2-} > [Pb(Succ)(Im)]$$

4. Conclusion

Pb(II) can be determined polarographically in the presence of both $Succ^{2-}$ and imidazole.

Acknowledgement

The award of a senior research fellowship by CSIR, New Delhi, to one of the authors (MS) is gratefully acknowledged.

References

Madhu Shivhare and Singh M 1981a *J. Inorg. Nucl. Chem.* **43** 1599
Madhu Shivhare and Singh M 1981b *J. Inorg. Nucl. Chem.* **43** 2885
Madhu Shivhare and Singh M 1981 *J. Electrochem. Soc. India* **30** 277
DeFord D D and Hume D N 1951 *J. Am. Chem. Soc.* **73** 5321
Schaap W B and McMaster D L 1961 *J. Am. Chem. Soc.* **83** 4699
Crow D R 1969 *Polarography of Metal Complexes* (New York: Academic Press) p. 70
Bidkar R G, Dhuley D G and Bhobe R A 1977 *Indian J. Chem.* **A15** 63
Gaur J N and Palrecha M M 1968 *Talanta* **17** 593
Chaberek S and Martell A E 1953 *J. Am. Chem. Soc.* **75** 1430

Proc. Indian Acad. Sci. (Chem. Sci.), Vol. 92, No. 1, January 1983, pp. 99–106.
© Printed in India.

Addition products of dimethyl acetylenedicarboxylate to thioureas—studies on 2-(*p*-bromophenyl) imino-3-methyl-5-carbomethoxymethylidenethiazolidin-(4)-one†

K NAGARAJAN*, M D NAIR, S J SHENOY and G KARTHA**
CIBA-GEIGY Research Centre, Bombay 400 063, India
**Roswell Park Memorial Institute, Buffalo, New York 14263, USA

MS received 27 September 1982

Abstract. N-(*p*-bromophenyl)-N′-methylthiourea (1) undergoes addition to acetylenedicarboxylic acid (3) and its dimethyl ester (4) to form 2-(*p*-bromophenyl) imino-3-methyl-5-carboxymethylidenethiazolidin-(4)-one (5) and its methyl ester (6) respectively. Alkaline hydrolysis of (6) leads to a mixture of (5) and 2-(*p*-bromophenyl) imino-3,4-dihydro-3-methyl-4-oxo-2H (1,3)-thiazine-6-carboxylic acid (7). Several reactions of (5) and (7) are described. The structures of (5) and (7) are established by x-ray crystallographic and ^{13}C NMR studies.

Keywords. Thiazolidinone; thiourea; addition products; dimethyl acetylenedicarboxylate.

1. Introduction

Dinucleophiles like thioureas undergo facile regioselective, sometimes regiospecific addition to acetylenedicarboxylic esters. The structures of the products have been the subject of controversy (Vögeli *et al* 1978; Acheson and Wallis 1981), only a few having been solved by x-ray crystallographic studies (Cameron *et al* 1970; Adman *et al* 1975; Mckillop *et al* 1978). We have demonstrated earlier (Vögeli *et al* 1978; Nagarajan *et al* 1979) for the first time that ^{13}C NMR spectroscopy was ideally suited to provide satisfactory answers in this area, by studying the products from a number of dinucleophiles, mostly thioureas. In one case, *viz.* that of the addition product (6) of N-(*p*-bromophenyl-N′-methylthiourea) (1) and dimethylacetylenedicarboxylate (4), we had undertaken x-ray crystallographic studies as well. We wish to present in this paper results of these studies and incidental interesting chemical observations which demonstrated facile conversion of thiazolidones to thiazinones.

2. Addition of thiourea (1) to acetylenedicarboxylic acid derivatives to form thiazolidones (5) and (6)

The reaction of thiourea (1) with diester (4) provided the thiazolidinone (6) in 60% yield as slender, yellow needles. During attempts to grow crystals suitable for x-ray studies, nice crystals were obtained by the fortuitous use as solvent, of acetone

† Contribution No. 596 from CIBA-GEIGY Research Centre.
* To whom all correspondence should be made.

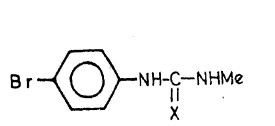

(1) X = S
(2) X = O

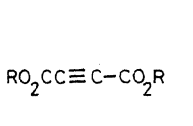

(3) R = H
(4) R = Me

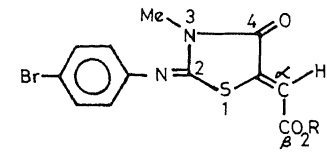

(5) R = H
(6) R = Me

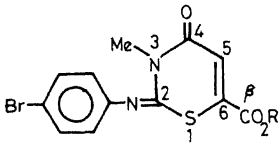

(7) R = H
(8) R = Me

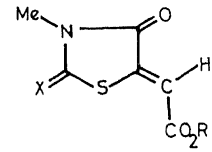

(9) X = O ; R = H
(10) X = MeN ; R = Me

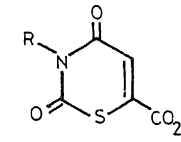

(11) R = Me
(12) R = p-Br-C_6H_4-

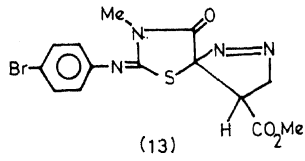

(13)

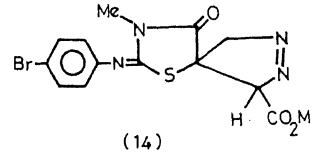

(14)

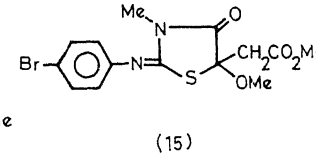

(15)

containing some dilute hydrochloric acid, but these turned out to be those of acid (5) corresponding to (6). Acid (5) was obtained directly from (1) in 70% yield by using acetylenedicarboxylic acid (3). Mild esterification of (5) employing stoichiometric amount of diazomethane afforded (6), while an excess of the reagent led to the formation of the pyrazoline (13), also obtained from (6) with excess diazomethane. Structure (13) was preferred to (14) for this product because of the appearance of signals in its ^{1}H NMR spectrum for the protons of a $-CH_2-CH-$ unit with appropriate chemical shifts. Treatment of (5) or (6) with hot hydrochloric acid in acetic acid resulted in the formation of 3-methyl-5-carboxymethylidene-thiazolidin-2,4-dione (9). This acid was also obtained by hot acid treatment of the thiazolidone (10) which was formed from N,N′-dimethylthiourea and diester (4). Rearrangement concomittant with acid hydrolysis to the thiazinone (11) had not happened, because in the ^{13}C NMR spectrum of (9), C-β was seen as a singlet, while C-2 was a quartet and C-4, a multiplet. Structure (11) would have required C-β to be a doublet with significant ($\sim$6Hz) $^3J_{CH}$ coupling (*vide infra*).

3. Alkaline hydrolysis of thiazolidone ester (6) to corresponding acid and thiazinone (7)

Interesting results were obtained when ester (6) was subjected to alkaline hydrolysis in dioxane solution. Brief treatment followed by acidification resulted in the formation of thiazolidone (5) and thiazinone (7) in nearly equal proportions. A small amount of urea (2) was also formed under these conditions, which was the sole product when hydrolysis was carried out for a longer period. The structures of (5) and (7) were established by single crystal x-ray crystallographic studies as shown later. Additional confirmation came from ^{13}C NMR spectral studies. In the carbonyl region, (6) had a

quartet for C-β due to coupling with methoxyl protons ($J = 4$ Hz) with further fine structure due to C-α H ($J = 1.1$ Hz), a multiplet for C-4, due to coupling with C-α H ($J = 5.3$ Hz) and N-CH_3 protons ($J = 2.6$ Hz). The signal due to C-4 in the analogous thiazolidone (10) was complex and was not amenable to first order analysis. But decoupling experiments allowed the extraction of the coupling constants with C-α H and N-methyl protons respectively as 6 and 2.8 Hz. In the ^{13}C NMR spectrum of acid (5), the splitting pattern seen for C-4 in (6) was retained, while C-β was a doublet ($^2J_{CH} = 1.2$ Hz). On the other hand, acid (7) exhibited a larger doublet for C-β, due to coupling with C-5 H ($^3J_{CH} = 6.3$ Hz) and 2 quartets for C-4 H, due to couplings with C-5 and N-methyl protons to 2.5 and 1.5 Hz respectively. The thiazinone structure of (7) was thus secure, although the 2 bond coupling of C-4 with C-5 H was larger than the ones we had seen for similar structures earlier.

4. Esterification of thiazinone carboxylic acid (7)

Mild esterification of (7) with diazomethane gave ester (8) which, despite its m.p. being identical with that of (6), was definitely different (mixed m.p. and spectral parameters). Unfortunately, its ^{13}C NMR spectrum did not show sufficient resolution in the C=O region (perhaps due to lack of adequate concentration). Treatment of (7) with hot acid removed the *p*-bromoaniline group to afford thiazinone (11), along with a small percentage of (12) formed presumably by rearrangement.

5. Alkali-promoted interconversion of 5 and 7

Surprisingly, although alkali induced a partial rearrangement of thiazinone (7) to thiazolidone (5) (NMR, isolation and identification), the latter did not suffer a similar transformation, being recovered totally under mild conditions or affording urea (2) under stress. It appeared possible that during alkali treatment, (6) partially isomerised to (8) by attack of the nucleophile at the lactam C=O group and cyclisation at the ester terminus. Addition of (1) to (4) in the presence of dry potassium hydroxide, 4-dimethylaminopyridine or a trace of sodium methoxide always led to (6), with no sign of formation of (8). Efforts to isomerise (6) at least partly to (8) using the above bases or insufficient quantity of aqueous alkali in methanol or dioxane were unsuccessful. In the presence of a larger quantity of sodium methoxide, (6) was partly transformed to (15) by the addition of methoxide to the unsaturated ester group at C-5 (NMR, mass). We are thus obliged to postulate that only in the presence of aqueous alkali (6) is isomerised to (8), which undergoes instant hydrolysis to (7).

6. Spectral studies on thiazolidones and thiazinones

The study provided us with pairs of thiazolidone and thiazinone derivatives (5) and (7), (6) and (8) and (9) and (11), for which UV, IR, ^{1}H and ^{13}C NMR and mass spectral data are presented in the experimental section. While there are differences between pairs, except by the use of ^{13}C NMR data, it appears doubtful whether an unambiguous structural assignment can be made when only one isomer is available. In the UV, the 2-iminothiazolidones (5), (6) and (10) had λ^{max} at 307–310 nm and the 2-oxoimidazolidinone (9) at 302 nm while the 2-iminothiazinones (7) and (8) showed

maxima at 271–275 nm and the 2-oxothiazinones (11) and (12) at 293 and 285 nm respectively. In the mass spectra of thiazolidinones (5) and (6) as also of the thiazinones (7) and (8), the radical ions due to N–(*p*-bromophenyl)–N′–methyl carbodimide (m/e 208, 210) were very prominent.

7. Conclusions

That study confirmed our earlier contention (Vögeli *et al* 1978) that the primary products of addition of thioureas and acetylene-dicarboxylic acid derivatives are thiazolidones, which may isomerise to thiazinones. Further thiazolidones and thiazinones of the type handled here tend to interconvert under alkaline and in some cases also under acidic conditions and structure assignments using chemical correlation have to be treated with caution.

8. X-ray crystallographic studies

Crystals of (5) and (7) were studied by single crystal x-ray diffraction methods. Both structures were solved by the heavy atom method and the atomic parameters refined by least squares techniques to the usual R index less than 6%. The structural and conformational details are shown in figures 1 and 2.

9. Experimental

M.p.s are uncorrected. UV spectra were recorded with a Beckman DK 2A spectrophotometer for solution in aqueous ethanol (95%). IR spectra were recorded on nujol mulls with Perkin-Elmer Infra cord and model 421 IR spectrophotometers. ^{1}H NMR

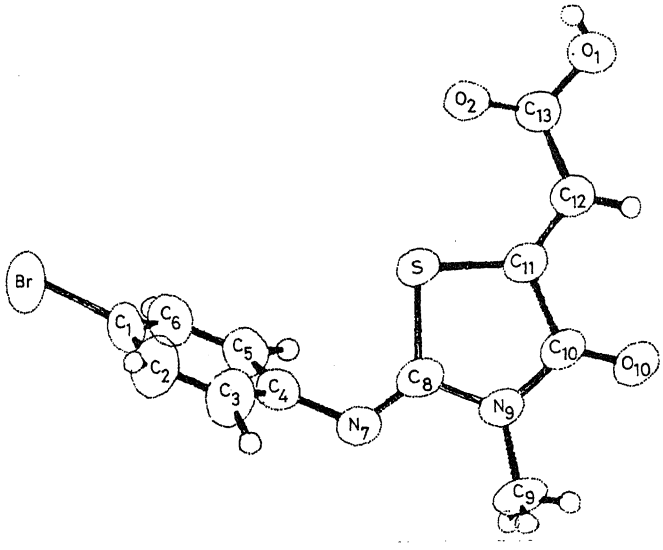

Figure 1. Crystal structure of 2-(*p*-bromophenyl-imino)-5-carboxymethylidenethiazolidin-4-one (5).

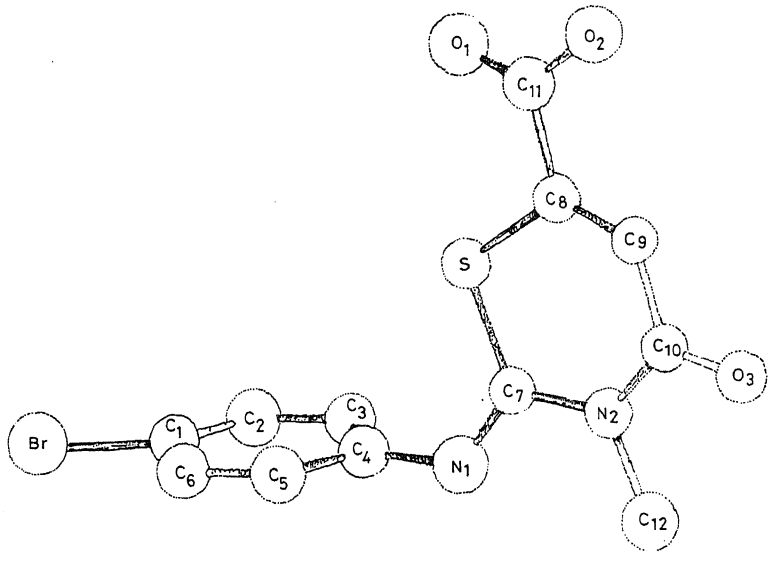

Figure 2. Crystal structure of 2-(*p*-bromophenyl-imino)-3,4-dihydro-3-methyl-4-oxo-2H-(1,3)-thiazine-6-carboxylic acid (7).

spectra were run on a Varian A60 or Bruker WH 90 spectrometer, with tetramethylsilane as internal standard. ^{13}C NMR spectra were obtained from the latter instrument at 22.63 MHz. Mass spectra were recorded with a Varian Mat CH 7 mass spectrometer. X-ray diffraction data were collected first on a manual GE XRD5 machine and later remeasured on an automated ENRAF Nonivus CAD4 diffractometer.

9.1 *2-(p-Bromophenylimino)-5-carbomethoxymethylidenethiazolidin-4-one (6)*

To a warm solution of N-(*p*-bromophenyl)-N′-methyl thiourea (1) (9.8 g, m.p. 145°, from *p*-bromoaniline and methylisothiocyanate in boiling benzene) in MeOH (70 ml) was added dimethyl acetylenedicarboxylate (4) (5.7 g). A yellow precipitate appeared within 15 minutes. The product was filtered off after 16 hr and recrystallized from acetone-MeOH to give (6) (8.6 g) as bright, yellow needles, m.p. 138–140° (Found: C, 43.81; H, 3.34; N, 7.95. $C_{13}H_{11}BrN_2O_3S$ requires C, 43.96; H, 3.12; N, 7.89%); λ_{max} 243, 308 nm (log ϵ 4.14; 4.16); γ 1730, 1650, 1620 cm^{-1}; ^{1}H NMR ($CDCl_3$): δ 7.48 (m, 2H, ArH); 6.91 (s, 1H, C–α.H), 6.85 (m, 2H, ArH); 3.81 (s, 3H, OMe), 3.42 (s, 3H, N–Me); ^{13}C NMR ($CDCl_3$): δ 165.8 (m, C–β); 164.4 (m, C–4); 118.2 (d, C–α), 52.4 (q, O$\underline{C}H_3$), 29.4 (q, N$\underline{C}H_3$); m/e at 356, 354 (M^+); 212, 210 (ArN=C=NCH_3)$^+$.

9.2 *2-(p-Bromophenylimino)-5-carboxymethylidenethiazolidin-4-one* (5)

An aqueous solution of diacid (3) (from 1.5 g of the monopotassium salt in 20 ml water and 4.5 ml of 2N HCl) was added to a warm solution of thiourea (1) (2.45 g) in MeOH (50 ml). An orange precipitate appeared 30 min. The mixture was set aside overnight and filtered to give acid (5) as orange crystals (2.4 g) (from MeOH–Et_2O), m.p. 216–220° (Found: C, 42.15; H, 2.81; N, 8.57; M^+ at m/e 340, 342. $C_{12}H_9BrN_2O_3S$ requires C, 42.25; H, 2.60; N, 8.21%; M, 340, 342).

9.3 *Alkaline hydrolysis of adduct* (6) *to* (5) *and* (7)

To a solution of (6) (3 g) in dioxane (20 ml) was added 10% aqueous NaOH (20 ml) with stirring. After 1 min, water (50 ml) was added and the clear solution was acidified to give a solid (2.3 g) which was essentially a mixture of the thiazolidone (5) and thiazinone (7) acids in the ratio of 6:5 (^{1}H NMR); m.p. 180–190°. Slow evaporation of an acetone solution and manual separation of orange and yellow crystals gave (5) and (7) respectively. A small amount of the urea (2) was also obtained as white crystals, m.p. and mixed m.p. with authentic sample, 216–8°, M^+ at m/e, 228, 230. This was the sole product when the hydrolysis was carried out for 1 hr.

Acid (5) (from acetone–Et_2O), m.p. 216–220° was identical with the earlier sample (Found: C, 42.50; H, 3.02; N, 8.52%); λ_{max} 245 (sh), 307 nm (log ϵ 4.23, 4.14); γ 1730, 1680, 1640, 1600 cm^{-1}; ^{1}H NMR ($CDCl_3$): δ 7.50 (m, 2H, ArH); 6.95 (s, 1H, C-α H); 6.85 (m, 2H, ArH); 3.43 (s, 3H, N-CH_3); ^{13}C NMR ($CDCl_3$ + DMSO-d_6), δ 167.1 (d, C-β); 165.0 (m, C-4); 122.7 (d, C-α); 29.2 (q, N-$\underline{C}H_3$); m/e 342, 340 (M^+), 212, 210 ($ArN{=}C{=}NCH_3)^+$.

Acid (7) (from acetone–Et_2O) had m.p. 177–80° (Found: C, 42.46; H, 3.03; N, 8.57%); λ_{max} 242 (sh), 275 nm (log ϵ 4.39, 4.04); γ 1700, 1620 cm^{-1}; ^{1}H NMR ($CDCl_3$), δ 7.47 (m, 2H, ArH); 7.17 (s, 1H, C-5H); 6.75 (m, 2H, ArH); 3.56 (s, 3H, N-CH_3); ^{13}C NMR ($C\underline{D}Cl_3$ + DMSO-d_6): δ 162.8 (d, C-β); 162.5(m, C-4); 121.1 (d, C-5); 30.6 (q, N-$\underline{C}H_3$); m/e at 342, 340 ($\underline{M}^+$), 298, 296 (M^+–CO_2), 212, 210 ($ArN{=}C{=}NCH_3)^+$.

9.4 *Reaction of acid* (5) *with diazomethane*

(i) Acid (5) (0.35 g, 1 mmole) in MeOH (5 ml) was treated with diazomethane (1 mmole) in Et_2O (10 ml) for 2 hr. The solvents were evaporated and the residue separated into the methyl ester (6) (0.15 g) and recovered acid (5) (0.1 g) by column chromatography over silica gel, (6) and (5) being eluted by $CHCl_3$ and $CHCl_3$–3% MeOH respectively. The ester thus obtained had m.p. 138–140° and was identical with the earlier sample (mixed m.p., tlc).

(ii) Acid (5) (0.15g) in MeOH (10 ml) was treated with excess diazomethane (from 5 g nitrosomethyl urea) in Et_2O (20 ml). After 16 hr, the solution was evaporated and the residue crystallized from CH_2Cl_2–hexane to give pyrazoline (13) (0.1 g) as white crystals, m.p. 115–117° identical with the sample below. (Found: N, 14.15. $C_{14}H_{13}BrN_4O_3S$ requires N, 14.11%).

9.5 *Pyrazoline* (13) *from ester* (6)

Ester (6) (0.5 g) in MeOH (10 ml) and CH_2Cl_2 (5 ml) was treated with excess diazomethane (from 5 g nitrosomethylurea) in Et_2O (20 ml) for 16 hr to afford pyrazoline (13) (0.5 g), white crystals (from Et_2O), m.p. 118–120°C (Found: C, 42.49; H, 3.63; N, 14.27. $C_{14}H_{13}BrN_4O_3S$ requires C, 42.33; H, 3.30; N, 14.11%); ν 1720, 1650; ^{1}H NMR ($CDCl_3$): δ 7.46 (m, 2H, ArH), 6.85 (m, 2H, ArH), 5.05 (d, J = 7Hz; CH_2); 3.68 (s, 3H, OCH_3); 3.62 (t, J = 7Hz, 1H, C$\underline{H}$-CO_2Me); 3.41 (s, 3H, NCH_3); m/e at 370, 368 ($M^+ - N_2$), 338, 336 (M^+–N_2–MeOH), 311, 309 (M^+–N_2–CO_2Me), 212, 210 ($ArN{=}C{=}NCH_3)^+$.

9.6 *Esterification of acid (7)*

Acid (7) (0.51 g, 1.5 mmole) in MeOH (5 ml) was treated with diazomethane (3 mmoles) in ether (20 ml) overnight. The ester (8) (60 mg) was obtained along with unreacted acid (0.15 g) and separated by chromatography on silica gel. Crystallisation from CH_2Cl_2–hexane gave pale yellow crystals of (8), m.p. 138–140°, which depressed the m.p. of (6) upon admixture (Found: C, 44.10; H, 3.30; N, 7.82%); λ_{max}243, 271 (log ϵ4.26, 4.08); γ 1720, 1685, 1620 cm^{-1}; ^{1}H NMR ($CDCl_3$) δ 7.49 (m, 2H, ArH), 7.13 (s, 1H, C–5H); 6.73 (m, 2H, ArH); 3.87 (s, 3H, OCH_3); 3.55 (s, 3H, N–CH_3); ^{13}C NMR ($CDCl_3$): δ 162.2 (m, C–β), 161.7 (m, C–4); 122.1 (d, C–5); 53.6 (q, O$\underline{C}H_3$); 30.9 (q, N–$\underline{C}H_3$); m/e at 356, 354 (M^+), 212, 210 (ArN=C=NMe)$^+$.

9.7 *Treatment of ester (6) with sodium methoxide*

Ester (6) (0.5 g) in MeOH (40 ml) containing sodium methoxide (from 50 mg sodium) was left overnight at 25°, made just acidic with 2N HCl and concentrated to 10 ml to give recovered starting material (0.2 g). The mother liquor was evaporated to dryness and the residue treated with water and a few drops of MeOH to give (15) as a white solid, m.p. 110°; ^{1}H NMR ($CDCl_3$); δ 7.56 (m, 2H, ArH); 7.17 (m, 2H, ArH); 3.61 (s, 3H, CO_2CH_3); 3.43 (s, 3H, OCH_3); 3.35 (s, 3H, NCH_3); 3.17 (d, J = 18 Hz, C–α H); m/e at 388, 386 (M^+), 357, 355 (M^+–OMe), 315, 313 (M^+–CH_2CO_2Me).

9.8 *Hydrolysis of acid (5) to (9)*

Acid (5) (0.35 g) in acetic acid (10 ml) was heated under reflux with 4N HCl (10 ml) for 3 hr. The solution was concentrated to about 6 ml and cooled. Colourless crystals of (9) separated and were filtered off; 0.2 g, m.p. 188–190° (from Et_2O-hexane) identical with other samples obtained as shown below. The acidic filtrate was made basic with 10% NaOH to give *p*-bromoaniline (0.1 g), m.p. and mixed m.p. 65°. Acid (9) (Found: C, 38.35; H, 2.96; N, 7.55. $C_6H_5NO_4S$ requires C, 38.51; H, 2.69; N, 7.49%).

9.9 Acid (9) from ester (6)

Hydrolysis of ester (6) (0.5 g) as before gave acid (9) (0.2 g), m.p. and mixed m.p. 188–190°.

9.10 *Acid (9) from ester (10)*

A solution N,N′-dimethylthiourea (2.6 g) in MeOH (20 ml) was left with diester (4) for 10 min to afford the thiazolidone ester (10) (4.5 g), m.p. 152–4° (from CH_2Cl_2–Et_2O) (Found: C, 45.17; H, 5.09; N, 12.80. $C_8H_{10}N_2O_3S$ requires C, 44.86; H, 4.71; N 13.08%); λ_{max} 310 nm (log ϵ 4.15); γ 1720, 1700, 1660, 1620 cm^{-1}; ^{1}H NMR ($CDCl_3$) δ6.90 (s, 1H, C–α H); 3.85 (s, 3H, OCH_3); 3.30, 3.29 (2s, 3H each, N–CH_3); ^{13}C NMR ($CDCl_3$ + DMSO–d_6); δ 166.2 (m, C–β); 164.7 (m, C–4); 115.3 (d, C–α), 52.2 (q, O$\underline{C}H_3$); 38.8 (q, $\underline{C}H_3$N=C); 29.1 (q, C(=O)–N–$\underline{C}H_3$); m/e at 214 (M^+); 183 (M^+–OMe), 155 (M^+–CO_2Me), 144 (M^+–MeN=C=NMe).

The above ester (2.1 g) in acetic acid (20 ml) was hydrolysed as before with 4N HCl (60 ml) under reflux to give acid (9) (1.8 g), m.p. 188–190° (from Et_2O) (Found: C, 38.79; H, 3.00; N, 7.58%); λ_{max} 249, 302 nm (log ϵ 3.94, 3.89); γ 1755, 1700, 1660, 1620 cm^{-1}; ^1H NMR ($CDCl_3$+DMSO-d_6): δ 6.92 (s, 1H, C-αH); 3.17 (s, 3H, N-CH_3); ^{13}C NMR: δ 169.0 (q, C-2); 166.3 (s, C-β); 164.8 (m, C-4); 120.2 (d, C-α), 27.4 (q, N-$\underline{C}H_3$); m/e at 187 (M^+), 130 (M^+-MeNCO).

9.11 *Acidic hydrolysis of acid (7)*

Acid (7) (1.6 g) in acetic acid (20 ml) was heated under reflux with 4N HCl (45 ml) for 30 min. The initially yellow solution became colourless and deposited crystals. The mixture was cooled and filtered to give the *p*-bromophenylthiazinone (12) (70 mg), m.p. >300° (decomp.) (Found: C, 40.44; H, 2.05. $C_{11}H_6BrNO_4S$ requires C, 40.27; H, 1.84%); λ_{max} 285 nm (log ϵ 3.97); γ (KBr) 1780, 1700, 1635 cm^{-1}; ^1H NMR ($CDCl_3$+DMSO-d_6): δ 7.64 (m, 2H, ArH), 7.22 (m, 2H, ArH); 7.09 (s, 1H, C-5H); m/e at 329, 327 (M^+), 301, 299 (M^+-CO), 199, 197 (ArN=C=O)$^+$.

The filtrate was concentrated to a small volume, diluted with 50% aqueous MeOH and the solution passed through a column of Dowex-50 (20–50 mesh; H^+ form). The column was eluted further with 50% aqueous MeOH. The combined eluates were evaporated to dryness and the residue crystallised from CH_2Cl_2–Et_2O to give (11) (0.15 g), m.p. 158° (Found: C, 38.79; H, 2.95; N, 7.71%); λ_{max} 293 nm (log ϵ 3.68); γ (KBr) 1700, 1640 cm^{-1}; ^1HNMR ($CDCl_3$+DMSO-d_6): δ 7.24 (s, 1H, C-5H); 3.40 (s, 3H, N-CH_3); ^{13}C NMR ($CDCl_3$+DMSO-d_6): δ 164.7 (q, C-2), 163.6 (m, C-β), 162.7 (m, C-4), 121.8 (d, C-5), 28.3 (q, N-$\underline{C}H_3$), m/e at 187 (M^+); 144 (M^+CO_2), 130 (M^+-MeNCO).

Acknowledgement

We thank Dr S Selvavinayakam and his associates for analytical and spectral data.

References

Acheson R M and Wallis J D 1981 *J. Chem. Soc. Perkin I* 415
Adman E T, Jensen L H and Warrener R N 1975 *Acta Crystallogr.* **B31** 1915
Cameron A G, Hair N J, Elmore N F and Taylor P J 1970 *Chem. Commun.* 890
Mckillop A, Bellinger G C A, Preston P N, Davidson A and King T J 1978 *Tetrahedron Lett.* 2621
Nagarajan K, Nair M D and Desai J A 1979 *Tetrahedron Lett.* 53
Vögeli U, Philipsborn W von, Nagarajan K and Nair M D 1978 *Helv. Chim. Acta* **61** 607

Proc. Indian Acad. Sci. (Chem. Sci.), Vol. 92, No. 1, January 1983, pp. 107–112.
© Printed in India.

Oxidation of phenylmethylcarbinols by bromamine-*T*

S GUNASEKARAN and N VENKATASUBRAMANIAN†*
Department of Chemistry, Ramakrishna Mission, Vivekananda College, Madras 600 004, India

MS received 6 August 1981; revised 16 November 1982

Abstract. The kinetics of oxidation of phenylmethylcarbinol and substituted phenylmethylcarbinols by bromamine-*T* have been studied in aqueous acetic acid medium in the presence of sulphuric acid. The effects of added toluene-*p*-sulphonamide and sodium bromide have been investigated. The solvent effect and temperatures effect on these reactions have also been studied. The Hammett correlation gives a ρ value of −2.5. A suitable mechanism consistent with the experimental observations has been suggested.

Keywords. Bromamine-*T*; phenylmethylcarbinols; oxidation; Hammett plot; activation parameters.

1. Introduction

A useful class of halogen containing oxidants is the group referred to as N-halo compounds which are potential sources of a positive halonium ion or a derivative thereof, which have good oxidising capabilities (Stewart 1964; Waters 1964; Wiberg 1965; Filler 1963; Barker 1964; Carr and England 1958; Campbell and Johnson 1978). Bromamine-*T* (BAT) is one such compound increasingly used in organic chemistry (Kremlev *et al* 1969). The present work reports the kinetic and mechanistic aspects of the oxidation of several substituted phenylmethylcarbinols by BAT with phenylmethylcarbinol (PMC) as the reference compound.

2. Experimental

Bromamine-*T* was prepared by the bromination of chloramine-*T* (CAT) in alkaline medium. The various substituted phenylmethylcarbinols used were of extra pure variety and were used without further purification.

The rate of reaction was followed by titrimetric methods, the disappearance of BAT being monitored iodometrically. The reactions were carried out in binary solvent mixtures of acetic acid and water to over 75% conversion. The rate constants were evaluated by using the respective integrated rate expression. Further oxidation or bromination of the product, acetophenone, was independently checked to be negligible under the conditions employed.

† Present address: IDL-Nitro Nobel Basic Research Institute, Bangalore 560 003, India
* To whom all correspondence should be made.

3. Results and discussion

The rates of the reactions of PMC with BAT have been determined under a variety of conditions of concentrations of BAT, alcohol, mineral acids, added sulphonamide and $NaClO_4$. The effect of changes in solvent polarity, temperature and structural modifications in the alcohol moiety has also been investigated (tables 1 to 6)

Table 1. Order dependence on [BAT] and [PMC]
$[H_2SO_4] = 0.1M$. 30° C. 50% HOAc–50% H_2O (V/V)

10^3[BAT] M	10^2[PMC] M	$10^4 k_{obs}$ sec^{-1}	$10^3 k_2$ lit mole^{-1} sec^{-1}
1.26	4.26	4.14	—
1.69	4.26	4.19	—
2.42	4.26	4.16	—
3.38	4.26	4.17	—
4.45	4.26	4.12	—
1.69	2.13	2.10	9.86
1.69	6.39	6.29	9.84
1.69	8.52	8.39	9.85
1.69	10.70	10.50	9.86

Table 2. Effect of acidity
$[PMC] = 1.95 \times 10^{-2}$M. $[BAT] = 1.84 \times 10^{-3}$ M.30° C
50% HOAc – 50% H_2O (V/V)

$[H_2SO_4]$ M	$10^4 k_{obs}$ sec^{-1}	$[HClO_4]$	$10^4 k_{obs}$ sec^{-1}
0.0	0.237	0.0	0.142
0.1	2.24	0.1	4.14
0.2	3.77	0.2	7.15
0.3	5.48	0.3	9.80
0.4	6.76	0.4	12.00
0.8	12.00	0.8	20.90
1.0	20.20	1.0	34.60

Table 3. Effect of added TSA and NaBr
$[PMC] = 2.23 \times 10^{-2}$M. $[BAT] = 1.84 \times 10^{-3}$M
$[H_2SO_4] = 0.2$ M. 30° C. 50%
HOAc–50%-H_2O (V/V)

10^4[TSA] M	$10^4 k_{obs}$ sec^{-1}	10^2[NaBr] M	$10^4 k_{obs}$ sec^{-1}
0.00	4.01	0.0	4.01
2.12	2.98	1.0	5.37
6.40	2.21	2.0	5.12
8.26	2.02	4.0	4.68
12.4	1.84	8.0	3.47
24.1	1.02	10.0	2.69

Table 4. Effect of solvent polarity
$[PMC] = 2.06 \times 10^{-2}$M. $[BAT] = 1.85 \times 10^{-3}$M
$[H_2SO_4] = 0.3$ M. 30° C

Solvent composition % HOAc–% H_2O (V/V)	$10^4 k_{obs}$ sec^{-1}
20–80	7.03
30–70	5.89
40–60	5.26
50–50	5.07
60–40	4.18
70–30	3.73
80–20	2.44

Table 5. Effect of structural modification
$[BAT] = 1.87 \times 10^{-3}$. $[H_2SO_4] = 0.16$ M.
50% HOAc–50% H_2O (V/V). 30° C.

RC_6H_4 $CH(OH)CH_3$	10^2[substrate] M	$10^5 k_{obs}$ sec^{-1}	$10^3 k_2$ lit mole^{-1} sec^{-1}
H	1.99	26.50	13.30
	3.98	52.10	13.10
4-ph	2.01	121.00	60.40
	4.22	256.00	60.60
4-Me	1.89	198.00	105.00
	4.02	414.00	103.00
4-Cl	1.97	9.97	5.06
	4.11	20.90	5.09
4-Br	2.12	10.70	5.07
	3.86	19.60	5.08
3-Cl	2.01	2.85	1.42
	3.97	5.72	1.44
3-Br	2.14	3.01	1.40
	3.56	4.91	1.38

Table 6. Activation parameters.

RC_6H_4 $CH(OH)CH_3$ R =	Ea kcal/mole	$\Delta H^{\ddagger}$ kcal/mole	$\Delta S^{\ddagger}$ e.u	$\Delta G^{\ddagger}$ kcal/mole
H	14.2	13.6	22.4	20.4
4-Ph	9.93	9.32	33.3	19.4
4-Me	9.13	8.52	34.9	19.1
4-Cl	13.5	12.9	26.4	20.9
4-Br	13.5	12.9	26.5	20.9
3-Cl	15.5	14.9	22.6	21.7
3-Br	15.8	15.2	21.6	21.7

The oxidation of phenylmethylcarbinols under investigation obeys the following rate-law:

$$\frac{-d[BAT]}{dt} = k\,[\text{alcohol}]\,[BAT]\,[H^+]^x \tag{1}$$

where $1 < x > 0$. The first order dependence both on [BAT] and [PMC] indicates that the slow step of the reaction involves an interaction between one molecule of substrate and one molecule of oxidant.

The following scheme is in keeping with the rate-law and other observations.

$$BAT^- + \overset{+}{H_3O} \overset{K_1}{\rightleftharpoons} BATH^- + H_2O \tag{2}$$

$$BATH + H\text{-}X \overset{K_2}{\rightleftharpoons} X\text{-}Br + TSA \tag{3}$$

(where X = OH or OAc)

$$C_6H_5CH(OH)CH_3 + X\text{-}Br \xrightarrow{K_2} C_6H_5COCH_3 + HBr + H\text{-}X. \tag{4}$$

Basically, the mechanism assumes one or more pre-equilibria for the formation of active oxidant species followed by a slow rate-determining interaction with the alcohol moiety to give the products. Applying equilibrium conditions for the formation of the oxidant species X-Br, one can arrive at the following rate expression (5)

$$\frac{-d\,[BAT]}{dt} = k_{obs}\,[BAT] = \frac{k_2 K_1 K_2\,[PMC]\,[BAT^-]_i\,[H_3O^+]}{[TSA]\,\{1 + K_1\,[H_3O^+]\}} \tag{5}$$

where $[BAT^-]_i$ = initial concentration of BAT.

The rate expression (5) is identical with the experimental rate-law and it also explains the fractional order dependence on $[H^+]$. The above expression would demand a linear relationship between [substrate]/k_{obs} versus $1/[H^+]$ with a finite intercept as has been realised.

An alternative way in which the fractional order dependence of the rate on the concentration of acid can be explained is to assume that two pathways are available for the oxidation of the alcohol—that is acid-dependent pathway and an acid independent one.

$$\frac{-d[BAT]}{dt} = k_{obs}\,[BAT] = k_2'\,[BAT]\,[PMC] + k_3''\,[BAT]\,[PMC]\,[H^+] \tag{6}$$

wherefrom it can be seen that

$$\frac{k_{obs}}{[PMC]} = k_2' + k_3''\,[H^+] \tag{7}$$

a relationship which would require a linear correlation in a plot of $k_{obs}/[PMC]$ versus $[H^+]$ with a finite intercept on the Y-axis. Such plot is brought out in figure 1

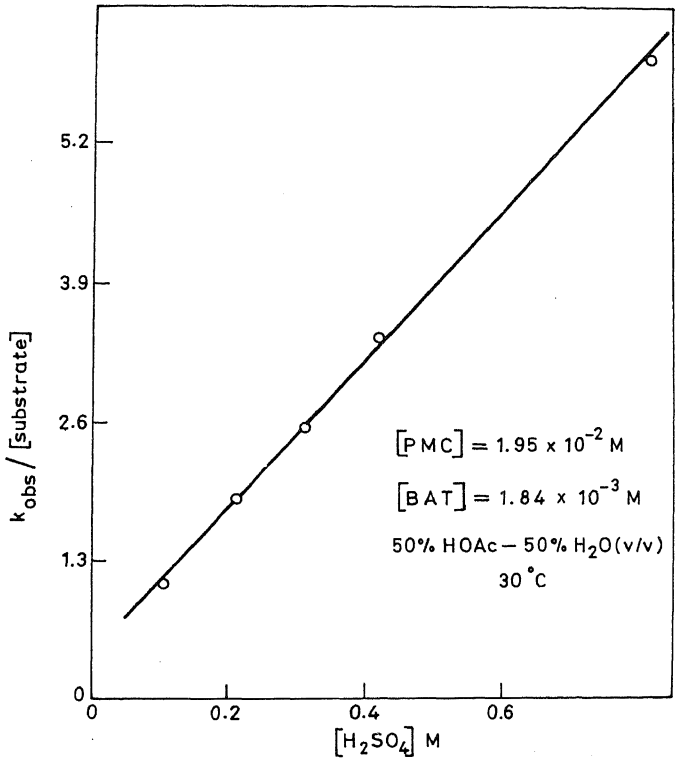

Figure 1. Plot of k_{obs}/(substrate) *vs* (acid).

confirming the operation of two such pathways. This formalism is probably on the right lines as could be seen from the fact that the acid-independent pathway for the oxidation of PMC has a k_2', value which is greater than that for the oxidation of the less reactive alcohol, benzyl alcohol by BAT (Gunasekaran and Venkatasubramanian 1980) ($k_2' = 5.01 \times 10^{-3}$ lit mole^{-1} sec^{-1} for PMC-BAT system and $k_2 = 9.78 \times 10^{-4}$ lit mole^{-1} sec^{-1} for benzylalcohol-BAT system under identical conditions). The finer details of the slow step could be picturised as

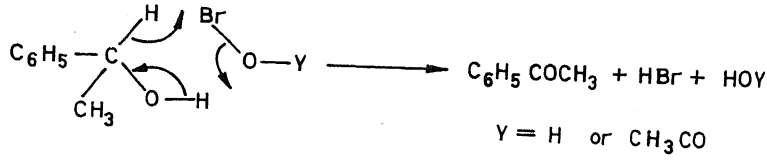

The slow step in the oxidation of PMC by BAT should proceed by an abstraction of the hydrogen on the α-carbon atom as a hydride ion, for the generation of a carbocationic centre in the transition state could be expected to be stabilized by electron-realising substituents in the phenyl group of PMC and an opposite effect for electron-withdrawing substituents. A Hammett analysis of the rate-data of this reaction yields a ρ value of –2.5 substantiating the above proposal. It may be recalled here that the Hammett ρ obtained for the oxidation of PMC by the related oxidant NBS is

-2.4 further underscoring the mechanistic similarities (Thiagarajan and Venkatasubramanian 1967). The faster oxidation of PMC than of benzyl alcohol is also in keeping with this picture for the additional $-CH_3$ on the α-carbon atom would not only facilitate the loss of the hydride ion but would also stabilise the developing carbonyl double bond in the transition state by hyperconjugation. The foregoing discussion is also in accord with the formalism that the reaction is essentially between two dipolar molecules. Such a reaction, according to Laidler and Eyring (1940), would proceed with a faster rate when the solvent is changed to a more polar one.

The observed acceleration in rate in the presence of initially added bromide ions is also consistent with the proposed mechanism, for, the added Br^- ions would react with BATH and generate molecular bromine which would be a better oxidising agent than HOBr or CH_3COOBr. However, further additions of the Br^- would tend to convert the active Br_2 into the inactive Br_3^- leading to rate retardations.

Acknowledgements

One of the authors (SG) thanks the University Grants Commission, New Delhi for a fellowship.

References

Barker I R L 1964 *Chem. Ind. London* 1936
Campbell M M and Johnson G 1978 *Chem. Rev.* **78** 65
Carr M D and England B D 1958 *Proc. Chem. Soc.* 350
Derbyshire A E and Waters W A 1950 *J. Chem. Soc.* 564
Filler R 1963 *Chem. Rev.* **63** 21
Gunasekaran S and Venkatasubramanian N–(unpublished work)
Kremlev M M, Kodachenko G F and Baranovskaya V F 1969 *Zh. Org. Khim.* **5** 914; 1969 *Chem. Abst.* **71** 38507
Laidler K J and Eyring J 1940 *Ann.N. Y. Acad. Sci.* **39** 303
Stewart R 1964 Oxidation Mechanisms (New York: Benjamin W A)
Thiagarajan V and Venkatasubramanian N 1967 *Tetrahedron Lett.* 3349
Waters W A 1964 *Mechanism of oxidation of organic compounds* (London: Methuen)
Wiberg K B 1965 *Oxidations in organic chemistry* (New York: Academic Press)

Proc. Indian Acad. Sci. (Chem. Sci.), Vol. 92, Number 2, April 1983, pp. 113–126.
© Printed in India.

Stability of mixed ligand complexes of copper(II): ESR studies

B S PRABHANANDA
Chemical Physics Group, Tata Institute of Fundamental Research, Bombay 400005, India

MS received 18 September 1982

Abstract. Three new mixed ligand complexes of Cu(II) obtained by combining any two of the three ligands, diethyldithiocarbamate, N-benzoyl-N'-diethylthiocarbamide and acetylacetonate have been identified in reaction mixtures using electron spin resonance (ESR), by estimating the equilibrium constant K associated with the ligand exchange reaction. The K values were also determined for fifteen other mixed ligand complexes of Cu(II) reported earlier. The stability of these mixed ligand complexes was correlated with the difference in the strengths of covalent bonding between the metal ion and the two ligands. The bondings involving both the $d_{x^2-y^2}$ and d_{xy} orbitals on the metal were necessary. In addition, the extent of metal 4s-orbital mixed in the unpaired electron orbital contributed to the magnitude of K. The diagrams similar to the ones used in our correlation could be useful in predicting the probable yield of mixed ligand complexes in reaction mixtures.

Keywords. Mixed ligand complex; electron spin resonance; cupric complexes; stability.

1. Introduction

Electron spin resonance (ESR) has been used to study a large number of mixed ligand transition metal complexes. (Dietzch *et al* 1977; Krishnamoorthy and Prabhananda 1978; Baratova *et al* 1982 and references cited therein). In our earlier studies we had shown that mixed ligand complexes are quite useful in inferring the mechanism of spin transfer to ligands. In the present work, we are mainly concerned with the stability of these complexes. A mixed ligand copper(II) complex of two bidentate ligands X and Y can be prepared by an appropriate mixture of $Cu(X)_2$ and $Cu(Y)_2$ in solutions by ligand exchange reactions.

$$Cu(X)_2 + Cu(Y)_2 \rightleftharpoons Cu(X)(Y) + Cu(Y)(X) \tag{1}$$

In this reaction, both X and Y coordinate to the metal ion. Even if we can identify two coordinating regions on the metal ion (thereby distinguish $Cu(X)(Y)$ from $Cu(Y)(X)$) there is no reason for X to coordinate preferentially at one of these regions. Thus the concentrations of $Cu(X)(Y)$ and $Cu(Y)(X)$ will be the same. By experiments such as ESR it is not possible to distinguish the mixed ligand complex $Cu(X)(Y)$ from $Cu(Y)(X)$. Therefore, if the measured mixed ligand complex concentration is $[Cu(X)(Y)]_m$, we can write

$$[Cu(X)(Y)] = [Cu(Y)(X)] = [Cu(X)(Y)]_m/2 \tag{2}$$

The equilibrium constant K for reaction (1) can then be written as

$$K = \frac{[Cu(X)(Y)]_m^2}{4.[Cu(X)_2][Cu(Y)_2]} \tag{3}$$

1

(This expression gives the expected value of $K = 1$ if there is no free energy change associated with reaction (1)).

In our previous studies, we had identified the mixed ligand complexes by the ligand hyperfine structures and had determined the equilibrium concentrations of the paramagnetic species in the reaction mixtures by comparing the observed ESR spectra with computer-simulated spectra. These had shown that K depends on the choice of ligands X and Y (Krishnamoorthy and Prabhananda 1978). Dietzch *et al* (1977) noticed that the mixed ligand complexes formed with maleonitrile dithiolate (MNT) as one of the ligands, had much higher values of K than other mixed ligand complexes studied. Their extended Hückel molecular orbital calculations also indicated such a trend in the values of K. They suggested that when the metal ion forms a four-membered ring with one ligand and a five-membered ring with a second ligand there is considerable energy gain for the mixed ligand complex formation. Such a simple rule is not applicable to the results obtained earlier (Prabhananda *et al* 1977; Krishnamoorthy and Prabhananda 1978). A better understanding of the stability of mixed ligand complexes can be gained by looking for some sort of correlation between K and ESR determined parameters. This could also help in guessing the probable yield of new mixed ligand complexes in reaction mixtures.

The value of K associated with 18 mixed ligand complexes prepared by various combinations of seven ligands (shown in figure 1) is examined. Equilibrium concentrations determined by computer simulations (Prabhananda *et al* 1977; Krishnamoorthy and Prabhananda 1978; Krishnamoorthy *et al* 1978), were used to obtain K in the case

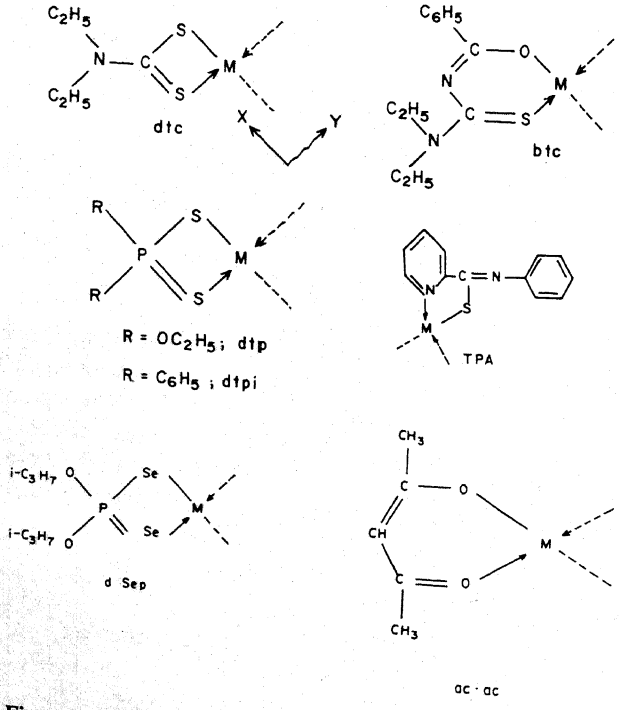

Figure 1. Ligands used in the present study. M is a metal ion to which they coordinate.

of eight complexes. For seven of the complexes we had not simulated the spectra to match the experimental ESR spectra from their reaction mixtures, in our earlier studies (Krishnamoorthy and Prabhananda 1980 and references therein). After determining the equilibrium concentrations of the paramagnetic species in the reaction mixtures the K value associated with these seven complexes was determined by obtaining the computer-simulated spectra and these values agree with the reported spectra.

Three new mixed ligand complexes of copper(II) prepared by the combinations of diethyldithiocarbamate (dtc), N-benzoyl-N′-diethylthiocarbamide (btc) and acetylacetonate (ac.ac) have also been reported in the present work. These complexes do not show ligand hyperfine structures. Nevertheless, the spectrum of mixed ligand complex can be identified as follows. In the complex ESR spectra obtained from the reaction mixtures one can easily identify the lines due to species $Cu(X)_2$ and $Cu(Y)_2$ (since their spectra can be obtained separately). The remaining lines could be assigned to the mixed ligand complex. That such an assignment is correct could be confirmed by estimating the concentrations from the observed spectra and plotting $[Cu(X)(Y)]_m^2/[Cu(X)_2]$ against $[Cu(Y)_2]$. From (3) the plot should be a straight line passing through the origin, the slope of which can be used to get an estimate of K. Further confirmation could be obtained if the g_0 value of the mixed ligand complex in liquid solutions can be determined. Our previous studies (Krishnamoorthy and Prabhananda 1980 references cited therein) have shown that g_0 of $Cu(X)(Y)$ is close to the average of those of $Cu(X)_2$ and $Cu(Y)_2$. Such a cross-check has been possible in the case of two new mixed ligand complexes reported in this work. A possible correlation between K and the bonding inferred from ESR parameters is also suggested in this paper.

2. Experimental

The complexes $Cu(dtc)_2$, $Cu(btc)_2$ and $Cu(ac.ac)_2$ which have been used in the preparation of mixed ligand complexes were prepared as described earlier (Krishnamoorthy and Prabhananda 1978, 1980). Reaction mixtures with Cu(dtc)(btc), Cu(btc)(ac.ac) and Cu(dtc)(ac.ac) at different concentrations were obtained according to equation (1), by mixing the chloroform solutions of the complexes in different proportions. Cupric acetate enriched to $> 90\,\%$ with ^{63}Cu was used in all preparations. X-band ESR spectra of the solutions were recorded at 25°C. Computer-simulated spectra were obtained using a program written earlier (Baratova *et al* 1982).

3. Results

Figure 2 gives the derivative ESR spectra obtained from typical reaction mixtures in the preparation of Cu(dtc)(btc), Cu(dtc)(ac.ac) and Cu(btc)(ac.ac). In the case of Cu(dtc)(btc) (figure 2a) all the four lines corresponding to ^{63}Cu hyperfine components can be seen in the spectrum. The high field components (which are well resolved) can be used to directly estimate the concentrations of the three paramagnetic species, since they are proportional to (peak-to-peak width)^2 × peak-to-peak height of the corresponding derivative lines. The concentrations thus obtained from different reaction mixtures give the expected linear plot (figure 2a′) supporting our identification of the spectrum from the mixed ligand complex. The g_0 corresponding to this spectrum (table 1) has the expected value. In figure 2b apart from the lines corresponding to

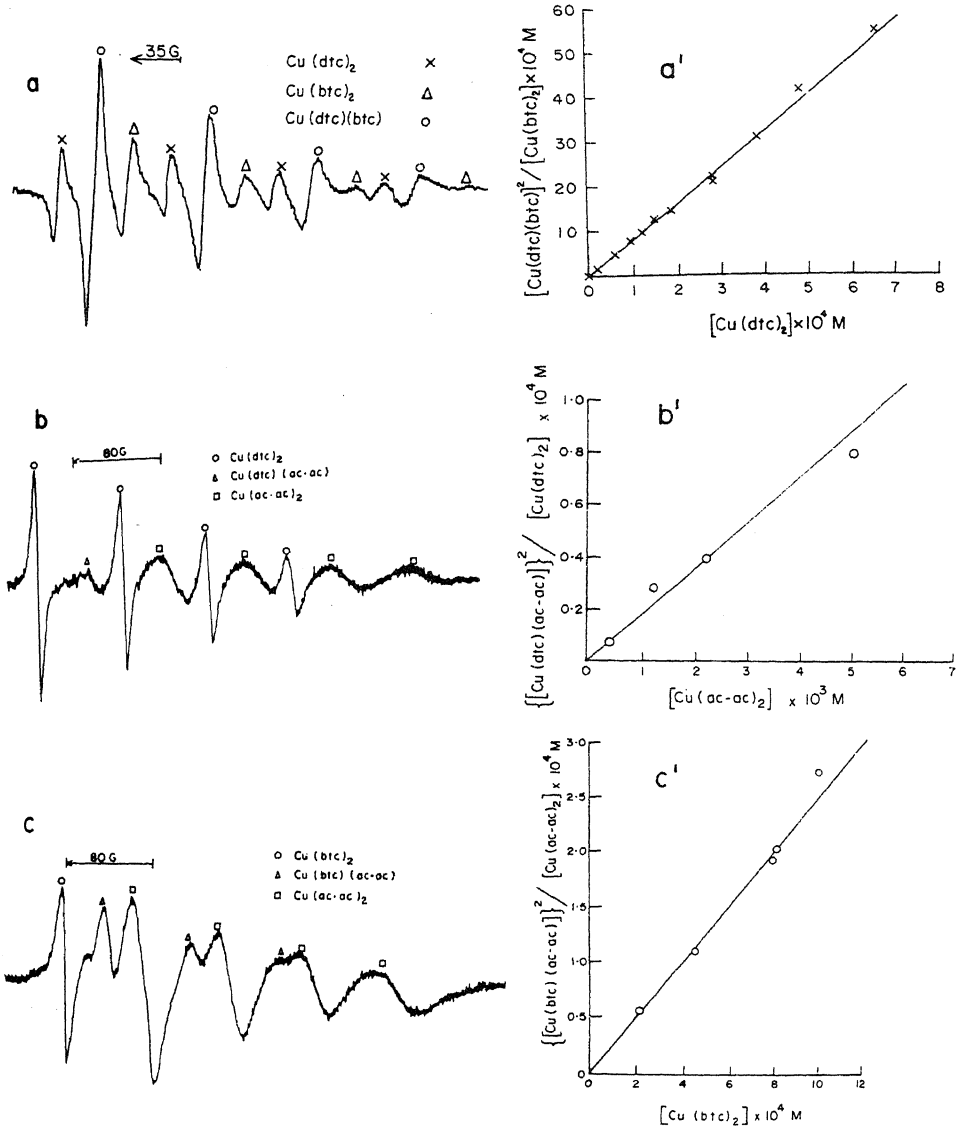

Figure 2. ESR spectra obtained from typical reaction mixtures in the preparations of (**a**) Cu(dtc)(btc), (**b**) Cu(dtc)(ac.ac) and (**c**) Cu(btc)(ac.ac). The plots used in the determination of K of these mixed ligand complexes are (**a'**), (**b'**) and (**c'**).

$Cu(dtc)_2$ and $Cu(ac.ac)_2$ one extra line is noted which is in the high field region. The estimation of concentrations, assigning this extra line to Cu(dtc)(ac.ac), gives a linear plot (figure 2b') consistent with such an assignment. However, this could not be confirmed from the g_0 measurements since none of the other three hyperfine components (of the spectrum of this complex) could be identified, due to considerable overlap from the spectra due to $Cu(dtc)_2$ and $Cu(ac.ac)_2$. In figure 2c even though there is considerable overlap, the positions of at least three hyperfine components of a

Table 1. ^{63}Cu hyperfine constant A_0 and g_0 determined from the ESR spectra of chloroform solutions at 25°C[a].

Complex	A_0 in G	g_0
$Cu(dtc)_2$	78·0	2·0480
$Cu(btc)_2$	79·6	2·0826
$Cu(ac.ac)_2$	76·2	2·1235
Cu(dtc)(btc)	77·7	2·0650
Cu(btc)(ac.ac)	78·6	2·1046

[a] The absolute errors in A_0 and g are $\pm 2G$ and $\pm 0{\cdot}002$ respectively.

spectrum could be determined, apart from those of $Cu(btc)_2$ and $Cu(ac.ac)_2$. These could be assigned to Cu(btc)(ac.ac), since the concentrations estimated (with this assignment) from the spectra of different reaction mixtures (figure 2c′) and the estimated g_0 (table 1) showed the expected behaviour.

Since there is considerable overlap of the lines in the spectra similar to figure 2c, the simple procedures adopted for figures 2(a–b) cannot be used in this case. The concentrations of the three species (C_i, $i = 1, 3$) in the reaction mixtures can be determined by measuring the ESR signal heights $S_0(H_j)$ at three convenient magnetic fields H_j, and solving the simultaneous equations

$$S_0(H_j) = C_1 S_1(H_j) + C_2 S_2(H_j) + C_3 S_3(H_j) \tag{4}$$

$S_1(H_j)$, $S_2(H_j)$ and $S_3(H_j)$ are the signal height at H_j of the three species when their concentrations are unity. These were determined by matching a computer-simulated spectrum with the observed ESR spectrum from one convenient reaction mixture at a particular field region. Procedures used earlier (Prabhananda *et al* 1972a; Krishnamoorthy and Prabhananda 1978) were used in the matching of the spectra and the data plotted in figure 2c′. The K estimated from figures 2(a′–c′) are given in table 2. Figure 3a gives the observed and computer-simulated spectra used to determine $S_1(H_j)$, $S_2(H_j)$ and $S_3(H_j)$ for this system.

It can be seen from figures 2(a′–c′) that the errors in the estimated K for the above three systems are less than 20%. The value of K estimated from analysing one reaction mixture is sufficiently good (with errors of the above order) if it is ensured that (i) an equilibrium has been reached and (ii) the signal height contributions of the three species are good. (Even if the concentration of the complex is small, it is possible to estimate this if the linewidth associated with this complex is small compared to that of the others.) The above procedure has been followed for other systems reported in this paper. However, the estimated K have been cross-checked by comparing the observed and simulated spectra for a second reaction mixture, using the same value of K.

In the spectra of reaction mixtures with Cu(btc)(ac.ac), Cu(TPA)(ac.ac) or Cu(dtc)(dtpi) the lines due to all the three species could be easily distinguished (figures 3a–c) only for the high field ^{63}Cu hyperfine component ($m_I = 3/2$). On the other hand, in Cu(dtc)(dseP), one could identify the lines (figure 3d) only for the low field ^{63}Cu hyperfine component ($m_I = -3/2$). While such identification could be easily made for $m_I = 3/2$ and $m_I = 1/2$ components in the reaction mixtures of Cu(btc)(dtp), this was possible only for the $m_I = 1/2$ component for the mixture with Cu(btc)(dtpi). Thus computer simulations have been carried out to include both these components in these

Table 2. Equilibrium constants K and other relevant parameters associated with the mixed ligand complexes of Cu(II).

Ligands and near neighbours of metal X	Y	δ^a in G	K^b	Reference
btc (S, O)	TPA (S, N)	9·0	270·0	K & P 1980[c]
dtc (S, S)	dtp (S, S)	0·3	14·0	K & P 1978
dtc (S, S)	TPA (S, N)	5·0	12·8	P *et al* 1977[c]
dtc (S, S)	dtpi (S, S)	0·0	9·6	K & P 1978[c]
dtp (S, S)	TPA (S, N)	4·0	3·1	P *et al* 1977
dtp (S, S)	dtpi (S, S)	0·0	2·2	K & P 1978
dtc (S, S)	btc (S, O)	−1·0	2·0	This work
dtc (S, S)	dSeP (Se, Se)	0·6	1·9	K *et al* 1978[c]
dtpi (S, S)	TPA (S, N)	5·0	1·6	P *et al* 1977
TPA (S, N)	ac.ac (O, O)	8·4	1·1	K & P 1980[c]
dSeP (Se, Se)	dtp (S, S)	0·8	1·1	K *et al* 1978
dSeP (Se, Se)	dtpi (S, S)	0·8	1·0	K *et al* 1978
dtpi (S, S)	btc (S, O)	−2·0	0·84	K & P 1978[c]
dtp (S, S)	btc (S, O)	−3·2	0·76	K & P 1978[c]
dSeP (Se, Se)	btc (S, O)	−2·0	0·5	K *et al* 1978
dSeP (Se, Se)	TPA (S, N)	1·4	0·4	K *et al* 1978
btc (S, O)	ac.ac (O, O)	0·7	0·06	This work
dtc (S, S)	ac.ac (O, O)	—	0·005	This work

[a] δ is a measure of the mixing of metal 4s-orbital in the unpaired electron orbital. See equation (5) in text.
[b] See text for the discussions on the errors in K. Errors in δ are of $\sim \pm 0{\cdot}3$ G.
[c] Computer simulations carried out in this work.

two systems (figures 4c and 4d). In the spectra obtained from the reaction mixtures containing Cu(btc)(TPA) and Cu(dtc)(TPA), the lines due to $Cu(btc)_2$ and $Cu(dtc)_2$ considerably overlapped with the lines due to other species throughout the spectra. In these two cases, the concentrations of $Cu(btc)_2$ and $Cu(dtc)_2$ were estimated by varying them to get minimum deviation between the observed and calculated line shapes in the high field region. In figures 4a and 4b these small contributions are marked by dotted lines in the simulated spectra. Table 2 gives the K value estimated for these systems and also the K calculated from the equilibrium concentrations used in the simulation of the spectra, for the reaction mixtures containing Cu(dtc)(dtp), Cu(dtp)(dtpi) (Krishnamoorthy and Prabhananda 1978. The concentrations of Cu(dtp)(dtpi) and $Cu(dtpi)_2$ have been erroneously interchanged in figure 3 of this paper), Cu(TPA)(dtp), Cu(TPA)(dtpi) (Prabhananda *et al* 1977), Cu(dtp)(dSeP), Cu(dtpi)(dSeP), Cu(btc)(dSeP) and Cu(TPA)(dSeP) (Krishnamoorthy *et al* 1978).

Small deviations between the observed and simulated spectra are noticed in many cases. Departure of the experimental line shape from Lorentzian (especially due to the finite amplitude of field modulation used for detecting the signal), presence of unidentified paramagnetic species in small concentrations are some of the causes for these deviations. However, the K values for different systems cannot be very different from those given in table 2, since K can be used to predict the spectra from other reaction mixtures (of these systems) also, which agree reasonably well with the observed spectra.

Diluting a typical reaction mixture changes the concentration of the three

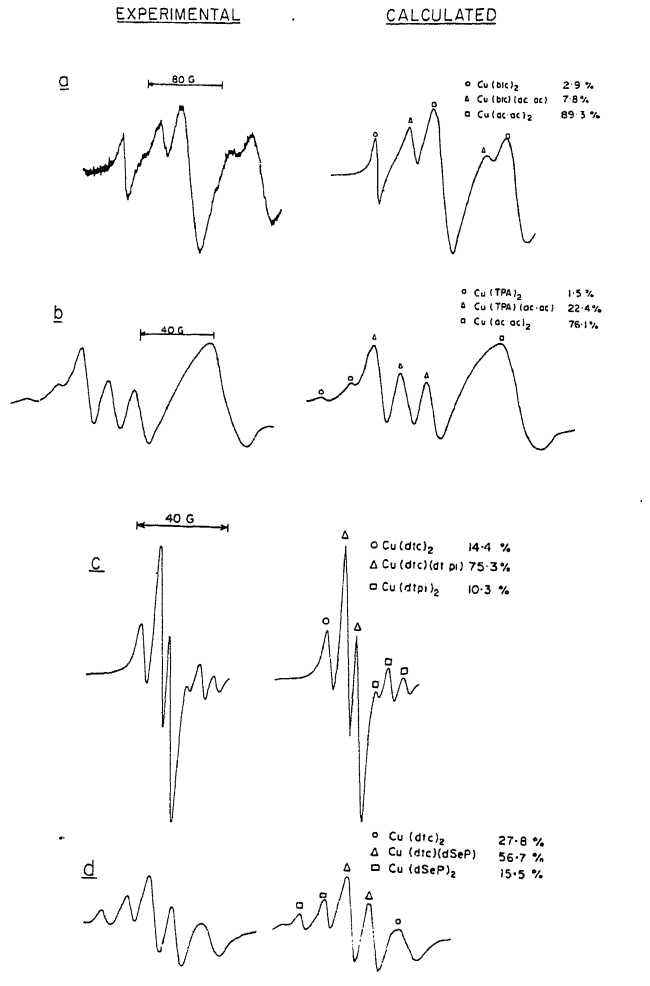

Figure 3. Experimentally observed and computer simulated ESR spectra for the reaction mixtures containing (**a**) Cu(btc)(ac.ac), (**b**) Cu(TPA)(ac.ac), (**c**) Cu(dtc)(dtpi) in the high field region and (**d**) Cu(dtc)(dSeP) in the low field region.

paramagnetic species by the same factor. This is expected from (3) and adds confidence to our identification of the reaction as that given by (1). Changing the hydrogen bonding property and the dielectric constant of the solvent (by using methanol) does not affect the estimated K for typical systems. It is therefore clear that the stability of the mixed ligand complex is mainly determined by internal factors.

3.1 *Relative ordering of the ligands on the basis of the strengths of their interaction with copper(II)*

It is natural to expect that K is correlated with the relative strengths of ligand-metal interactions. In previous studies (Krishnamoorthy and Prabhananda 1980), we had placed the ligands in the increasing order of covalent bonding of the metal $d_{x^2-y^2}$

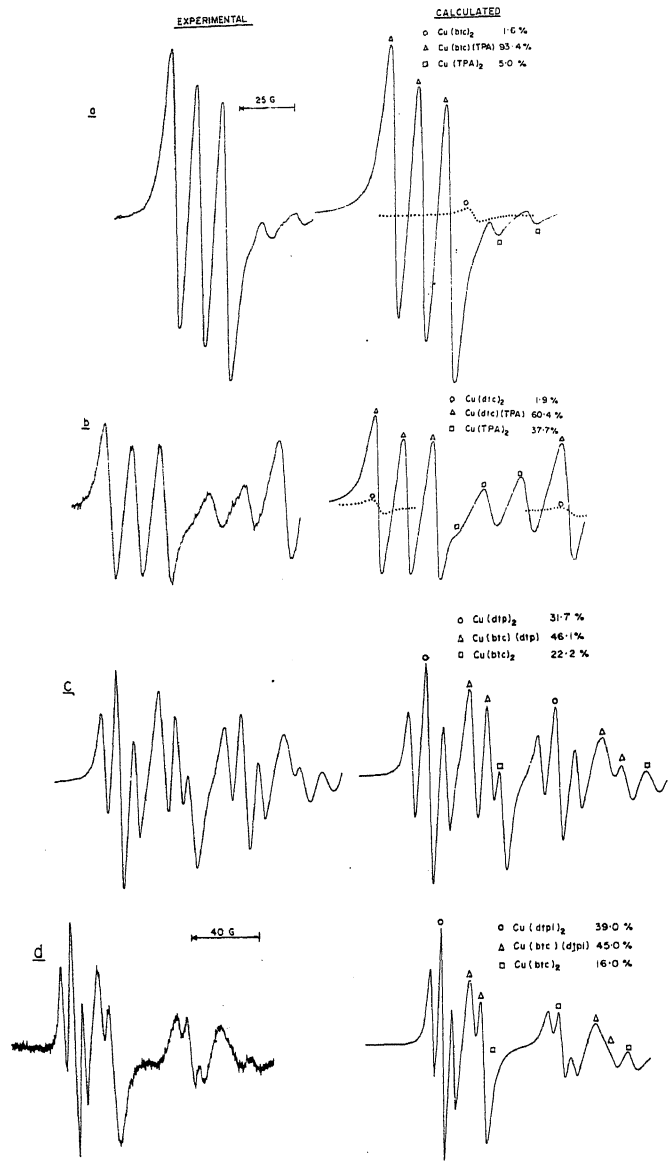

Figure 4. Experimentally observed and computer simulated ESR spectra for the reaction mixtures containing (**a**) Cu(btc)(TPA), (**b**) Cu(dtc)(TPA), (**c**) Cu(btc)(dtp) and (**d**) Cu(btc)(dtpi) in the high field region. Dotted lines in (a) and (b) correspond to $Cu(btc)_2$ and $Cu(dtc)_2$ components respectively.

orbital with the near neighbours as follows:

$$\text{ac.ac} < \text{btc} < \text{TPA} < \text{dtp} < \text{dtc} < \text{dSeP}$$

(In our coordinate system the lobes of $d_{x^2-y^2}$ point towards the near neighbours.) In figure 5, the above ordering is along the vertical direction.

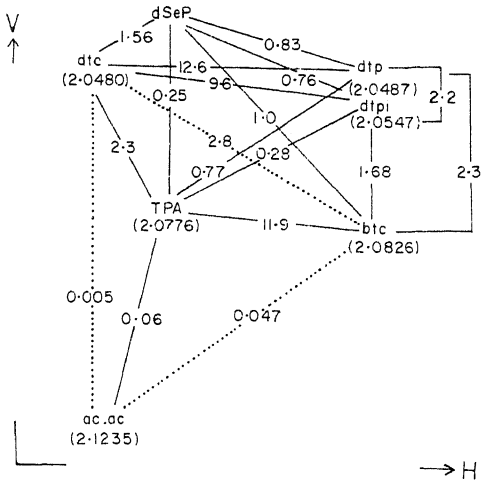

Figure 5. Schematic diagram used in correlating K_0 with the bonding characteristics. The g_0 associated with $Cu(L)_2$ are given within brackets. K_0 associated with Cu(X)(Y) are given between the line connecting X and Y.

If we subtract the contribution of spin-orbit interaction at the ligands from the measured g_0 and designate it by g'_0, we note that g'_0 differs from g_0 substantially in the case of $Cu(dSeP)_2$ (due to spin orbit interaction on Se). This can be seen in the calculations of Attanasio *et al* (1976). Spin-orbit interaction on the ligands L is quite small for the other complexes $Cu(L)_2$ discussed here. Thus, the g_0 given earlier (Prabhananda 1979; Krishnamoorthy and Prabhananda 1980) can be used as the estimates of g'_0 (figure 5). In view of the dependence of g_0 on the interaction of the ligands with the metal $d_{x^2-y^2}$ orbital, we have separated the ligands L along the vertical direction of figure 5, following the pattern seen in the g_0 of $Cu(L)_2$. Attanasio *et al* (1976) show that inclusion of 4*d*-orbitals of Se is necessary in $Cu(dSeP)_2$ to reproduce the experimentally determined g-tensor by calculations. If the spin-orbit interaction on this ligand orbital is neglected, we get $g_0 \sim 2{\cdot}046$ (Attanasio *et al* 1976). Therefore dSeP should be placed above dtc. Covalency considerations mentioned above also require dSeP to be placed above dtc in figure 5. Further, we should expect the separation between dtc and dSeP to be more than that between dtp and dtpi, since the coordinating atoms of the two ligands are different in the former case whereas they are all sulphurs in the latter case. This intuitive consideration is used while placing the ligand dSeP in figure 5.

Earlier studies (Prabhananda *et al* 1972b and the later works cited here) had shown that the next neighbour ligand hyperfine splittings observed in the complexes were due to the covalent bonding involving the metal d_{xy} orbital. Studies on the next neighbour hyperfine splittings in mixed ligand complexes (Krishnamoorthy and Prabhananda 1978) had shown that the covalent transfer of electrons in the bonds with stronger bonding ligand increases at the expense of the weaker bonding ligand. This is similar to the observations of Eaton and Phillips (1965). Since these hyperfine interactions are due to configuration interaction mechanism in Cu(II) complexes, the next neighbour hyperfine splittings associated with the stronger bonding ligands actually decrease as a

consequence of increased delocalisation in that bond, as explained earlier (Krishnamoorthy and Prabhananda 1978). Thus the next neighbour hyperfine splittings can be used to arrange the ligands in the increasing order of interaction of the ligand with the metal d_{xy} orbital (see table 2). In figure 5 this interaction increases along the horizontal direction.

The Cu(II) complexes formed by combinations of dtp, dtpi and btc do not show significant changes in the ^{31}P hyperfine splittings. Thus their horizontal coordinates in figure 5 will be similar. The decrease in the ^{31}P hyperfine splitting associated with dtp on forming Cu(dtp)(dSeP) and Cu(TPA)(dSeP) is comparable. Therefore, their horizontal coordinates in figure 5 cannot be much different. Formation of Cu(dtc)(dSeP) decreases the ^{31}P splitting associated with dSeP by a small amount. Thus dSeP (and hence TPA) is placed close to dtc along the horizontal direction. The position of ac.ac along the horizontal direction is not definite, since we have not been able to make observations on Cu(dtp)(ac.ac). However, predictions regarding the relative stabilities of the complexes made later in this paper are not significantly altered by changing the position of ac.ac along the horizontal direction of figure 5.

3.2 *Changes in the metal 4s-mixing*

In our previous work (Krishnamoorthy and Prabhananda 1980) we had noted that if A^X, A^Y and A^{XY} are the ^{63}Cu hyperfine constants of $Cu(X)_2$, $Cu(Y)_2$ and $Cu(X)(Y)$, measured from their ESR spectra in liquid solutions,

$$\delta = A^{XY} - (A^X + A^Y)/2 \neq 0 \tag{5}$$

This non-zero value of δ is due to the change in the mixing of metal 4s orbital in the unpaired electron orbital. The experimentally determined δ are given in table 2.

4. Discussion

The Cu(II) complexes studied are nearly square planar. One can look for correlation between the magnitude of K and the bonding characteristics by referring to figure 5 and table 2. Among the 18 mixed ligand complexes listed in table 2, Cu(btc)(TPA) has the largest value of K ($\sim$ 270). Therefore, the characteristics associated with it can be used to find the conditions for stabilisation of the mixed ligand complex. (a) The coordinates of btc and TPA in figure 5 differ substantially along H-direction. But this difference is not much along V-direction. (b) The δ associated with Cu(btc)(TPA) has a large positive value (table 2). The first characteristic feature is the highly stable Cu(dtc)(dtp) ($\sim$ 14). It may be reasonable to infer that the smaller value of K for Cu(dtc)(dtp) when compared to that for Cu(btc)(TPA) is to be associated with the differences in the δ values (table 2).

4.1 *Stabilisation associated with change in metal 4s-mixing*

Kuska *et al* (1967) used a value of 0·0975 cm^{-1} for the hyperfine constant associated with a 4s-electron in Cu(II) complexes, based on the calculations of Watson and Freeman (1961). Converting this into magnetic field units and a part of the unpaired electron density with $3d^8\ 4s^1$ character ρ gets converted into $3d^9$ character, the hyperfine constant changes by approximately 1000ρ. The δ given in table 2 will correspond to changes in the metal 4s-mixing of the unpaired electron orbital by $\delta/1000$. Using the estimate of energy difference between the configurations $3d^8\ 4s^1$ and

$3d^9$ given by Abragam and Pryce (1951), $\sim$ 70,000 cm^{-1} (= 8·68 eV), the above change would correspond to a free energy decrease $\sim 8{\cdot}68\,\delta/1000$ eV. At room temperature ($kT \sim 1/40$ eV), this would correspond to an increase in the K by a factor exp (0·347 δ). For Cu(btc)(TPA), this factor has a value of $\sim$ 22. Thus it is not surprising that K associated with this complex has a large value. K_0 defined by

$$K \exp(-0{\cdot}347\,\delta) \tag{6}$$

can be used to discuss the stabilisation of the complex excluding the above factor. The K_0 values thus determined are given in figure 5 on the line connecting the ligands of the mixed ligand complex. For example, $K_0 = 12{\cdot}6$ is associated with Cu(dtc)(dtp) and $K_0 = 2{\cdot}8$ with Cu(dtc)(btc).

The mixing of metal 4*s*-orbital in the unpaired electron orbital (which has $d_{x^2-y^2}$ character on the metal) has been attributed to the mixing of d_{z^2} (which has the correct symmetry to mix with 4*s*) with $d_{x^2-y^2}$. This could be due to a vibronic mechanism or due to the lower symmetry environment of the metal (Kuska *et al* 1967). Thus in reality we have two contributions to free energy changes associated with a change in the 4*s* mixing. (i) that associated with a change in configuration from $3d^8\,4s^1$ to $3d^9$ as discussed above; (ii) that associated with the change in vibronic mixing or with change in the symmetry of coordination (to a higher symmetry when there is a reduction in 4*s* mixing and to a lower symmetry when there is an increase) which could affect the overlap of the metal orbitals with the ligand orbitals. (The reason for such changes on forming the mixed ligand complexes is not clear at present.) The first factor is taken care of by expressing K in terms of K_0 and δ. The importance of the second factor is not yet clear in our system. We can correlate K_0 with bonding characteristics only if we assume that the second factor is negligible.

3.3 *Correlation between K_0 and bonding characteristics*

The magnitude of K_0 is mainly determined by the difference in the H-coordinates of the ligands forming the mixed ligand complex, when the difference in the V-coordinates is small (figure 5). This can be seen by comparing the K_0 associated with Cu(dtc)(dtp) and Cu(btc)(TPA). Similarly, a comparison of K_0 associated with Cu(dtc)(TPA) and Cu(btc)(dtp) shows that K_0 is mainly determined by the difference in V-coordinates, when the difference in the H-coordinates is small. From this, we conclude that K_0 is mainly decided by the differences in the bonding characteristics of the two ligands with the metal d_{xy} and $d_{x^2-y^2}$ orbitals.

The terms 'bond energy' or 'bond strength' is used in reference to the covalent bonds involving the ligand orbitals and the metal $d_{x^2-y^2}$ and d_{xy} orbitals. The actual total bond energy could have other contributions also. If V_x and H_x are the coordinates of the ligand X (figure 5) (along the vertical and horizontal directions), $V_x + p.H_x$ is a measure of the strength of the Cu-X bond coming from the covalent bonds involving the metal $d_{x^2-y^2}$ and d_{xy} orbital. (The contributions to strengths are additive in nature. The parameter p takes care of the differences in the scales of V and H axes.) The magnitude of the difference in the strengths of Cu-X and Cu-Y bonds in Cu(X)(Y) is given by

$$D = |V_x - V_y + p(H_x - H_y)| \tag{7}$$

An intuitive understanding of the dependence of K_0 and D can be gained by

visualising reaction (1) as that involving fictitious diatomic molecules,

$$(A-A)+(B-B) \rightleftharpoons (A-B)+(B-A). \tag{8}$$

Here, A takes the place of Cu-X bond and B takes the place of Cu-Y bond (see appendix). If this could be done, we can make an analysis similar to that of Pauling (1960) and arrive at the following conclusion (as shown in the appendix). (I) For small D, K_0 increases with D reaching a maximum value corresponding to an 'optimum value' of D. (II) For D greater than this 'optimum', K_0 decreases with increase in D. One can examine 153 pairs ($= {}^{18}C_2$) of K_0 (figure 5), in an attempt to qualitatively understand the relative magnitudes of K_0 on the basis of this conclusion. Some simple examples of such comparisons are given below.

When $D = 0, K_0 = 1$. Thus $K_0 \sim 2$ for Cu(dtp)(dtpi) can be understood on the basis of situation (I). However, when we go from Cu(dtc)(TPA) to Cu(TPA)(ac.ac), K_0 decreases corresponding to situation (II). For Cu(dtc)(dSeP), $V_x - V_y$ and $H_x - H_y$ have the same signs, whereas for Cu(dtp)(dSeP) they have opposite signs. Therefore, D associated with Cu(dtc)(dSeP) is greater than that associated with Cu(dtp)(dSeP). For the case (I), we can expect K_0 to show the same behaviour as D. Experimental observations are consistent with this. A similar situation is encountered in comparing Cu(TPA)(dSeP) and Cu(btc)(dSeP). However, in this case D can be more than the 'optimum' which would then correspond to case II. Thus, it is not surprising that K_0 of Cu(TPA)(dSeP) is less than that of Cu(btc)(dSeP). The above type of correlation of K_0 with D can be seen by comparing several pairs of mixed ligand complexes of our earlier studies. However, the magnitude of K_0 of Cu(btc)(dtpi) and of Cu(TPA)(dtpi) shows small deviations from the expected trend, when we compare them with the K_0 of Cu(btc)(dtp) and Cu(TPA)(dtp) respectively. One could attribute this to the approximations made in the 'assumption' mentioned earlier. Errors in δ which contribute to additional errors in K_0 (when compared to that in K) could also be responsible for such small deviations.

If we are satisfied with the above correlation for the complexes reported earlier the order of magnitude of K_0 could be predicted for the complexes prepared in this work (indicated by dotted lines in figure 5) as follows. From figure 5, we note that a comparison of K_0 of Cu(dtc)(TPA) and Cu(dtc)(btc) will be similar to that of Cu(TPA)(dSeP) and Cu(btc)(dSeP), as discussed above. Thus K_0 of Cu(dtc)(btc) could be greater than 2·3. K_0 of Cu(dtc)(ac.ac) can be much less than that of Cu(TPA)(ac.ac) when a similar comparison between the K_0 associated with Cu(dtc)(TPA) and Cu(TPA)(dSeP) or Cu(TPA)(ac.ac) is made. K_0 associated with Cu(btc)(ac.ac) will be less than that of Cu(TPA)(ac.ac) by anology with a similar situation involving Cu(dtc)(TPA) and Cu(dtp)(TPA). The experimentally determined K_0 are in accordance with the predictions for all the three complexes.

In view of the approximations involved in the assumptions, it is not appropriate to make quantitative predictions of K_0. Nevertheless, our results have shown that diagrams of the type shown in figure 5 could be useful in predicting the relative magnitudes of K_0. Relative stabilities of various mixed ligand complexes could also be guessed, if we take note that certain ligands, such as, TPA favour a reduction in 4*s*-mixing on forming the mixed ligand complex and the ligands such as btc favour an increase in 4*s*-mixing (except when in combination with TPA). Our discussion also shows the importance of bonding involving the metal $d_{x^2-y^2}$ and d_{xy} orbitals in the stabilisation of mixed ligand complex of Cu(II). In addition, changes in 4*s*-mixing in the unpaired electron orbital also play a significant role.

Acknowledgement

The author is grateful to Prof. P M Solozhenkin, Dr Melnik and Dr G Krishnamoorthy with whose help the spectra reported in the earlier studies had been obtained. The author thanks Prof. B Venkataraman for going through the manuscript and for useful discussions.

Appendix

The equilibrium constant associated with reaction (8) involving diatomic molecules varies as exp (Δ/RT) where

$$\Delta = E_{AB} - (E_{AA} + E_{BB})/2$$

$E_{AA'}$ refers to bond energy of diatomic molecule (A–A'). We can also define

$$\Delta' = E_{AB} - (E_{AA} \cdot E_{BB})^{1/2}$$

It is easy to see that

$$P = \Delta' - \Delta = (E_{AA} + E_{BB})/2 - (E_{AA} \cdot E_{BB})^{1/2} \geqslant 0$$

P increases when $|E_{AA} - E_{BB}|$ increases. In the absence of ionic character in the bond A–B, $\Delta' = 0$. However, if the electron density of one atom increases at the expense of other, the bond will have an ionic character which requires the inclusion of ionic structures in the valence bond calculations (Pauling 1960 see eqn 3-2). According to Pauling (1960) quantum mechanical calculations support the hypothesis that Δ' increases with increase in the ionic character of the bond which could come from increase in $|E_{AA} - E_{BB}|$. Thus in the expression

$$\Delta = \Delta' - P$$

both Δ' and P increase with increase in $|E_{AA} - E_{BB}|$. Experimental results on halogen halides and alkali metal hydrides cited by Pauling (1960) appear to indicate that for small values of $|E_{AA} - E_{BB}|$ the variation of Δ' dominates and for large values of $|E_{AA} - E_{BB}|$ the variation of P dominates in the expression for Δ. Thus Δ and the equilibrium constant could increase or decrease with $|E_A - E_B|$ depending on its magnitude.

Reaction (1) is visualised as (8) in order to bring out the similarities in our results and those discussed by Pauling (1960). In doing so, we take note of the following equivalences. A takes the place of Cu–X bond and B takes the place of Cu–Y bond. Bond energies of $Cu(X)_2$ and $Cu(Y)_2$ are equivalent to bond energies E_{AA} and E_{BB} of the fictitious diatomic molecules (A–A) and (B–B). Thus, the difference D in the bond strengths of Cu–X and Cu–Y bonds of Cu(X)(Y) is related to $|E_{AA} - E_{BB}|$. The experimental observation that spin density on one ligand (and hence on the bond associated with it) increases at the expense of the other (due to increased delocalisation on the stronger bond) is equivalent to the increase of electron density on one atom at the expense of the other due to the ionic character of the bond $A - B$, when $|E_{AA} - E_{BB}| > 0$. Thus even for reaction (1) one obtains $\Delta = \Delta' - P$, where Δ' and P show the above mentioned behaviour. It is not unreasonable to expect that the variation of Δ and P in our system will be similar to those of diatomic molecules discussed by Pauling (1960). This leads to the conclusion mentioned in this paper.

References

Abragam A and Pryce M H L 1951 *Proc. R. Soc. London* **A206** 164
Attanasio D, Keijzers C P, van de Berg J P and de Boer E 1976 *Mol. Phys.* **31** 501
Baratova Z R, Semenov E V, Solozhenkin P M and Prabhananda B S 1982 *Inorg. Chem.* **21** 57
Dietzch W, Reinhold J, Kirmse R, Hoyer E, Marov I N and Belyaeva V K 1977 *J. Inorg. Nucl. Chem.* **39** 1377
Eaton D R and Phillips W D 1965 *J. Chem. Phys.* **43** 392
Krishnamoorthy G and Prabhananda B S 1978 *J. Magn. Res.* **30** 273
Krishnamoorthy G, Prabhananda B S and Solozhenkin P M 1978 *Proc. Indian Acad. Sci. (Chem. Sci.)* **A87** 395
Krishnamoorthy G and Prabhananda B S 1980 *J. Phys. Chem.* **84** 637
Kuska H A, Rogers M T and Drullinger R E 1967 *J. Phys. Chem.* **71** 109
Pauling L 1960 *The Nature of the chemical bond* 3rd edn. (Ithaca Cornell University Press) pp 79–83
Prabhananda B S 1979 *Indian J. Chem.* **A18** 290
Prabhananda B S, Shah S J and Venkataraman B 1972a *Proc. Indian Acad. Sci.* **A76** 231
Prabhananda B S, Shah S J and Venkataraman B 1972b *Indian J. Pure Appl. Phys.* **10** 365
Prabhananda B S, Solozhenkin P M and Panemangalor A V 1977 *Dokl. Akad. Nauk Tajik SSR* **20** 27
Watson R E and Freeman A J 1961 *Phys. Rev.* **123** 2027

Proc. Indian Acad. Sci. (Chem. Sci.), Vol. 92, Number 2, April 1983, pp. 127–131.
© Printed in India.

On the vibrational structure involving C=O stretch in the vapour phase phosphorescence of *p*-benzoquinone-h_4 and -d_4

V N PANDEY† and S N THAKUR*

Department of Physics, Banaras Hindu University, Varanasi 221 005, India
†On leave from Pt. Jawaharlal Nehru College, Banda 210001, India.

MS received 12 August 1982; revised 9 February 1983

Abstract. The high resolution spectrum of vapour phase phosphorescence from *p*-benzoquinone exhibits a mixing of normal modes involving symmetric C=O stretching and C=C stretching vibrations. The vibrational bands due to these mixed vibrations have been assigned on the basis of relative intensities of these bands in the vapour phase and also, using solid neon host.

Keywords. Vibrational structure; C=O and C=C stretching vibrations; *p*-benzoquinone; vapour phase phosphorescence; triplet-singlet transition.

1. Introduction

The two non-bonding orbitals of para-benzoquinone (PBQ) are in accidental degeneracy and its visible spectrum results from an electron promotion to the lowest π^* orbital (Hollas 1964). The splitting between the two singlet states ($^1B_{1g}$ and ^1Au) resulting from this electron promotion has been determined by studying the spectrum in a supersonic jet (Horst and Kommandeur 1979). It has also been found that the splitting between the two triplet states ($^3B_{1g}$ and ^3Au) is less than 0·5 cm^{-1} (Kommandeur private communication). Another interesting aspect in this molecule is the occurrence of vibrational perturbation in the ground electronic state in the energy range 1650 to 1690 cm^{-1} (Goodman and Brus 1978). In the present paper we report the results on our high resolution studies of the vapour phase phosphorescence spectra ($^3Au \rightarrow {}^1Ag$) of para-benzoquinone-h_4 and -d_4.

2. Experimental

The vapour phase phosphorescence was excited by a Schüler-type transformer discharge and by using a tesla coil of 4 MHz frequency. The spectra were recorded on a $f/8{\cdot}4$ one meter Spex grating spectrograph in the first order using Kodak Spectrum Analysis No 1 plates.

3. Results and discussion

The vibrational analysis of the spectrum is straightforward except in the region of the vibronic band involving one quantum of C=O stretching vibration in the ground state

* To whom all correspondence should be addressed.

of PBQ-h_4 (figure 1). This region is dominated by intense emission bands at 16993, 17006·9 and 17017·4 cm^{-1}. The origin band of the vapour phosphorescence in PBQ-d_4 lies at 18682·8 cm^{-1} showing a blue shift of about 1 cm^{-1} with respect to the corresponding origin band of PBQ-h_4. In this case however there is only one strong band at 17021·6 cm^{-1} in the region corresponding to one quantum of C=O stretching vibration in the ground state (figure 2).

Goodman and Brus (1978) observed the phosphorescence spectrum of PBQ in solid neon host and found the $^3B_{1g} \rightarrow {}^1Ag$ emission also which is forbidden in the free molecule. The vibrational structure of $^3Au \rightarrow {}^1Ag$ system is very different from the former and the strongest band of this system involves a ground state vibrational frequency of 1676 cm^{-1} in PBQ-h_4 and of 1668 cm^{-1} in PBQ-d_4. The interval of 1676 cm^{-1} is in good agreement with that of 1675 cm^{-1} associated with the band at 17006·9 cm^{-1} in PBQ-h_4 in our work. In the case of PBQ-d_4 however there are two weak bands involving ground state vibrational intervals of 1667·5 and 1670·3 cm^{-1} whose average separation (1669 cm^{-1}) is in good agreement with the vibrational interval of 1668 cm^{-1} reported by Goodman and Brus (1978).

It has been suggested that the symmetric C=O stretch (ν_3) and the C=C stretch (ν_2) are both strongly mixed-vibrations (Goodman and Brus 1978). It is therefore likely that in the solid state neon host ν_3 becomes more prominent in the case of PBQ-h_4 whereas ν_2 is more prominent in the case of PBQ-d_4. In our vapour phase phosphorescence we assume that it is the C=O stretching vibration (ν_3) which corresponds to the most intense band in both the molecules (17006·9 cm^{-1} in PBQ-h_4 and 17021·6 cm^{-1} in PBQ-d_4). This has been done in view of the fact that $n \rightarrow \pi^*$ electron promotion is largely localized in the C=O bond region and the effects of external perturbations are minimal in the vapour phase. This leads to the assignment of the band at 16993·0 cm^{-1} in PBQ-h_4 as due to C=C stretching vibration (ν_2) which has an interval of 1689 cm^{-1}. The corresponding interval in PBQ-d_4 may be taken as 1669 cm^{-1} (average value). It is to be noted that the bands involving C=C stretching vibration in both PBQ-h_4 and PBQ-d_4 are weak in comparison to the respective bands involving symmetric C=O stretching vibration.

The band at 17017·4 cm^{-1} in PBQ-h_4 has a vibrational interval of 1665 cm^{-1} and has been assumed to involve one quantum of antisymmetric C=O stretching vibration. This is in good agreement with the assignments of Dunn and Francis (1974) and of Anno and Sado (1958). In the case of PBQ-d_4 (figure 2) we get three closely-spaced weak bands with an average ground state interval of 1646 cm^{-1} and this has been assigned as due to antisymmetric C=O stretching vibration in the light of an observed band at 1648 cm^{-1} in the vapour phase infrared spectrum of this molecule (Goodman and Brus 1978).

4. Conclusion

We have been able to assign three prominent bands in the vapour phosphorescence spectrum of PBQ-h_4 and one prominent and two weak bands in the corresponding spectrum of PBQ-d_4 on the basis of our high resolution work.

Acknowledgements

The authors are thankful to Dr J M Hollas of Reading University of providing experimental facilities to SNT and to the UGC (New Delhi) for a Teacher Fellowship to VNP.

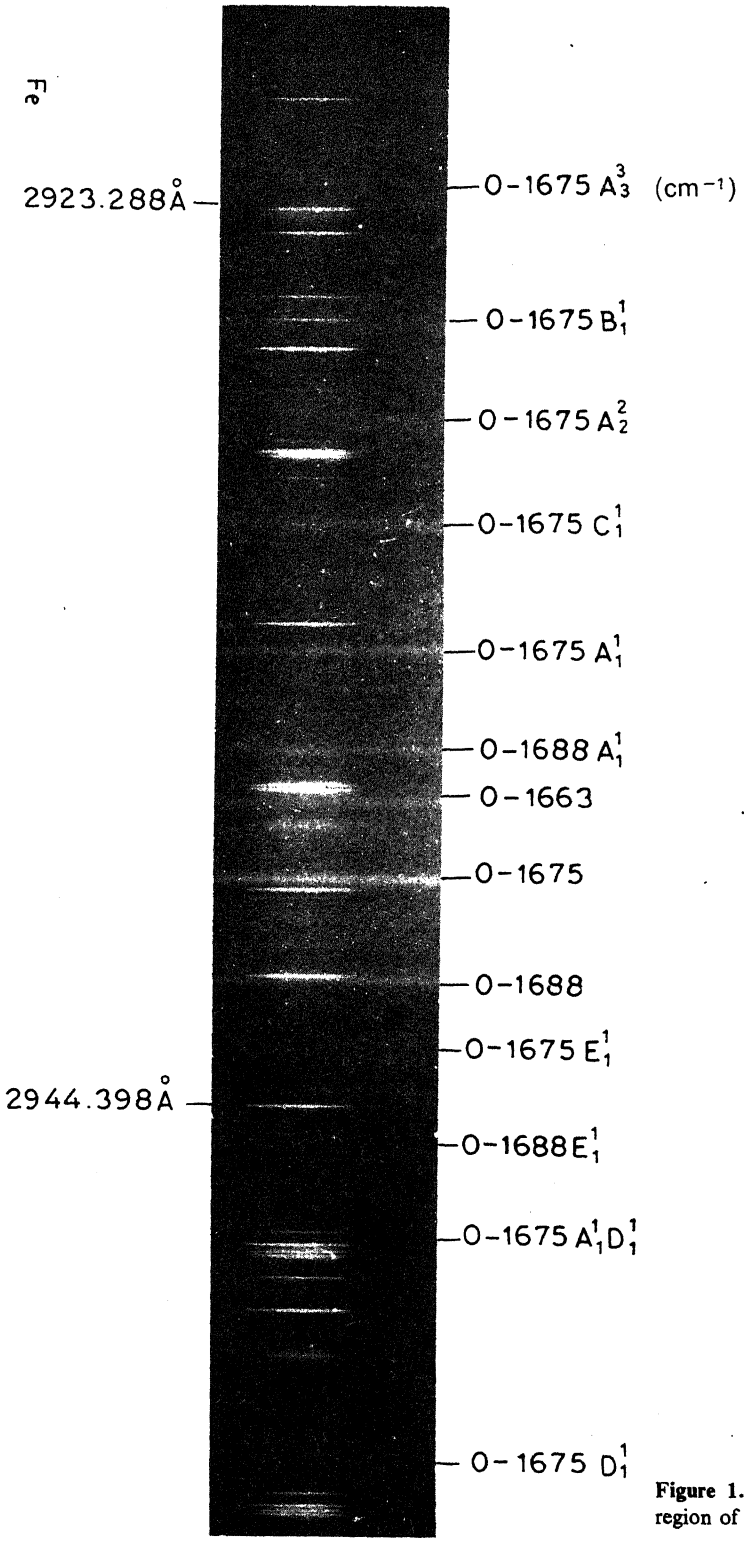

Figure 1. The C=O stretching region of PBQ-h_4.

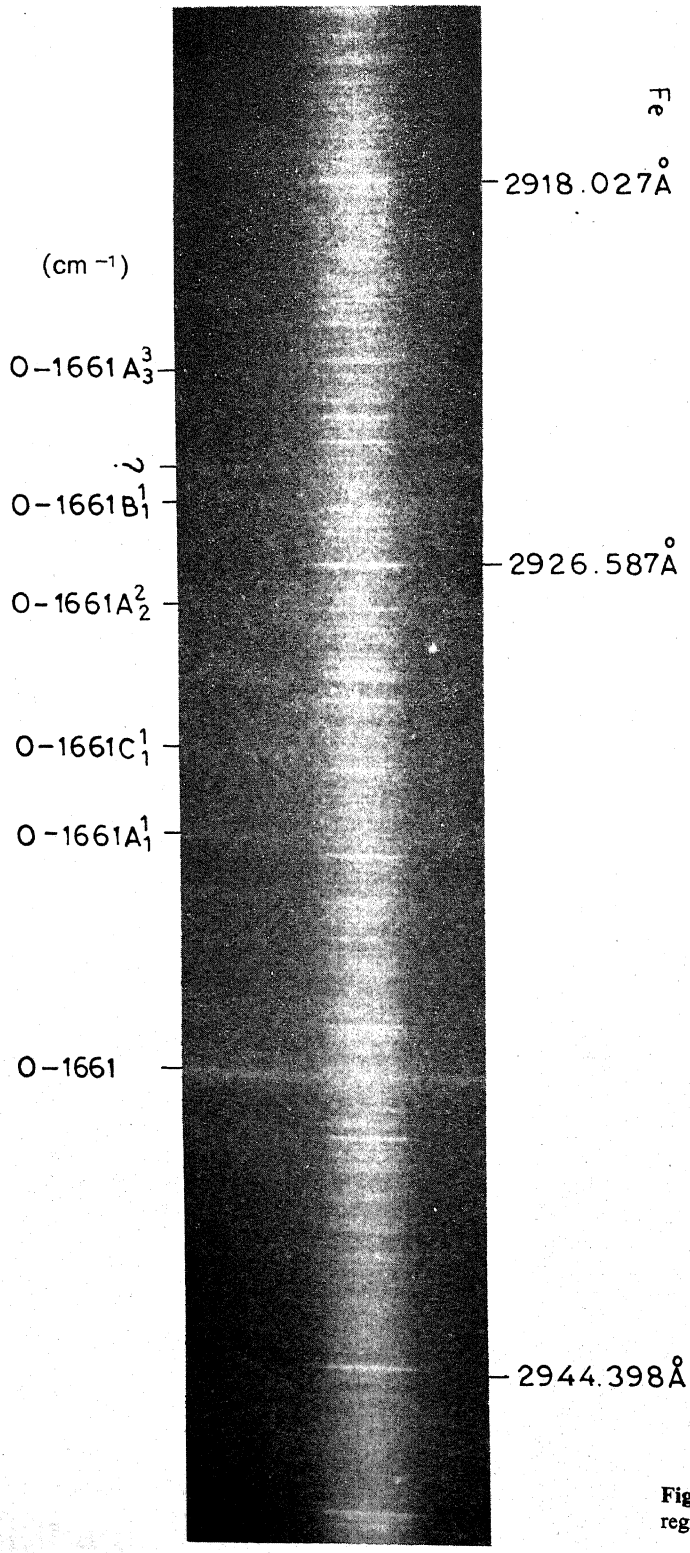

Figure 2. The C=O stretchi
region of PBQ-d_4.

References

Anno T and Sado A 1958 *Bull. Chem. Soc. Jpn.* **31** 734
Dunn T M and Francis A H 1974 *J. Mol. Spectrosc.* **50** 14
Goodman J and Brus L E 1978 *J. Chem. Phys.* **69** 1604
Hollas J M 1964 *Spectrochim. Acta* **20** 1563
Horst G T and Kommandeur J 1979 *Chem. Phys.* **44** 287

Proc. Indian Acad. Sci. (Chem. Sci.), Vol. 92, Number 2, April 1983, pp. 133–138.
© Printed in India.

The near UV vapour absorption spectra of 1-hydroxynaphthalene and 2-hydroxynaphthalene

V N PANDEY† and S N THAKUR*
Department of Physics, Banaras Hindu University, Varanasi 221 005, India
†On leave from Pt. Jawaharlal Nehru College, Banda 210 001, India.

MS received 12 August 1982; revised 9 February 1983

Abstract. Vibrational analyses, of the electronic bands of 1-hydroxynaphthalene and 2-hydroxynaphthalene corresponding to the 312 nm electronic transition in naphthalene, have been carried out from the vapour phase absorption spectra recorded under high resolution. It is found that the prominent vibronic bands owe their large intensities to a different vibronic interaction than that in naphthalene.

Keywords. UV vapour absorption spectra; hydroxynaphthalene; vibrational analyses.

1. Introduction

The effect of substituents on the excited electronic states of naphthalene can only be deduced from absorption spectra. Since the electronic wavefunctions of molecules are free from any external perturbations in the vapour phase these spectra are the least complicated to interpret. The greater number of allowed vibrations in the substituted naphthalenes, however, makes their spectra much more complex in appearance than the spectrum of naphthalene because of their lower symmetry. The perturbational role of molecular vibrations on the one hand and inductive substituents on the other is complementary in the electronic spectroscopy of alternant hydrocarbons but the recent studies on two-photon spectra of benzenes show that the complementarity of vibronic and inductive perturbations for a given electronic transition gets reversed as compared to that in one-photon spectra [Goodman and Rava 1982]. It has been possible to see these changes in perturbation effects due to the availability of vast amount of data on the one-photon absorption spectra of substituted benzenes. In substituted naphthalenes, however, there is paucity of data from the high resolution vapour phase absorption spectroscopy. In the present paper we summarize the results of our vibrational analyses of electronic bands of 1-hydroxynaphthalene (1-HN) and 2-hydroxynaphthalene (2-HN) corresponding to the 312 nm system of the parent naphthalene molecule.

2. Experimental

The absorption bands were developed in a pyrex cell fitted with quartz windows at temperatures 60°C for 1-HN and 100°C for 2-HN and were recorded on a 3·4 m Jarrell-

*To whom all correspondence should be addressed.

Ash grating spectrograph using photographic plates. The plates were measured on a Russian comparator, the uncertainty of measurements being 0·1 cm^{-1} for sharp bands and 0·5 cm^{-1} for weak and diffuse bands.

3. Discussion

The O_0^0 bands of 1-HN and 2-HN have been assigned in the light of hot electronic bands and the vibrational frequencies determined from the infrared spectra (Hollas and Thakur 1973, 1974). In the present work about 200 bands in the spectra of both 1-HN and 2-HN were analysed. The prominent sequence bands in the neighbourhood of the O_0^0 band are shown in figures 1 and 2, for 1-HN and 2-HN respectively, where A, B, C etc., stand for sequence bands in the order of decreasing intensities.

The 312 nm electronic spectrum of the parent molecule consists of two parts—the Franck-Condon part of the intensity as represented by the O_0^0 band and the others involving totally symmetric vibrations which are small in comparison to the vibronic part of the intensity which is associated with the b_{3g} vibrations. The vibronic intensity arises from Herzberg-Teller type intensity stealing from the second excited state $^1B_{1u}$ of naphthalene (Craig *et al* 1961).

In the case of 1-HN and 2-HN both the first and the second excited states have A′ symmetry of the C_s point group and any differences in the intensities of vibronic bands should reflect the effect of substituent site. The strong vibronic bands at 0–317 cm^{-1} in 2-HN and at 0–274 cm^{-1} in 1-HN have the same rotational contours as the corresponding O_0^0 bands and this implies that there are no changes in the orientation of the transition moments. It has been shown earlier that the electronic transition moments of 1-substituted naphthalenes are polarized largely along the long in-plane axis whereas those of 2-substituted naphthalenes are polarized largely along the short in-plane axis (Hollas and Thakur 1973, 1974). The weak vibronic bands at 0–531 cm^{-1} in 1-HN and at 0–522 cm^{-1} in 2-HN may be correlated to the ring distortion vibration of b_{3g} symmetry (506 cm^{-1}) in naphthalene which gives rise to the most active vibronic band in naphthalene. This observation shows that the bands at 0–274 cm^{-1} in 1-HN and 0–317 cm^{-1} in 2-HN may involve a intensity borrowing from an electronic state other than the second excited singlet state. One of the possibilities is the involvement of charge-transfer states corresponding to the promotion of an electron from a molecular orbital localized on the substituent to that localized on the ring. This idea gets support from the fact that the vibrational structures observed in the spectra of 1-fluoronaphthalene and 2-fluoronaphthalene (Singh 1981) are different from those of corresponding naphthols.

The vibrational intervals in the ground and the first excited states as determined from the present work are summarized in table 3 and the prominent vibronic bands are given in tables 1 and 2 for 1-HN and 2-HN respectively. It is seen that the rotational contours of the vibronic bands involving out-of-plane vibrations (symmetry a'') are not well-developed. The present analysis supersedes the earlier analyses from the low resolution work (Singh and Singh 1965, 1966).

It is also interesting to note that the normal modes of vibrations appearing strongly in the hot bands do not give rise to similarly intense cold bands. This may result from the different amounts of mixing between two or more vibrational modes in the two electronic states which can change the form of a particular mode of vibration in going

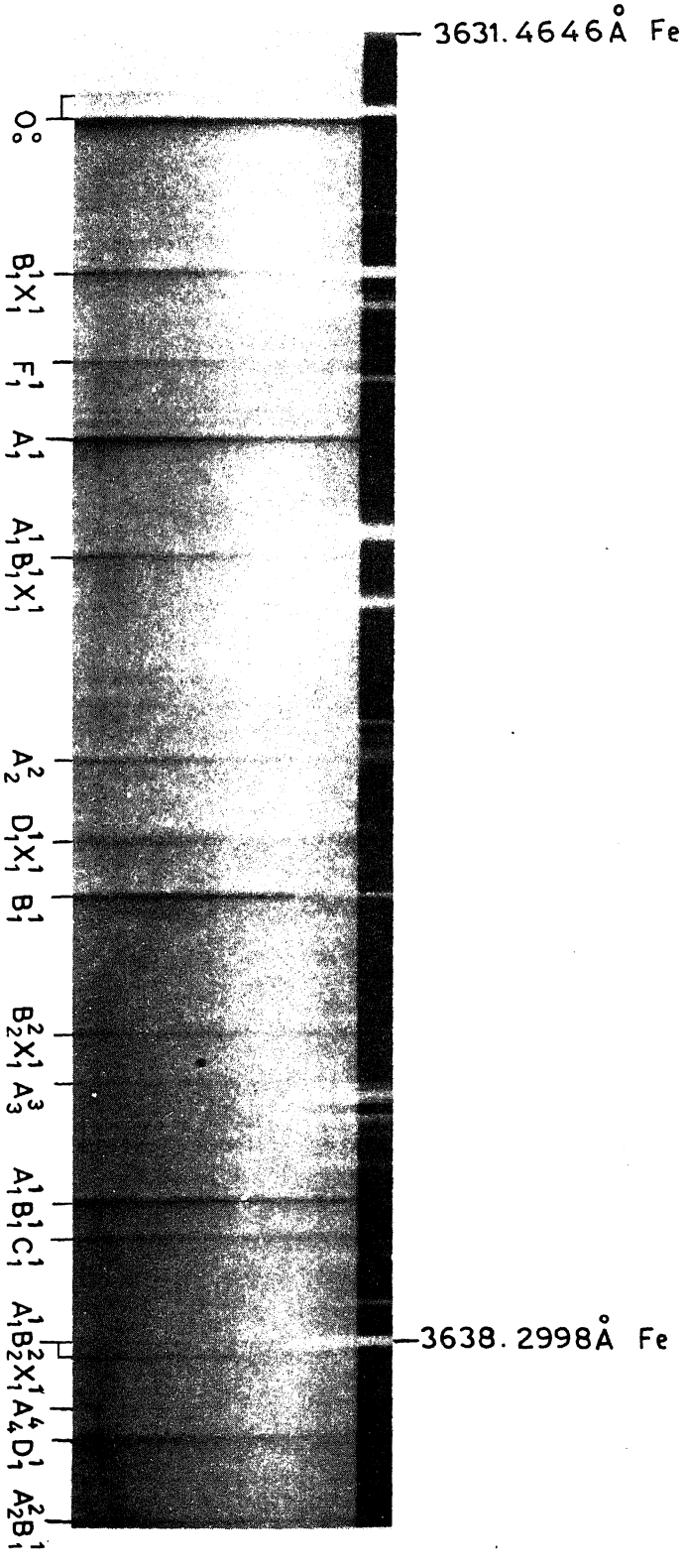

Figure 1. The O_0^0 band region of 1-hydroxynaphthalene.

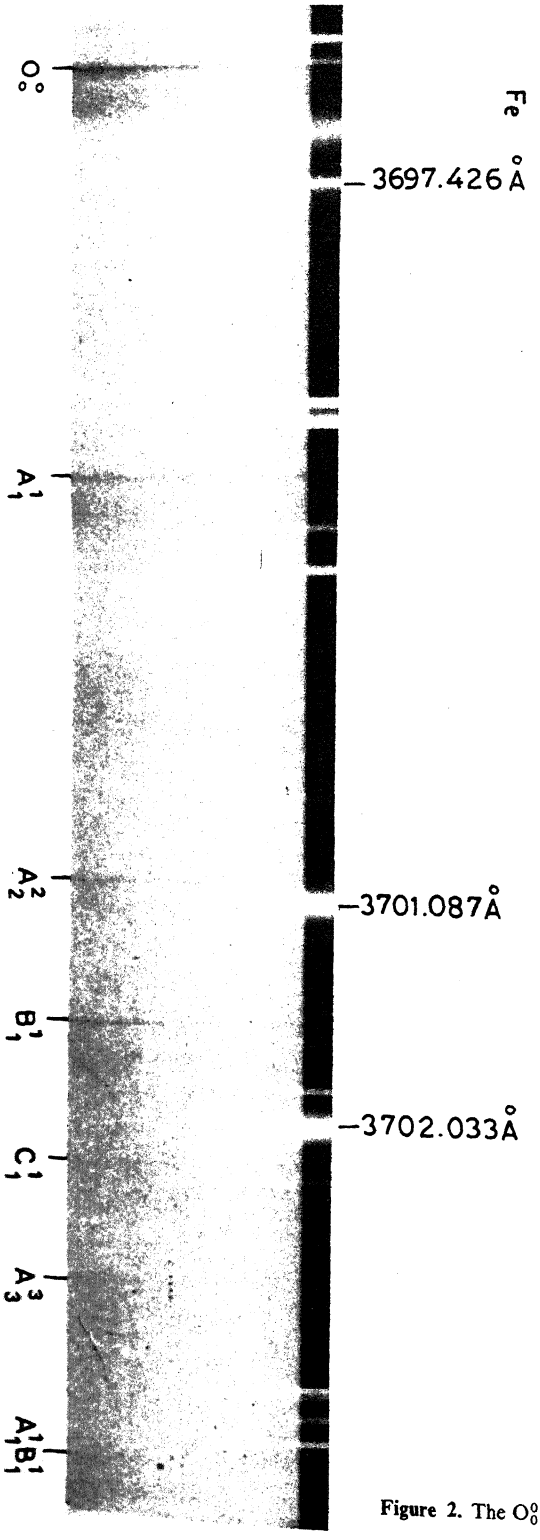

Figure 2. The O_0^0 band region of 2-hydroxynaphthalene.

Table 1. Prominent bands in the $S_1 \leftarrow S_0$ vapour absorption of 1-hydroxynaphthalene.

Wave number (cm^{-1})	Relative intensity	Separation from O_0^0 band (cm^{-1})	Assignments
30925	2	−531·0	0–531
31029	2·5	−427·1	0–427
31182	5	−274·4	0–274
31260	2	−196·7	0–197
31345	4	−111·6	E_1^1
31377	2	−79·7	G_1^1
31407	4	−49·1	C_1^1
31422	8	−34·2	
31422	8	−34·1	B_1^1
31422	8	−34·0	
31433	2	−23·8	H_1^1
31442	6	−14·0	A_1^1
31446	2	−10·6	F_1^1
31456·5	10	0–0	O_0^0
31457	1	+0·7	
31457	1	+0·9	Y_1^1
31458	1	+1·1	
31483	6	+26·9	X_1^1
31564	3	+107·4	0+107
31731	6	+274·4	0+274
31869	5	+412·4	0+412
31908	3	+452·0	0+452
32140	4	+683·2	0+683

Table 2. Prominent bands in the $S_1 \leftarrow S_0$ vapour absorption of 2-hydroxynaphthalene.

Wave number (cm^{-1})	Relative intensity	Separation from O_0^0 band (cm^{-1})	Assignments
30383	1·5	−522·1	0–522
30495	3	−410·9	0–411
30589	8	−316·8	0–317
30703	2	−202·1	0–202
30778	1	−127·1	0–127
30779	1	−126·7	
30815	1·5	−90·5	D_1^1
30859	2·5	−46·4	C_1^1
30865	3	−40·5	B_1^1
30888	2	−17·3	A_1^1
30905	10	0–0	O_0^0
30923	1·5	+17·9	X_1^1
30986	2	+80·7	0+81
31197	1	291·5	0+292
31301	1·5	+395·5	0+395
31309	1·5	+403·4	0+403
31625	2	+719·3	0+719

Table 3. Correlation of ground and excited state frequencies of 1-hydroxy and 2-hydroxy naphthalene.

Molecule	Ground state (cm^{-1})	Excited state (cm^{-1})	Sequence internal (cm^{-1})
1-hydroxynaphthalene	156 (*a*″)	107 (*a*″)	−49
	197 (*a*″)	163 (*a*″)	−34
	274 (*a*′)	260 (*a*′)	−14
	470 (*a*′)	412 (*a*′)	−58
	531 (*a*′)	452 (*a*′)	−79
	740 (IR) (*a*′)	683 (*a*′)	
	770 (Raman) (*a*′)		
2-hydroxynaphthalene	127	81	−46
	202	162	−40
	317		
	411	395	−17
	522		
	740 (IR)	719	
	765 (Raman)		

from the ground to the excited electronic state. This effect makes the task of correlating ground and excited state vibrational frequencies very difficult. The observed sequence intervals have been used in making such correlations wherever possible and are shown in table 3 for the two molecules.

Acknowledgements

The authors are thankful to Dr J M Hollas of Reading University for providing experimental facilities to SNT and to UGC (New Delhi) for a teacher fellowship to VNP.

References

Craig D P, Hollas J M, Redies M F and Wait S C Jr 1961 *Philos. Trans. R. Soc. (London)* **A253** 543

Hollas J M and Thakur S N 1973 *Mol. Phys.* **25** 1315

Hollas J M and Thakur S N 1974 *Mol. Phys.* **27** 1001

Goodman L and Rava R P 1982 *Advances in Chemical Physics* **54** (eds) I Prigogine and S A Rice (New York: Wiley) Chap 2

Singh R A 1981 *Spectra and structural studies of some monosubstituted naphthalenes* Ph.D. Thesis, Banaras Hindu University

Singh R D and Singh R S 1965 *Indian J. Pure Appl. Phys.* **3** 418

Singh R D and Singh R S 1966 *Curr. Sci.* **15** 287

Proc. Indian Acad. Sci. (Chem. Sci.), Vol. 92, Number 2, April 1983, pp. 139–145.
© Printed in India.

Structural, electrical and reflectance studies of the system $ZnMn_{2-2x}Ni_xTi_xO_4$

B A MULLA and V S DARSHANE*

Chemistry Department, Institute of Science, Bombay 400032, India

MS received 6 September 1982; revised 24 February 1983

Abstract. X-ray, electrical conductivity and reflectance studies of the system $ZnMn_{2-2x}Ni_xTi_xO_4$ have been carried out. The system is tetragonal in the range $0 \leqslant x \leqslant 0{\cdot}25$ and cubic in the range $0{\cdot}5 \leqslant x \leqslant 1$. Electrical resistivity temperature behaviour obeys Wilson's law for all the compounds and the thermoelectric coefficient values vary between 325 and $-290\ \mu V/K$. The activation energy and ρ_{RT} decrease gradually with increase in concentration of charge carriers at *B*-site except for $ZnNiTiO_4$. Reflectance spectral studies indicate the presence of Ni^{2+} at the octahedral site.

Keywords. Spinel; x-ray; electrical conductivity; Seebeck coefficient; reflectance spectra.

1. Introduction

Compounds of AB_2O_4 type with spinel structure have been investigated by a number of workers (Blasse 1965; O'Keeffe 1961; Goodenough 1963; Ghare and Sinha 1968; Rao and Subba Rao 1970) as they show interesting structural, electrical and magnetic properties which vary with the nature of the ions, their charge and site distribution amongst tetrahedral and octahedral sites. Literature survey indicated that although considerable work has been done on zinc manganite, no work has been reported on the system $ZnMn_{2-2x}Ni_xTi_xO_4$. With a view to investigating the effect of cations of different charges and radii on structural parameter as well as mode of conduction, the above mentioned system has been studied. Similarly the cation distribution has been determined using x-ray analysis, electrical conductivity and reflectance spectroscopic studies.

2. Materials and methods

The compositions of the system $ZnMn_{2-2x}Ni_xTi_xO_4$ were prepared by mixing the component oxides (GR grade) in acetone in appropriate molar proportions. The pellets of these compositions were prepared using 2% solution of polyvinylacetate as a binder which were first slowly heated at 773 K for 20 hr to remove the binder and then fired at 1173 K for 100 hr. The samples were cooled slowly in air at 50 K/hr. X-ray powder patterns (Philips diffractometer) were taken using Cu-K_α radiation with Ni-filter. The areas under different (*hkl*) peaks were determined by counting the squares on the cm-graph paper and their values obtained in relation to the peak for 311 reflections which was taken as 100. The {*hkl*} reflections 220, 222, 400, 422 and 440 are sensitive to cation

*To whom all correspondence should be addressed.

distribution at both the sites in the spinel lattice. To determine the cation distribution and its variation, if any, with the composition the intensity ratios 220/400, 400/422, 400/440 and 422/440 were calculated for different possible models of cation distribution and were compared with the observed ratios. The relative integrated intensity I of the given $\{hkl\}$ reflection was calculated by using a diffractometer with flat plate sample holder. The following formula suggested by Burger (1960) was used.

$$I = |F_{hkl}|^2 P \cdot L_p, \tag{1}$$

where F is the structure factor, P the multiplicity factor and L_p the Lorentz polarisation factor. The atomic scattering factors for various ions were taken from International Tables (1974).

The electrical resistivity was measured using LCR Marconi bridge. The faces of each pellet were coated with a thin layer of conducting silver paste and measured from 303 to 773 K using two-probe technique. Thermoelectric coefficient was measured from room temperature to 573 K. The thermoelectric coefficient value is considered positive if the cold end is positive, indicating p-type of semiconduction. Reflectance spectra in the range 300 to 1200 nm (33000 to 8000 cm^{-1}) were recorded (Carl Zeiss VSU-2P spectrophotometer) using $MgCO_3$ as a reference.

3. Results and disussion

3.1 *X-ray analysis*

The results of the x-ray analysis are summarised in table 1 and the lattice constant *vs* composition is plotted in figure 1. The system $ZnMn_{2-2x}Ni_xTi_xO_4$ is tetragonal in the range $0 \leqslant x \leqslant 0{\cdot}25$ and cubic in the range $0{\cdot}50 \leqslant x \leqslant 1$. The values of the lattice constants of the end members, $ZnMn_2O_4$ and $ZnNiTiO_4$ observed (table 1) are well within those reported earlier (Mason 1947; Yamaguchi 1953).

The compound $ZnMn_2O_4$ showed tetragonal symmetry ($a' = 8{\cdot}06$ and $c' = 9{\cdot}23$A) due to the presence of Mn^{3+} (J–T) ion at B-site. Table 1 and figure 1 show that more than 50% of Mn^{3+} ions are required at the B-site to cause tetragonal distortion in the

Table 1. Lattice parameter, resistivity, activation energy and thermo e.m.f. for the system $ZnMn_{2-2x}Ni_xTi_xO_4$.

Composition	Colour	Structure type	Lattice parameters (A)	ρ at RT (ohm-cm)	ΔE (eV)	α (μV/°C)
$ZnMn_2O_4$	Brownish black	T	$a' = 8{\cdot}06$ $c' = 9{\cdot}23$	$1{\cdot}20 \times 10^9$	0·67	325
$ZnMn_{1{\cdot}5}Ni_{0{\cdot}25}Ti_{0{\cdot}25}O_4$	Brownish black	T	$a' = 8{\cdot}047$ $c' = 9{\cdot}15$	$1{\cdot}01 \times 10^9$	0·61	77
$ZnMn_{1{\cdot}0}Ni_{0{\cdot}5}Ti_{0{\cdot}5}O_4$	Brownish black	C	$a = 8{\cdot}36$	$9{\cdot}81 \times 10^8$	0·53	40
$ZnMn_{0{\cdot}5}Ni_{0{\cdot}75}Ti_{0{\cdot}75}O_4$	Brown	C	$a = 8{\cdot}40$	$8{\cdot}15 \times 10^8$	0·46	−19
$ZnNiTiO_4$	Yellowish green	C	$a = 8{\cdot}45$	$> 10^{12}$	1·08	−290

C = cubic, T = tetragonal.

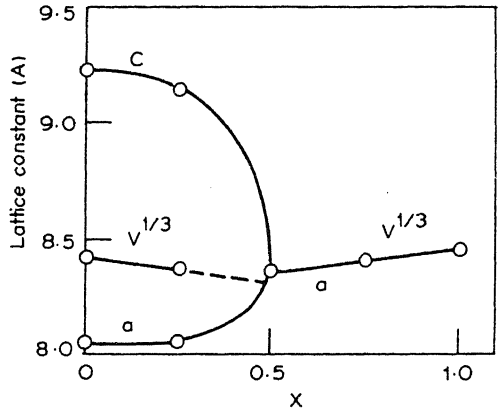

Figure 1. Plot of lattice constant and $V^{1/3}$ *vs* composition for the system $ZnMn_{2-2x}Ni_xTi_xO_4$.

lattice. This higher value (62·5 %) of critical fraction suggests the presence of ions with different charges and/or radii at *B*-site (Jain and Darshane 1981). Figure 1 also shows that the plot of $V^{1/3}$ *vs* composition shows a break at the transition region, similar to the studies reported in Zn-Ge-Co-Mn (Wickham and Croft 1958) and $ZnMnFeO_4$-$GaCoMnO_4$ (Jain and Darshane 1981) oxide spinel systems. The sudden change in the volume at the critical composition can be attributed to the change in the elastic energy of the crystal (Goodenough and Loeb 1955).

The cation distribution in oxidic type compounds can be obtained by x-ray diffraction intensity calculations. The observed and calculated intensities were computed for the composition taking into consideration the structure factors for the planes 220, 400, 422 and 440 which are quite sensitive to cation distribution. Intensity was calculated for different models in which (i) Ni^{2+}, Ti^{4+} and Mn^{3+} (ii) Ni^{3+}, Ti^{4+}, Ti^{2+} and Mn^{3+} (iii) Ni^{3+}, Ti^{3+} and Mn^{3+} and (iv) Ni^{2+}, Ti^{4+}, Mn^{2+} and Mn^{4+} are present at *B*-site. Intensity ratios for the compound $ZnNi_{0.5}Ti_{0.5}MnO_4$ are given in table 2. The calculated intensity ratios show better agreement with the observed intensity ratios in which Zn^{2+} occupy *A* site and Ni^{2+}, Ti^{4+} and Mn^{3+} are at *B* site. This model is also supported by site preference energy values (Miller 1959). Hence the ionic configuration of the system can be written as $Zn^{2+}[Mn^{3+}_{2-2x}Ni^{2+}_x\ Ti^{4+}_x]O^{2-}_4$.

Table 2. Comparison of intensity ratios for $Zn[Ni_{0.5}Ti_{0.5}Mn]O_4$.

Cations at		220/400		400/422		400/440		422/440	
A-Site	*B*-Site	Obs.	Calc.	Obs.	Calc.	Obs.	Calc.	Obs.	Calc.
Zn^{2+}	$Ni^{2+}_{0.5}Ti^{4+}_{0.5}Mn^{3+}$		2·90		0·90		0·36		0·40
Zn^{2+}	$Ni^{3+}_{0.5}Ti^{2+}_{0.25}Ti^{4+}_{0.25}Mn^{3+}$	2·88	2·95	0·94	0·87	0·37	0·40	0·39	0·44
Zn^{2+}	$Ni^{3+}_{0.5}Ti^{3+}_{0.5}Mn^{3+}$		2·95		0·88		0·42		0·44
Zn^{2+}	$Ni^{2+}_{0.5}Ti^{4+}_{0.5}Mn^{4+}_{0.5}Mn^{2+}_{0.5}$		2·96		0·88		0·43		0·46

3.2 *Electrical properties*

The room temperature dc resistivity in all the compounds varied between 10^8 and 10^{12} ohm-cm and the activation energy between 0·49 and 1·08 eV. Electrical resistivity-temperature behaviour obeyed Wilson's law ($\rho = \rho_0 \exp \Delta E/kT$) indicating the semiconducting nature of the compounds (figure 2). High resistivity values of the compounds indicate that the elements with only one stable oxidation state are present at *B*-site. In transition metal oxides, electrical resistivity is low if the compound contains the cations of the same element situated at the similar site but with their valency differing by unity *e.g.* $Fe^{3+}[Fe^{2+}Fe^{3+}]O_4^{2-}$ ($\rho_{RT} \simeq 10^{-2}$ ohm-cm) (Verwey *et al* 1951).

The plot of thermoelectric voltage (μV) *vs* temperature (ΔT) is given in figure 3. A positive sign indicates that the sample is of *p*-type and the negative shows *n*-type. It is seen that the compounds where $x \leqslant 0{\cdot}5$ are *p*-type and for $x > 0{\cdot}5$ they are *n*-type semiconductors. Thermoelectric power of $ZnNiTiO_4$ is negative and decreases with temperature in the range 30 to 120°C and increases with temperature in the range 120 to 300°C. This is due to the fact that the mobility of *n*-type carriers is higher than that of *p*-type (up to 120°C) and as temperature increases the mobility of *p*-type carriers rises rapidly compensating for *n*-type carriers.

The conduction mechanism in the present system can be explained as follows. In the first three compounds ($x \leqslant 0{\cdot}5$) *p*-type semiconduction was observed. This is attributed

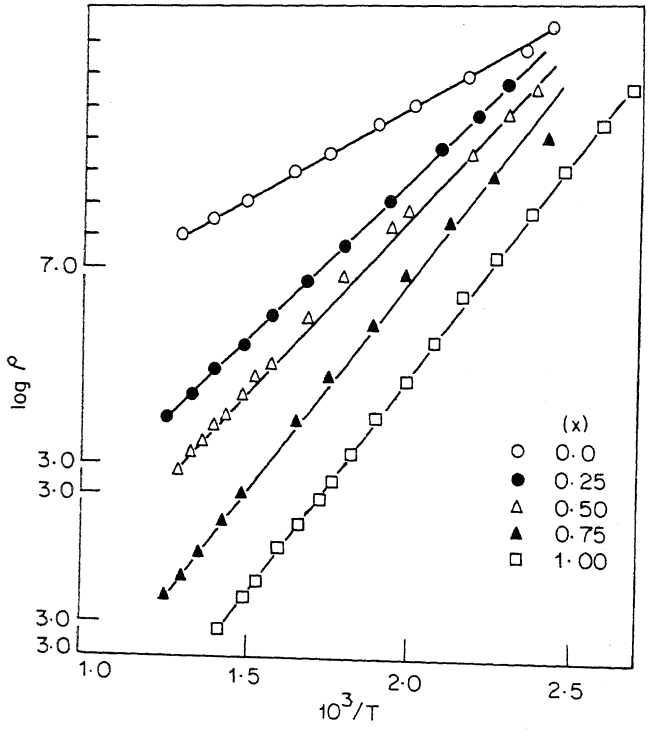

Figure 2. Plot of log ρ *vs* $10^3/T$ for the system $ZnMn_{2-2x}Ni_xTi_xO_4$.

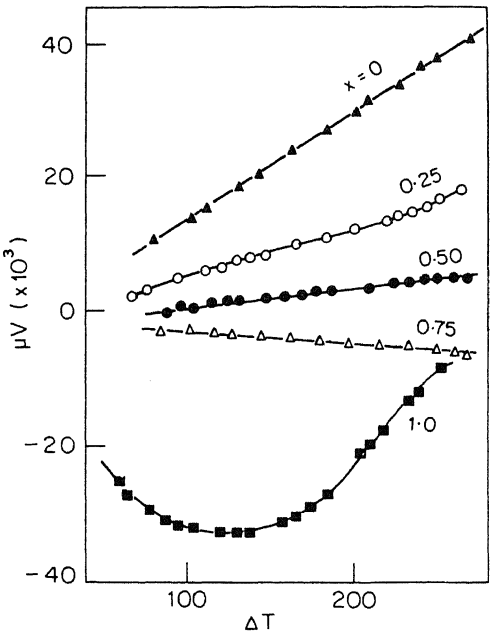

Figure 3. Plot of μV *vs* ΔT for the system $ZnMn_{2-2x}Ni_xTi_xO_4$.

to the following process:

$$Mn^{3+} + Mn^{4+} \rightarrow Mn^{4+} + Mn^{3+},$$

where the motion of Mn^{4+} ion acts as a hole. However in the last two compounds $x \geqslant 0{\cdot}75$.

Slight departure from stoichiometry produces Ti^{3+} ion in the lattice which acts as donor with respect to Ti^{4+} ion and donor levels are introduced near 3*d* bands. These Ti^{3+} ions (donors) produce conduction electrons near 3*d* levels and are ultimately responsible for *n*-type conduction in $ZnNiTiO_4$ and $ZnNi_{0{\cdot}75}Ti_{0{\cdot}75}Mn_{0{\cdot}5}O_4$. Increasing concentration of Ti^{4+} ions in the lattice ($x \geqslant 0{\cdot}75$) indicates that $Ti^{3+} \rightarrow Ti^{4+}$ mechanism becomes more predominant as compared to $Mn^{3+} \rightarrow Mn^{4+}$ and, therefore, shows *n*-type behaviour in the last two cases. This is also one of the reasons for the decrease in ΔE and ρ_{RT} in our compounds (table 1). The high values of ΔE and ρ_{RT} in $ZnNiTiO_4$ are attributed to the presence of nickel and titanium in 2+ and 4+ oxidation states only.

3.3 *Reflectance spectra*

Reflectance spectra can conveniently detect octahedrally and tetrahedrally co-ordinated nickel ions in solids. Three bands were observed in the region 8,000 to 33000 cm^{-1} for all the compounds while for $ZnNiTiO_4$ the bands were observed at (i) 9750 (ii) 15250 and (iii) 27500 cm^{-1} (figure 4). The positions of bands of the spectra closely agree with those of Porta *et al* (1974) and Schmidz-Du Mont *et al* (1965) who have investigated zinc-nickel-aluminate and zinc-magnesium-aluminate spinels. Besides the above bands Schmidz-Du Mont *et al* (1965) observed a band around

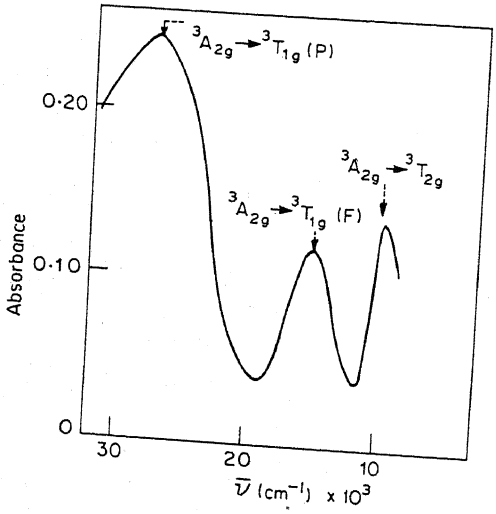

Figure 4. Reflectance spectrum for $ZnNiTiO_4$.

17000 cm^{-1} which is due to tetrahedrally co-ordinated nickel. The above band is not observed in our compositions since nickel is present at octahedral site only, which is supported by x-ray investigation and site preference energy values (Miller 1959). As pointed out by Schmidz Du Mont *et al* (1965) the bands (i), (ii) and (iii) are due to

$$^3A_{2g} \rightarrow {}^3T_{2g},\ {}^3A_{2g} \rightarrow {}^3T_{1g}\ (F) \text{ and } {}^3A_{2g} \rightarrow {}^3T_{1g}\ (P)$$

transitions respectively. The assignment of the above bands to octahedrally co-ordinated nickel is also supported by the study of transition metal complexes (Drago 1965).

4. Conclusions

(i) The system $ZnMn_{2-2x}Ni_xTi_xO_4$ is tetragonal in the range $0 \leqslant x \leqslant 0{\cdot}25$ and cubic in the range $0{\cdot}5 \leqslant x \leqslant 1$. (ii) X-ray analysis and electrical conductivity data suggest the ionic configuration as $Zn^{2+}[Mn^{3+}_{2-2x}Ni^{2+}_xTi^{4+}_x]O_4$. (iii) The compounds for $x \leqslant 0{\cdot}5$ are *p*-type while for $x > 0{\cdot}5$ are *n*-type semiconductors. (iv) Reflectance measurements suggest the presence of Ni^{2+} at octahedral site only.

Acknowledgements

One of the authors (BAM) is thankful to UGC, New Delhi, for a teacher fellowship. VSD is thankful to UGC for financial support.

References

Blasse G 1965 *Philips Res. Rep.* **20** 529
Burger M J 1960 *Crystal structure analysis*, (New York: John Wiley) p. 46
Drago R S 1968 *Physical methods in inorganic chemistry* (New Delhi: East-West Press) p. 167

Ghare D B and Sinha A P B 1968 *J. Phys. Chem. Solids* **29** 865
Goodenough J B 1963 *Magnetism and chemical bond* (New York, London: John Wiley) p. 120
Goodenough J B and Loeb A L 1955 *Phys. Rev.* **98** 391
International Tables for X-ray Crystallography Vol III (Birmingham: Kynoch Press) 1974
Jain P S and Darshane V S 1981 *Nucl. Phys. Solid. State. Phys. Sym.* (Silver Jubilee Vol 24c) BARC, Bombay 529
Mason B 1947 *Am. Minerol.* **32** 426
Miller M 1959 *J. Appl. Phys. Suppl.* **30** 24s
O'Keeffe M 1961 *J. Phys. Chem. Solids.* **21** 172
Porta P, Stone F S and Turner R G 1974 *J. Solid. State. Chem.* **11** 135
Rao C N R and Subba Rao G V 1970 *Phys. Status Solidi* **A1** 597
Schmidz-Du Mont O, Lule A and Reinen D 1965 *Ber Bunsenges Phys. Chem.* **69** 76
Verwey E J W, Braun P B, Gorter E W, Romeijn F C and Van Santen J H 1951 *Phys. Chem.* **198** 6
Wickham D G and Croft W J 1958 *J. Phys. Chem. Solids.* 7 361
Yamaguchi an 1953 *Bull. Chem. Soc. Jpn.* **26** 204

Proc. Indian Acad. Sci. (Chem. Sci.), Vol. 92, Number 2, April 1983, pp. 147–152.
© Printed in India.

Viscometry in the study of molecular complexes

BHARATI BHATTACHARJEE and S N BHAT*
Department of Chemistry, North-Eastern Hill University, Shillong 793 003, India

MS received 1 January 1983

Abstract. Viscometric method has been used to study the interaction between the weak interacting systems such as benzene-CCl_4-cyclohexane, toluene-CCl_4-cyclohexane and *o*-xylene-CCl_4-cyclohexane. The equilibrium constants and other thermodynamic parameters have been reported and compared with literature data.

Keywords. Viscometry; molecular complexes; weak interacting systems.

1. Introduction

There has been an increasing interest in the study of molecular complexes and a number of different experimental procedures have been used to investigate the interaction between electron donors and electron acceptors with or without a third component. All the methods available to study the molecular structure and the nature of chemical bond also apply to molecular complexes. However, in spite of the fact that in principle, the interaction between molecules and the composition of the complex formed can be established from a study of the characteristic abrupt departure of some physical properties from ideal behaviour, like dielectric constant, refractive index, optical absorption, surface tension, viscosity etc, many of these methods are hardly used. Recently Bhat *et al* (1979); Bhat and Singh (1981, 1982) used non-spectral methods like surface tension, refractive index measurements, constant activity method etc., to study the interaction between the molecules in solutions, and demonstrated their applicabilities in obtaining the equilibrium constant directly. Although the measurements of various thermodynamic excess functions of binary solutions have been the subject of much research (from viscosity measurements) there is hardly any report on using viscosity measurement method for ternary systems except that of Irving and Smith (1969). It was therefore felt worthwhile to study the interaction of electron donors with electron acceptors in suitable media viscometrically and to obtain the equilibrium constant directly. The systems, chosen for the studies are benzene, alkyl benzenes-carbon tetrachloride-cyclohexane.

2. Material and method

Cyclohexane, carbon tetrachloride, benzene, toluene and *o*-xylene, were purified by standard procedures. The densities and the boiling points of the liquids agree with literature values.

* To whom all correspondence should be addressed.

The densities and viscosities of pure samples and those of 'binary mixtures' of known compositions (mole fractions) of benzene, toluene, xylene, and carbon tetrachloride in cyclohexane were determined at 25, 30, 35 and 40°C (±0·1°C) using Ostwald's viscometer and the coefficients of viscosities calculated. Similarly the densities and viscosities of ternary systems (of known compositions) of benzene-CCl_4-cyclohexane etc, were determined. The experiments were repeated at least twice and the results were reproducible within the experimental error of $\pm 0{\cdot}015 \times 10^{-3}$ poise.

The stoichiometry of the 'complex' was determined by Job's (1928) continuous variation method.

The nonlinear plot of any physical property of a 'mixed solution' against the concentration of the components, *i.e.*, the deviation from ideal behaviour of the pure components in solution is an indication of the interaction between the two species, namely the donor D, and the acceptor A (after deducting the solvent contributions). If one can assume that the deviation is entirely due to the complex alone, then the deviation should be proportional to the concentration of the complex. Baur *et al* (1969) developed a procedure for obtaining equilibrium constant of a complex by studying the change in polarizability of the species. However, it is felt that the equilibrium constant K_c can be calculated by modifying the procedure of Yoshida and Osawa (1965) which is of more general nature.

For an equimolar mixture of D and A (with total concentration C), the maximum deviation RS of any of the physical properties, (here η) from the additivities can be written as

$$RS = \alpha x, \tag{1}$$

where α is a proportionality constant and x is the concentration of the complex. When the total concentration is changed from C to C', then

$$R'S' = \alpha x', \tag{2}$$

therefore

$$RS/R'S' = \alpha x/\alpha x' = x/x' = k \tag{3}$$

In the present case K_c is given by

$$K_c = x/[(C/2) - x]^2 = x'/[(C'/2) - x']^2. \tag{4}$$

Combining (3) and (4) and rearranging, we obtain

$$K_c = 2\sqrt{k}\{\sqrt{k}(C + C') - (C + kC')\}/(C - kC')^2 \tag{5}$$

As the plot of $\Delta\eta$ *vs* mole fraction is not always symmetrical, k is actually the ratio of the area under the curves.

3. Results and discussion

The viscosities of benzene, toluene, *o*-xylene and carbon tetrachloride in cyclohexane were determined at 25, 30, 35 and 40°C. The viscosities of benzene and alkylbenzenes in cyclohexane decrease with increase in concentration whereas that of carbon tetrachloride in cyclohexane increases with concentration. Here it can be recalled that benzene and alkylbenzenes are electron donors whereas carbon tetrachloride is an electron acceptor. Therefore the interaction between benzenes and cyclohexane and

carbon tetrachloride and cyclohexane is of different type. The viscosities of all the mixtures studied are lower than the expected values, *i.e.*

$$\Delta\eta^E = \eta_S - (\eta_A X_A + \eta_B X_B),$$

where η_S is the observed viscosity, η_A and η_B are the viscosities and X_A and X_B are the mole fractions of the components A and B respectively. The deviation of viscosity from the ideal behaviour with a maximum deviation of 0·4 and 0·5 molefraction of alkylbenzenes shows that there is an interaction between the systems. Our present data go in parallel with the data of heat of mixing. The maximum deviation of the plot of $\Delta\eta$ against the molefraction of benzene in benzene-cyclohexane appears at 0·5 molefraction of benzene whereas for toluene and *o*-xylene the excess of viscosity maximum appears at 0·4 molefraction indicating the presence of 2:3 complex. Similar observations were made by Lorimer and Jones (1977) for chloroform-propionitrile and chloroform-butylonitrile and they are of the opinion that this is due to the resultant of specific and non-specific interactions. As the deviation from the ideal behaviour is due to the interaction between the two different types of molecules, the relative deviation should be an indication of the strength of interaction between the molecules. From the present data it is clear that the strength of interaction between cyclohexane and alkylbenzenes vary in the order, benzene-cyclohexane > toluene-cyclohexane > *o*-xylene-cyclohexane (figure 1). This trend is maintained at all the temperatures studied. This is an indication that the strength of the interaction depends on the substituent (steric effect) rather than on the polarizability of the molecule. This trend is in good agreement with the observations made by Nigam *et al* (1980) for aromatic hydrocarbons-nitromethanes. The activation energy for the viscosities of benzene, toluene, *o*-xylene, carbon tetrachloride and cyclohexane are 9·23, 9·25, 10·98, 11·43 and 13·58 kJ mol^{-1}

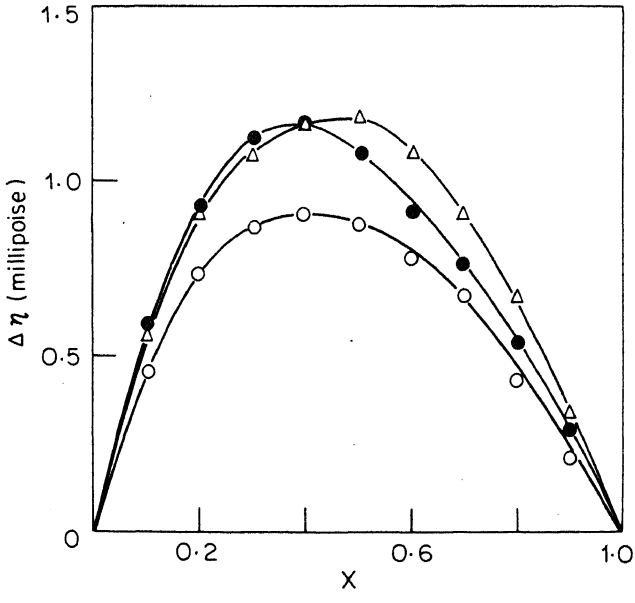

Figure 1. Variation of $\Delta\eta$, the difference between η_{cal} and η_{obs}, with the molefraction of alkylbenzenes at 25°C. (Δ-benzene cyclohexane; ●-toluene cyclohexane and O-*o*-xylene cyclohexane).

respectively. The increase in the activation energy with increase in size of the molecule (for alkyl benzenes) again confirm our earlier observations that the size and shape of the molecule is to be considered in determining the strength of interaction rather than the polarizability. The difference in the energy of activation (*i.e.* E_{obs} and E_{cal}) varies in the order, *o*-xylene-cyclohexane > toluene-cyclohexane > benzene-cyclohexane. From these data we believe that the effect of *o*-xylene-cyclohexane complex on the energy of activation is much more than that of benzene-cyclohexane.

The viscosities of ternary systems, namely alkyl benzenes-CCl_4-cyclohexane of different composition were determined at different temperatures (25, 30, 35 and 40°C). No maxima are found in the viscosity curves but the nonlinear plot of the difference in viscosities of the mixed solutions (*i.e.* $\eta_{cal} - \eta_{obs}$) against the concentration of benzene indicates the presence of a complex. For brevity, only one such set of data is given in table 1. A continuous variation plot of $\Delta\eta$, the difference in viscosity between the 'mixed solutions' and the calculated viscosities of the two solutions, shows the presence of only a 1:1 complex in the experimental range of concentrations. The deviation between the observed and calculated values is due to the interaction between the two species. From figure 2, it is clear that there is an interaction between the alkylbenzenes and carbon tetrachloride which increases with the electron-donating nature of the donor molecules, keeping the electron acceptor constant. The equilibrium constants and the free energies of formation of complexes (table 2) show that the equilibrium constants calculated from (5) are slightly higher than the literature data (obtained by different methods). However the values are increasing from benzene-CCl_4 to *o*-xylene-CCl_4. The ΔH^0 values are also slightly higher and decrease from benzene-CCl_4 to *o*-xylene-CCl_4. Our values of K_c cannot be compared with literature data as the latter make no mention about the solvent used. Secondly we have a higher concentration of solutions whereas in the literature the concentration range is very small. Our higher values may be due to the concentration effect since K_c depends on the concentration of the sample used. It is seen that although the equilibrium constants increase from benzene-CCl_4 to *o*-xylene-CCl_4 (which is expected on the strength of *n*-electron-donor

Table 1. Viscosities of mixed solutions of benzene-carbon tetrachloride in cyclohexane at 25°C.

Benzene (mol)	Carbon-tetra-chloride (mol)	Calculated viscosity (millipoise)	Observed viscosity (millipoise)	$\Delta\eta$ (millipoise)
0·0	1·0	8·4031	8·1792	0·2239
0·1	0·9	8·3649	8·0636	0·3013
0·2	0·8	8·3271	7·997	0·3301
0·3	0·7	8·2892	7·9304	0·3588
0·4	0·6	8·2514	7·8469	0·4045
0·5	0·5	8·2137	7·762	0·4520
0·6	0·4	8·1756	7·6921	0·4835
0·7	0·3	8·1313	7·6114	0·5199
0·8	0·2	8·0924	7·5614	0·5310
0·9	0·1	8·0538	7·5110	0·5430
1·0	0·0	8·0249	7·4491	0·5758

Error limit ±0·015

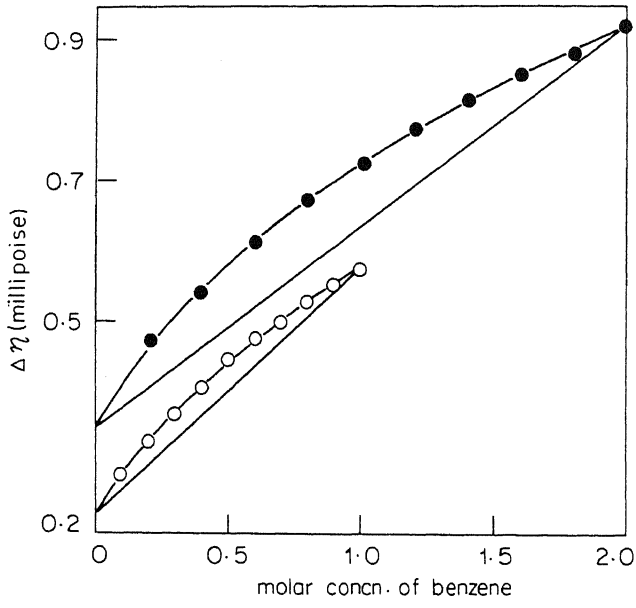

Figure 2. Variation of $\Delta\eta$ with the molar concentration of benzene in the benzene-CCl_4-cyclohexane system at 25°C.

Table 2. Equilibrium constants and other thermodynamic parameters of alkylbenzenes-carbontetrachloride in cyclohexane.

System	K_c^* 25°M^{-1}	$-\Delta H°^\dagger$ (kJ/mol)	$-\Delta F°$ (kJ/mol)
Benzene-CCl_4	1·70 (0·21)	24·5 (25·4)	1·32
Toluene-CCl_4	3·20 (0·41)	17·7 (21·3)	2·88
o-xylene-CCl_4	4·07 (−)	12·2 (−)	3·47

Error limit: $* = \pm 0{\cdot}05$; $\dagger = \pm 1{\cdot}5$
The values in parentheses are taken from Glashan *et al* (1969)

ability) the enthalpies vary in the reverse order. Similar calorimetric observations were made by Glashan (1969). Irving and Smith (1969) are of the opinion that the viscometric method can be used satisfactorily in the case of strong complexes.

As it stands the present procedure demands very careful measurements of viscosities involving long flow times to realise significant differences between solvent and dilute solutions. In addition there are experimental difficulties such as accurate measurement of flow times, precise temperature control, dust-free grease materials etc. Moreover, the measurements are time-consuming. However, this method is useful where no alternative is available.

Acknowledgement

One of the authors (BB) is thankful to CSIR (India) for the award of a Fellowship.

References

Baur M E, Morsma D A, Knobler C M and Perz P 1969 *J. Phys. Chem.* **73** 641
Bhat S N, Singh R A and Mishra S P 1979 *Proc. Indian Acad. Sci. (Chem. Sci.)* **89** 139
Bhat S N and Singh R A 1982 *Bull. Chem. Soc. Jpn.* **55** 1623
Bhat S N and Singh R A 1981 *Can. J. Chem.* **59** 1212
Glashan M L, Stubley D and Watts H 1969 *J. Chem. Soc.* A 673
Irving H M N and Smith J S 1969 *J. Inorg. Nucl. Chem.* **31** 159
Jobs P 1928 *Ann. Chim.* **9** 197
Lorimer J W and Jones D E 1977 *Can. J. Chem.* **55** 2980
Nigam R K, Singh P P, Mishra R and Singh M 1980 *Can. J. Chem.* **58** 1468
Yoshida Z and Osawa E 1965 *Bull. Chem. Soc. Jpn.* **38** 140

Proc. Indian Acad. Sci. (Chem. Sci.), Vol. 92, Number 2, April 1983, pp. 153–161.
© Printed in India.

Kinetics and mechanism of anation of hydroxopenta-aquo chromium(III) ion by DL-alanine in aqueous solution

B K NIOGY and G S DE*

Department of Chemistry, University of Burdwan, Burdwan 713 104, India

MS received 17 June 1982; revised 28 December 1982

Abstract. The kinetics of substitution of aquo-ligand from hydroxopenta-aquo chromium(III) by DL-alanine in aqueous medium has been studied spectrophotometrically. The rate law involving the formation of ion-pair has been established in the pH range 4·5–5·4. The reaction rate is higher compared to water exchange and other substitution reactions of hydroxopenta-aquo chromium(III) ion. Activation parameters have been evaluated. A lower ΔH^+ value for the reaction suggests that both bond-breaking and bond making are equally important in the transition state.

Keywords. Anation; hydroxopenta-aquo chromium(III) ion; amino acid; ion-pair; hydrogen-bonding; associative interchange.

1. Introduction

Anation reactions of hexaaquo chromium(III) ion and hydroxopenta-aquo chromium(III) ion by different ligands have been studied extensively (Hamm *et al* 1958; Banerjea and Chatterjee 1969; Banerjea and Sarkar 1972; Bhattacharya and De 1981; Mandal and De 1980; Postmus and King 1955; Phatak *et al* 1970, 1976) and some generalisations have been made regarding the reaction mechanism. Anation rate constants for $Cr(H_2O)_5OH^{2+}$ with Cl^-, Br^-, I^-, NO_3^-, SCN^- and NCS^- at 25°C span a range of 0·26–8·5 $\times 10^{-5}$ M^{-1} sec^{-1} (Espenson 1969; Thusius 1971) and for $Cr(H_2O)_6^{3+}$, with the aforementioned anions at 25°C cover a range of 0·08–73 $\times 10^{-8}$ M^{-1} sec^{-1}. This result has been interpreted as implying that bond-making plays a significant role in these reactions as evidenced by the small but definite dependence of the formation rates on the nature of the ligand. The difference in the range of rates spanned by $Cr(H_2O)_5OH^{2+}$ is smaller as compared to that by $Cr(H_2O)_6^{3+}$ with the same anions. This may be explained on the basis that coordinated OH^- facilitates a dissociative mechanism through its π-bonding ability. Anation of $Cr(H_2O)_6^{3+}$ by glycine has been reported (Banerjea and Dutta Choudhuri 1968) to proceed 10 times faster than the water exchange rate. On this basis Banerjea and Dutta Choudhuri 1968 have advanced an associative interchange (Ia) mechanism. However, Hartley suggested a dissociative mechanism for the anation of $Cr(H_2O)_6^{3+}$ by $-COO^-$ in wool. Thus despite the large amount of work done on chromium(III) complexes, controversy regarding its mechanism persists. Further the aquo-ligand substitution in hexa-aquo chromium(III) ion by amino acids except glycine has not been studied so far and similar substitution in hydroxopenta-aquo chromium(III) ion has not received any

* To whom all correspondence should be addressed.

attention. Hydroxopenta-aquo chromium(III) complex is distinctly different from hexa-aquo complex. Hydroxide ion is not only a strong σ-bonding ligand but is a strong π-donor as well. It is therefore planned to study the kinetics of substitution of aquo ligands in $[Cr(H_2O)_5OH]^{2+}$ by alanine, β-alanine, phenylalanine, aspartic acid and other related amino acid ligands. In this paper the results on alanine are presented.

2. Materials and methods

Analar quality chemicals were used. The reactant $[Cr(H_2O)_6](ClO_4)_3$ was prepared by the method of Moor and Basolo (1965); λ_{max} 410 nm (log ε, 1·52), 572 nm (log ε, 1·20). The solution of $[Cr(H_2O)_5OH]^{2+}$ (Complex-I) was prepared *in situ* from $[Cr(H_2O)_6](ClO_4)_3$ by adjusting pH to 5: pK_a of $[Cr(H_2O)_6]^{3+}$ being 3·8, a solution of this at pH 5 with λ_{max} 430 nm (log ε, 1·44) and 590 nm (log ε, 1·24), represents complex (I) (figure 1). DL-alanine (pK_1 2·34 due to the dissociation of –COOH, and pK_2 9.69 due to dissociation of $-NH_3^+$), at pH 5 remains in the Zwitter ionic form, $H_3N^+-CH(CH_3)-COO^-$ (PI, isoelectric point being 6) (Fox and Foster 1957). The product of the reaction between $[Cr(H_2O)_5OH]^{2+}$ and alanine was prepared by mixing them in different molar ratios of 1:1, 1:2, 1:3 and 1:5 at pH 5. The deep red (maroon) coloured solution when placed over concentrated H_2SO_4 gave a product with the composition $[Cr(Alanine)_2(OH)H_2O]$, complex-II. The composition of the complex (1:2) formed in the reaction mixtures was checked by the Jobs' method of continuous variation which was confirmed by the studies of Green and Ang (1955). The values of λ_{max} 400 nm (log ε, 1·53) and 540 nm (log ε, 1·61) (figure 1) of our product is nearly identical with that of Green and Ang.

3. Kinetic run

The temperature-equilibrated solution of DL-alanine and complex (I), prepared in

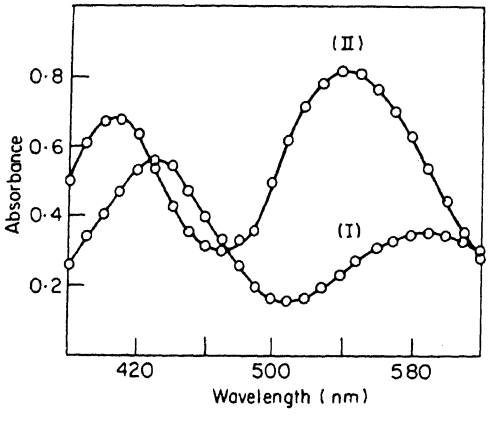

Figure 1. Absorption spectra. (I) $[Cr(H_2O)_5OH]^{2+}$, 0·01 M, pH = 5.
(II) $[Cr(H_2O)_5OH]^{2+}$, 0·01 M, alanine 0·1 M, pH = 5. Spectrum recorded after keeping the mixture at 40°C for 24 hr.

solution at pH 5 of desired concentrations were mixed in the reaction vessels and its optical density measured (Hilger UVISPEK spectrophotometer), at 540 nm, and there was a substantial difference in the spectra of the complexes $[Cr(H_2O)_5OH]^{2+}$ and $[Cr(alanine)_2OH.H_2O]$. DL-alanine does not absorb at this wavelength. The assumption that only hydroxopentaaquo chromium(III) is involved in the reaction is reasonable since under the experimental condition (pH 5) the percentage of hexa-aquo chromium(III) is very small. The pseudo-first order rate constants for the substitution reaction were obtained by plotting log $(D_\alpha - D_0)/(D_\alpha - D_t)$ against time where D_α, D_0 and D_t are the optical density values at infinite time, at the beginning and end of time t respectively. The pseudo-first order plots were linear (figure 2). However the rate constants were calculated on the basis of the least square method were reproducible within $\pm 3\%$.

4. Results and discussion

4.1 *Effect of varying concentration of complex (I)*

In the first set of experiments the concentration of $[Cr(H_2O)_5OH]^{2+}$, (complex I) was varied at a fixed concentration (0·15 M) of alanine. The ionic strength (0·06 M), and pH (5) was also kept constant. The value of k_{obs} ($\times 10^5$) was found to be 15·2, 15·4, 15·82 and 15·9 sec^{-1} at varied concentrations of [complex I] 0·005, 0·0075, 0·01 and 0·015 M respectively at a temperature of 35°C. The reaction rate is of first order with respect to [complex I] *i.e.*

$$d[\text{complex-II}]/dt = k[\text{complex-I}]$$

4.2 *Effect of varying pH on rate constant*

At fixed [complex I] (0·01 M), [alanine] (0·15 M) and $\mu = 0{\cdot}03$ M the values of pseudo-first order rate constant (k_{obs}) ($\times 10^5$) at 35°C were 6·9, 12·4, 15·5, 25·6 and 40·2 sec^{-1} at pH 4·5, 4·8, 5, 5·2 and 5·4 respectively (figure 5). The pH dependence of rate constant indicates that the rate constant decreases with decreasing pH. To explain the effect of

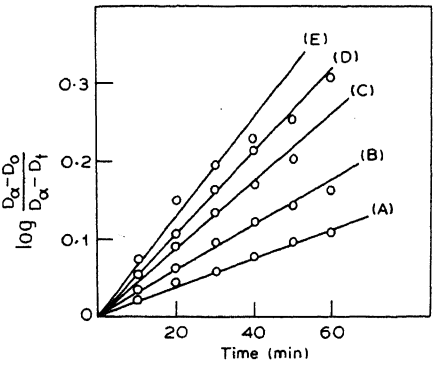

Figure 2. Graphical presentation of k_{obs} (35°C), $\mu = 0{\cdot}03$ alanine variation: $[Cr(H_2O)_5OH]^{2+}$, 0.01 M, pH = 5. [alanine], 0·05 (A), 0·1 (B), 0·15 (C), 0·2 (D) and 0·25 M (E).

pH variation the following equilibrium is considered necessary (Basolo and Pearson 1967)

$$Cr(H_2O)_6^{3+} \rightleftharpoons Cr(H_2O)_5OH^{2+} + H^+$$
$$(pK_a = 3{\cdot}8 \text{ at } 25°C)$$

As the pH of the reaction medium decreases the ratio of [hydroxopenta-aquo chromium(III)]: [hexa-aquo chromium(III)] decreases which in turn decreases the reaction rate. Hydroxopenta-aquo complex due to its π-bonding ability is a very reactive species compared to hexa-aquo complex. Alanine, an α-amino mono-carboxylic acid, at pH $\leqslant$ 2 has two dissociable groups $H_3\overset{+}{N}-CH(CH_3)-COOH$, one uncharged in the carboxylic acid (–COOH) and the other in the cationic form ($-\overset{+}{N}H_3$). With the pH range (4·5 to 5·4) studied the following equilibria are also significant

$$H_3\overset{+}{N}-CH(CH_3)-COOH \underset{+H^+}{\overset{-H^+}{\rightleftharpoons}} H_3\overset{+}{N}-CH(CH_3)-COO^-$$
$$pK_1 = 2{\cdot}34 \text{ at } 25°C,$$

and

$$H_3\overset{+}{N}-CH(CH_3)-COO^- \underset{+H^+}{\overset{-H^+}{\rightleftharpoons}} H_2N-CH(CH_3)-COO^-$$
$$pK_2 = 9{\cdot}69 \text{ at } 25°C.$$

It can be assumed that within the pH range studied for the substitution reaction the ligand alanine exists in the dipolar (Zwitter ionic) form $\overset{+}{N}H_3$–$CH(CH_3)$–COO^-. Thus the effect of pH on the reaction rate is solely due to the change in the ratio of [hydroxopenta-aquo chromium(III)]: [hexa-aquo chromium(III)]ion.

4.3 *Effect of varying alanine concentration*

The concentration of alanine ($\overline{O}{\cdot}OC{\cdot}CH(CH_3)$–$\overset{+}{N}H_3$) was varied in the range 0·05 to 0·25 M at a fixed [complex-I] (0·01 M). In these experiments the ionic strength and pH were kept constant at 0·03 M and 5 respectively. The results in table 1, show that the rate increases with increasing alanine concentration and at high concentration a limiting rate is reached (figure 3), which invokes a completion of the ion-pair formation.

The following reaction scheme can be proposed to explain the variation of rate due to

Table 1. Variation of rate constant k_{obs} with [alanine] at different temperatures (°C). $[Cr(H_2O)_5OH]^{2+} = 0{\cdot}01$ M, ionic strength $\mu = 0{\cdot}03$ M, pH = 5.

[Alanine] (M)	k_{obs} ($\times 10^5$ sec^{-1})				
	25	30	35	40	45
0·05	6·01	6·42	7·29	9·38	18·9
0·10	10·01	10·42	11·05	14·87	29·9
0·125				17·72	33·9
0·15	13·14	13·96	15·52	20·52	38·6
0·20	15·17	17·14	19·81		
0·25			22·06		

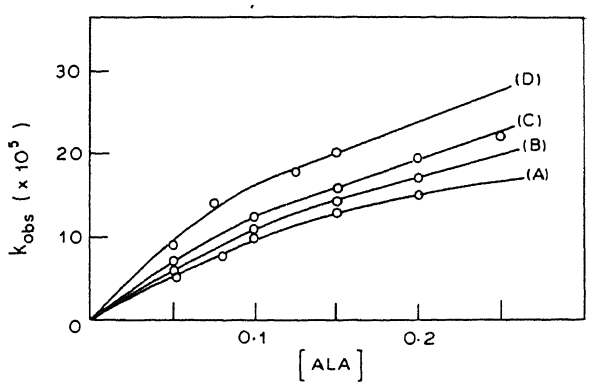

Figure 3. Dependence of k_{obs} on alanine concentration $[Cr(H_2O)_5OH]^{2+}$, 0·01 M, pH = 5; (A) 25, (B) 30, (C) 35 and (D) 40°C.

change in concentration of incoming ligand:

$$[Cr(H_2O)_5OH]^{2+} + \text{alanine} \overset{K_E}{\rightleftharpoons} [Cr(H_2O)_5OH]^{2+}, \text{alanine}$$
$$\text{A} \qquad\qquad \text{L} \qquad\qquad \text{IP}$$

$$[Cr(H_2O)_5OH]^{2+}, \text{alanine} \xrightarrow[k]{\text{slow}} [Cr(H_2O)_3OH\ \text{alanine}]^{1+} + H_2O + H_3O^+$$

$$[Cr(H_2O)_3OH\ \text{alanine}]^{1+} + \text{alanine} \xrightarrow{\text{fast}} [Cr(\text{alanine})_2OH \cdot H_2O] + H_2O + H_3O^+$$
$$\text{B}$$

In such a case the rate equation for the anation reaction is derived as follows:

$$d[B]/dt = k[IP] \tag{1}$$

and

$$[A]_{total} = [A] + [IP] \tag{2}$$

where k = anation rate constant for the slow step.

$[A]_{total}$ is the total amount of unreacted complex, $[A]$ = unreacted free $[Cr(H_2O)_5OH]^{2+}$ and [IP] = unreacted ion-pair concentration. From ion-pair equilibrium,

$$K_E = [IP]/[A]\,[L] \tag{3}$$

where K_E = ion pair equilibrium constant.
or,

$$[IP] = K_E[A][L]. \tag{4}$$

From (4) and (2) we get,

$$[A]_{total} = [A] + K_E[A][L] \tag{5}$$

or,

$$[A] = \frac{[A]_{total}}{1 + K_E[L]}. \tag{6}$$

From (6), (4) and (1) we get

$$\frac{d[B]}{dt} = \frac{k \cdot k_E[A]_{total}[L]}{1 + K_E[L]}, \tag{7}$$

i.e.

$$\frac{d[Cr(alanine)_2OH \cdot H_2O]}{dt} = \frac{k \cdot K_E[Cr(H_2O)_5OH]^{2+}_{total}[alanine]}{1 + K_E[alanine]}$$

$$= k_{obs}[Cr(H_2O)_5OH]^{2+}_{total}, \tag{8}$$

and

$$k_{obs} = \frac{k \cdot K_E[alanine]}{1 + K_E[alanine]}, \tag{9}$$

or,

$$1/k_{obs} = 1/k + 1/k \cdot K_E[alanine]. \tag{10}$$

From (10) the plot of $1/k_{obs}$ *vs* $1/[alanine]$ should be linear with an intercept, $1/k$ and slope, $1/k \cdot K_E$ (figure 4). The values of k ($\times 10^5$) and K_E thus obtained are given in table 2. The K_E values remain almost constant at all temperatures. The k values (anation rate constant) are much greater than the rate constant for isotopic water exchange under identical experimental condition [$< 10 \times 10^{-5}$ sec^{-1} at 25°C, Thusius 1971].

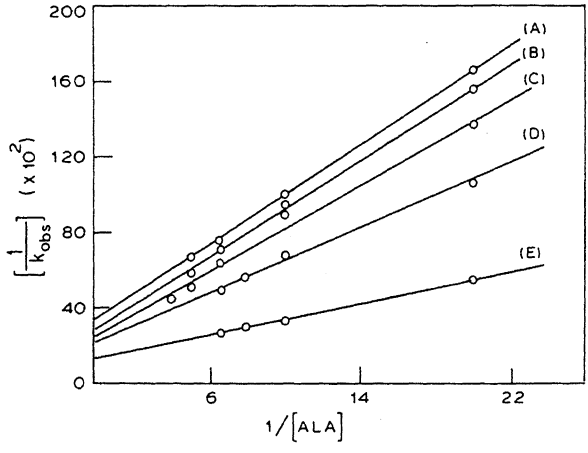

Figure 4. Plot of $1/k_{obs}$ vs 1/ligand concentration at various temperatures (A) 25, (B) 30, (C) 35, (D) 40 and (E) 45°C.

Table 2. Values of k ($\times 10^5$) sec^{-1} and K_E for the anation of $[Cr(H_2O)_5OH]^{2+}$ by alanine at different temperatures.

Temperature (°C)	k ($\times 10^5$) sec^{-1}	K_E
25	30·18	4·78
30	34·93	4·46
35	39·90	4·35
40	44·74	5·26
45	75·86	6·60

4.4 *Effect of ionic strength on reaction rate*

The ionic strength of the reaction mixture was adjusted by adding sodium perchlorate, considering the net charge of alanine to be zero (isoelectronic nature). The pseudo-first order rate constants ($\times 10^5$) at 35°C are found to be 11·05, 15·9, 19·84 and 22·69 sec^{-1} at ionic strengths of 0·03, 0·15, 0·3 and 0·45 M respectively at [complex-I] = 0·01 (M) and [alanine] = 0·1 M (figure 6). The increase in rate, k_{obs} with increase in ionic concentration indicates the easy removal of coordinated water molecule from the ion pair.

4.5 *Effect of temperature on reaction rate*

The temperature effect on the reaction rate was studied at five different temperatures for different ligand concentrations. The values for anation rate constants (k) are calculated by the least square method and are given in table 2.

Activation parameters are also calculated by the least square method using the Eyring plot of log k vs $1/T$. A much lower ΔH^+ amounting to 8.14 kcal/mol and ΔS^+, −48·23 e.u. was obtained.

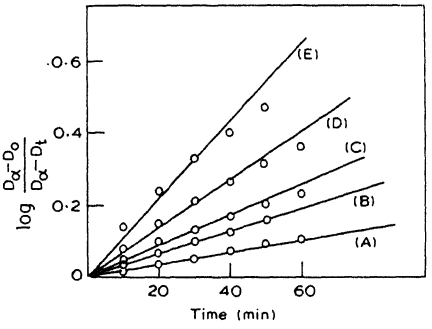

Figure 5. Effect of pH on reaction rate: pH for curve (A) 4·5, (B) 4·8, (C) 5, (D) 5·2 and (E) 5·4.

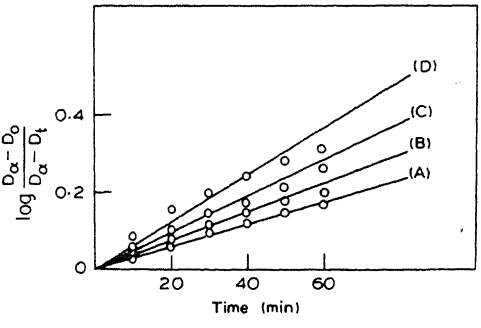

Figure 6. Effect of ionic strength on reaction rate: (A) μ = 0·03, (B) 0·15, (C) 0·3 and (D) 0·45 M.

5. Mechanism and conclusion

The reaction between $[Cr(H_2O)_5OH]^{2+}$ and alanine (in Zwitter ionic form) involves outersphere association between the two reacting species followed by an associative interchange process in which both bond-breaking and bond-making are equally important. The following mechanism (figure 7) can be proposed to explain the rate data and activation parameters of alanine substitution in $[Cr(H_2O)_5OH]^{2+}$.

Ligand OH^- which is electron donating facilitates the loss of a water ligand in the *trans* position by increasing the electron density in the chromium(III) d_{z^2} orbital. Further the activated complex formation through outersphere association is stabilized by hydrogen bonding. In this activated complex, carboxylate ion of alanine is able to form a weak bond. These assumptions are supported by the rate data and activation parameters. The rate of anation by alanine is much faster than that of isotopic water exchange and other anation processes (Thusius 1971). Further the aquo ligand substitution in $[Cr(H_2O)_5OH]^{2+}$ by alanine is much faster than that in $[Cr(H_2O)_6]^{3+}$ by glycine. The presence of OH^- in the complex facilitates the easy rupture of Cr (III)–OH_2 bond. Activation parameters (ΔH^+ and ΔS^+) of the present system are evaluated from the Eyring plot. A lower ΔH^+ value as compared to other anation reactions of $[Cr(H_2O)_5OH]^{2+}$ suggests significant associative character of the interchange process. In the associative interchange process the rupture of the Cr(III)–OH_2 bond already present and formation of new Cr(III)–L bond are equally important in the activated state. In this process positive enthalpy change due to rupture of Cr(III)–OH_2 bond is partially compensated by negative enthalpy change due to the bond formation by the incoming ligand.

The high rate of alanine substitution in $[Cr(H_2O)_5OH]^{2+}$ over the rate of water exchange and other substitution reactions of $[Cr(H_2O)_6]^{3+}$ is due to the presence of OH^- in $[Cr(H_2O)_5OH]^{2+}$ which facilitates the cleavage of Cr(III)–OH_2 bond. This in turn favours the entry of outersphere ligand and its subsequent coordination to chromium(III).

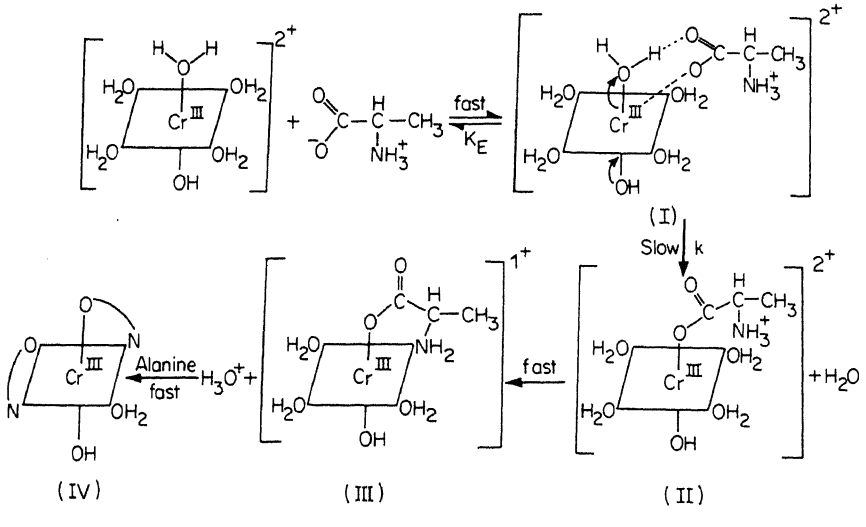

Figure 7. Probable mechanism for the anation process.

Acknowledgement

The authors thank Prof. S K Siddhanta for his encouragement and valuable suggestions. BN is indebted to the UGC, New Delhi, for a fellowship.

References

Banerjea D and Dutta Chaudhuri S 1968 *J. Inorg. Nucl. Chem.* **30** 871
Banerjea D and Chatterjee C 1969 *J. Inorg. Nucl. Chem.* **31** 3845
Banerjea D and Sarkar S 1972 *Z. Anorg. Allg. Chem.* **393** 301
Basolo F and Pearson R G 1977 *Mechanism of inorganic reactions* (New Delhi: Wiley Eastern) p. 32
Bhattacharyya M and De G S 1981 *Indian J. Chem.* **A20** 780
Espenson J H 1969 *Inorg. Chem.* **8** 1554
Fox S W and Foster J F 1957 Protein Chemistry (New York: John Wiley) p. 26
Green R W and Ang K P 1955 *J. Am. Chem. Soc.* **77** 5482
Hartley F R 1968 *Aust. J. Chem.* **21** 2723
Hartley F R 1970 *Aust. J. Chem.* **23** 275
Hamm R E, Johnson R L, Perkins R H and Davis R E 1958 *J. Am. Chem. Soc.* **80** 4469
Moor P and Basolo F 1965 *Inorg. Chem.* **4** 1671
Mandal J N and De G S 1980 *Indian J. Chem.* **A19** 25
Postmus C and King E L 1955 *J. Phys. Chem.* **59** 1208, 1217
Phatak G M, Bhat T R and Shankar J 1970 *J. Inorg. Nucl. Chem.* **32** 1305
Phatak G M, Rama Rao and Shankar J 1976 *Proc. Indian Acad. Sci.* **A83** 243
Thusius D 1971 *Inorg. Chem.* **10** 1106

Proc. Indian Acad. Sci. (Chem. Sci.), Vol. 92, Number 2, April 1983, pp. 163–166.
© Printed in India.

Preparation and structural studies of a new series of bimetallic complexes

T N OJHA*† and S B SHARMA

Chemistry Department, M L K Post-Graduate College, Balrampur 271201, India
† Department of Pharmaceutics, Institute of Technology, Banaras Hindu University, Varanasi 221005, India

MS received 29 October 1982; revised 28 January 1983

Abstract. A new series of bimetallic Lewis acid, $Cu(NCO)_2(NCS)_2Hg$, and its complexes, $L_2Cu(NCO)_2(NCS)_2Hg$ (L = THF, DMSO, pyridine, nicotinamide and Ph_3P are prepared and studied by physical and spectroscopic methods.

Keywords. Bimetallic; thiocyanate; cyanate; magnetic moment; tetragonal; bridged; softness values; symmetry; Jahn-Teller distortion.

Introduction

There has been much interest (Bailey *et al* 1971) in the bonding capabilities of ambidentate ligands, NCS^-, $NCSe^-$ and NCO^-. Makhija *et al* 1973 prepared and studied some bimetallic tetrathiocyanate complexes, $MM'(NCS)_4$ and $L_2MM'(NCS)_4$ and the coordination behaviour of the thiocyanate ion, NCS^-. Singh *et al* (1980) extended this work to include the corresponding tetraselenocyanate $MM'(NCSe)_4$ and mixed dithiocyanato-diselenocyanates, $MM'(NCSe)_2(NCS)_2$. The effect of the various ligands on the bonding modes adopted by $NCSe^-$ and NCS^- ions is further discussed. Since the cyanate ion, NCO^-, also possesses two potential donor sites, it was thought worthwhile to study the coordination behaviour of this and the thiocyanate ions together in a mixed-metal system as there appears no such report in literature.

Experimental

Synthesis of the Lewis acid

An aqueous solution of $Cu(NCO)_2$ was prepared by stirring hydrated Cu(II) nitrate (10 mmol) with KNCO (> 80 mmol) for 6 hr. To this, 35 mmol of $Hg(SCN)_2$ was added and the whole content was stirred for 3 days. A light green product formed which was suction-filtered, washed, *inter alia*, with water and acetone and dried over anhydrated silica gel. The compound, m.p. 283°C, μ_{eff} = 1.96 B.M., was analysed for $Hg(NCO)_2(NCS)_2$. Found: C, 10·88%; N, 11·97%; S, 13·78%; Cu, 13·52%; requires for $CuHg(NCO)_2(NCS)_2$: C, 10·34%; N, 12·07%; S, 13·79%; Cu, 13·68%.

* whom all correspondence should be addressed.

2.2 *Synthesis of the complexes (L = THF, DMSO, py, nia or Ph_3P)*

The THF and DMSO complexes were synthesised by stirring a small amount of the Lewis acid with an excess of the required ligand for 12 hr. For the synthesis of the remaining complexes, > 4 mmol of the ligand dissolved in acetone was stirred with 1 mmol of the Lewis acid followed by usual working of the products. In all the examples, complexes analysing for $L_2CuHg(SCN)_2(OCN)_2$ were obtained. The *bis*-pyridine and *bis*-nicotinamide complexes could also be synthesised by an alternative procedure. First, $CuL_4(NCO)_2$ was prepared by the reaction between an aqueous solution of $Cu(NCO)_2$ and an excess of py (or nia) dissolved in alcohol. Further, 1 mmol of this was suspended in acetone-alcohol mixture and stirred with 1 mmol of $Hg(SCN)_2$ for 3 days. Complexes of the composition $L_2CuHg(SCN)_2(OCN)_2$ were obtained.

2.3 *Analysis of the complexes*

Cu was estimated as its salicylaldoximate, Hg as HgS, S as $BaSO_4$ and C and N were analysed at CDRI, Lucknow.

2.4 *Physical measurements*

Magnetic moments were measured on a Gouy balance using $CoHg(SCN)_4$ as calibrant. Molar conductance of the complexes was measured in purified DMF using a Philip PR 9500 conductivity bridge. Electronic spectra were recorded on a DMR-21 UV-vis spectrophotometer. IR spectra were measured on a Perkin-Elmer-621 spectrophotometer (4000–200 cm^{-1}) and on a FIR-30 spectrophotometer (650–100 cm^{-1}).

3. Results and discussion

3.1 *Molar conductance, electronic spectra and magnetism*

The calculated magnetic moment values (~ 1·9 B.M.) was greater than the theoretical value (1·73 B.M.) which was attributed to Jahn-Teller distortion effects. Electronic spectra exhibited a broad band (Forster and Goodgame 1965) around 12840–15400 cm^{-1}, assignable to $^2T_g \rightarrow {}^2E_g$ electronic transition. These features are consistent with a tetragonally distorted Cu(II) complex approximating to D_2 symmetry. The molar conductance values for these complexes suggest their non-electrolytic nature (Geary 1971). This criterion indicates the polymeric nature of the complexes.

3.2 *IR spectral studies*

The IR spectra of all the complexes and the Lewis acid exhibited ν_{CN}, ν_{CS} and δ_{NCS} bands in the region assignable to the bridged NCS groups only (Makhija *et al* 1973; Singh 1980). The bands due to ν_{CN} of the NCO groups appeared around 2240 cm^{-1} which is a much higher value than expected for a N-terminal, O-terminal or > N-bridged cyanate group (Bailey *et al* 1971; Nelson and Shepherd 1965). X-ray crystal analysis and IR analysis of a Ni(II) cyanate complex (Hudson and Hendrickson 1973) has recently supported the existence of a three centre-NCO-bridges. Our IR data closely resemble IR data of this complex and based on this analogy, three-atom-NCO-bridges are proposed between Cu(II) and Hg(II) in our complexes.

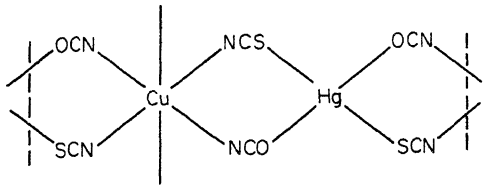

Chart 1.

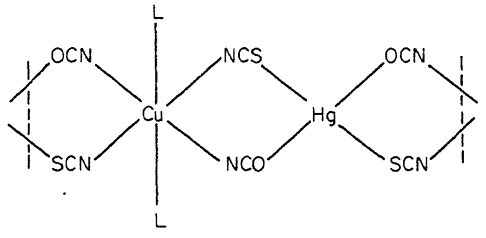

Chart 2.

Thus, all the NCO and NCS groups must be bridged between Cu(II) and Hg and a polymeric structure (chart 1) is proposed. In the Lewis acid, Cu(II) might acquire an octahedral coordination geometry through axial coordination of the adjacent NCS groups (chart 2). In the complexes, these weak axial bonds are replaced by the ligands.

The problem which now remains is the mode of coordination of the NCO and NCS groups between the two metal ions, Cu(II) and Hg(II). This could be overcome by calculating the Klopman's softness values (Klopman 1968) of the two coordinating sites of these ambidentate ligands. Using the procedure of Singh *et al* (1980), we have calculated the softness parameters ($E_m^{\ddagger}$) of the NCO^- and NCS^- ions. For the O-end and the S-end of these ions, the values are $-10{\cdot}47$ and $-7{\cdot}71$ eV respectively. For the two metal ions (Lewis acids), Cu^{2+} and Hg^{2+}, the softness values ($E_n^{\ddagger}$) are $-0{\cdot}73$ and $-4{\cdot}86$ eV respectively.

A higher negative value of softness of a base ($E_m^{\ddagger}$) indicates a more hard (Klopman 1968; Singh *et al* 1980) character whereas this sequence is reversed for the acids ($E_n^{\ddagger}$). Taking into account Pearson's (1968) HSAB theory which states that hard-hard (or soft-soft) interactions are more facile, it is proposed that Cu(II) must link to the N-ends of these ions whereas Hg(II) should link to the O-end (or S-end). Thus, the structure must consist of —$(NCS)_2$—Hg—$(OCN)_2$—Cu—$(NCS)_2$— units. The larger number of bands observed each for ν_{CN}, ν_{CS}, δ_{NCO} and δ_{NCS} modes is on account of the presence of a symmetry of order lower than C_{2v}.

3.3 *Structure of* $(Ph_3P)_2CuHg(SCN)_2(OCN)_2$

The IR spectra of the BIS-triphenylphosphine complex indicates only bridged-thiocyanate groups and terminal cyanate groups. The cyanate groups are N-bonded. This is to be expected on account of increased negative charge density (Wagner 1965) ($-0{\cdot}7712$ eV) on the N-end than on the O-end ($-0{\cdot}1846$). It is suggested that the reaction of Ph_3P with the Lewis acid ruptures the cyanate bridges and thus, monomeric complexes are formed.

3.4 *Effect of coordination on the IR spectra of ligands*

The ligands, THF and DMSO are coordinated to the metal through their O-ends as is evident from the characteristic changes (Nakamoto 1963) in the IR spectra of these when in the coordinated form. The upward shifting in the lowest ring vibrations of py and nia (at 405 and 604 cm^{-1} in uncomplexed molecules) indicates that these two ligands have coordinated through their ring nitrogen atoms.

3.5 *Far-IR spectra*

Absorption bands due to ν_{MN}, ν_{ML}, ν_{HgS}, $\delta_{N\text{-}M\text{-}N}$ and ν_{MP} modes were assigned by comparing with published data (Makhija *et al* 1973; Nakamoto 1963; Ferraro 1971). These support the assigned structures for the complexes.

Acknowledgements

The authors thank Dr P P Singh, for valuable suggestions. One of the authors (TNO) is thankful to CSIR, New Delhi for the award of a fellowship.

References

Bailey R A, Kozak S L, Michelsen T W and Mills W N 1971 *Coord. Chem. Rev.* **6** 407
Ferraro J R 1971 *Low frequency vibrations of inorganic and coordination compounds* 1st edn (New York: Plenum Press)
Forster D and Goodgame D M L 1965 *Inorg. Chem.* **4** 715
Geary W J 1971 *Coord. Chem. Rev.* **15** 81
Hudson D M and Hendrickson D N 1973 *Inorg. Chem.* **13** 2056
Klopman G 1968 *J. Am. Chem. Soc.* **90** 223
Makhija R, Padzernik L and Rivest R 1973 *Can. J. Chem.* **51** 2987
Nakamoto K 1963 *Infrared spectra of inorganic and coordination compounds* 1st edn (New York: John Wiley)
Nelson S M and Shepherd T M 1965 *J. Inorg. Nucl. Chem.* **27** 1803
Pearson R G 1968 *J. Chem. Educ.* **45** 581, 643
Singh P P 1980 *Coord. Chem. Rev.* **32** 33
Singh P P, Srivastava S K and Srivastava A K 1980 *J. Inorg. Nucl. Chem.* **42** 521
Wagner E L 1965 *J. Chim. Phys.* **43** 2728

Proc. Indian Acad. Sci. (Chem. Sci.), Vol. 92, Number 2, April 1983, pp. 167–172.
© Printed in India.

Effect of several auxiliary ligands on the extraction of cadmium (II) with 2-thenoyltrifluoroacetone

G N RAO* and ROMA LAHIRI
Department of Chemistry, Indian Institute of Technology, New Delhi 110016, India

MS received 16 July 1982; revised 2 December 1982

Abstract. The effect of tributylphosphate (TBP), trioctylphosphineoxide (TOPO), pyridine (PY) and some derivative bases of pyridine as auxiliary ligands on the extraction of cadmium (II) by 2-thenoyltrifluoroacetone (TTA) from an aqueous-buffered solution into benzene was studied. A synergistic enhancement was observed in all the systems. The equilibrium constant and adduct formation constant have been calculated. The results showed that the synergistic extraction was attributable to the formation of the base adducts Cd $(TTA)_2B$ and $Cd(TTA)_2B_2$. The main factor affecting the stability of the adduct was considered to be the base strength of the synergist.

Keywords. Synergistic extraction; thenoyltrifluoroacetone; extraction constant; adduct formation constant; cadmium.

1. Introduction

While extraction of several metals with thenoyltrifluoroacetone (TTA) has been investigated in detail (Marcus and Kertes 1969) no detailed report on cadmium (II) extraction with TTA has been published. In a general survey of the extraction of cadmium with different chelating agents a pH half (pH at which half of the total metal ion is extracted with 0·1 M TTA) value for extracting cadmium (II) with TTA into chloroform has been mentioned (Schweitzer and Randolph 1962). The current concern over increased cadmium level in the environment and the evidence that it has an adverse effect on immunologic phenomenon make this an object of immediate study. In the present paper,therefore, an attempt has been made to study cadmium (II) extraction with thenoyltrifluoroacetone and compare the coordinating abilities of tributylphosphate (TBP), trioctylphosphine oxide (TOPO), pyridine (PY), 3-methylpyridine (3MP), 4-methylpyridine (4MP), pyridineoxide (PO), 2-methylpyridineoxide (2MPO), 4-methylpyridine oxide (4MPO) towards *bis* (2-thenoyltrifluoroacetonato) cadmium (II).

2. Experimental

TTA, PO, 2-MPO, 4-MPO (Fluka), PY, 3-MP, 4-MP (BDH), TBP (IDPL), TOPO (Eastman Organic Chemicals) were used. Acetate buffers were used for pH variation studies. A constant ionic strength of 0·1 M was maintained by using potassium nitrate solution. Stock solutions were prepared by weighing AR grade chemicals. Analytical reagent grade benzene was used without further purification.

* To whom all correspondence should be addressed.

Ten ml of the aqueous layer containing 2 ml of 100 ppm cadmium acetate solution, 5 ml of buffer solution and 1 ml of 1 M potassium nitrate solution was equilibrated with 10 ml of benzene containing TTA and the auxiliary ligand at required concentrations for 2 hr in a thermostatic shaker at $30 \pm 1°C$. After equilibration the two layers were allowed to settle. Preliminary experiments indicated that equilibrium was attained after shaking for 1 hr but a shaking time of 2 hr was employed as a precautionary measure. The concentration of cadmium in the aqueous layer was measured by an SP 191 atomic absorption spectrophotometer. The pH of the aqueous layer was measured by an expanded scale pH meter (ECIL, India).

3. Results and discussion

Extraction behaviour of cadmium (II) with TTA can be understood by determining K_d values for different pH values keeping the ligand concentration constant at 0·01 M. Plot of $\log K_d$ *vs* pH gave a straight line with a slope of $\simeq 2$. A similar study of variation of K_d with ligand concentration at constant pH indicated the number of ligand molecules involved in the extracted species. Since the slope of the plot of $\log K_d$ *vs* pH at constant ligand concentration is $\simeq 2$ and the slope of $\log K_d$ *vs* $\log[HA]$ at constant pH is also $\simeq 2$, the extraction equilibrium may be represented as

$$Cd^{2+}_{aq} + 2HA_{org} \rightleftharpoons Cd\,A_{2org} + 2H^{+}_{aq}, \tag{1}$$

where HA represents the ligand (TTA). Equilibrium constant (also called extraction constant) for this equation is given by

$$K_{ex} = [Cd\,A_2]_{org}[H^+]^2_{aq}/[Cd^{2+}]_{aq}[HA]^2_{org}. \tag{2}$$

If it is assumed that CdA_2 concentration is negligible in the aqueous phase, the distribution ratio is given by

$$K_d = [Cd\,A_2]_{org}/[Cd^{2+}]_{aq}. \tag{3}$$

From (2) and (3) we have

$$\log K_{ex} = \log K_d - 2\log[HA]_{org} - 2\,\mathrm{pH}. \tag{4}$$

The value of K_{ex} is calculated from (4), using the experimental values of K_d, $[HA]$ and pH.

The effect of adding auxiliary ligands on cadmium (II) extraction with TTA has also been similarly investigated by determining K_d value as a function of concentration of auxiliary ligand (B) at constant pH and TTA concentration. From the plot of $\log K_d$ *vs* $\log[B]_{org}$ the number of molecules of B incorporated in the extracted species has been determined.

Extraction of cadmium (II) in the presence of auxiliary ligand B may be represented as

$$Cd^{2+}_{aq} + 2HA_{org} + mB_{org} \rightleftharpoons Cd\,A_2B_{m\,org} + 2H^{+}_{aq} \tag{5}$$

with equilibrium constant K'_{ex} given by

$$K'_{ex} = [Cd\,A_2B_m]_{org}[H^+]^2_{aq}/[Cd^{2+}]_{aq}[HA]^2_{org}[B]^m_{org} \tag{6}$$

and

$$\log K'_{ex} = \log K_d - 2\log[HA]_{org} - 2\,\mathrm{pH} - m\log[B]_{org} \tag{7}$$

K_s *i.e.* the adduct formation constant for the equilibrium Cd $A_{2org} + mB_{org} =$ Cd $A_2B_{m\,org}$ is given by

$$\log K_s = \log K'_{ex} - \log K_{ex} \tag{8}$$

One of the possible side reactions by adding pyridine base is the protonation of the base in the aqueous phase. When $[Cd]_{total} \ll [B]_{total}$, the following equation is obtained by mass balance,

$$[B]_{total} \simeq [B]_{org} + [B] + [BH^+], \tag{9}$$

to which the distribution coefficient P_B and dissociation constant K_{BH} for the protonated form of the base are introduced and the resulting situation is given by

$$[B]_{total} \simeq [B]_{org}(1 + P_B^{-1} + P_B^{-1} K_{BH^{-1}}[H^+]) = [B]_{org}\,\alpha B(H), \tag{10}$$

where $\alpha B(H)$ is a variable defined only by the concentration of hydrogen ion and the kind of base; $[B]_{org}$ for pyridine and pyridine *N*-oxides has been calculated by using (10).

Adduct stability constants (K_s) and the values of K'_{ex} are listed in table 2.

The values of P_B and PK_{BH} for the pyridines and pyridine N-oxides have been listed in table 1 (Al-Niami *et al* 1973).

Figure 1 shows the plots of log K_d against log $[B]_{org}$ for PY, 3-MP and 4-MP at pH 6·2, TBP (pH = 5·8) and TOPO (pH = 5·3) at constant ligand concentration (0·01 M of TTA). Two moles of PY, 3-MP, 4-MP, TBP or TOPO are present in the extracted adduct as indicated by a slope value of $\simeq 2$.

Table 1. Partition coefficients (P_B) and dissociation constant (pk_{BH}) values of the heterocyclic bases and heterocyclic N-oxides*

	PY	3MP	4MP	PO	2MPO	4MPO
P_B	3·52	11·86	14·52	0·0026	0·0143	0·0034
pk_{BH}	5·44	5·88	6·24	0·602	1·034	1·086

* Al-Niami *et al* (1973).

Table 2. Extraction constants and formation constants of the adducts formed between the complex Cd $(TTA)_2$ and various auxiliary ligands.

Auxiliary ligand	log K'^{*}_{ex}	log K_s*
PY	−3·26	7·74
3-MP	−2·92	8·08
4-MP	−2·70	8·30
Pyridine-N-oxide	−6·92	4·08
2-methylpyridine N-oxide	−6·27	4·73
4-methylpyridine N-oxide	−5·58	5·42
TBP	−5·12	5·88
TOPO	−1·48	9·52
Nil	−11·0	—

* Estimated uncertainty in the numerical values is ±0·1 unit.

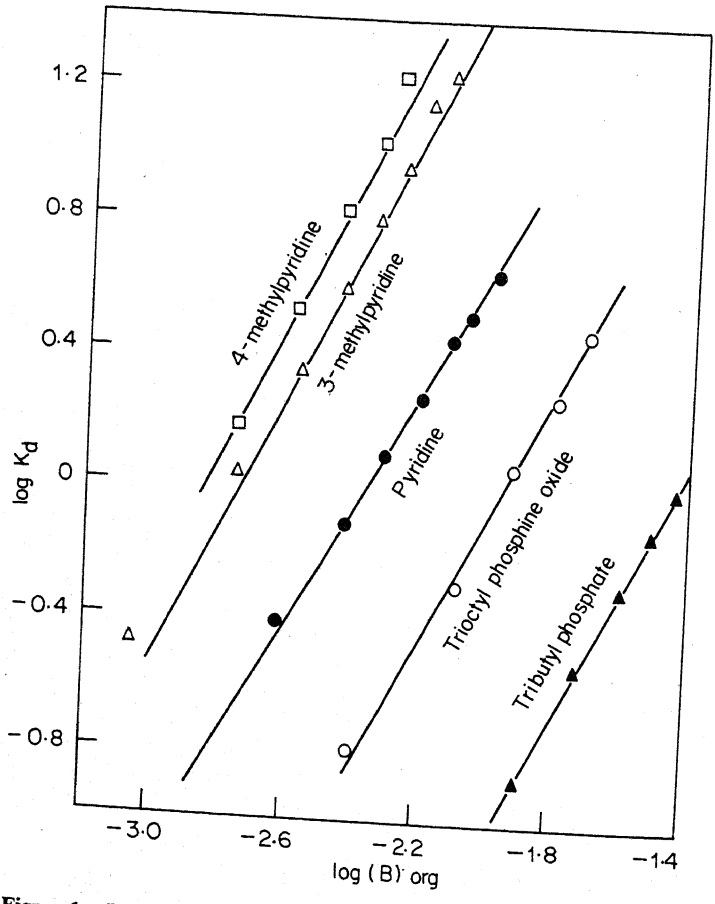

Figure 1. Plot of log K_d *vs* log $[B]_{org}$. The vertical axis has been shifted to the positive side by 0·2 and 0·6 log units in the case of pyridine and TOPO respectively. The axis has been shifted to the negative side by 0·2 log units in the case of tributyl phosphate.

Figure 2 shows the plots of log K_d *vs* log $[B]_{org}$ at constant pH (7·4, 7·3 and 6·9 respectively for PO, 2-MPO and 4-MPO) at constant ligand concentration (0·005 M TTA for PO and 2-MPO and 0·01 M TTA for 4-MPO).

One mole of PO, 2-MPO or 4-MPO is present in the extracted adduct as indicated by the slope value of $\simeq 1$.

A comparison of the values of K'_{ex} with that of K_{ex} indicates synergism in all these systems. The main factors affecting the synergistic extraction of a metal chelate are stability and organophilic property of the resulting adduct.

In pyridine bases a competing reaction between the formation of the adduct in question and that of BH^+ also affects the extent of synergism. The present results clearly indicate that the variation of the adduct formation constant is in accordance with the order of basicities of the auxiliary ligands. The formation constant of the adduct formed by $Cd(TTA)_2$ with an N-base is greater than that formed with the corresponding N-oxide. Synergistic extraction studies of $Cu(TTA)_2$ with N-bases and N-oxides have shown similar trends (Al-Niami and Rasoul 1974). On the other hand,

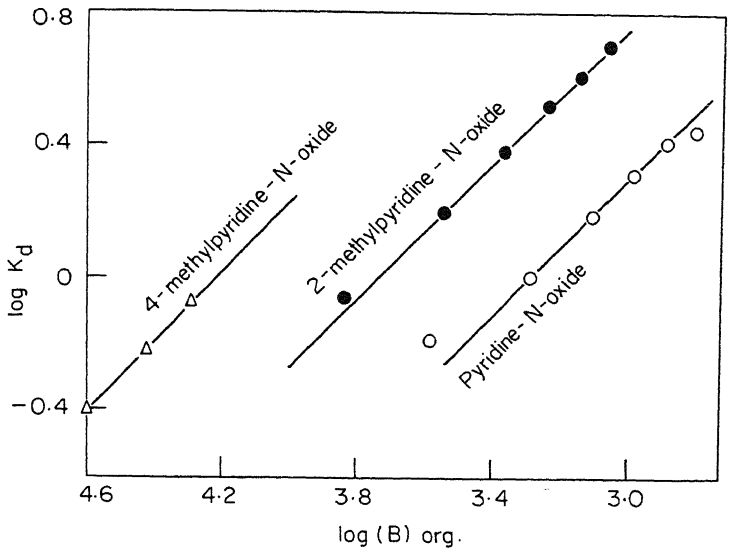

Figure. 2. Plot of log K_d *vs* log $[B]_{org}$.

formation constants of the adduct formed between $Co(PMBP)_2$ and N-oxides were greater than those formed with the N-base (Al-Niami *et al* 1973). These results can be interpreted by assuming metal to ligand back-bonding, which can be achieved by back donation of electrons from the filled metal *d*-orbitals to the empty π^* antibonding orbitals of the N–O bonds in the ligand. The energy level of this π^* orbital increases when a methyl group is introduced in the 4th position of the ring thereby decreasing the energy match between the filled orbitals of the metals and the π^* orbital and hence decreasing the contribution of back bonding.

There are not many reports where the effect of phosphorous esters is compared with those of heterocyclic bases or heterocyclic base N-oxides under identical conditions. This work indicates that TOPO exhibits the maximum synergistic effect among the ligands studied. Adduct formation constant value for TOPO is greater than that with TBP with the Lewis acid $Cd(TTA)_2$ as expected. It is interesting to note that TBP is more effective than all the N-oxides but less effective than all the N-bases studied. Formation constants of the adducts decreased in the order.

Trioctylphosphineoxide > 4-methylpyridine > 3-methylpyridine > pyridine > tributylphosphate > 4-methylpyridine oxide > 2-methylpyridine oxide > pyridine oxide.

Solvent extraction techniques are normally used for preconcentration before atomic absorption spectrophotometric determination of metals. The present results would be of interest in the preconcentration of traces of cadmium in pollution studies.

Acknowledgement

The authors wish to thank CSIR for financial assistance.

References

Al-Niami N S, Al-Karaghouli A R and Aliwi S M 1973 *J. Inorg. Nucl. Chem.* **35** 577
Al-Niami N S and Rasoul H A A 1974 *J. Inorg. Nucl. Chem.* **36** 2051
Marcus Y and Kertes A S 1969 *Ion exchange and solvent extraction of metal complexes* (London: Wiley Interscience) pp. 509
Schweitzer A K and Randolph D R 1962 *Anal. Chim. Acta* **26** 567

Proc. Indian Acad. Sci. (Chem. Sci.), Vol. 92, Number 2, April 1983, pp. 173–179.
© Printed in India.

3d-metal complexes of salicylaldehyde ethoxythiocarbonyl hydrazone

N K SINGH, S C SRIVASTVA and R C AGGARWAL*
Department of Chemistry, Banaras Hindu University, Varanasi 221 005, India

MS received 11 December 1982; revised 5 March 1983

Abstract. Salicylaldehyde ethoxythiocarbonyl hydrazone (H_2L) forms adducts as well as deprotonated complexes having 1 : 1 or/and 1 : 2 metal ligand ratio with the metal ions VO(IV), Ni(II), Co(III), Cu(II), Zn(II), Mn(II) and Fe(II). Based on magnetic, ESR, electronic, infrared and NMR spectral measurements, structures have been assigned to all the compounds. IR spectral studies show neutral bidentate behaviour of the ligand in the adducts and uninegative/binegative tridentate behaviour in the deprotonated complexes, the bonding sites being azomethine nitrogen and thione sulphur in the former type of complexes and phenolate oxygen, azomethine nitrogen and thione/thiolate sulphur in the latter type.

Keywords. 3*d* metal complexes; IR spectral studies; electronic; nuclear magnetic resonance; electron spin resonance; salicylaldehyde ethoxythiocarbonyl hydrazone.

1. Introduction

Although the transition metal complexes of ONO multidentate Schiff bases derived from salicylaldehyde and acid hydrazides are extensively studied (Sayed and Iskandar 1971; Narang and Aggarwal 1974; Iskandar and Aggan 1975; Biradar and Havinale 1976; Aggarwal *et al* 1981; Dutta and Sarkar 1981) comparatively little work has been done on the complexes of analogous ONS Schiff bases (Ablov and Gerbeleu 1964, 1965; Ali *et al* 1973). Also, no work seems to have been done todate on the complexes of salicylaldehyde ethoxythiocarbonyl hydrazone containing oxygen, nitrogen and sulphur as potential donor sites. The synthesis and structural studies of VO(IV), Mn(II), Fe(II), Co(III), Ni(II), Cu(II), and Zn(II) complexes of the above ligand were therefore undertaken and the results of these investigations are described in the present paper.

2. Experimental

2.1 *Materials*

All the chemicals used were of BDH or equivalent quality.

2.2 *Preparation of ligands*

Salicylaldehyde ethoxythiocarbonyl hydrazone, $C_6H_4(OH)CH:N\cdot NHC:S\cdot OC_2H_5(H_2L)$ was prepared by refluxing for ~1 hr the ethanolic solutions of ethoxythiocarbonyl hydrazide and salicylaldehyde taken in ~1 : 1·2 molar ratio. On cooling a white solid separated out which was filtered, washed with ethanol and

* To whom all correspondence should be addressed.

recrystallised from ethanol, m.p. 163–165°C. Ethoxythiocarbonyl hydrazide required for the purpose was prepared by the reported method (Jensen *et al* 1969). Analysis: C = 53·46, H = 5·5, N = 12·24, S = 13·62, N_2H_4 = 13·58 %, $C_{10}H_{12}O_2N_2S$ requires C = 53·58, H = 5·36, N = 12·5, S = 14·28, N_2H_4 = 14·28 %.

2.3 *Preparation of the complexes*

Adducts of Fe(II), Ni(II) and Cu(II) chlorides were prepared by adding ethanolic solutions of the respective metal(II) chloride to the solution of the ligand in the same solvent in ~1:2 molar ratio. $ZnCl_2(H_2L)$ was, however, prepared by using the ethereal solutions of the ligand and anhydrous $ZnCl_2$.

$VOL \cdot 2H_2O$ and Co(HL) (L) were prepared by mixing the ethanolic solutions of the ligand and the hydrated vanadyl/cobaltous chloride in ~1:2 molar ratio and stirring the reaction mixture. Few drops of dil HCl were added to the reaction mixture during the synthesis of Co(III) complex.

$MnL \cdot H_2O$ and ZnL·EtOH were obtained by refluxing the ethanolic solutions of the respective metal(II) acetate and the ligand in ~1:2 molar ratio.

$NiL \cdot NH_3$ was obtained as a red crystalline product by adding concentrated ammonia solution dropwise to the ethanolic solutions of $NiCl_2 \cdot 6H_2O$ and the ligand in a 1:1 molar ratio till present in slight excess and concentrating the red solution to incipient crystallization. The resulting compound was filtered, washed with ethanol and dried in air.

$Ni(HL)_2$ and $CuL \cdot H_2O$ were prepared by digesting for ~10–15 min the solutions of the respective hydrated metal(II) chloride and the ligand in ~1:2 molar ratio after raising the pH to ~5–6 with dil NH_4OH. $Fe(HL)_2$ was prepared by mixing and subsequent stirring of the ethanolic solutions of $FeCl_2 \cdot 4H_2O$, ligand and KOH in 1:2:2 molar ratio in hydrogen atmosphere to prevent the oxidation of Fe(II). The complexes thus obtained were suction-filtered and washed with ethanol/ether; however, the deprotonated complexes of Fe(II), Ni(II) and Cu(II) were washed first with water and then with ethanol. The complexes were dried *in vacuo*.

2.4 *Analysis*

The complexes were analysed for their metal contents employing standard literature procedures after destroying the organic matter at first with a mixture of nitric and hydrochloric acids and then with concentrated sulphuric acid. Sulphur was estimated as $BaSO_4$ and chloride as AgCl. Nitrogen was determined by microanalysis. Hydrazine was estimated volumetrically using KIO_3 (Vogel 1971) after submitting the complexes to acid hydrolysis for ~2–3 hr. The water or ethanol content of the complexes was determined by heating them in the range 100–140°C and finding out the loss in weight. The analytical data are given in table 1.

2.5 *Physical measurements*

The equipment and the methods employed for recording molar conductance, magnetic susceptibility, and electronic and infrared spectra were the same as described in our previous studies (Aggarwal *et al* 1981). The values of the various spectral parameters such as 10Dq, B′ and LFSE were calculated as described in Lever (1968a).

ESR spectra of $Cu(H_2L)_2Cl_2$ and $CuL \cdot H_2O$ were recorded at room temperature and

Table 1. Analytical data and general behaviour of the complexes.

Compound	Colour	% Metal		% N_2H_4		% Nitrogen		% Cl		% S		μ_{eff} (BM)	m.p. (°C)
		Found	Cal.	Found	Cal.	Found	Cal.	Found	Cal.	Found	Cal.		
$Fe(H_2L)Cl_2$	Dark brown	16·38	15·92	—	—	7·62	7·98	20·10	20·21	8·89	9·12	4·80	160
$Ni(H_2L)Cl_2 \cdot 2H_2O$	Green	15·22	15·07	8·86	8·21	6·98	7·18	17·90	18·20	8·01	8·21	3·30	>300
$Cu(H_2L)_2Cl_2$	Dark green	10·40	10·91	11·18	10·99	9·86	9·61	11·82	12·17	10·60	10·99	1·75	145
$Zn(H_2L)Cl_2$	Light yellow	18·40	18·15	9·05	8·88	7·39	7·77	19·28	19·67	8·34	8·88	dia-magnetic	175
$Fe(HL)_2$	Dark brown	10·86	11·13	—	—	10·90	11·16	—	—	12·42	12·76	4·82	205[d]
$Ni(HL)_2$	Yellowish green	11·40	11·63	12·26	12·69	11·48	11·10	—	—	12·98	12·69	3·24	235
Co(HL)(L)	Dark brown	11·42	11·69	13·07	12·70	11·40	11·11	—	—	12·36	12·70	dia-magnetic	255[d]
$VOL \cdot 2H_2O$	Light grey	15·16	15·68	10·01	9·84	8·58	8·62	—	—	9·24	9·84	1·70	250[d]
$MnL \cdot H_2O$	Light yellow	18·61	18·63	10·60	10·85	9·30	9·49	—	—	10·50	10·85	5·82	>300
$NiL \cdot NH_3$	Red	19·25	19·72	11·13	10·75	13·80	14·11	—	—	10·16	10·75	dia-magnetic	200[d]
$CuL \cdot H_2O$	Chocolate	21·05	20·94	10·03	10·54	9·60	9·22	—	—	10·40	10·54	1·78	258
$ZnL \cdot EtOH$	White	21·37	21·42	10·73	10·53	9·44	9·17	—	—	10·01	10·53	dia-magnetic	>300

d – decomposes

77 K in DMF and chloroform, respectively on a Varian X-band spectrometer, Model E-4, using DPPH as a g marker. The ESR magnetic parameters $g_{av}, g_{\parallel}, g_{\perp}, A_{iso}, A_{\parallel}$, and $A_{\perp}$ deduced from the analysis of the spectra are discussed.

The ^{1}H NMR spectra of the ligand and 1:1 deprotonated complexes of Zn(II) were recorded on a Varian A-60D spectrophotometer in $CDCl_3$ and $DMSO(d_6)$, respectively.

3. Results and discussion

The analytical data given in table 1 show the formation of 1:1 adducts with Fe(II), Ni(II) and Zn(II) chlorides, 1:2 adduct with Cu(II) chloride, and deprotonated complexes of the types $M(HL)_2$ [M=Fe(II) and Ni(II)] and $M'L \cdot nY$ [Y=H_2O for VO(IV), Mn(II), Cu(II); NH_3 for Ni(II) and EtOH for Zn(II); $n = 2$ for VO(IV) and one for others]. The loss of weight between 120–140°C for $ZnL \cdot EtOH$, $VOL \cdot 2H_2O$, $MnL \cdot H_2O$ and $CuL \cdot H_2O$ suggests the coordinated nature of the solvent molecule(s) which is further supported by ^{1}H NMR or IR spectral studies discussed later. The complexes are insoluble in water and non-polar organic solvents such as chloroform, benzene etc., (Ali and Livingstone 1974) but with a few exceptions they are soluble in ethanol, DMF and DMSO. The molar conductance values of the soluble complexes in DMF show them to be non-ionic in nature (Geary 1971).

3.1 *Magnetic moments*

The magnetic moment data given in table 1 show that $NiL \cdot NH_3$ and Co(HL)(L) are diamagnetic indicating that the former complex is square planar while the latter is a low-spin octahedral Co(III) complex. The magnetic moments of other Ni(II) complexes are consistent with spin-free octahedral geometry around Ni(II) and those of Mn(II) and Fe(II) complexes indicate them to be spin-free in nature (Ali and Livingstone 1974). μ_{eff} values of oxovanadium(IV) and copper(II) complexes are normal but give no specific information about the stereochemistry.

3.2 *Electronic spectra*

The electronic spectrum of the ligand in ethanol shows four bands at 30000, 32570, 42740 and 33900 cm^{-1} with ε_{max} values of 18400, 20000, 18400 and 16800, respectively. The first three bands may be attributed to $\pi \rightarrow \pi^*$ transition arising from the salicylaldimine part (Sacconi *et al* 1957) while the fourth to the >C=S chromophore (Walter and Reubke 1970) present in the ligand.

$VOL \cdot 2H_2O$ shows two bands at 10000 and 18180 cm^{-1} assigned to $d_{xy} \rightarrow d_{yz}, d_{xz}$ and $d_{x^2-y^2}$ transitions, respectively on the basis of octahedral geometry of the complex (Lever 1968b). 10Dq and LFSE have been calculated to be 18180 cm^{-1} and 89 kJ mol^{-1} respectively.

The spectra of $Fe(H_2L)Cl_2$ and $Fe(HL)_2$ yield one band at 17390 and 16670 cm^{-1} respectively which may be attributed to charge transfer transition (Lever 1968b).

The 18000 and 25000 cm^{-1} bands in the spectrum of Co(HL)(L) may be assigned to $^1A_{1g} \rightarrow {}^1T_{1g}$ and $^1T_{2g}$ transitions, respectively in octahedral geometry of Co(III) (Lever 1968b), the calculated value of B comes out to be 437 cm^{-1}. The spectrum of $NiL \cdot NH_3$ shows three $d-d$ bands at 16670, 20000 and 24000 cm^{-1} which may be assigned to

$^1A_{1g} \rightarrow {}^1A_{2g}$, $^1B_{1g}$ and $^1E_{1g}$ transitions respectively in square planar geometry. The single electron parameters Δ_1, Δ_2 and Δ_3 have been calculated as suggested by Gray and Ballhausen (1963) assuming after Shupack *et al* (1964) that $F_2 = 10F_4 = 800\ cm^{-1}$ and the calculated values are 19470, 4930 and 3600 cm^{-1} respectively.

$Ni(HL)_2$ and $Ni(H_2L)Cl_2 \cdot 2H_2O$ show two *d–d* transition bands at 11430, 16950 and 11430, 17390 cm^{-1}, respectively. These two bands in each case may be assigned to $^3A_{2g} \rightarrow {}^3T_{2g}(F)$ and $^3T_{1g}(F)$ transitions, respectively in octahedral environment of Ni(II) (Sacconi 1968). The values of 10Dq (cm^{-1}), B (cm^{-1}) and LFSE (kJ $mole^{-1}$) have been calculated for each of the complexes and they are 11430; 680, 602; and 164·2 respectively.

$Cu(H_2L)_2Cl_2$ and $CuL \cdot H_2O$ show a broad band at 14290 and 18180 cm^{-1}, respectively. The positions of these bands suggest octahedral geometry for the former complex which may be assigned to the envelope of $^2B_{1g} \rightarrow {}^2Eg$; $^2B_{2g}$ and $^2A_{1g}$ transitions and square planar geometry for the latter may be assigned to the envelope of $^2B_{1g} \rightarrow {}^2A_{1g}$; $^2B_{2g}$ and ^2Eg transitions, respectively (Sacconi and Ciampolini 1964; Procter *et al* 1968; Patel and Goldberg 1972). The 10Dq (cm^{-1}) and LFSE (kJ $mole^{-1}$) values of the complexes are calculated to be 14290, 18180 and 102·7, 130·6 respectively.

3.3 *ESR spectra*

$Cu(H_2L)_2Cl_2$ and $CuL \cdot H_2O$ show isotropic ESR spectra at room temperature and are axially symmetric at 77 K. The values of the various ESR magnetic parameters calculated from the spectra of $Cu(H_2L)_2Cl_2$ are: $g_{av} = 2{\cdot}0962$; $g_{\parallel} = 2{\cdot}2006$; $g_{\perp} = 2{\cdot}0441$; $A_{iso}(Cu) = 85\ G$; $A_{\parallel}(Cu) = 170\ G$; $A_{\perp}(Cu) = 43{\cdot}3\ G$ and $A_{iso}(^{14}N) = 15\ G$ and for $CuL \cdot H_2O$ the various values are: $g_{av} = 2{\cdot}0790$; $g_{\parallel} = 2{\cdot}1567$; $g_{\perp} = 2{\cdot}0401$; $A_{iso}(Cu) = 87\ G$; $A_{\parallel}(Cu) = 183\ G$ and $A_{\perp}(Cu) = 35{\cdot}83\ G$.

The trend $g_{\parallel} > g_{\perp} > ge$ (2·0023; free spin value) observed for the complexes under study indicates that the unpaired electron is most likely in the $d_{x^2-y^2}$ orbital of Cu(II). Further the ratio $(g_{\parallel}-2)/(g_{\perp}-2) \approx 4$ is also an evidence that $d_{x^2-y^2}$ ground state is present in these complexes (Procter *et al* 1968). The ESR spectrum of $Cu(H_2L)_2Cl_2$ at 77 K displays a well resolved super hyperfine splitting (*ca* 15G) arising from the interaction of the unpaired electron density of ^{63}Cu with ^{14}N atoms of the ligand (Kokoszka *et al* 1967; Danopoulos and Paraskewas 1981).

3.4 *Infrared spectra*

The IR spectrum of the ligand in $CHCl_3$ shows two bands at 3340 and 3160 cm^{-1} which may be assigned to ν(OH) and ν(NH) modes respectively. The positions of these bands remain practically unchanged or show some positive shifts in the spectra of the adducts indicating the non-involvement of imino nitrogen and phenolic oxygen in bonding.

The bands occurring at 1620, 965, 1480, 1310 and 800 cm^{-1} in the $CHCl_3$ solution spectrum of the ligand are assigned to ν(C=N), ν(N–N) (Braibanti *et al* 1968), thioamide bands: βNH + νCN (mainly βNH), νCN + βNH (high νCN) and ν(C=S), respectively (Burns 1968). The corresponding bands in the spectra of all the adducts are observed in 1590–1600, 985–1000, 1500, 1320–1350 and 770–790 cm^{-1} regions respectively. Negative shifts in ν(C=N) (20–30 cm^{-1}) and ν(C=S) (10–30 cm^{-1}) (Burns 1968) indicate coordination through azomethine nitrogen and thione sulphur. The bonding through these atoms are further supported by positive shifts in βNH + νCN (20 cm^{-1}), νCN + βNH (10–40 cm^{-1}) and ν(N–N) (20–35 cm^{-1}) modes (Braibanti *et al* 1968).

The ν(C–O) (phenolic) band observed in the ligand at 1270 cm^{-1} remains practically unchanged showing non-involvement of phenolic oxygen in bonding (Yamada 1959). In the spectra of $Fe(HL)_2$ and $Ni(HL)_2$ the disappearance of the above band and appearance of a new band due to ν_{asym}(C–O–M) at ~1530 cm^{-1} indicate bonding through phenolic oxygen with the metal ions and monodentate behaviour of C–O group (Sinn and Harris 1969). The spectral features in ν(N–H), ν(C=N) ν(N–N) and thioamide frequency regions in the spectra of 1 : 2 deprotonated complexes are the same as for the adducts discussed above. The IR spectral studies thus show mononegative tridentate behaviour of H_2L in 1 : 2 deprotonated complexes; the bonding sites being phenolate oxygen, azomethine nitrogen and thione sulphur as reported for salicylaldehyde thiosemicarbazone complexes (Ablov and Gerbeleu 1964, 1965). The tridentate behaviour of H_2L is consistent with the octahedral geometry of the above complexes inferred from magnetic and electronic spectral studies discussed earlier.

The disappearance of ν(OH), ν(N–H), and ν(C=S) bands in the spectra of anhydrous 1 : 1 deprotonated complexes and appearance of new bands due to ν_{asym} (C–O–M) and ν(C–S) (Geetharani and Sathyanarayana 1977) modes in 1520–1540 and 715–730 cm^{-1} regions, respectively indicate removal of the phenolic as well as thioenolic protons as a result of chelation. A negative shift in ν(C=N) (~25 cm^{-1}) and a positive shift in ν(N–N) (45–55 cm^{-1}) in the spectra of these complexes suggest coordination through azomethine nitrogen. The IR spectral studies thus indicate dinegative tridentate behaviour of the ligand in 1 : 1 deprotonated complexes.

The infrared spectral features of Co(HL)(L) are similar to those of 1 : 1 and 1 : 2 deprotonated complexes discussed above in the ν(OH), ν(C–O–M), ν(C=N) and ν(N–N) frequency regions indicating bonding through phenolate oxygen and azomethine nitrogen. But unlike the 1 : 1 and 1 : 2 deprotonated complexes which give only one band at ~720 and ~770 cm^{-1}, respectively, Co(HL)(L) yields two bands in 700–800 cm^{-1} region due to ν(C–S) and ν(C=S) modes. The above observation shows uni- and binegative tridentate behaviour of the two ligands attached to Co(III). The bands observed at 3320–3400 and 740–760 cm^{-1} regions in the spectra of the hydrated complexes but absent in the anhydrous complexes may be assigned to ν(OH) and $\rho_r(H_2O)$ modes of the coordinated water molecule (Nakagawa and Shimanouchi 1964). The non-ligand bands occurring at 330–350, 280–370, 300–420 and 280–400 cm^{-1} regions may be tentatively assigned to ν(M–Cl) (Speca *et al* 1976), ν(M–N) (Beeroff *et al* 1974; Lever and Mantovani 1971), ν(M–O) (Sathyanarayana and Patel 1968; Ohkaku and Nakamoto 1971) and ν(M–S) (Geetharani and Sathyanarayana 1977) modes, respectively.

3.5 ^1H *NMR spectra*

The ^1H NMR spectrum ($CDCl_3$) of salicylaldehyde ethoxythiocarbonyl hydrazone shows signals at δ 1·47 (*t*, J = 8 Hz, 3H, $-OCH_2\underline{CH_3}$), 4·70 (*q*, J = 8 Hz, 2H, $-O\underline{CH_2}CH_3$), 6·60–7·60 (*m*, 4H, aromatic), 8·10 (*s*, 1H, –<u>CH</u>=N–), 10·47 (br, –<u>NH</u>–) and 11·20 (*s*, –<u>OH</u>). The signals due to –NH– and –OH groups disappear on D_2O exchange. The ^1H NMR spectrum of 1 : 1 deprotonated complex of Zn(II) shows signals at δ 1·25 (*t*, J = 8 Hz, 3H, $-OCH_2\underline{CH_3}$), 4·28 (*q*, J = 8 Hz, 2H, $-O\underline{CH_2}CH_3$), 6·60–7·60 (*m*, 4H, aromatic) and 8·88 (*s*, 1H, –<u>CH</u>=N–). Additional signals observed at δ 1·07 (*t*, J = 7 Hz, 3H, $-CH_2\underline{CH_3}$) 3·43 (*q*, J = 7 Hz, 2H, $-\underline{CH_2}CH_3$) and 3·33 (*s*, –<u>OH</u>) may be attributed to the presence of coordinated ethanol. The absorption at

δ 3·33 disappears in the Zn(II) complex under investigation on deuteration as expected for the proton of the –OH group in ethanol.

Acknowledgements

One of the authors (SCS) is thankful to UGC, New Delhi for the award of a fellowship. Sincere thanks are due to RSIC, IIT Madras, for running the ESR spectra of the complexes and to Dr S P Mishra, for helpful discussions pertaining to ESR spectra.

References

Ablov A V and Gerbeleu N V 1964 *Russ. J. Inorg. Chem.* **9** 1260; 1965 *Russ. J. Inorg. Chem.* **10** 33
Aggarwal R C, Singh N K and Singh R P 1981 *Inorg. Chem.* **20** 2794
Ali M A, Livingstone S E and Phillips D J 1973 *Inorg. Chim. Acta.* **7** 179
Ali M A and Livingstone S E 1974 *Coord. Chem. Rev.* **13** 101
Beeroff B, Campbell M J M and Grezeskowiah R 1974 *J. Inorg. Nucl. Chem.* **36** 55
Biradar N S and Havinale B R 1976 *Inorg. Chim. Acta.* **17** 157
Braibanti A, Dallavalle F, Pellinghelli M A and Leoprati E 1968 *Inorg. Chem.* **7** 1430
Burns G R 1968 *Inorg. Chem.* **7** 277
Danopoulos A A and Paraskewas S M 1981 *Inorg. Chim. Acta.* **55** 141
Dutta R L and Sarkar A K 1981 *J. Inorg. Nucl. Chem.* **43** 57
Geary W J 1971 *Coord. Chem. Rev.* **7** 81
Geetharani K and Sathyanarayana D N 1977 *Aust. J. Chem.* **30** 1617
Gray H B and Ballhausen C J 1963 *J. Am. Chem. Soc.* **85** 260
Iskandar M F and Aggan A M E 1975 *Inorg. Chem. Acta.* **14** 167
Jensen K A, Anthoni U and Holm R 1969 *Acta Chem. Scand.* **23** 1916
Kokoszka G F, Reiman C W, Allen H C and Gordon G 1967 *Inorg. Chem.* **6** 1657
Lever A B P 1968a *J. Chem. Educ.* **45** 711
Lever A B P 1968b *Inorganic electronic spectroscopy* (Netherlands: Elsevier) pp. 301, 307, 342
Lever A B P and Mantovani F 1971 *Inorg. Chem.* **10** 817
Nakagawa I and Shimanouchi T 1964 *Spectrochim. Acta.* **20** 429
Narang K K and Aggarwal A 1974 *Inorg. Chim. Acta.* **9** 137
Ohkaku N and Nakamoto K 1971 *Inorg. Chem.* **10** 798
Patel K C and Goldberg D E 1972 *J. Inorg. Nucl. Chem.* **34** 637
Procter I M, Hathaway B J and Nicholls P 1968 *J. Chem. Soc.* **A** 1978
Sacconi L, Paoletli P and Maggio F 1957 *J. Am. Chem. Soc.* **79** 4067
Sacconi L 1968 In *Transition metal chemistry 4th edn* (ed) R L Carlin (New York: Marcel Dekker) p. 199.
Sacconi L and Ciampolini M 1964 *J. Chem. Soc.* **4** 276
Sathyanarayana D N and Patel C C 1968 *Indian J. Chem.* **6** 523
Sayed L E and Iskandar M F 1971 *J. Inorg. Nucl. Chem.* **33** 435
Shupack S I, Billig E, Clark R J H, Williams R and Gray H B 1964 *J. Am. Chem. Soc.* **86** 4594
Sinn E and Harris C M 1969 *Coord. Chem. Rev.* **4** 391
Speca A N, Karayannis N M and Pytlewski L L 1976 *Inorg. Chim. Acta.* **17** 29
Vogel A I 1971 *A textbook of quantitative inorganic analysis* (ELBS: Longmans) p. 380
Walter W and Reubke K L 1970 In *Chemistry of amides* (ed) J Zabicky (New York: Interscience) p. 493.
Yamada H 1959 *Bull. Chem. Soc. Jpn.* **32** 1051

Proc. Indian Acad. Sci. (Chem. Sci.), Vol. 92, Number 2, April 1983, pp. 181–187.
© Printed in India.

Chiral synthesis of optically active S(+)-2,6,7,7a-tetrahydro-1β-hydroxy-4-formyl-7aβ-methylindene

D K BANERJEE, T R KASTURI* and A SARKAR
Department of Organic Chemistry, Indian Institute of Science, Bangalore 560012, India

MS received 10 February 1983

Abstract. The chiral aldol cyclization of the prochiral triketone 3 using l-valine afforded the optically active compound 4 in high chemical and optical yield. The configuration and optical purity of (+)4 was determined by ORD, chemical resolution and NMR chiral LSR studies. The title compound (+)7 was prepared from (+)4 following our earlier reported procedure.

Key words. Chiral synthesis; chemical resolution; optical rotatory dispersion; chiral NMR shift reagent.

1. Introduction

An efficient synthesis of 2,6,7,7a-tetrahydro-1β-hydroxy-4-formyl-7aβ-methylindene (7), a potential synthon for stereospecific total synthesis of natural and modified steroids, was reported earlier (Banerjee *et al* 1976). Further improvements in the method for the preparation of the compound (7) in larger quantities have been effected. Replacing the Mannich base (1b) by the parent chloroketone (1a) in the annealation reaction with the diketone (2), an yield of 92% (reported 55%, Banerjee *et al* 1976) of enedione (4a) was obtained. An improved yield of 60% (reported 55%, Banerjee *et al* 1976) of the aldehyde (7) could also be obtained by suitably modifying the reaction condition.

In the present paper, the synthesis of the aldehyde (7) in the optically-active form required for the synthesis of natural steroids, has been described. For this purpose, the triketone (3) was cyclized using l-valine as the chiral catalyst to furnish the enedione (4*a*) with the specific rotation of +250° ($CHCl_3$) in 80% yield. To determine the optical purity of the above product, the resolution of the enedione (4*a*) was undertaken following the procedure adopted by Hajos *et al* (1968) and Dutcher *et al* (1976) for similar compounds.

The racemic enedione (4*a*) was selectively reduced by purified sodium borohydride in methanol under controlled conditions and the compound (4*b*) was obtained in 98% yield. The monophthalate (4*c*) of the keto alcohol (4*b*) was resolved with a molar quantity of brucine in boiling acetone. The salt which separated out on cooling, was repeatedly crystallized from acetone to the constant rotation of −4·5° ($CHCl_3$). The monophthalate, (−)4*c*, was regenerated by treating with dilute hydrochloric acid and crystallized twice from acetonitrile to the constant rotation of −71° (DMSO). Saponification followed by oxidation with pyridinium dichromate furnished the

Chart 1

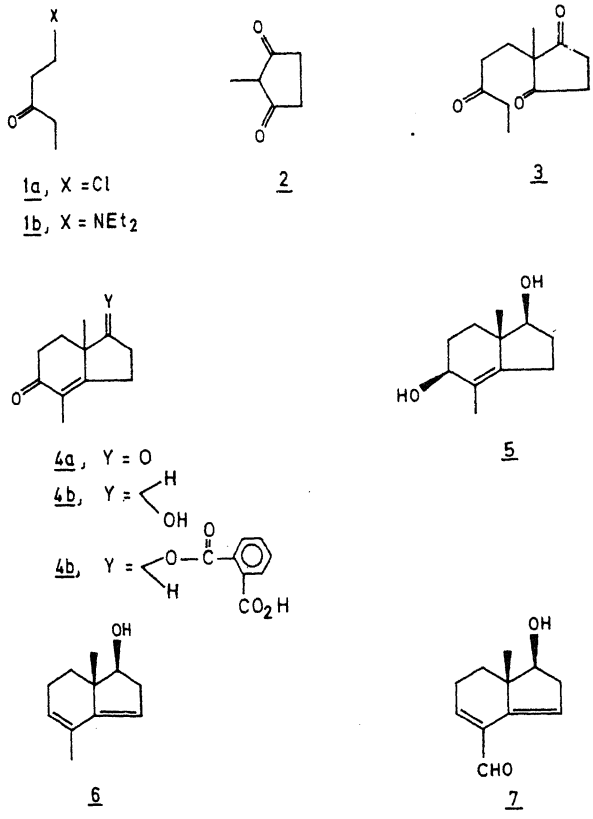

enantiomerically pure enedione (4*a*) which had a specific rotation of $-337°$ ($CHCl_3$).

The negative rotation and the inverted ORD curve (figure 1) of the resolved compound (4*a*) led us to suspect that the brucine salt of the *R*-isomer might have selectively precipitated out unlike the separation of the S-isomer in the case of Hajos' and Heathcock's compounds (Hajos *et al* 1968, Dutcher *et al* 1976). The formation of four isomers of the hydroxyenone (4*b*) is possible, as shown in chart 2, by the two possible pathways.

To clarify whether the borohydride reduction of the compound (4*a*) actually resulted in a higher proportion of the *trans* alcohol, the enedione (4*a*) was reduced with lithium tri-(*t*-butoxy)aluminumhydride (LTBA) in tetrahydrofuran and the entire process of resolution was repeated to obtain identical result, *i.e.* the isomer (−)4*a* was formed. On the basis of the absolute rotation obtained and assuming that the other antipode has identical magnitude of rotation with opposite sign, the optical yield in the chiral transformation has been found to be 74%. Analysis of the 270 MHz PMR spectrum of the compound (+)4*a*, in the presence of Eu^{III} (trifluoroacetylcamphorato) complex (substrate: LSR = 1 : 0·46 M) corroborated this result. Both the angular methyl and the allylic methyl singlets split into two distinct peaks; the integration of both the signals showed the same ratio (7 : 3), and this compared well with the enantiomeric excess determined by the chemical resolution. The configuration at C-13 (steroid nomencla-

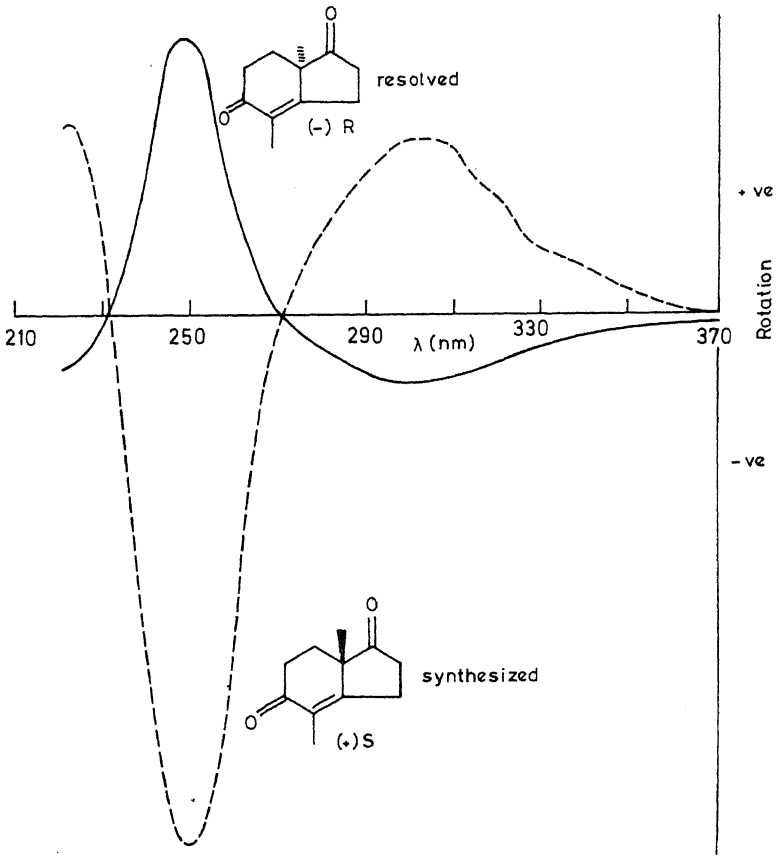

Figure 1. ORD spectrum of 4*a* in EtOH —— for (−) 4*a*; ---- for (+) 4*a*.

Chart 2

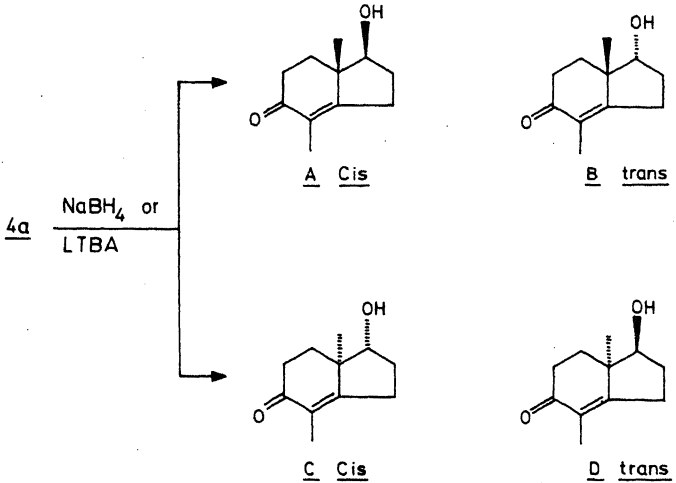

ture) was further confirmed to be 'S' by comparison of the CD-spectrum of the enedione (4*a*) with the data published by Hajos and Parrish (1974) for a related compound (figure 2).

The optically-active enedione (4*a*), possessing the required chirality for the synthesis of natural steroids, was then reduced with sodium borohydride to obtain the diol (5), m.p. 142°, $\alpha_D + 2{\cdot}5°$ (EtOH). The dienol (6), m.p. 74–75°, obtained after the acid-catalyzed dehydration of the diol (5), had a negative rotation of $-80°$ ($CHCl_3$). Such a change in the sign of the specific rotation is in accordance with an earlier report in the literature for the cholestane series (Fieser and Fieser 1959). Selenium dioxide oxidation resulted in a relatively improved yield (64%) of the title compound (7), mp. 84°, $\alpha_D + 12°$ ($CHCl_3$).

2. Experimental

All melting points (hot stage) and boiling points (bath-temperature) are uncorrected. The UV spectra were recorded in 95% ethanol on a Unicam SP 700A recording

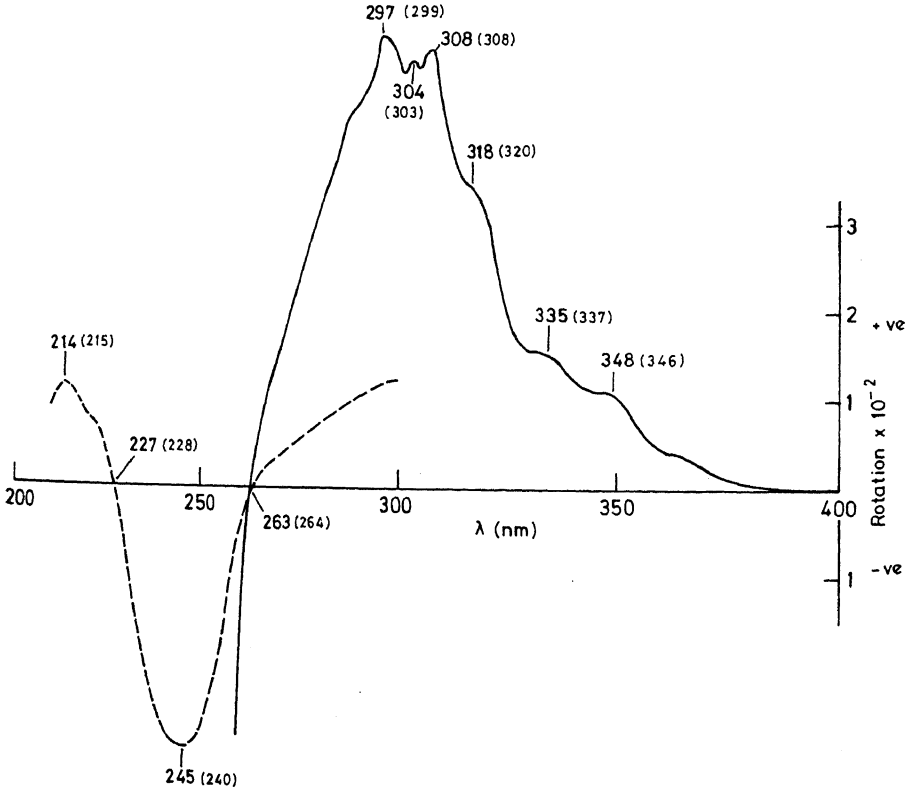

Figure 2. CD spectrum (dioxan) of (+) 4*a*. The figures in parentheses are taken from Hajos *et al* 1974.
—— Conc 3·5 mg/ml
--- Conc 0·7 mg/ml } in 1 mm cell.

spectrometer and Shimadzu double-beam UV spectrophotometer. The IR spectra were recorded on Perkin-Elmer 397 and Perkin-Elmer 700 spectrophotometers. The NMR spectra were recorded on a Varian T-60, Varian HA-100D or Bruker WH-270 FT NMR spectrometer. Chemical shifts are quoted relative to TMS ($\delta = 0$ ppm) as internal standard. Anhydrous sodium sulphate has been used for drying organic solutions. The optical rotations were recorded on a JASCO-J20 automatic recording ORD/CD machine.

2.1 2-*methyl*-2-(3-*oxopentyl*)-*cyclopentane*-1,3-*dione* (3)

Freshly-distilled ethyl vinyl ketone (14 g) and 2-methylcyclopentane-1,3-dione (2, 18·6 g) were stirred in 35 ml of demineralized water for 7 days at room temperature under nitrogen. Benzene (100 ml) was then added and the mixture filtered. The residue was repeatedly washed with boiling benzene (30 ml × 3). The combined benzene layer was concentrated and chromatographed over neutral alumina (600 g) using benzene-chloroform (3 : 1) as the eluent. The triketone (3) was obtained (19·9 g, 60%) as a pale yellow liquid, b.p. 145–150°/2 mm (reported 94°/0·01 mm, Swaminathan *et al* 1970); IR (neat): ν_{max} 1770, 1730, 1710 cm^{-1}; NMR (CCl_4): 0·95 (t, J = 7 Hz, 3H, $CH_2\underline{CH_3}$), 1·02 (s, 3H, CH_3), 1·80 (q, J = 7 Hz, 2H, $\underline{CH_2}CH_3$), 2·20–2·60 (m, 4H, methylenes) and 2·74 δ (s, 4H, ring methylenes).

2.2 (+)5,6,7,7*a*-*tetrahydro*-4,7*a*-*dimethylindane*-1,5-*dione* (4*a*)

A stirred mixture of the triketone (3, 3·4 g), l-valine (2·4 g), perchloric acid (0·7 ml) in acetonitrile (15 ml) was heated under reflux for 72 hr, filtered and concentrated. Dry benzene (20 ml) and a few crystals of *p*-toluene sulphonic acid were added to the concentrate and the solution heated for 4 hr in a Dean-Stark apparatus for azeotropic removal of water. The solution was concentrated and passed through silica gel (150 g). Elution with hexane-ethyl acetate (3 : 1) yielded 2·5 g (80%) of the (+) enedione (4*a*), b.p. 160–165°/6 mm (reported 120°/0·8 mm), $\alpha_D = +250°$ ($CHCl_3$), (Found: C 74·29 H 7·88; $C_{11}H_{14}O_2$ requires C 74·13, H 7·92%).

2.3 (+)5,6,7,7*a*-*tetrahydro*-1,5-*dihydroxy*-4,7*a*-*dimethylindane* (5)

This was prepared following the reported procedure for the preparation of the recemic compound (Banerjee *et al* 1976); from 4·5 g of the enone (+)4*a*, 1·25 g of sodium borohydride and 25 ml of ethanol was obtained the required diol (+)5 (3·8 g, 94%) m.p. 142°; $\alpha_D = +2·5°$ (EtOH); (Found: C 72·68, H 9·77; $C_{11}H_{18}O_2$ requires C 72·49, H 9·96%).

2.4 (−)2,6,7,7*a*-*tetrahydro*-1-*hydroxy*-4,7*a*-*dimethylindene* (6)

Following the earlier procedure for the preparation of the racemate from 2·1 g of the diol (+) 5, was obtained 1·75 g (92·5%) of the compound (−) 6, m.p. 74–75°; $\alpha_D = -80°$ ($CHCl_3$); (Found: C 80·53, H 9·62; $C_{11}H_{16}O$ requires 80·44, H 9·83%).

2.5 (+)2,6,7, 7*a*-*tetrahydro*-1-*hydroxy*-4-*formyl*-7*a*-*methylindene* (7)

This was prepared by modifying the reported procedure (Banerjee *et al* 1976). A mixture of 1·6 g of the dienol (−) 6 and 2·5 g of selenium dioxide was stirred in 25 ml of dimethyl sulphoxide under nitrogen at 120 for 1·5 hr. The mixture was poured into

water and extracted with ether. The ether layer was washed with water, aqueous $NaHCO_3$, water and brine and dried. The residue left on removal of the solvent was subjected to short path distillation (140–143°/2 mm) to afford the aldehyde (+)7 (7·1 g, 64%), m.p. 84°, $\alpha_D = +12°$ ($CHCl_3$). (Found: C 74·25, H 7·79; $C_{11}H_{14}O_2$ requires C 74·15, H 7·86%).

2.6 (±)5,6,7,7*a*-*tetrahydro*-4,7*a*-*dimethylindane*-1,5-*dione* (4*a*)

This was prepared following the procedure of Zoretic *et al* (1976), but was obtained in a much better yield. Thus, from 32·3 g of β-chloroethyl ethylketone and 25 g of 2-methylcyclopentane-1, 3-dione, was obtained 36·5 g (92%, reported [Eder *et al* 1971] 78%) of the title compound, b.p. 160–165°/6 mm (reported 94–98°/0·01 mm).

2.7 (±)5,6,7,7*a*-*tetrahydro*-1-*hydroxy*-4,7*a*-*dimethylindan*-5-*one* (4*b*)

This was earlier prepared by Crispin *et al* (1970), but now we report different methods which considerably improved the yield.

(a) A solution of 18·5 g of the enedione (4*a*) in methanol (400 ml) was treated with purified sodium borohydride (0·989 g) at 0–5° in small portions for 90 min. The course of the reaction was monitored by TLC. One drop of acetic acid was added to the reaction mixture and the solvent distilled off. Usual work-up afforded the pure compound (4*b*), b.p. 134–136°/1 mm (reported 128–130°/0·5 mm, Crispin *et al* 1970) as a pale yellow liquid (18·65 g, 97%).

(b) To a stirred suspension of lithium tri-*t*-butoxyaluminumhydride, prepared from 3·8 g of lithium aluminumhydride and 25 ml of *t*-butanol in THF (100 ml), maintained at 0°, was added dropwise a solution of 16·8 g of the enedione (4*a*) in 60 ml of THF. After 30 min, 15 ml of acetone and 200 ml of water were carefully added to the mixture, followed by acidification with 2N H_2SO_4 and extraction with ether. The ether layer was washed with brine and dried. Removal of the solvent yielded 15·7 g of the compound as an yellow oil (TLC single spot) (93%).

2.8 (±)5,6,7,7*a*-*tetrahydro*-1-*phthaloyloxy*-4,7*a*-*dimethylindan*-5-*one* (4*c*)

A mixture of hydroxy enone (4*b*, 11 g), resublimed phthalic anhydride (10 g) and 50 ml of pyridine was stirred under nitrogen at room temperature for two days. It was then poured into ice-water and carefully acidified with 2N HCl. The solid, which separated on cooling, was crystallized from acetonitrile to yield the analytically pure compound (4*c*) in 40% yield (8 g), m.p. 225–226°; IR (nujol): ν_{max} 2625, 2500, 1720, 1710, 1620, 1600 and 1590 cm^{-1}; NMR (DMSO-d_6): 1·2 (s, 3H, CH_3), 1·65 (s, 3H, vinylic CH_3), 1·7–2·8 (*m*, 8H, methylenes), 5·0 (bt, J = 10 Hz, 1H, –CH–O-phthaloyl), 7·65 (m, 4H, Ar-H) and 11·15δ (broad peak, 1H, CO_2H, exchanges with D_2O); Mass: M^+ m/z 328; (Found: C 69·11, H 6·3; $C_{19}H_{20}O_5$ requires C 69·5, H 6·14%).

2.9 (−)5,6,7,7*a*-*tetrahydro*-1-*phthaloyloxy*-4,7*a*-*dimethylindan*-5-*one* (4*c*)

The brucine salt of 4*c* was prepared as follows: To a hot solution of 6 g of the monophthalate (4*c*) in boiling acetone (250 ml) was slowly added 9·2 g of brucine dissolved in 120 ml of hot acetone. The solution was concentrated to a volume of 80 ml. Refrigeration for three days yielded crystals which were thrice crystallized from acetone

to furnish the brucine salt of 4*c* having the constant rotation of $-4{\cdot}5°$ ($CHCl_3$), 3·5 g, m.p. 154–155°; NMR ($CDCl_3$); 1·25 (s, 3H, CH_3), 1·67 (bs, 3H, vinylic CH_3) and 4·98 δ (dd, J = 7 Hz, 1H, –CH–COOAr).

A solution of the above brucine salt (2 g) in 30 ml of acetone was slowly added to ice and water containing 3 ml of 5% HCl. The product was crystallized twice from acetonitrile to afford the constant rotation $\alpha_D = -71°$ ($CHCl_3$), m.p. 224–226° (Found: C 69·21, H 6·15; $C_{19}H_{20}O_5$ requires C 69·50, H 6·14%).

2.10 (−)5,6,7,7*a*-*tetrahydro*-4,7*a*-*dimethylindane*-1,5-*dione* (4*a*)

A stirred mixture of 602 mg of the compound (−) 4*c* and 10 ml of 40% aqueous KOH was attached to a continuous extraction apparatus and extracted with ether at room temperature for 24 hr. The ether was removed to obtain the hydroxy enone (4*b*, 309 mg), a stirred solution of which in 5 ml of methylene chloride was oxidized by 1 g of pyridinium dichromate at room temperature under nitrogen for 22 hr. The mixture was diluted with ether (50 ml) and filtered through $MgSO_4$ to obtain the pure enedione, (−) 4*a* (257 mg) $\alpha_D = -337°$ ($CHCl_3$) (Found: C 74·35, H 7·86; $C_{11}H_{14}O_2$ requires C 74·13, H 7·92%).

Acknowledgements

This paper is based on the Ph.D thesis of one of the authors (AS). The authors wish to thank Dr S K Brahmachari of the Molecular Biophysics Unit, for the CD and ORD spectra and the Bangalore NMR facility for their kind cooperation. One of the authors (AS) thanks UGC and CSIR, New Delhi, for financial assistance.

References

Banerjee D K, Vittal Rao A S, Venkataramu S D, Surendranath V and Angadi V B 1976 *Synthesis* 307
Crispin D, Vanstone A E and Whitehurst J S 1970 *J. Chem. Soc.* **C** 10
Dutcher J S, Macmillan J G and Heathcock C H 1976 *J. Org. Chem.* **41** 2663
Eder U, Sauer G and Weitchert R 1971 *Angew. Chem. Int. Ed.* **10** 496
Fieser L and Fieser M 1959 *Steroids* (New York: Reinhold) pp. 26, 263
Hajos Z G, Parrish D R and Oliveto E P 1968 *Tetrahedron* **24** 2039
Hajos Z G and Parrish D R 1974 *J. Org. Chem.* **39** 1615
Swaminathan S, Srinivasan K G and Venkataramani P S 1970 *Tetrahedron* **26** 1453
Zoretic P A, Bendiksen B and Branchand B 1976 *J. Org. Chem.* **41** 3767

Proc. Indian Acad. Sci. (Chem. Sci.), Vol. 92, Number 2, April 1983, pp. 189–196.
© Printed in India.

Synthesis and characterisation of some novel β-aminodiketones

STEPHEN P ROE and JOHN O HILL*

Department of Inorganic and Analytical Chemistry, La Trobe University, Bundoora, Victoria, 3083, Australia

MS received 27 December 1982

Abstract. The synthesis and characterisation of five new β-aminodiketones is reported: (a) 3,3,5,8,10,10-hexamethyl-5,8-diazadodecane-2,11-dione; (b) 3,3,11,11-tetramethyl-5,8-diazatridecane-2,12-dione; (c) 3,3,12,12-tetramethyl-5,10-diazatetradecane-2,13-dione; (d) 3,3,10,10-tetramethyl-5,8-diphenyl-5,8-diazadodecane-2,11,dione and (e) 6,7-benzo-3,3,10,10-tetramethyl-5,8-diazadodecane-2,11-dione. These compounds are discussed as potential precursors in the synthesis of tetra-aza macrocyclic complexes.

Keywords. β-aminodiketone; tetra-aza macrocyclic complexes; nuclear magnetic resonance; mass spectra.

1. Introduction

The synthesis of β-aminodiketones is of interest since these compounds are possible precursors in the synthesis of model systems of naturally occurring tetra-aza macrocyclic systems such as the corrinoids and porphyrins. A variety of β-aminodiketones have been synthesised which have resulted in the preparation of a wide variety of tetra-aza macrocyclic complexes exhibiting variation in ring size, ring substitution and degree of saturation within the ring system. The synthesis of such model systems is achieved by one of two general procedures—a metal template synthesis as described by Curtis and House (1961) and Busch and Blinn (1968) or by metal insertion into a preformed tetra-aza macrocyclic ligand, formed by condensation of an aminodiketone with a primary amine. Love and Powell (1968) synthesised 4,4,9,9-tetramethyl-5,8-diazadodecane-2,11-dione [1], Green and Tasker (1968) synthesised 4,7-diaza-2,3,8,9-dibenzodecane-1,10-dione [2] and Bishop *et al* (1978) synthesised 1,10-phenanthroline-2,9-dicarboxaldehyde [3], all of which have served as precursors for a variety of Ni(II) tetra-aza macrocyclic complexes formed *via* a metal template synthesis. The α-aminodiketone [3] is an interesting example of the requirement of a dicarbonyl compound in general to contain one or more donor atoms between two carbonyl groups to achieve a facile *in situ* metal directed condensation, as discussed by Lindoy and Busch (1971). Further examples of synthetic β-aminodiketones include *bis*(acetylacetone)ethylenediamine [4], Martell *et al* (1955), N,N′-*bis*(2-acetyl-2-methylpropyl)piperazine [5], Lesnewski (1978) and 3,3,10,10-tetramethyl-5,8-diazadodecane-2,11-dione [6], Roe *et al* (1982). Compounds [5] and [6] were prepared by condensing appropriate diaminedihydrochloride with formaldehyde and methylisopropyl ketone, according to the Mannich reaction scheme.

* To whom all correspondence should be addressed.

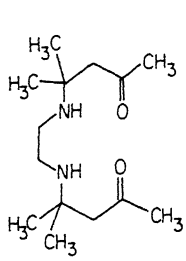

[1]

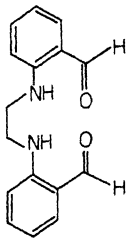

[2]

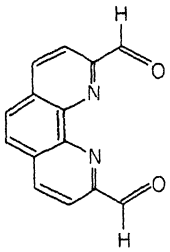

[3]

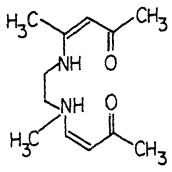

[4]

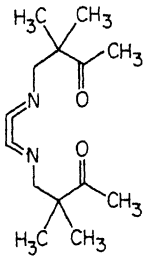

[5]

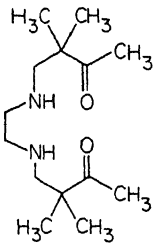

[6]

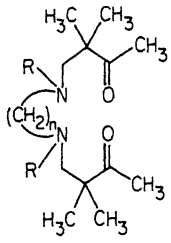

[7]

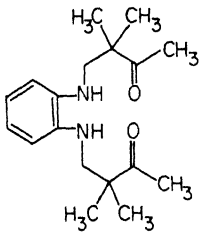

[8]

(7a) R = CH_3 , n = 2
(7b) R = H , n = 3
(7c) R = H , n = 4
(7d) R = C_6H_5 , n = 2

In the present study, five new β-aminodiketones [7 a–d], [8], structurally related to [1], [5] and [6] are synthesised and characterised from corresponding infrared, proton NMR, electronic and mass spectral data.

2. Experimental

All chemicals used were of reagent grade. Elemental analyses were provided by the Australian Microanalytical Service, Melbourne.

β-aminodiketones were prepared according to the procedure described by Roe *et al* (1982) for compound [6] or a modification thereof.

IR spectra in the range 4000–250 cm^{-1} were obtained on a Perkin-Elmer 457 spectrophotometer using the NaCl disc method.

Proton NMR spectra were obtained on a Perkin-Elmer R32 high resolution nuclear magnetic resonance spectrometer using Me_4Si as an internal reference and a sample spinning rate of 30 Hz.

Electron impact and chemi-ionisation mass spectra were obtained using a JEOL-JMSD 100 mass spectrometer and an ionising voltage of 70 eV with isobutane as carrier gas for the chemi-ionisation mode. Boiling points were obtained using a Swoloboff apparatus as described by Vogel (1972). It is apparent that these β-aminodiketones form azeotropes with either water or ether. Electronic spectra were recorded on a Shimadzu UV-240 recording spectrophotometer using 1 cm quartz cells and acetonitrile-190 as solvent.

2.1 3,3,5,8,10,10-*hexamethyl*-5,8-*diazadodecane*-2,11-*dione* [*7a*]

Using the general procedure described by Roe *et al* (1982), N,N′-dimethylethylenediamine dihydrochloride (12·0 g); methyl isopropyl ketone (12·0 g); formaldehyde (37% w/v, 11·7 cm^3) were refluxed to yield 5·0 g (42·2%) of a red oil b.p. 135°. i.r. $\nu_{max}(cm^{-1})$: 3400 sb (O–H str, H_2O), 2950 s, 2830 s, (C–H str, N–CH_3), 2965 s, 2870 s, (C–H str, CH_3), 2800 s (C–H str, CH_2), 1705 *vs* (C=O str), 1465 s, (C–H def, CH_2 scissor), 1380 s, 1355 s, (C–H def, gem–Me), 1260 s, 1185 s, 1110 s, 1035 s, (C–N str), 955 m, 835 m (C–C str).

^{1}H-NMR ($CDCl_3$): 1·17, s, 12H, gem–Me; 2·15, s, 6H, N-Me; 2·20, s, 6H, MeC=O; 2·50, d, 4H, CH_2; 2·62, s, 4H, CH_2 Mass Spectrum (c.i.) *m/z* 285 (molecular ion), 142 ($CH_2N(Me)CH_2C(Me)_2COMe$), 100($H_2CNH \cdot CH_2CH_2NMe \cdot CH_2$), 86 ($CH(Me)_2COMe$), 71($CH(Me)_2CHO$), 58($HNCH_2CH_2NH$), 43(MeCO), 28 ($CH_2CH_2$).

Microanalysis. (Found: C, 66·6, H, 11·20; N, 9·85. $C_{16}H_{32}N_2O_2$, 0·25 H_2O requires C, 66·51; H, 11·33; N, 9·7%).

2.2 3,3,11,11-*tetramethyl*-5,8-*diazatridecane*-2,12-*dione* [*7b*]

Using the general procedure, 1,3-diaminopropane dihydrochloride (13·2 g), methyl-isopropyl ketone (21·4 g), formaldehyde (37% w/v, 19·39 cm^3) were refluxed to yield 13·14 g (41%) of a red oil. b.p. 91°. i.r. $\nu_{max}(cm^{-1})$: 3400 *sb* (O–H) str, H_2O), 3330 s, (N–H str), 2960 s, 2870 s, (C–H str, CH_3), 2930 s, 2820 s, (C–H str, CH_2), 1705 *vs* (C=O str with shoulder at 1645 m), 1590 m (N–H def), 1465 s (C–H def, CH_2 scissor), 1380 m, 1355 s, (C–H def, gem–Me), 1265 m, 1190 m, (C–N str), 1050 m, 965 m, 950 mb, 880 m (C–C str). Strong bands at 1120 s, 1100 s imply a C–O str vibration. ^{1}H-NMR (d_6-DMSO): 1·1, s, 12H, gem–Me; 2·2, m, 6H, MeC=O, 3·2, s, 2H, NH; 4·57; s, 2H, H_2O. Chemical shifts at 3·7, 3·62, 3·54, 3·47, q, and 1·2, 1·12, 0·97, *t* indicate the presence of ether resulting from the extraction procedure. It is apparent that decomposition of the diketone occurs prior to complete removal of ether. Mass spectrum (c.i.): *m/z* 270 (molecular ion), 86 ($HC(Me)_2COMe$), 84 ($CH_2C(Me)_2CO$), 43(MeCO), 28 (CH_2CH_2). Fragments at *m/z* 74 and 45 correspond to ether fragments ($MeCH_2OCH_2Me$) and (OCH_2Me) respectively.

Microanalysis: (Found: C, 58·12; H, 11·32; N, 7·63. $C_{15}H_{30}N_2O_2$, 2·5 H_2O requires C, 58·57; H, 11·64; N, 7·19%).

2.3 3,3,12,12-*tetramethyl*-5,10-*diazatetradecane*-2,13-*dione* [*7c*]

Using the general procedure with a revised stoichiometry 1 mol of diamine dihydrochloride, 5 mol methylisopropyl ketone, 2·5 mol formaldehyde, 0·2 cm^3 hydrochloric acid (32% w/w) in anhydrous methanol (200 cm^3) were refluxed at 68° under N_2 for

12 hr, the reactants of 1,4-diaminobutane dihydrochloride (10·6 g), methyl isopropyl ketone (28·4 g) and formaldehyde (37% w/v, 13·4 cm^3) produced a yellow oil of yield 6·5 g (34·5%), b.p. 76°. IR ν_{max} (cm^{-1}): 3375 sb (N–H str), 2942 s, 2910 s (C–H str, CH_2), 1690 s (C=O str), 1455 s (C–H def, CH_2 scissor), 1375 m, 1350 s, (C–H def, gem-Me), 1185 w, 1120 s (C–N str). ^{1}H-NMR (d_6-DMSO): 1·08, s, 12H, gem-Me; 1·98, s, 6H, MeC=O, 3·03, s, 12H, CH_2. Mass spectrum (c.i.): *m/z* 142 ($MeCOC(Me)_2CH_2NHCH_2CH_2$), 86 ($MeCOC(Me)_2H$), 57 ($CH_2NHCH_2CH_2$), 43 (MeCO), 42 ($Me_2C$). Microanalysis: (Found: C, 67·56; H, 11·34; N, 9·84; $C_{16}H_{32}N_2O_2$, 0·25 $C_4H_{10}O$ requires C, 67·39; H, 11·47; 9·24%).

2.4 3,3,10,10-*tetramethyl*-5,8-*diphenyl*-5,8-*diazadodecane*-2,11-*dione* [7*d*]

Using the revised procedure as for [7c], N,N′-diphenylethylenediamine dihydrochloride (7·0 g), methyl isopropyl ketone (10·6 g), formaldehyde (37% w/v, 5·0 cm^3) were refluxed to produce a red-oil of yield 3·6 g (36%). b.p. 151°. i.r. ν_{max} (cm^{-1}): 3070 m, 3040 s, 3000 s (C–H str on C_6H_5), 3340 s, (O–H str, H_2O), 2950 s, 2850 s (C–H str, CH_3), 2920 s (C–H str, CH_2), 1695 s (C=O str), 1660 s, 1590 s, 1495 sb, 1430 m (C=C str of C_6H_5), 1460 m (C–H def, CH_2 scissor), 1375 m, 1350 s (C–H def, gem–Me), 1300 m, 1290 m, 1255 s, 1215 s, 1185 m, 1150 m (C–N str), 1110 s, 1090 m, 1070 m, 1025 m, 975 s, 880 s, 830 m, 800 m (C–C str), 750 s, 690 s (C–H def, monosubstituted aromatic, C_6H_5, out of plane).

^{1}H-NMR (d_6-DMSO): 1·11, 1·13, d, 12H, gem-Me, 2·13, s, 6H, CH_3C=O, 4·52, *s*, 4H, CH_2, 4·58, s, 4H, CH_2 on *en* bridge, 6·83 sextuplet, J = 7 Hz, ϕ, 7·43, s, 12H, CH ϕ. Mass Spectrum (e.i.) *m/z*: 238($CH_2N(C_6H_5)CH_2CH_2N(C_6H_5)CH_2$), 133 ($CH_2N(C_6H_5)CH_2CH_2$), 119 ($CH_2N(C_6H_5)CH_2$), 86 ($(Me)_2CCOMe$), 43 (MeCO), 42 ($Me_2C$).

Microanalysis: (Found: C, 74·53; H, 8·67; N, 9·07. $C_{26}H_{36}N_2O_2$ 0·5 H_2O requires C, 74·78; H, 8·93; N, 6·70%).

2.5 6,7-*benzo*-3,3,10,10-*tetramethyl*-5,8-*diazadodecane*-2,11-*dione* [8]

Using the revised procedure as for [7c], *o*-phenylenediamine dihydrochloride (10·0 g), methyl isopropyl ketone (26·7 g), formaldehyde (37% w/v, 11·2 cm^3) were refluxed to produce a red-oil of yield 14·0 g (84%). b.p. 130°. IR ν_{max} (cm^{-1}): 3400 sb (N–H str), 3040 m (C–H str, C_6H_4), 2950 s, 2910 s (C–H str, CH_3), 2850 s, (C–H str, CH_2), 1695 s (C=O str), 1675 s, 1590 s, 1490 w, 1450 wb (C=C str on C_6H_4), 1505 w (N–H def), 1380 w, 1350 w, (C–H def, gem–Me), 1030 m, 1095 m (C–N str), 735 s (C–H def out of plane disubstituted aromatic, C_6H_4).

^{1}H-NMR (d_6-DMSO): 1·1, s, 12H, gem–Me; 2·07, s, 6H, MeC=O; 3·19, s, 2H, NH; 7·1, *q*, 4H, ϕ. Mass spectrum (e.i.): *m/z* 261 ($Me_2CCH_2NH(C_6H_4)NHCH_2C(Me)_2COMe$) 219 ($CH_2NH(C_6H_4)NHCH_2C(Me)_2COMe$), 86 ($Me_2CCOMe$) 73 ($Me_2CHCH_2NH_2$), 71 ($Me_2CHCO$), 43 (MeCO), 42 ($Me_2C$).

Microanalysis: (Found: C, 64·68; H, 9·52; N, 10·09. $C_{18}H_{28}N_2O_2 \cdot 1{\cdot}5H_2O$ requires C, 65·22; H, 8·97; N, 8·45%).

3. Results and Discussion

3.1 $^1H_{NMR}$ *Spectral assignments*

With respect to structure [7a], the singlet at 1·11 δ is assigned to the geminal dimethyl

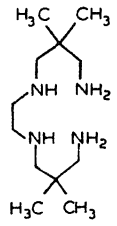

[9]

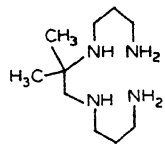

[10]

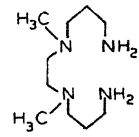

[11]

groups; the singlet at 2·5 δ is assigned to the N–Me function and singlet at 2·2 δ is assigned to the MeC=O function. These assignments for the geminal dimethyl groups and the N–Me function are in accordance with the assignments of Barefield *et al* (1976) for structures [9], [10] and [11]: (gem–Me, 0·86 δ [9], 1·0 δ [10] and N–Me 2·18 δ, [11]). For structure [7b], the singlet at 3·2 δ is assigned to the N–H group, which is in contrast to the singlet at 1·5 δ for structure [10] and [11] as assigned to N–H by Barefield *et al* (1976). The assignments for the geminal dimethyl groups and for the MeC=O function are also in agreement with the corresponding assignments 1·1 and 2·14 δ respectively made by Lesnewski (1978) for structure [5].

For structure, [7c], [7d] and [8], the chemical shifts corresponding to the MeC=O function are moved upfield by 0·22, 0·07 and 0·13 δ respectively, reflecting expansion and contraction of the carbon chain length between the amine functions. Structure [7d] exhibits a doublet at 1·11 and 1·13 δ for the geminal-methyl groups, possibly due to an anisotropic effect, that is, the geminal-methyl groups resonate at different chemical shift positions due to shielding of one methyl group relative to the double bond of the MeC=O function.

3.2 *IR spectral assignments*

IR assignments for the β-aminodiketones synthesised in the present work are made on the basis of the definitive group assignments provided by Kemp (1975), Jones (1959) and Silverstein *et al* (1974).

The most characteristic band for these compounds is that due to the C=O stretching vibration in the region of 1700 cm^{-1}. All five compounds indicate such a band within the narrow range 1700 ± 5 cm^{-1} which is indicative of a similar environment for carbonyl groups within the series.

Further characteristic bands for aminodiketones according to Kemp (1975) and Jones (1959) are those associated with C–H deformation modes of geminal methyl groups in the region of 1390 and 1360 cm^{-1} respectively. For the five β-aminodiketones studied, these bands appear at 1380 ± 5 cm^{-1} and 1350–1355 cm^{-1}. Compounds [7a], [7b] and [7c], which have a $(CH_2)_n$ bridge between secondary or tertiary amine groups, exhibit a CH_2 scissor vibration at 1460 ± 5 cm^{-1}.

Compounds [7b], [7c] and [8] exhibit an N–H stretching vibration at 3330, 3375 and 3400 cm^{-1} respectively.

The phenyl groups attached to the tertiary nitrogen atoms in compound [7d] are identified by the following bands: C–H stretching vibrations at 3070 cm^{-1} (s), 3040 cm^{-1} (s) and 3000 cm^{-1} (s), C=C stretching vibrations at 1660 cm^{-1} (s), 1590 cm^{-1} (s), 1495 cm^{-1} (sb) and 1430 cm^{-1} (m). The main fingerprint bands are the

C–H deformation out-of-plane bands at 750 cm^{-1} (s) and 690 cm^{-1} (s), typical of mono-substituted aromatic compounds. The *o*-phenylene group in compound [8] is identified by C=C stretching vibrations at 1675 cm^{-1} (s), 1590 cm^{-1} (s), 1490 cm^{-1} (w) and 1450 cm^{-1} (wb), with the main fingerprint band at 735 cm^{-1} (s) corresponding to the C–H deformation out-of-plane mode for a di-substituted aromatic compound.

IR spectra over the range 1800–1300 cm^{-1} for compounds [6], [7b] and [7d] indicating C=O str., C–H def. CH_2 str. and C–H def (gem–Me) bands are shown in figure 1.

3.3 *Mass spectral assignments*

In general, mass spectra derived *via* the chemi-ionisation mode indicate molecular ions whereas mass spectra derived *via* the electron impact mode show fragment ions only.

All five β-aminodiketones exhibit α cleavage—a common fragmentation pathway according to McLafferty (1973). Such cleavage occurs between pairs of carbon atoms C_1–C_2, $C_{1'}$–$C_{2'}$, C_2–C_3, $C_{2'}$–$C_{3'}$ [12] resulting in common fragment ions of *m/z* 86 ($CH(Me)_2COMe$, 43 (COMe) and 42 (CMe_2).

Further α type cleavage occurs for compounds [7a] and [7c] within the ethylenediamine and 1,3-diaminobutane bridges respectively, yielding fragment ions of *m/z* 142 ($CH_2N(Me)CH_2C(Me)_2COMe$) [7a] and 142 ($MeCOC(Me)_2CH_2NHCH_2 \cdot CH_2$) [7c]. Compound [7d] gave a fragment ion at *m/z* 119 ($CH_2N(C_6H_5)CH_2$), however such cleavage within the ethylenediamine bridge is secondary to the α cleavage

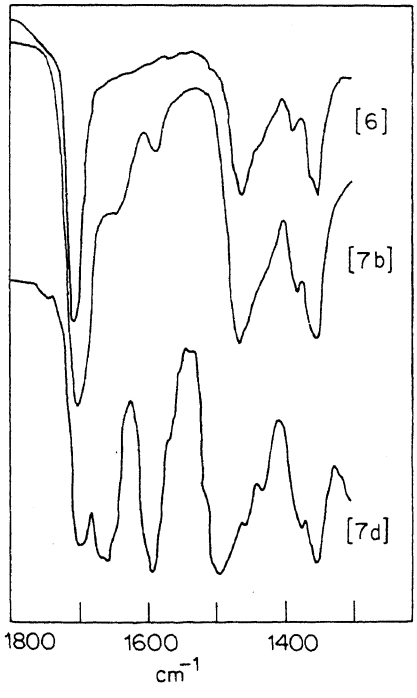

Figure 1. IR spectra of compounds [6], [7b] and [7d] in the region of 1800 cm^{-1} to 1300 cm^{-1}.

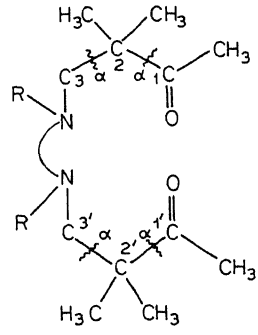

[12]

between C_1–C_2 and C_2–C_3 type segments since a fragment ion corresponding to $(CH_2N(C_6H_5)CH_2C(Me)_2COMe)$ does not appear in the mass spectrum of this compound.

3.4 *Electronic spectral assignments*

The principal UV-visible spectral bands within the range 190–900 nm for various β-aminodiketones are listed in table 1.

The assignment of bands is made on the basis of the definitive data of Silverstein *et al* (1974); a band in the region of 280 nm, $\varepsilon_{max} = 15$ is assigned to the $n \rightarrow \pi^*$ forbidden transition in the carbonyl chromophore. Methylisopropyl ketone, the precursor of the β-aminodiketones studied, indicates an electronic absorption band at 280 nm, $\varepsilon_{max} = 23{\cdot}5$ (acetonitrile solvent). The $n \rightarrow \sigma^*$ and $\pi \rightarrow \pi^*$ allowed transitions for such ketones are of higher energy $n \rightarrow \sigma^*$ (185 nm) and $\pi \rightarrow \pi^*$ (160 nm) and are outside the scanning range studied. All β-aminodiketones studied exhibit the $n \rightarrow \pi^*$ forbidden transition, which is essentially the fingerprint transition for these compounds.

The additional bands associated with compound [8] are assigned to the $\pi \rightarrow \pi^*$ transitions of the C_6H_4 moiety: 283 nm ($A_{1g} \rightarrow B_{2u}$), 275 nm ($A_{1g} \rightarrow B_{1u}$) and 248 nm ($A_{1g} \rightarrow E_{1u}$), as compared to those of benzene at 204 nm ($A_{1g} \rightarrow B_{1u}$) 256 nm ($A_{1g} \rightarrow B_{2u}$) and 184 nm ($A_{1g} \rightarrow E_{1u}$). The substantial bathochromic shift accompanied by a diminished fine structure is due to the non-bonding pair substituents of NH_2. The fine structure is lost due to n–π conjugation and the shift is due to conjugation between the

Table 1. Electronic spectra of β-aminodiketones (acetonitrile solvent).

Compound	λ_{max} (nm) (ε_{max})(10^{-2} M^2 mol^{-1})			
	$n \rightarrow \pi^*$	$A_{1g} \rightarrow B_{2u}$	$A_{1g} \rightarrow B_{1u}$	$A_{1g} \rightarrow E_{1u}$
[7b]	312 (1317)	—	—	—
[7c]	292 (38)	—	—	—
[7d]	379 (252·5)	—	—	—
[8]	304 (2475)	283 (3197)	275 (3919)	248 (7529)
[6]	297·5 (70·3)	—	—	—
[5]	279 (366)			

non-bonding electrons of nitrogen and the π-electron system of the ring.

It is interesting that only one band is observed for compound [7d] at $\lambda_{max} = 379$ nm ($\varepsilon_{max} = 252{\cdot}5$) which probably results from the overlap of a shifted $n \rightarrow \pi^*$ forbidden transition in the carbonyl chromophore and a shifted $A_{1g} \rightarrow B_{2u}$ allowed transition associated with the aromatic substituents on the nitrogen atoms.

4. Conclusion

The physical data for the five β-aminodiketones synthesised in the present work are essentially consistent with their proposed structures. Such compounds increase the range of known aminodiketones, in particular, those reported by Martin *et al* (1980), Busch and Blinn (1968) Martell *et al* (1955), Holm *et al* (1973), Lesnewski (1978), Roe *et al* (1982), Barefield *et al* (1976), Martell *et al* (1958), Belford *et al* (1956), Jager (1964, 1968), Truex and Holm (1972), Tasker and Fleischer (1970), Van Leeuwen (1968), Nakamura and Kawaguchi (1968), Bamfield (1969), Patterson and Holm (1975), and Black *et al* (1972) which have been employed in the synthesis of a wide variety of tetra-aza macrocyclic complexes.

References

Bamfield P 1969 *J. Chem. Soc.* A 2021

Barefield E K, Wagner F and Hodges K D 1976 *Inorg. Chem.* **15** 1370

Belford R L, Martell A E and Calvin M 1956 *J. Inorg. Nucl. Chem.* **2** 11

Bishop M M, Lewis J, O'Donoghue T D and Raithby P R 1978 *Chem. Commun.* 476

Black D, St. C. and Greenland H 1972 *Aust. J. Chem.* **25** 1315

Busch D H and Blinn E 1968 *Inorg. Chem.* **7** 820

Curtis N F and House D A 1961 *Chem. Ind.* 1708

Green M and Tasker P A 1968 *Chem. Commun.* 518

Holm R H, Tang S C, Koch S, Weinstein G N and Lane R W 1973 *Inorg. Chem.* **12** 2589

Jager E G 1964 *Z. Chem.* **4** 437

Jager E G 1968 *Z. Chem.* **8** 30, 392

Jones R N 1959 Infrared spectra of organic compounds: Summary charts of principal group frequencies. (Ottawa: National research council of Canada)

Kemp W 1975 *Organic Spectroscopy* (New York: Macmillan) pp. 8–75

Lesnewski G 1978 M.Sc. Thesis La Trobe University Melbourne Australia 121

Lindoy L F and Busch D H 1971 *Prep. Inorg. Reactions* **6** 1

Love J L and Powell H K J 1968 *Chem. Commum.* 39

Martell A E, McCarthy P J, Hovey R J and Ueno K 1955 *J. Am. Chem. Soc.* **77** 5820

Martell A E, Belford R L, and Calvin M 1958 *J. Inorg. Nucl. Chem.* **5** 170

Martin J W L, Timmons J H and Martell A E 1980 *J. Coord. Chem.* **10** 251

McLafferty R W 1973 *Interpretation of mass spectra* (New York: Benjamin) 48–56

Nakamura Y and Kawaguchi S 1968 *Chem. Commun.* 716

Patterson G S and Holm R H 1975 *Bioinorg. Chem.* **4** 257

Roe S P, Cullis P G, Derrick P J and Hill J O 1982 *Aust. J. Chem.* **35** 287

Silverstein R M, Bassler G C and Morrill T C 1974 *Spectrometric identification of organic compounds* (New York: Wiley) pp. 135–152

Tasker P A and Fleischer E B 1970 *J. Am. Chem. Soc.* **92** 7072

Truex T J and Holm R M 1972 *J. Am. Chem. Soc.* **94** 4529

van Leeuwen P W N M 1968 *Rec. Trav. Chim.* **87** 396

Vogel A I *Practical Organic Chemistry* (New York: Longman) p. 85

Proc. Indian Acad. Sci. (Chem. Sci.), Vol. 92, No. 3, June 1983, pp. 197-201.
© Printed in India.

Electronic spectra of paramethoxy benzyl alcohol and parachloro benzyl cyanide

A K SARKAR, P K MALLICK, S CHAKRAVORTI and S B BANERJEE*
Department of Optics, Indian Association for the Cultivation of Science, Jadavpur, Calcutta 700 032, India.

MS received 24 May 1982; revised 10 December 1982.

Abstract. The electronic absorption spectra of paramethoxy benzyl alcohol (PMBA) and parachloro benzyl cyanide (PCBC) are described. The broad features of the spectra of the molecules are consistent with allowed transition for C_{2v} symmetry. However, the solid state and glass matrix spectra of PMBA at 77K indicate possible deviation from planarity in the structure of the molecule. In PCBC, it is pointed out that intensity borrowing may be responsible for the large intensity of the vibrationally-induced part of the spectra, in which non-totally symmetric vibrations are excited.

Keywords. Solid phase spectrum; glass matrix spectrum; intensity borrowing; paramethoxy benzyl alcohol; parachloro benzyl cyanide.

1. Introduction

Complete vibrational assignments of paramethoxy benzyl alcohol (PMBA) and parachloro benzyl cyanide (PCBC) molecules were recently described (Chakravorti *et al* 1982). This paper concerns recording and analysis of hitherto unreported electronic absorption spectra of PMBA in the vapour and solid states and in an isobutyl alcohol rigid glass at 77K and of PCBC in the solid phase and in an ethanol rigid glass at 77K. Both are para-disubstituted benzene molecules with one or more large substituents. In PMBA, both substituents (OCH_3 and CH_2OH) are electron releasing while in PCBC, one substituent (Cl) is electron releasing and the other (CH_2CN) is electron withdrawing. In interpreting the results attention has been paid to probable structure and symmetry of the molecules, with which the symmetry of vibrational modes involved in an electronic transition is known to be intimately related.

2. Experimental

The compounds PMBA and PCBC were of purum grade and were obtained from Fluka AG (Switzerland) and E. Merck (Germany) respectively. They were used after repeated vaccum distillation. Isobutyl alcohol and ethanol of spectroscopic purity were supplied by BDH (London). Experimental arrangements were the same as described elsewhere (Mallick and Banerjee 1974).

*To whom all correspondence should be made.

3. Interpretation of the results

In making vibrational assignments of the ring vibrations, the molecules were assumed to belong to symmetry species C_{2v} (Chakravorti *et al* 1982). If the assumption is valid, then with recommended choice of axes (Mulliken 1955) the π-electronic transition would be $^1B_2 \leftarrow {}^1A_1$ corresponding to $^1B_{2u} \leftarrow {}^1A_{1g}$ of benzene with dipole moment in the plane of molecules and along Y direction *i.e.* perpendicular to C_2 axis. The expected vibrational structure of the electronic spectra of such molecules is well established. The spectra should exhibit a strong O, O band and progressions of totally symmetric (a_1) vibrations. Non-totally symmetric vibrations (b_2 type) may couple with the transition but only weakly.

3.1 *PMBA*

The f-value of the transition, which is allowed, is measured in cyclohexane solution and found to be 2.59×10^{-2}. The O, O band in the vapour spectrum is identified with the band 35539 cm^{-1}. Modes 1 and 12 of benzene, which are substituent sensitive in para–substituted benzenes, yield two trigonal modes (Chakravorti *et al* 1982) assigned as ν_9 (851 cm^{-1}) and ν_{10}(818 cm^{-1}). The excited state frequency 820 cm^{-1} may be reasonably correlated with ν_9. The excited state vibration 313 cm^{-1} represents the a_1 component of the a(CCC) mode 6 of benzene, the corresponding ground state vibration being 374 cm^{-1} (ν_{11}). These two vibrations are the most prominent in the vapour spectrum. Another a_1 vibration 1127 cm^{-1} is also observed in the band at 36646 cm^{-1} (table 1), which is broad due to the presence of a second unresolved band 0 + 313 + 820. The spectrum shows presence of one nontotally symmetric planar b_2 vibration which appears in the weak band at 36877 cm^{-1}.

The two excited state a_1 vibrations related to ν_{11} and ν_9, observed in the vapour spectrum, are also strongly excited in the spectra of PMBA in the solid phase and in isobutyl alcohol glass matrix at 77K (tables 2 and 3). The solid state spectrum consists of sharper bands and a b_2 vibration 198 cm^{-1} couples

Table 1. Absorption bands of PMBA vapour.

Wave no in cm^{-1} and intensity	Assignment
35143 wb	0 – 376
35519 w	0, 0
35832 m	0 + 313
36339 m	0 + 820
36646 sb	0 + 1127; 0 + 313 + 820
36877 w	0 + 1358
37122 wb	0 + 2 × 820
37484 wb	0 + 820 + 1127

Table 2. Absorption bands of PMBA in isobutyl alcohol rigid glass and in solid phase at 77K.

Isobutyl alcohol rigid glass at 77K		Solid at 77K	
Wave number in cm^{-1} intensity	Assignment	Wave number in cm^{-1} and intensity	Assignment
35164 m	0 – 0	35127 m	0 – 0
35275 s	0 + 111	35227 sb	0 + 100
		35325 vs	0 + 190
35501 vs	0 + 337	35451 vs	0 + 324
35987 vs	0 + 823	35948 m	0 + 821
36326 vs	0 + 1162;	36277 vs	0 + 1150;
	0 + 337 + 823		0 + 324 + 821
36713 vs	0 + 2 × 823	36713 vs	0 + 2 × 821
37136 svb	0 + 337 + 2 × 823;	37095 vs	0 + 324 + 2 × 821;
	0 + 823 + 1162		0 + 821 + 1150
		37510 s	0 + 3 × 821
		37925 mb	0 + 324 + 3 × 821;
			0 + 2 × 821 + 1150
		38259 m	0 + 4 × 821

Table 3. Correlation between ground and excited state frequencies of PMBA in cm^{-1}.

Ground state				Excited state		
Raman	IR	UV	Vapour	Solid at 77	Glass at 77K	Symmetry species*
–	120	–	–	100	111	b_1 (ν_{20})
226	–	–	–	198	–	b_2 (ν_{30})
374	–	376	313	324	337	a_1 (ν_{11})
851	–	–	820	821	823	a_1 (ν_9)
1204	1182	–	1127	1150	1162	a_1 (ν_6)
1249	1260	–	–	–	–	a_1 (ν_5)
–	1428	–	1358	–	–	b_2 (ν_{24})

* Discussion in the text

with the transition. Both the solid state and rigid glass spectra are characterised by the appearance of an excited state frequency *ca* 111 cm^{-1} corresponding to the out of plane b_1 vibration 120 cm^{-1} (ν_{20}) in the ground state (Chakravorti *et al* 1982) representing an X – sensitive mode. Since such b_1 vibration should be forbidden in a $^1B_2 \leftarrow {}^1A_1$ transition, it is possible that the molecule may be distorted from planar structure in the solid phase and also in isobutyl alcohol matrix at 77K. Similar conclusions drawn in the case of benzene (Kanda and Shimada 1961; Kanda *et al* 1961) and 1,3,5-trimethoxy benzene (Chakravorti *et al* 1979 may) be noted.

3.2 *PCBC*

The computed *f*-value in cyclohexane solution is 2.9×10^{-3}. This shows that

Table 4. Absorption bands of PCBC in ethanol glass and solid phase at 77K.

Ethyl alcohol rigid glass		Solid at 77K	
Wave number in cm^{-1} and intensity	Assignment	Wave number in cm^{-1} and intensity	Assignment
36379 m	0, 0	36155 m	0, 0
		36406 s	0 + 251
		36713 s	0 + 558
37152 vs	0 + 773	36944 s	0 + 789
37442 vw	0 + 1063	37219 mb	0 + 1064
37653 m	0 + 1274	37442 s	0 + 1287
		37526 msh	0 + 1371
		37611 m	0 + 1456
37913 vw	0 + 1534;	37710 m	0 + 1555;
	0 + 2 × 773		0 + 2 × 789
		37839 m	0 + 251 + 1456
		37968 m	0 + 789 + 1064
		38055 w	0 + 2 × 558+789
38142 s	0 + 1763 (?)		
38381 w	0 + 773 + 1274	38200 w	0 + 789 + 1287
38667 w	0 + 3 × 773;	38464 s	0 + 1064 + 1287;
	0 + 1063 + 1274		0 + 3 × 789
		38569 ssh	0 + 3 × 558+789
38881 vw	0 + 2 × 1274	38718 msh	0 + 2 × 1287
		38854 w	0 + 1287 + 1456
		39235 m	0 + 4 × 789

Table 5. Correlation of ground and excited state vibrational frequencies of PCBC in cm^{-1}.

Ground state		Excited state		
Raman	IR	Rigid Glass at 77K	Solid at 77K	Symmetry species*
–	260 or 358	–	251	b_2 (ν_{29}) or (ν_{30})
637	635	–	558	b_2 (ν_{28})
808	800	773	789	a_1 (ν_9)
1069	1070	1063	1064	a_1 (ν_7)
1322	1314	1274	1287	b_2 (ν_{25})
–	1485	–	1371	a_1 (ν_4)
1583	1578	–	1456	b_2 (ν_{23})
1600	1615	1534	1555	a_1 (ν_3)

*Discussion in text.

the electronic transition though allowed by symmetry is of weaker nature than that in PMBA. The vapour phase spectrum of this compound is not well structured and the vibronic analysis of electronic bands had to be confined to the solid phase and ethanol glass matrix spectra at 77K. As shown in table 4 the O, O band is identified at 36379 cm^{-1} and 36155 cm^{-1} in the spectra due to the rigid glass and the solid respectively. An upper state a_1 vibration 789 cm^{-1} is the most prominent and is excited several quanta in the spectra. Two other a_1 vibrations 1064 and 1371 cm^{-1} are also involved in the transition. One notable feature is a b_2 vibration of frequency 558 cm^{-1} (tables 4 and 5) which represents the α(CCC) mode derived from the e_{2g} mode 6 of benzene. This vibration is quite prominent and several quanta of it appear in combination with the 789 cm^{-1} vibration. A few other bands arising from excitation of b_2 vibrations 251, 1287 and 1456 cm^{-1} appear with considerable intensity. Several combinations of these are observed in the spectra. The excitation of these b_2 vibrations which constitute the so-called 'forbidden part' is quite high and may be attributed to intensity borrowing, effected through vibronic mixing of the B_2 state concerned in the $B_2 \leftarrow A_1$ transition with an upper A_1 state derived from E_{1u} state of benzene by excitation of b_2 vibration (Herzberg 1966; Mallick and Banerjee 1977). It was pointed out by Chakravorti *et al* (1977) that vibronic mixing of states is facilitated by crystal forces in the solid phase. However, in the case of the molecule PCBC, all the vibrations are planar (a_1 or b_2) and as such there is no indication of deviation from planar structure either due to crystal fields in the solid phase or in the ethanol matrix at 77K.

References

Chakravorti S, Sarkar A K, Mallick P K and Banerjee S B 1977 *Chem. Phys. Lett.* **52** 377

Chakravorti S, Sarkar A K and Banerjee S B 1979 *Chem. Phys. Lett.* **61** 568

Chakravorti S, Sarkar A K, Mallick P K and Banerjee S B 1982 *Indian J. Phys.* **B56** 96

Herzberg G 1966 *Electronic spectra and electronic structure of polyatomic molecules* (New York: D. van Nostrand) p. 140

Kanda Y and Shimada R 1961 *Spectrochim. Acta* **17** 7

Kanda Y, Gondo Y and Shimada R 1961 *Spectrochim. Acta* **17** 424

Mallick P K and Banerjee S B 1974 *Chem. Phys. Lett.* **27** 503

Mallick P K and Banerjee S B 1977 *Indian J. Phys.* **B51** 173

Mulliken R S 1955 *J. Chem. Phys.* **23** 1979

Specific conductances of 2×10^{-8} mho cm^{-1} (EG) and 9.5×10^{-9} mho cm^{-1} (DEG) were observed at 25°C. Conductivity water was prepared by distilling doubly-distilled water, to which a trance of permanganate and a few sodium hydroxide pellets were added, over an all-glass apparatus. Hydrogen chloride gas, generated according to the method described earlier (Kalidas and Palit 1961), was bubbled into the solvent mixture of the desired composition and standardised against a freshly standardised solution of aqueous NaOH and solutions of HCl of the desired concentration were prepared from this stock solution. A precision conductance bridge model WBR/TAV (Wissenschaftliche Technische Werkstatten GmbH, West Germany) operating on 220 V and 50 cycles/sec was used for all conductance measurements. A logarithmic indicator amplifier with a built-in 1000 cycles/sec generator was used as the balance indicator. The resistance measurements are generally accurate to $\pm 0.1\%$. A conductance cell similar to that reported by Daggett and Kraus (1951) with a cell constant 0.5524 cm^{-1} was used. The temperature was maintained to within ± 0.01°C by circulating liquid paraffin at the given temperature through the annular space of the double-walled cell used in the measurements. The viscosities and dielectric constants of EG-DEG mixtures were determined at 25°C (Sivaprasad and Kalidas 1979) by an Ostwald viscometer and a DK meter 60 GK respectively while the same data for water-EG and water-DEG mixtures were taken from literature (Gallant 1967; Akerlof 1932). The general procedure in the conductance measurements has been described earlier (Kalidas and Rao 1976) and usually HCl concentrations in the range 1 to 7 ± 10^{-3} eqv/l were employed.

3. Results and discussion

The conductance data on the acid in the various solvent mixtures were analysed by the Fuoss-Onsager (1965) three parameter equation given by (Fuoss *et al* 1965)

$$\Lambda = \Lambda_0 - SC^{1/2}\gamma^{1/2} + 2EC\gamma \log(\tau\gamma^{1/2}) + LC\gamma - AC\gamma \exp(-2T\gamma^{1/2})\Lambda \quad (1)$$

wherein the various terms have their usual significance. The calculations were performed on an IBM 360 computer. The results analysed showed no appreciable association of the acid ($K_A < 10$) in all the three systems and hence the 1965 Fuoss-Onsager two-parameter equation given by (Fuoss *et al* 1965)

$$\Lambda = \Lambda_0 - SC^{1/2} + 2EC \log(\tau) + LC \quad (2)$$

was used in further analysis of the data. The terms in (2) have been explained elsewhere (Fuoss *et al* 1965). The correction for the solvent conductance was small and hence neglected. The conductance data, the Λ_0 values and the standard deviation for each run obtained from the computer analysis of the data at

Table 1. Conductance data of HCl in water-EG mixtures at 25°C.

$c \times 10^4$ mol lit^{-1}	Λ	$\Delta\Lambda^*$	$c \times 10^4$ mol lit^{-1}	Λ	$\Delta\Lambda^*$
	20 wt% EG			40 wt% EG	
9.397	196.95	0.06	11.49	120.32	0.07
14.17	196.14	−0.05	15.14	119.90	−0.02
20.65	195.36	−0.05	20.60	119.46	−0.05
28.59	194.68	0.07	27.38	119.08	0.01
36.94	193.82	−0.06	34.33	118.67	−0.01
48.63	193.00	0.00	42.86	118.26	−0.00
66.16	191.89	0.01	59.23	117.57	0.01
	60 wt % EG			80 wt % EG	
13.75	65.81	−0.01	15.82	29.87	−0.02
19.20	65.53	0.00	24.34	29.58	−0.03
24.55	65.28	−0.01	31.83	29.44	0.03
29.90	65.10	0.02	38.95	29.30	0.05
37.91	64.81	0.01	44.40	29.14	0.00
46.19	64.55	0.01	53.86	28.96	−0.02
57.06	64.21	−0.02	62.19	28.77	0.04
			68.91	28.56	0.04

* represents the difference between the measured Λ and that calculated from (2). Λ and $\Delta\Lambda$ are given in ohm^{-1} cm^2 cm^2 mol^{-1}.

Table 2. Conductance data of HCl in water-DEG mixtures at 25°C.

$c \times 10^4$ mol lit^{-1}	Λ	$\Delta\Lambda^*$	$c \times 10^4$ mol lit^{-1}	Λ	$\Delta\Lambda^*$
	20 wt% DEG			40 wt% DEG	
18.17	182.94	0.09	19.81	94.30	0.04
26.40	181.84	−0.02	22.69	94.01	−0.04
34.33	180.97	−0.04	28.58	93.65	0.01
43.85	180.00	−0.10	34.57	93.22	−0.06
52.96	179.34	0.03	48.85	92.57	0.10
61.89	178.58	0.00	56.15	92.07	−0.03
68.46	178.11	0.05	68.13	91.51	−0.02
	60 wt % DEG			80 wt % DEG	
11.91	45.40	−0.04	18.35	16.62	0.05
14.84	45.31	0.00	25.49	16.39	−0.03
20.98	45.05	−0.01	33.35	16.23	−0.04
31.43	44.78	0.06	45.13	16.06	−0.01
38.07	44.56	0.02	53.40	15.95	0.00
46.38	44.32	−0.01	61.38	15.82	−0.01
53.24	44.19	0.01	68.90	15.76	0.03
61.47	43.97	0.03			

* represents difference between the measured Λ and that calculated from (2). Λ and $\Delta\Lambda$ are given in ohm^{-1} cm^2 mol^{-1}.

Table 3. Conductance data of HCl in EG-DEG mixtures at 25°C.

$c \times 10^4$ mol lit^{-1}	Λ	$\Delta\Lambda^*$	$c \times 10^4$ mol lit^{-1}	Λ	$\Delta\Lambda^*$
	20 wt% DEG			40 wt% DEG	
10.83	16.39	0.01	13.17	13.69	0.11
18.74	16.10	−0.01	18.15	13.31	−0.07
27.97	15.86	0.00	23.80	13.09	−0.08
35.52	15.70	0.01	34.38	12.81	−0.02
44.58	15.52	0.00	44.99	12.53	0.02
52.32	15.38	−0.01	55.52	12.27	0.04
62.61	15.26	0.03	66.03	11.95	−0.01
69.44	15.12	0.02			
	60 wt % DEG			80 wt % DEG	
12.48	9.82	0.05	15.47	7.66	−0.01
19.43	9.63	0.00	29.27	7.46	0.08
24.52	9.51	−0.03	33.65	7.31	0.02
31.34	9.37	−0.07	37.99	7.16	−0.06
45.83	9.29	0.04	46.18	7.01	−0.07
53.65	9.17	0.01	54.15	6.94	−0.01
62.18	9.07	0.00	62.18	6.85	0.02
			68.79	6.76	0.03

* Represents the difference between the measured Λ and that calculated from (2). Λ and $\Delta\Lambda$ are given in ohm^{-1} cm^2 mol^{-1}.

Table 4. Data of Λ_0(HCl) and $\sigma\Lambda^*$ in the various mixtures of water-EG, water-DEG and EG- DEG mixtures at 25°C. Λ_0 given in ohm^{-1} cm^2 mol^{-1}.

Wt% DEG/EG	0	20	40	60	80	100
Water-EG	426.75[a]	199.89	122.39	67.35	30.93 ± 0.03	32.77[b]
wt % EG		± 0.05	± 0.03	± 0.01		
$\sigma\Lambda$		0.06	0.04	0.02	0.03	
Water-DEG	426.75[a]	187.07	96.97	46.54	17.35 ± 0.03	9.76 ± 0.05[c]
wt% DEG		± 0.07	± 0.06	± 0.03		
$\sigma\Lambda$		0.07	0.06	0.04	0.03	0.05
EG-DEG	32.77[b]	17.01	14.43	10.26	8.28 ± 0.05	9.76 ± 0.05[c]
wt% DEG		± 0.02	± 0.06	± 0.04		
$\sigma\Lambda$		0.02	0.07	0.04	0.05	0.05

* $\sigma\Lambda$'s represent standard deviation of the individual points; [a] Stokes (1961); [b] Convington and Dickinson (1973); [c] Srinivas Rao and Kalidas (1976).

25°C are recorded in tables 1 to 4. The walden products $\Lambda_0\eta_0$ in all the solvent mixtures and their viscosities at 25°C are given in table 5. The two-parameter equation fits the data fairly well as evidenced from the small differences in $\Delta\Lambda$ and the small values of $\sigma\Lambda$ for each run (tables 1-3). Further the plots of Λ' given by

$$\Lambda' = \Lambda - \Lambda_0 + SC^{1/2} - EC\log C \qquad (3)$$

Table 5. Viscosities of the solvent mixtures (η_0) and walden products ($\Lambda_0\eta_0$) of HCl in various water-EG, water-DEG and EG-DEG mixtures at 25°C. η_0 is given in poise, $\Lambda_0\eta_0$ is given in ohm^{-1} cm^2 mol^{-1} poise.

Wt % DEG/EG		0	20	40	60	80	100
water-EG system	η_0	0.0089	0.0135	0.025	0.042	0.080	0.169
wt % EG	$\eta_0\Lambda_0$ (HCl)	3.80	2.70	3.06	2.83	2.43	5.54
Water-DEG system	η_0	0.0089	0.017	0.03	0.066	0.147	0.3055
wt % DEG	$\eta_0\Lambda_0$ (HCl)	3.8	3.18	2.91	3.07	2.55	2.98
EG-DEG system	η_0	0.169	0.1945	0.2138	0.2295	0.2485	0.3055
wt % DEG	$\eta_0\Lambda_0$ (HCl)	5.54	3.31	3.09	2.34	2.06	2.98

against concentration of the acid in all the mixed solvents are fairly linear lending further support (Evans and Kay 1966) to the complete dissociation of the acid in all solvent mixtures.

3.1 *Variation of Λ_0 and $\Lambda_0\eta_0$ as a function of solvent composition*

It is seen from table 4 that a small minimum observed for Λ_0 of HCl at 80 wt % EG in water-EG mixtures is not observed in water-DEG mixtures which is most possibly due to the large differences in the viscosity and dielectric constant of EG and DEG which affect the conductance values in the pure solvents to widely varying extent. Selvarajan and Kalidas (1974) and Srinivas Rao and Kalidas (1976) observed that Λ_0 (HCl) (taking into account the glycol-rich region) passes through a minimum at 2.5 wt % water and 1.4 wt % water in mixtures of water-EG and water-DEG respectively and this sharp decrease in Λ_0 (HCl) on the addition of small amount of water was interpreted on the basis of the abnormal conductance in EG or DEG according to

$$R^+(OH_2) + H_2O \rightleftarrows ROH + H_3O^+ \qquad (4)$$

where

$$R = CH_2OH.CH_2 \text{ or } CH_2OH.O.CH_2CH_2$$

In the water-rich region, the large decrease in Λ_0 on the addition of organic solvent to an infinitely dilute solution of HCl in water may be attributed to the breakdown of the H-bonded structure of water resulting in the disruption of the abnormal proton conductance in spite of the fact that the protons are virtually present as H_3O^+ ions right up to 90 wt % organic solvent in these mixtures as shown by our earlier studies (Selvarajan and Kalidas 1974). Shedlovsky and Kay (1956) arrived at similar conclusions in their conductance studies on HCl in methanol-water mixtures.

Examination of $\Lambda_0\eta_0$ data (table 5) in water-EG mixtures shows that it decreases initially up to 20 wt % EG and then increases slightly up to 40 wt % EG. The region from 40-80 wt % EG is marked by a gradual decrease and finally an increase in pure EG. The variation in water-DEG mixtures is in general similar to that in water-EG mixtures. The viscosity of the solvent mixtures, however, (table 5) increases continuously with the addition of the organic component in both water-EG and water-DEG mixtures. The large decrease in $\Lambda_0\eta_0$ in water-EG mixtures parallels the decrease of Λ_0 observed on the addition of small amounts of water (in the region of 80 wt % EG) to an infinitely dilute solution of HCl in EG. It is plausible to conclude that the changes in $\Lambda_0\eta_0$ in this region are not predominantly controlled by the changes in the viscosity of the medium but only by the structural changes occurring on addition of water. Similar conclusions apply for the variation of $\Lambda_0\eta_0$ with solvent composition in the water-rich region up to about 40 wt % organic solvent.

To get further information on the variation of the walden product with solvent composition, the cationic and anionic walden products were estimated in water-EG mixtures assuming

$$\lambda^0_{K^+} \approx \lambda^0_{NO_3} \approx \lambda^0_{Cl^-} \tag{5}$$

which was found to be valid (within $\pm$ 5%) from an examination of the conductance data for these ions in water (Robinson and Stokes 1959), EG, ethanol and methanol (Covington and Dickinson 1973). For obtaining the ionic walden products in the mixture of water-EG, the Λ_0 (KNO_3) data of Beradelli and Sesta (1972) in water-EG mixtures were utilised and the results so obtained are given in table 6. It is seen from this table that the changes in the walden product for chloride ion are more gradual with a small maximum at 40 wt % EG while considerable decrease of the same for H^+ ion is observed at the extreme compositions. It may be mentioned that the walden product variation of chloride ion in water-EG mixtures is similar to that observed in water-ethanol mixtures (Shedlovsky and Spivey 1967). Thus the variation of $\Lambda_0\eta_0$ of HCl in water-EG mixtures (and possibly in water-DEG) is largely dictated by the changes occuring in the value for the proton.

Table 6. Limiting single ion conductances and walden products of H^+ and Cl^- ions in water-EG mixtures at 25°C. λ^0s are given in $ohm^{-1}\ cm^2\ mol^{-1}$ and $\lambda^0\eta_0$ are given in $ohm^{-1}\ cm^2 mol^{-1}$ poise.

Wt % EG	0	20	40	60	80	100
$\lambda^0\ H^+$	349.80	150.69	83.39	48.60	21.68	27.70
$\lambda^0 Cl^-$	76.35	49.20	39.00	18.75	9.25	5.07
$\lambda^0 H^+ \eta_0$	3.11	2.03	2.09	2.04	1.73	4.68
$\lambda^0 Cl^-\ \eta_0$	0.68	0.66	0.98	0.79	0.74	0.86

The results in EG-DEG mixtures show (table 4) that Λ_0 (HCl) initially decreases up to 80 wt % DEG on the addition of small amounts of EG to an infinitely dilute solution of HCl in DEG and then gradually increases up to pure EG the rise being steep in the region of pure EG. The variation of the walden product with solvent composition is similar to that of Λ_0.

The decrease of Λ_0 may be attributed to the decrease of the abnormal conductance of the proton in DEG caused by the addition of small amounts of EG due to the proton partition equilibrium between DEG and EG. The proton jump mechanism is restored due to EGH^+ formation when considerable amount of EG is added and Λ_0 increases rather steeply as pure EG is approached.

In the EG-rich region, the continuous decrease of Λ_0 up to 80 wt % EG may thus be attributed to the disruption of hydrogen bonded structure of EG and hence the decrease of the abnormal proton conductance. It may be added that this explanation is also supported (Sivaprasad 1978) by considerable decrease of enthalpy of transfer of HCl from EG to EG-DEG mixtures.

References

Akerlof G 1932 *J. Am. Chem. Soc.* **54** 4125

Baradelli M and Sesta B 1972 *Electrochim. Acta* **77** 915

Covington A K and Dickinson T 1973 *Physical chemistry of organic solvent systems* (New York: Plenum Press) p. 674

Daggett H M and Kraus C A 1951 *J. Am. Chem. Soc.* **73** 799

De Lisi R and Goffredi M 1971 *Electrochim. Acta* **16** 2181

Evans D F and Kay R L 1966 *J. Phys. Chem.* **70** 366

Fuoss R M, Onsager L and Skinner J F 1965 *J. Phys. Chem.* **69** 2581

Gallant W 1967 *Hydrocarbon Processing* **46** 183

Goffredi M and Shedlovsky T 1967 *J. Phys. Chem.* **71** 2182

Kalidas C and Palit S R 1961 *J. Chem. Soc.* 3998

Kalidas C and Rao V S 1974 *J. Chem. Eng. Data* **19** 201

Robinson R A and Stokes R H 1959 *Electrolyte solutions* (London: Butterworths) p.463

Selvarajan V M and Kalidas C 1974 *Trans. Soc. Adv. Electrochem. Sci. Technol.* **9** 111

Shedlovsky T and Kay R L 1956 *J. Phys. Chem.* **60** 151

Shedlovsky T and Spivey H O 1967 *J. Phys. Chem.* **71** 2165

Sivaprasad P 1978 *Ion solvent interactions in isodielectric binary mixed solvents,* Ph.D. thesis, Indian Institute of Technology, Madras

Sivaprasad P and Kalidas C 1979 *Adv. Chem. Ser.* (ed) W F Further (Washington: Am. Chem. Soc.) Vol. 1, p. 77, 345

Srinivas Rao V and Kalidas C 1976 *Bull. Chem. Soc. Jpn.* **49** 203

Srinivas Rao V and Kalidas C 1976 *Indian J. Chem.* **A14** 129

Stokes R H 1961 *J. Phys. Chem.* **65** 1242

Strehlow H 1960 *Z. Phys. Chem. NF* **24** 240

Proc. Indian Acad. Sci. (Chem. Sci.), Vol. 92, No. 3, June 1983, pp. 211-220.
© Printed in India.

Isotopic invariants of pyramidal symmetrical XY_3 molecules and evaluation of molecular constants

A NATARAJAN* and V A CHINNAPPAN

Department of Physics, Bharathidasan University, Tiruchirapalli 620 023, India.

MS received 9 July 1982; revised 13 January 1983

Abstract. The isotopic invariants of pyramidal symmetrical XY_3 molecules are calculated in terms of frequencies, Coriolis coupling constants, molecular geometry parameters and masses of the constituent atoms. These invariants are used to evaluate force constants, compliance constants and mean amplitudes of vibration of four sets of 12 isotopic molecules.

Keywords. Isotopic invariants; pyramidal XY_3 molecules; force constants; mean amplitudes of vibration.

1. Introduction

The theory of isotopic substitution of nonlinear triatomic molecules of Parker (1975) has been generalised recently by Jagannathan *et al* (1980) applicable to molecules of the type X_mY_n whose G matrix contains 1×1 and 2×2 diagonal blocks in a mass-independent coordinate system. The same has been applied (Chinnappan *et al* 1978; Chinnappan and Savariraj 1979) for the nonlinear symmetrical XY_2 molecules and the planar symmetrical XY_3 molecules to derive expressions involving vibrational frequencies, Coriolis coupling constants, molecular geometry and masses of the constituent atoms that are invariant under symmetrical isotopic substitution. These invariants have been used to calculate the molecular constants such as force constants, centrifugal distortion constants and mean amplitudes of vibration for these molecules. In this paper, the expressions for the isotopic invariants of pyramidal XY_3 molecules are derived based on the theory of Jagannathan *et al* (1980). The numerical values are computed using the harmonic frequencies, the Coriolis coupling constants, geometry parameters and the masses of the constituent atoms for 4 sets of 12 isotopic molecules and these invariants are used to calculate the force constants, the compliance constants and the mean amplitudes of vibration of these molecules.

2. Theory

Throughtout this paper, the symbols, definitions of standard matrices, molecular geometry parameters and the orientation of coordinate axes are as in Cyvin (1968). The regular pyramidal XY_3 molecule belongs to C_{3v} point

*To whom all correspondence should be made.

group symmetry giving rise to six fundamental normal modes of vibration which are distributed among the different species according to

$$\Gamma_{\text{vib}} = 2A_1 + 2E \tag{1}$$

where E is doubly degenerate.

The G matrix of such a regular pyramidal XY_3 molecule in the internal symmetry coordinate system has two diagonal blocks each of them being of order 2×2 and they are

$$G(A_1) = \begin{bmatrix} (4\cos^2 A - 1)\mu_X + \mu_Y & -2(4\cos^2 A - 1)\tan A\ \mu_X \\ -2(4\cos^2 A - 1)\tan A\ \mu_X & (4 - \sec^2 A)(4\sin^2 A\ \mu_X + \mu_Y) \end{bmatrix} \tag{2}$$

$$\text{and } G(E) = \begin{bmatrix} 2\sin^2 A\ \mu_X + \mu_Y & 2\sin^2 A\tan A\ \mu_X \\ 2\sin^2 A\tan A\ \mu_X & 2\sin^2 A\tan^2 A\ \mu_X + (1 + \tfrac{1}{2}\sec^2 A)\ \mu_Y \end{bmatrix} \tag{3}$$

where μ_{XY} and μ_{YX} are the reciprocal masses of the atoms X and Y respectively and $2A$ is the YXY bond angle. Incidently, angle B which is the angle between the symmetry axis and the $X-Y$ bond is related to the YXY bond angle according to

$$3\sin^2 B = 2(1 - \cos 2A)$$

$$\text{or} \qquad \sin B = (2/\sqrt{3})\sin A \tag{4}$$

Following the notation and theory of Jagannathan *et al* (1980), the explicit expressions for g, d and Γ matrices for A_1 and E species are given by

$$g(A_1) = \begin{bmatrix} 1 & -2\tan A \\ -2\tan A & (\sec^2 A - 4) \end{bmatrix},$$

$$d(A_1) = \begin{bmatrix} [(4\cos^2 A - 1)(\mu_X + \tfrac{1}{3}\mu_Y)]^{1/2} & 0 \\ 0 & (\tfrac{1}{3}\mu_Y \cos^2 A)^{1/2} \end{bmatrix},$$

$$\Gamma(A_1) = \begin{bmatrix} \cos\theta & -\sin\theta \\ \sin\theta & \cos\theta \end{bmatrix},$$

$$g(E) = \begin{bmatrix} 1 & \tan A \\ \tan A & -(1 + \tfrac{1}{2}\sec^2 A) \end{bmatrix},$$

$$d(E) = \begin{bmatrix} [2\mu_X \sin^2 A + \tfrac{1}{3}\mu_Y(2\cos^2 A)+1]^{1/2} & 0 \\ 0 & (\tfrac{2}{3}\mu_Y \cos^2 A)^{1/2} \end{bmatrix},$$

$$\Gamma(E) = \begin{bmatrix} \cos\alpha & -\sin\alpha \\ \sin\alpha & \cos\alpha \end{bmatrix}, \tag{5}$$

where θ and α are the two parameters introduced for A_1 and E species respectively. It can be easily verified that

$$G(A_1) = g(A_1)\, d(A_1)^2\, g(A_1)^{\dagger},$$

and

$$G(E) = g(E)\, d(E)^2\, g(E)^{\dagger}. \tag{6}$$

The parameters θ and α can be determined from the Coriolis coupling constants as follows. According to the choice of the coordinate axes, there exists the Coriolis coupling matrix elements for the $A_1 \otimes E$ coupling with respect to Y axis and for the $E \otimes E$ coupling with respect to X axis and Z axis. Now the relation for the Coriolis coupling constant matrix ζ^{α} and L matrix (Cyvin 1968) is

$$\zeta^{\alpha} = L^{-1} C^{\alpha} L^{-1\dagger} \tag{7}$$

where $\alpha = x,y,z$.

Making use of the explicit values of C^{α} (skew symmetric matrix) for the various couplings from Cyvin (1968) and the relation (Jagannathan *et al* 1980).

$$L = gd\Gamma \tag{8}$$

we get the ζ elements in terms of the parameters θ and α as

$$\zeta^{Y}_{1,3a} = -C(D\cos\theta + E\sin\theta)\cos\alpha; \qquad \zeta^{Y}_{1,4a} = -C(D\cos\theta + E\sin\theta)\sin\alpha;$$

$$\zeta^{Y}_{2,3a} = -C(E\cos\theta - D\sin\theta)\cos\alpha; \qquad \zeta^{Y}_{2,4a} = C(E\cos\theta - D\sin\theta)\sin\alpha;$$

$$\zeta^{X}_{3a,4b} = -(m_X/6MI_{XX})^{1/2}\, R\cos B; \qquad \zeta^{Z}_{3a,3b} = K\cos^2\alpha - \sin^2\alpha;$$

$$\zeta^{Z}_{3a,4b} = \zeta^{z}_{4a,3b} = -(K+1)\sin\alpha\cos\alpha; \qquad \zeta^{Z}_{4a,4b} = K\sin^2\alpha - \cos^2\alpha \tag{9}$$

where

$$C = \left(\frac{6R^2 m_Y}{MI_{XX}}\right)^{1/2}, \qquad D = \left(\frac{M}{4\cos^2 A - 1}\right)^{1/2} \sin A \cos B,$$

$$E = \tfrac{1}{2} m_X^{1/2} \cos B, \quad K = I_{ZZ}/2I_{XX}$$

$$\text{with } I_{XX} = \frac{R^2 m_Y}{M}\,[6m_Y \sin^2 A + m_X(2\cos^2 A + 1)],$$

$$I_{ZZ} = 4R^2 m_Y \sin^2 A; \quad M = m_X + 3m_Y$$

Here m_X and m_Y are the masses of the X and Y atoms respectively and R the $X-Y$ bond length.

Incidently the following sum rules are evident:

$$\text{(i)}\quad (\zeta^Y_{1,3a})^2 + (\zeta^Y_{1,4a})^2 + (\zeta^Y_{2,3a})^2 + (\zeta^Y_{2,4a})^2 = \frac{I_{ZZ}}{4I_{XX}} + \frac{1}{2}$$

$$\text{(ii)}\quad \zeta^Y_{1,3a}\ \zeta^Y_{2,4a} = \zeta^Y_{1,4a}\ \zeta^Y_{2,3a},$$

$$\text{(iii)}\quad \zeta^Z_{3a,3b}\ \zeta^Z_{4a,4b} = \frac{R^2 m_X m_Y}{MI_{XX}}(1 - 4\cos^2 A),$$

$$\text{(iv)}\quad \zeta^Z_{3a,3b}\ \zeta^Z_{4a,4b} - (\zeta^Z_{3a,4b})^2 = -\frac{I_{ZZ}}{2I_{XX}}$$

$$\text{(v)}\quad \sum_{t=1}^{2}\sum_{t=3}^{4} (\zeta^Y_{i,ta})^2 + \tfrac{1}{2}[\zeta^Z_{3a,3b}\ \zeta^z_{4a,4b} - (\zeta^Z_{3a,4b})^2] = \tfrac{1}{2} \qquad (10)$$

The sum rules (i) and (ii) are given by Hoy *et al* (1972) and the rules (iii) and (iv) are given in Cyvin (1968 p. 341). The rule (v) is another sum rule of the Coriolis coupling constants and it is obtained by using the sum rules (i) and (iv).

According to (21)–(23) of Jagannathan *et al* (1980) and from (5), the invariants of the regular pyramidal XY_3 molecules in terms of the parameters θ and α are given by

$$I_{11} = \frac{3m_X m_Y}{M(4\cos^2 A - 1)}(\lambda_1 \cos^2\theta + \lambda_2 \sin^2\theta),$$

$$I_{12} = \frac{3m_Y}{\cos A}\left(\frac{m_X}{M[4\cos^2 A - 1]}\right)^{1/2}(\lambda_1 - \lambda_2)\sin\theta\cos\theta,$$

$$I_{22} = \frac{3m_Y}{\cos^2 A}(\lambda_1 \sin^2\theta + \lambda_2 \cos^2\theta), \qquad (11)$$

$$I_{33} = \frac{3m_X m_Y}{6m_Y \sin^2 A + m_X(2\cos^2 A + 1)}(\lambda_3 \cos^2\alpha + \lambda_4 \sin^2\alpha),$$

$$I_{34} = \frac{3m_Y}{\cos A}\left[\frac{m_X}{12m_Y \sin^2 A + 2m_X(2\cos^2 A + 1)}\right]^{1/2}\sin\alpha\cos\alpha(\lambda_3 - \lambda_4),$$

$$I_{44} = \frac{3m_Y}{2\cos^2 A}(\lambda_3 \sin^2\alpha + \lambda_4 \cos^2\alpha), \qquad (12)$$

where $\lambda_i = 4\pi^2 c^2 \omega_i^2$ with ω_i the vibrational frequency of the ith mode of vibration.

The parameter θ in (11) is determined using the geometry parameters of the molecule and the Coriolis coupling constants from the relation

$$\theta = \tan^{-1}\left\{\frac{[m_X(4\cos^2 A - 1)]^{1/2}\,\zeta^Y_{1,3a} - 2M^{1/2}\sin A\,\zeta^Y_{2,3a}}{2M^{1/2}\sin A\,\zeta^Y_{1,3a} + [m_X(4\cos^2 A - 1)]^{1/2}\,\zeta^Y_{2,3a}}\right\} \tag{13}$$

and the parameter α in (12) is eliminated and the equations are rewritten as

$$I_{33} = m_X m_Y R^2\left[\frac{(\lambda_3 - \lambda_4)(1 + \zeta^Z_{3a,3b})}{I_{ZZ} + m_X R^2} + \frac{3m_Y\lambda_4}{MI_{XX}}\right]$$

$$= m_X m_Y R^2\left[\frac{3m_Y\,\lambda_3}{MI_{XX}} - \frac{(\lambda_3 - \lambda_4)(1 + \zeta^Z_{4a,4b})}{I_{ZZ} + m_X R^2}\right],$$

$$I_{34} = \frac{(\lambda_3 - \lambda_4)\,R\;\zeta^Z_{3a,4b}}{(I_{ZZ} + m_X R^2)\cos A}\,(\tfrac{1}{2}\,Mm_X m_Y I_{XX})^{1/2}$$

$$I_{44} = \frac{1}{2\cos^2 A}\left[\frac{(\lambda_3 - \lambda_4)\,MI_{XX}\,(1 + \zeta^Z_{4a,4b})}{I_{ZZ} + m_X R^2} + 3m_Y\lambda_4\right]$$

$$= \frac{1}{2\cos^2 A}\left[3m_Y\,\lambda_3 - \frac{(\lambda_3 - \lambda_4)\,MI_{XX}\,(1 + \zeta^Z_{3a,3b})}{I_{ZZ} + m_X R^2}\right] \tag{14}$$

It can be noticed that these invariants are calculated using observable quantities in addition to the molecular parameters.

3. Applications of the invariants

3.1 *Calculation of force constants*

From (19) of Chinnappan *et al* (1978), viz., $F = g^{-1^{\dagger}}\,Ig^{-1}$ the symmetrised force constants of the regular pyramidal XY_3 molecule are worked out to be

$$F_{11} = \tfrac{1}{9}[(4\cos^2 A - 1)^2 I_{11} + \sin^2 2A\;I_{22} - 2(4\cos^2 A - 1)\sin 2A\;I_{12}]$$

$$F_{12} = \tfrac{1}{9}[-(4\cos^2 A - 1)\sin 2A\,I_{11} + \sin 2A\cos^2 A\,I_{22} + (\sin^2 2A - 4\cos^2 A - 1\cos^2 A)I_{12}]$$

$$F_{22} = \tfrac{1}{9}[\sin^2 2A\,I_{11} + \cos^4 A\,I_{22} + 2\sin 2A\,\cos^2 A\,I_{12}]$$

$$F_{33} = \tfrac{1}{9}\,[(2\cos^2 A + 1)^2 I_{33} + \sin^2 2AI_{44} + 2\sin 2A\,(2\cos^2 A + 1)\,I_{34}]$$

$$F_{34} = \tfrac{1}{9}\,[\sin 2A\,[(2\cos^2 A + 1)\,I_{33} - 2\sin 2A\cos^2 A\,I_{44} + (\sin^2 2A - 2\cos^2 A + 1\;\;2\cos^2 A)\;I_{34}]$$

$$F_{44} = \tfrac{1}{9}[\sin^2 2A\, I_{33} + 4\cos^4 A\, I_{44} - 4\sin 2A \cos^2 A\, I_{34}] \tag{15}$$

3.2 *Calculation of compliance constants*

The compliance constant matrix is given by (Cyvin 1968)

$$N = L\sigma L^{\dagger} \tag{16}$$

where $\sigma_i = 1/\lambda_i$. Using (5), (8), (11) and (14) in (16) the elements of the symmetrised compliance constants are found to be

$$N_{11} = P\{Q[4m_X\sin^2 A - M(4\cos^2 A - 1)] + 2Mm_X I_{12}(4\cos^2 A - 1)\sin 2A + 3m_X m_Y[M\lambda_1(4\cos^2 A - 1) + 4m_X\lambda_2 \sin^2 A]\},$$

$$N_{12} = P(4\cos^2 A - 1)\{2Q(M + m_X)\tan A + Mm_X I_{12}(4\cos 2A - 1) - 6m_X m_Y \tan A(M\lambda_1 - m_X\lambda_2)\},$$

$$N_{22} = P(4 - \sec^2 A)\{Q[m_X(4\cos^2 A - 1) - 4M\sin^2 A] - 2Mm_X I_{12}(4\cos^2 A - 1)\sin 2A + 3m_X m_Y[4M\lambda_1\sin^2 A + m_X\lambda_2(4\sin^2 A - 1)]\},$$

$$N_{33} = T\{(3m_X m_Y\lambda_4 - SI_{33})(S - 2m_X\sin^2 A) - 2SI_{34}\sin 2A - 3m_X m_Y[S\lambda_3 + 2m_X\lambda_4\sin^2 A]\},$$

$$N_{34} = T\{S(3m_X m_Y\lambda_4 - SI_{33})\tan A + Sm_X I_{34}(2\cos^2 A + 1) + 3m_X m_Y\tan A[S\lambda_3 - m_X\lambda_4(2\cos^2 A + 1)]\},$$

$$N_{44} = T\{(SI_{33} - 3m_X m_Y\lambda_4)[\tfrac{1}{2}m_X(2\cos^2 A + 1)^2 - S\tan^2 A] + Sm_X I_{34}(2\cos^2 A + 1)\sin 2A + 3m_X m_Y[S\lambda_3\tan^2 A + \tfrac{1}{2}m_X\lambda_4(2\cos A + \sec A)^2]\}, \tag{17}$$

where $P = (9m_X^2 m_Y^2\lambda_1\lambda_2)^{-1}$, $Q = MI_{11}(4\cos^2 A - 1) - 3m_X m_Y\lambda_2$,

$T = (9m_X^2 m_Y^2\lambda_3\lambda_4)^{-1}$, $S = 6m_Y\sin^2 A + m_X(2\cos^2 A + 1)$.

3.3 *Calculation of mean amplitudes of vibration*

The matrix of the mean square amplitudes of vibration is given as (Cyvin 1968)

$$\Sigma = L\,\delta\,L^{\dagger} \tag{18}$$

Substituting (5), (8), (11) and (14) in (18), the elements of the symmetrised mean square amplitudes of vibration are as follows:

$$\Sigma_{11} = U\{V[4m_X\sin^2 A - M(4\cos^2 A - 1)] + 2Mm_X I_{12}(4\cos^2 A - 1)\sin 2A\} + (3m_X m_Y)^{-1}[M\delta_2(4\cos^2 A - 1) + 4m_X\delta_1\sin^2 A],$$

$$\Sigma_{12} = U(4\cos^2 A - 1)\{2V(M + m_X)\tan A + Mm_X I_{12}(4\cos^2 A - 1)\} - (3m_X m_Y)^{-1}\,2\tan A(M\delta_2 - m_X\delta_1),$$

$$\Sigma_{22} = U(4 - \sec^2 A)\{V[m_X(4\cos^2 A - 1) - 4M\sin^2 A] - 4Mm_X I_{12}\cos^2 A(4\cos^2 A - 1)\tan A\} + (3m_X m_Y)^{-1}(4 - \sec^2 A)[m_X \delta_1 (4\cos^2 A - 1) + 4M\delta_2 \sin^2 A]$$

$$\Sigma_{33} = W\{(3m_X m_Y \lambda_4 - SI_{33})(S - 2m_X \sin^2 A) - 2Sm_X I_{34}\sin^2 A\} + (3m_X m_Y)^{-1}(2m_X \delta_3 \sin^2 A + S\delta_4),$$

$$\Sigma_{34} = W\{S(3m_X m_Y \lambda_4 - SI_{33})\tan A + Sm_X I_{34}(2\cos^2 A + 1)\} + (3m_X m_Y)^{-1}\tan A[S\delta_4 - m_X \delta_3(2\cos^2 A + 1)]$$

$$\Sigma_{44} = W\sec^2 A\{(SI_{33} - 3m_X m_Y \lambda_4)[\tfrac{1}{2}m_X(2\cos^2 A + 1)^2 - S\sin^2 A] + Sm_X I_{34}(2\cos^2 A + 1)\sin 2A\} + (3m_X m_Y)^{-1}\sec^2 A[\tfrac{1}{2}m_X \delta_3(2\cos^2 A + 1)^2 + S\delta_4 \sin^2 A], \quad (19)$$

where $U = [9m_X^2 m_Y^2(\lambda_1 - \lambda_2)]^{-1}(\delta_2 - \delta_1)$,

$V = MI_{11}(4\cos^2 A - 1) - 3m_X m_Y \lambda_2$,

$W = [9m_X^2 m_Y^2(\lambda_3 - \lambda_4)]^{-1}(\delta_4 - \delta_3)$,

$\delta_i = h/8\pi^2 c\omega_i \coth(hc/kT)\omega_i$,

$= 16.85748/\omega_i \coth(0.719399/T)\omega_i$.

The mean amplitudes of vibration of the bonded and the non-bonded atoms are given as (Cyvin 1968)

$$l(X\text{——}Y) = [\tfrac{1}{3}(\Sigma_{11} + 2\Sigma_{33})]^{1/2},$$

$$l(Y\cdots Y) = \{\tfrac{1}{3}[(4\Sigma_{11} + 2\Sigma_{33})\sin^2 A + 2(\Sigma_{12} - \Sigma_{34})\sin^2 A + (\Sigma_{22} + 2\Sigma_{44})\cos^2 A]\}^{1/2}. \quad (20)$$

4. Results and discussion

The isotopic invariants for the four sets of 12 molecules of regular pyramidal XY_3 type (the trihydrides of the group V elements X = N, P, As, Sb and Y = H, D, T) are calculated taking the frequencies and the Coriolis coupling constants from Cyvin (1968) and the geometrical parameters as given by Thyagarajan *et al* (1969) and are given in table 1. These invariants show a very good consistency thereby justifying the assumption that the molecular force field and the geometry remain unaltered under isotopic substitution. The calculated symmetrised force constants using these invariants are listed in table 2 and they show agreement with the values given by Periseau *et al* (1963). It is noted that the force constant F_{33} which involves the stretching constant is nearly 10 times F_{44} which involves the bending constant. Similar relation is noticed between F_{11} and F_{22}. Also, the stretching and bending force constants decrease characteristically with the increase in the mass of the apex atom. The calculated values of the compliance constants are presented in table 3. It is quite striking to observe the invariance of the compliance constants due to the isotopic substitution from table 3 thereby conforming the basic assump-

Table 1. The isotopic invariants of pyramidal XY_3 molecules.

Molecule	I_{11}	$-I_{12}$	I_{22}	I_{33}	I_{34}	I_{44}
NH_3	6.7720	12.6044	56.7034	7.7658	7.4110	17.6267
ND_3	6.7213	12.6007	56.6811	7.7692	7.4093	17.6210
NT_3	6.7208	12.5859	56.7119	7.7679	7.4026	17.6211
PH_3	5.7895	6.4059	14.9647	3.8049	2.8937	5.6973
PD_3	5.7900	6.4085	14.9627	3.8024	2.8927	5.6891
PT_3	5.7921	6.4106	14.9625	3.8048	2.8942	5.6935
AsH_3	5.1569	5.0644	11.0072	3.0074	2.4441	4.7322
AsD_3	5.1586	5.0669	10.9929	3.0076	2.4471	4.7317
AsT_3	5.1558	5.0670	10.9999	3.0069	2.4425	4.7334
SbH_3	3.9653	4.2498	8.7431	2.4748	1.9434	3.3438
SbD_3	3.9739	4.2538	8.7295	2.4760	1.9435	3.3397
SbT_3	3.9771	4.2536	8.7227	2.4759	1.9442	3.3400

Table 2. The symmetrised force constants (md/A) of pyramidal XY_3 molecules.

Molecule	F_{11}	$-F_{12}$	F_{22}	F_{33}	$-F_{34}$	F_{44}
NH_3	7.0721	−0.7792	0.5313	7.0388	0.1758	0.6650
	(7.018)	(−1.098)	(0.6401)	(6.881)	(0.195)	(0.680)
PH_3	3.4004	0.0618	0.3402	3.4639	0.0399	0.3763
	(3.439)	(0.057)	(0.290)	(3.283)	(0.163)	(0.410)
AsH_3	2.7758	0.0069	0.3135	2.8904	0.0976	0.3021
	(2.850)	(0.077)	(0.270)	(2.865)	(0.237)	(0.330)
SbH_3	2.2735	0.1990	0.2113	2.2983	0.2005	0.2075
	(2.184)	(0.374)	(0.213)	(2.215)	(0.131)	(0.224)

The values in parentheses are from Pariseau (1963).

Table 3. The compliance constants (A/md) of pyramidal XY_3 molecules.

Molecule	N_{11}	N_{12}	N_{22}	N_{33}	N_{34}	N_{44}
NH_3	0.1687	−0.2475	2.2453	0.1429	0.2002	1.5123
ND_3	0.1687	−0.2473	2.2454	0.1428	0.2001	1.5122
NT_3	0.1686	−0.2473	2.2450	0.1429	0.2001	1.5117
PH_3	0.3045	0.1797	3.0443	0.2894	0.2770	2.6609
PD_3	.03046	0.1798	3.0456	0.2892	0.2767	2.6620
PT_3	0.3048	0.1793	3.0457	0.2891	0.2767	2.6619
AsH_3	0.3881	0.3114	3.4383	0.3509	0.4287	3.3589
AsD_3	0.3881	0.3114	3.4368	0.3510	0.4287	3.3573
AsT_3	0.3881	0.3113	3.4364	0.3507	0.4282	3.3563
SbH_3	0.4803	0.4528	5.1687	0.4345	0.4992	4.7967
SbD_3	0.4799	0.4518	5.1635	0.4344	0.4990	4.7992
SbT_3	0.4801	0.4527	5.1669	0.4344	0.4991	4.7974

Table 4. The mean amplitudes of vibration (Å units) of pyramidal XY_3 molecules.

Molecules	T = 0 K		T = 298 K	
	l(X— Y)	l(Y·····Y)	l(X— Y)	l(Y·····Y)
NH_3	0.07144 (0.07146)	0.11048 (0.11569)	0.07146 (0.07147)	0.11060 (0.11578)
ND_3	0.06113 (0.06113)	0.09311 (0.09755)	0.06116 (0.06116)	0.09389 (0.09790)
NT_3	0.05613 (0.05614)	0.08421 (0.08837)	0.05615 (0.05618)	0.08484 (0.08906)
PH_3	0.08414 (0.0841)	0.14548 (0.1498)	0.08416 (0.0841)	0.14601 (0.1503)
PD_3	0.07130 (0.0713)	0.12245 (0.1261)	0.07132 (0.0713)	0.12434 (0.1282)
PT_3	0.06491 (0.0649)	0.11080 (0.1142)	0.06499 (0.0650)	0.11417 (0.1179)
AsH_3	0.08807 (0.0880)	0.15390 (0.1586)	0.08809 (0.0880)	0.15472 (0.1596)
AsD_3	0.07425 (0.0743)	0.12286 (0.1335)	0.07436 (0.0744)	0.13105 (0.1368)
AsT_3	0.06736 (0.0673)	0.11706 (0.1207)	0.06760 (0.0676)	0.12210 (0.1264)
SbH_3	0.09279 (0.0928)	0.16832 (0.1735)	0.09283 (0.0929)	0.17061 (0.1760)
SbD_3	0.07819 (0.0782)	0.14175 (0.1459)	0.07836 (0.0784)	0.14777 (0.1528)
SbT_3	0.07085 (0.0708)	0.12808 (0.1320)	0.07125 (0.0713)	0.13775 (0.1427)

The values in parentheses are from Cyvin (1968).

tion of the isotopic invariants. In table 4, the calculated mean amplitudes of vibration at temperature 0 K and 298 K are given. These values agree very well with the values given by Cyvin (1968) at these temperatures. It is observed that as the end atoms are substituted by heavier atoms, the mean amplitudes of vibration decrease as expected.

It is interesting to note that when once the isotopic invariants of a pyramidal XY_3 molecules are found using reliable observable quantities like frequencies, etc., the other molecular constants of the same molecule and its isotopic substituents can be easily calculated.

References

Chinnappan V A, Jagannathan R and Savariraj G A 1978 *Indian J. Pure Appl. Phys.* **16** 668

Chinnappan V A and Savariraj G A 1979 *Indian J. Pure Appl. Phys.* **17** 423

Cyvin S J 1968 *Molecular vibration and mean square amplitude* (Amsterdam: Elsevier) p. 341

Hoy A R, Stone J M R and Watson J K G 1972 *J. Mol. Spectrosc.* **42** 393

Jagannathan R, Chinnappan V A and Savariraj G A 1980 *Indian J. Pure Appl. Phys.* **18** 964

Pariseau M, Wu E and Overend J 1963 *J. Chem. Phys.* **39** 217

Parker P M 1975 *J. Mol. Spectrosc.* **58** 344

Thyagarajan G, Sarma C R and Subhedar M K 1969 *J. Mol. Spectrosc.* **31** 100

Proc. Indian Acad. Sci. (Chem. Sci.), Vol. 92, No. 3. June 1983, pp. 221–225.
© Printed in India.

Uncatalysed oscillations in the bromate – pyrogallol system

R RAMASWAMY* and S RAMANATHAN
Department of Chemistry, Indian Institute of Technology, Madras 600 036, India

MS received 19 May 1981; revised 30 December 1982

Abstract. Studies on the bromate-pyrogallol system with sulphuric and perchloric acids are presented. The addition of acrylamide and acrylonitrile to the oscillatory system indicates the presence of free radicals. The apparent energy of activation for the overall process is 10.1 ± 1 and 20 ± 0.5 kcal mol^{-1} respectively for sulphuric and perchloric acids. The static potential measurements with different constituents together with double recording of oscillations with a platinum and Ag/AgBr indicator electrode establish that oscillations are caused by continuous change in the concentration of bromine and bromide ions.

Keywords. Oscillatory reaction; periodic reaction; uncatalysed oscillations; bromate-sulphuric acid/perchloric acid-pyrogallol system; effect of monomer; activation energy.

1. Introduction

Oscillatory reaction in the bromate system with Mn^{2+}/Ce^{3+} has been extensively studied (Noyes and Field 1977; Ganapathisubramanian *et al* 1980). Pyrogallol gives oscillations in the bromate system without the presence of metal ion (Orban and Koros 1978). The addition of [iron (1, 10 phenanthroline)$_3$]$^{2+}$ or [Ru ($\alpha\alpha'$ dipyridyl)$_3$]$^{2+}$ has been reported to inhibit the oscillations (Orban and Koros 1979).

2. Experimental

Sulphuric acid and pyrogallol were taken in a polythene beaker and thermostated. Thermostated potassium bromate was added to trigger off the oscillations. The oscillations were followed by continuous recording of the potential between a platinum indicator electrode and a saturated calomel electrode connected through a potassium nitrate bridge. The solution was well-stirred for homogeneity with a magnetic stirrer. The difficulty in obtaining reproducible results in the iodate and bromate systems had been overcome by the choice of the reaction vessel and the pretreatment of the electrode (Ramaswamy *et al* 1978, 1980).

3. Results and discussion

The concentration of the constituents have a profound influence on the oscil-

*To whom all correspondence should be made.

latory behaviour of the system and help in identifying the species causing the oscillations. The addition of acrylonitrile or acrylamide affects the oscillatory pattern of the systems differently.

The apparent energy of activation for the overall process has been evaluated. The double recordings obtained with platinum and Ag/AgBr indicator electrodes and the static potential measurements with different compositions of the constituents enable identification of the species causing the oscillations.

Simulation of oscillatory pattern by the periodic addition of a constituent provides visual and direct evidence of the conclusions drawn in identifying the species causing oscillations.

3.1 *Effect of concentration*

3.1.a Pyrogallol concentration: The concentration of pyrogallol was varied in the range 0.03 to 0.08 M with constant concentrations of potassium bromate (0.1 M) and sulphuric acid (2 M) at 30°C. Eleven oscillations were recorded in 2 min at 0.03 M with an induction time of 0.33 min. The number of oscillations decreased to 4 in 6.5 min at 0.07 M. The system did not oscillate at 0.08 M pyrogallol. The range of concentration of pyrogallol in which the system gives oscillations with perchloric acid (3.22 M) and potassium bromate (0.1 M) at 30°C is 0.3 to 0.06 M. Standard conditions produced ten oscillations in 6.5 min with an induction time of 1.2 min (figure 1). The optimum con-

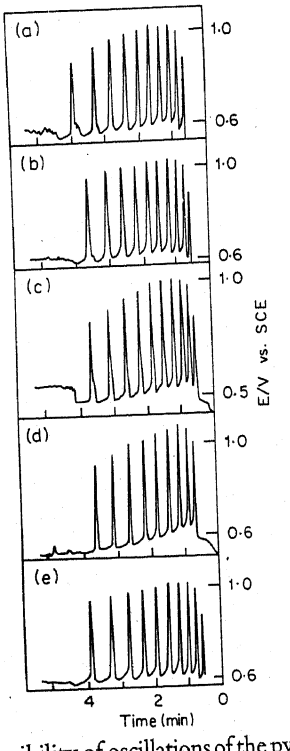

Figure 1. Reproducibility of oscillations of the pyrogallol-sulphuric acid-bromate system. Bromate = 0.1 M; pyrogallol = 0.05 M; Sulphuric acid = 2 M; temperature 30°

centrations of pyrogallol employed in subsequent studies were 0.05 M and 0.06 M in sulphuric acid and perchloric acid systems respectively.

3.1.b Bromate concentration: The concentration of potassium bromate was varied in the range 0.06 to 0.16 M. The optimum concentration of potassium bromate employed subsequently for both the systems was 0.1 M.

3.1.c Acid concentration: Sulphuric acid concentration was varied in the range 1 to 3 M, while that of perchloric acid from 3 to 3.7 M. There was a decrease in the amplitude and increase in the frequency of oscillations at higher concentrations of the acids. The concentration of sulphuric and perchloric acids employed for detailed study were 2 M and 3.6 M respectively. Ten oscillations in 4 min and 23 oscillations in 2.7 min were observed under these conditions respectively with the two systems.

3.2 Effect of temperature

The reaction was studied in the temperature range 5 to 60°C for both systems. Increase in temperature resulted in an increase in frequency of oscillations and the amplitude. The amplitude increased from 200 mV at 5°C to 430 mV at 48°C in the sulphuric acid system. The apparent energy of activation for the overall process has been evaluated (Ganapathisubramanian *et al* 1978) from the linear plot of log $1/t$ *vs* $1/T$ on the basis that the rate constant is inversely proportional to time (t). For this purpose, the total duration, oscillating time and the time for a definite number of oscillations were considered. The apparent energy of activation for the overall process respectively for sulphuric acid and perchloric acid systems are 10.1 ± 1 and 20 ± 0.5 kcal mol^{-1}.

3.3 *Effect of monomers*

The addition of arcylonitrile to the pyrogallol-bromate-sulphuric acid system reduced the amplitude to a considerable extent. After the termination of the oscillations the reaction mixture yielded, on standing, a solid non-polymeric precipitate. The IR spectrum of the compound indicated the presence of a cyano group.

3.3a *Addition of acrylamide:* The addition of acrylamide to the system brought about a considerable change in the oscillatory behaviour. Acrylamide (1 ml of 5% solution) added before the start of the oscillations increased the duration of oscillation from 4 to 7 min. However the duration decreased to 1.2 min for an addition of 2 ml acrylamide. The same trend was maintained when the addition of acrylamide was made 1 min after the start of the reaction. The response of the oscillatory system to the addition of different amounts of acrylamide after the first oscillation is presented in figure 2. The pattern is characterised by double peaks in the presence of acrylamide and the peak shoulder position shifts with the addition of different amounts of acrylamide.

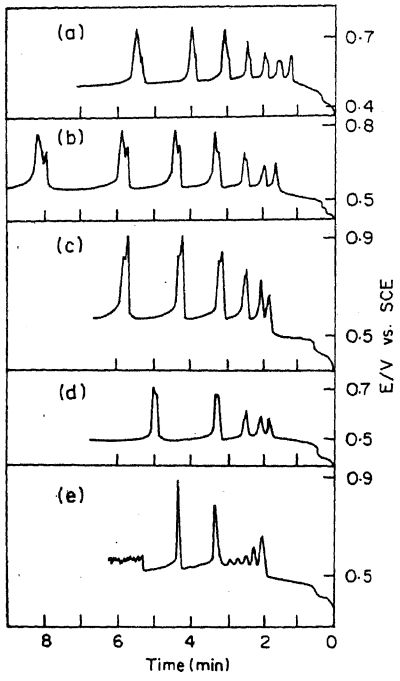

Figure 2. Effect of addition of acrylamide on bromate pyrogallol-perchloric acid system after the first oscillation.

Bromate = 0.1 M; Pyrogallol = 0.06 M; Perchloric acid = 3.22 M; Temperature 30°C. Acrylamide (5% solution) added (ml) a. 2.5, b. 1.0, c. 0.5, d. 0.3, e. nil.

3.4 *Species causing oscillations*

The oscillations recorded with Ag/AgBr indicator electrode establish that the concentrations of bromide are 10^{-6} and 10^{-5} M at the peak and base regions respectively. Static potential values of the platinum electrode measured with different constituents present show that in the binary system with a constant bromide concentration of 10^{-3}M, the potential was 0.14 V (*vs* SCE) with 10^{-5} M bromine and 0.8 V (*vs* SCE) with 10^{-4} M bromine. The potential of the platinum electrode with the oxidised product of pyrogallol is 0.25 V (*vs* SCE).

The addition of ferroin (0.002 M) or iron $\alpha\alpha'$ dipyridyl (0.002 M) to the uncatalysed bromate system leads to a switch over of the oscillations to a new oscillatory phase with an amplitude of about 100 mV in the range of 0.95 to 1.05 V (*vs* SCE). The exchange current density for $Pt/Br_2/Br^-$ is about 10^{-5}

amp/cm^2 and for Pt/Fe^{3+}/Fe^{2+} is nearly 10^{-3}amp/cm^2. The oscillatory behaviour of the system is thus controlled by the relative magnitudes of the exchange current density of the different species involved. These facts establish that oscillations in such systems are caused by the periodic concentration change of bromine and bromide ion.

Acknowledgements

One of the authors (SR) is thankful to UGC, New Delhi for the award of a fellowship and to the Government of Tamilnadu for deputation to the Ph.D. programme at IIT, Madras. The authors thank Drs J C Kuriacose and B Viswanathan for helpful discussions.

References

Ganapathisubramanian N, Jaya S and Ramaswamy R 1978 *Curr. Sci.* **47** 770

Ganapathisubramanian N, Ramaswamy R and Kuriacose J C 1980 *Proc. Indian Acad. Sci. (Chem. Sci.)* **89** 235

Noyes R M and Field R J 1977 *Acc. Chem. Res.* **10** 273

Orban M and Koros E J 1978 *J. Phys. Chem.* **82** 1672

Orban M and Koros E J 1979 *Symposium on kinetics of Physicochemical oscillations, Aachen* (FRG) preprints Vol. 1. p. 83

Ramaswamy R, Ganapathisubramanian N, Kuriacose J C and Doss K S G 1978 *Proc. Indian Acad. Sci. (Chem. Sci.),* **A 87** 253

Ramaswamy R, Jaya S and Ganapathisubramanian N 1980 *Proc. Indian Acad. Sci. (Chem. Sci.)* **89** 65